UNIVERSITY OF CORDOBA

DEPARTMENT OF PHYSICAL CHEMISTRY AND

APPLIED THERMODYNAMICS

Experimental and numerical study on hybrid HVAC systems activated at low temperature based on desiccant wheels and indirect evaporative coolers

Estudio experimental y numérico de sistemas híbridos de climatización activados a baja temperatura basados en ruedas desecantes y enfriadores evaporativos indirectos

Thesis submitted in partial fulfillment of the requirements for the

Degree of Doctor of Advanced Computing, Energy and Plasmas

FRANCISCO COMINO MONTILLA

supervised by

Dr. Manuel Ruiz de Adana Santiago

Cordoba, September 2017

TITULO: *ESTUDIO EXPERIMENTAL Y NUMÉRICO DE SISTEMAS HÍBRIDOS DE CLIMATIZACIÓN ACTIVADOS A BAJA TEMPERATURA BASADOS EN RUEDAS DESECANTES Y ENFRIADORES EVAPORATIVOS INDIRECTOS*

AUTOR: *Francisco Comino Montilla*

© Edita: UCOPress. 2017
Campus de Rabanales
Ctra. Nacional IV, Km. 396 A
14071 Córdoba

www.uco.es/publicaciones
publicaciones@uco.es

TÍTULO DE LA TESIS: ESTUDIO EXPERIMENTAL Y NUMÉRICO DE SISTEMAS HÍBRIDOS DE CLIMATIZACIÓN ACTIVADOS A BAJA TEMPERATURA BASADOS EN RUEDAS DESECANTES Y ENFRIADORES EVAPORATIVOS INDIRECTOS

DOCTORANDO: FRANCISCO COMINO MONTILLA

INFORME RAZONADO DEL DIRECTOR DE LA TESIS

(se hará mención a la evolución y desarrollo de la tesis, así como a trabajos y publicaciones derivados de la misma).

El doctorando Francisco Comino Montilla ha realizado bajo mi dirección la tesis doctoral titulada "*Estudio experimental y numérico de sistemas híbridos de climatización activados a baja temperatura basados en ruedas desecantes y enfriadores evaporativos indirectos*".

Francisco Comino Montilla presentó sus primeros resultados en esta línea de investigación con el TFM "*Modelado y optimización de una rueda desecante mediante diseño de experimentos*" presentado en septiembre de 2014 dentro del Máster de Control de Procesos Industriales de la Universidad de Córdoba.

Francisco Comino Montilla ha trabajado dentro de esta línea de investigación, en el marco de varios proyectos. Cabe destacar su participación activa en esta línea de trabajo dentro del proyecto de investigación "*DESSECA: Investigación y deshumectación y secado de aire*", desde 15/02/2013 a 31/01/2015. También ha colaborado en otros proyectos de investigación como el proyecto "NATURCOOL: Investigación en ciclos de refrigeración y climatización con fluidos alternativos", desde 01/11/2015 a 30/06/2016. Ha recibido ayudas del programa I+D+i Emplea Joven, desde 01/02/2015 a 31/10/2015, del Plan Propio Galileo "PPGALILEO-2016-MI-TEP-169" de la Universidad de Córdoba desde 01/12/2016 a 31/01/2017 y también ayudas del Plan Propio "XXI PP. Mod. 1 (2016) - TEP-0169 BIOSAHE", de la Universidad de Córdoba desde 01/02/2017 a 30/06/2017.

Francisco Comino Montilla realizó parte de la tesis en el Laboratorio de Investigación en Climatización de la Universidad de Córdoba. Esta instalación experimental ha permitido

alcanzar resultados de investigación significativos en el estudio y caracterización de ruedas desecantes activadas a baja temperatura.

El avance en esta línea de trabajo propició una estancia de investigación de 3 meses en el Dipartimento di Energia del Politecnico di Milano, bajo la supervisión del Profesor Stefano De Antonellis, realizada en el periodo comprendido entre el 01/09/2016 y el 30/11/2016. Durante esta estancia se realizó el estudio y caracterización experimental de equipos enfriadores evaporativos indirectos, aprovechando las instalaciones experimentales disponibles en el grupo de investigación Airlab.

Una vez concluida su estancia de investigación, Francisco Comino Montilla ha desarrollado la última etapa de la tesis consistente en evaluar el potencial de sistemas híbridos basados en ruedas desecantes y enfriadores evaporativos indirectos para la climatización de edificios pequeños con altas cargas latentes así como su comparación con los sistemas tradicionales.

El trabajo de investigación de Francisco Comino Montilla ha requerido el desarrollo de numerosos estudios experimentales y numéricos. Los resultados de estos trabajos de investigación han dado lugar a distintas publicaciones entre las que cabe destacar: dos artículos publicados en revistas internacionales de impacto, así como distintas comunicaciones en cinco congresos de carácter nacional e internacional. En los últimos meses, se han enviado dos artículos a revistas internacionales de impacto, los cuales se encuentran actualmente en proceso de revisión.

Del doctorando, aparte de su excelente calidad humana, me gustaría destacar, entre otras cualidades, su extraordinaria capacidad de trabajo, así como su constancia, tesón y disciplina, valores que han soportado todo el trabajo de investigación desarrollado y que han contribuido a resolver las numerosas dificultades que han aparecido a lo largo de un trabajo de esta naturaleza. Considero que este periodo ha permitido que Francisco Comino Montilla desarrolle las cualidades propias de un excelente investigador.

Concluyendo, la metodología, calidad científica y resultados de investigación de esta tesis se valoran de forma MUY FAVORABLE.

Por todo ello, SE AUTORIZA LA PRESENTACIÓN DE LA TESIS DOCTORAL.

Córdoba, 21 de Septiembre de 2017

Firma del director

Fdo.: Manuel Ruiz de Adana Santiago

A mi familia con todo mi amor.

Quiero agradecer a todos aquellos que de una forma u otra han estado a mi lado durante la realización de esta Tesis Doctoral.

A todos mis compañeros, por la ayuda prestada durante el desarrollo de este trabajo, por el día a día, y por supuesto, por las buenas experiencias compartidas dentro y fuera de la universidad. Fernando, por tu colaboración y soporte en este trabajo de investigación. Miguel y Félix, por los momentos vividos en la sala de becarios y por compartir conmigo esta aventura, seguro que pronto obtendréis la recompensa por la que estáis peleando. Pepelu, por tu amistad y por hacer más entretenidos los días de trabajo. Javi S. e Inés, por vuestra disponibilidad y por las divertidas conversaciones durante los almuerzos. Paco y David, por el café de las mañanas durante los cuales he recibido muchos consejos interesantes. Sara, por tu ayuda brindada en mis inicios con la técnica del Diseño de Experimentos. Pilar, Isa y Pepe, por vuestra amabilidad y disponibilidad. A todos los que han pasado por el departamento y me han ayudado, en especial a Javi V. por su colaboración en el laboratorio.

A la empresa CIATESA por la financiación y apoyo técnico recibido durante parte de esta tesis. Al Dr. Miguel Zamora, Adoración Cerezuela y el resto de componentes del departamento de I+D+i, por su contribución en este trabajo.

Al grupo de investigación AirLab, del departamento de Energía en el Politecnico di Milano.

Vorrei ringraziare Samanta Milani, il professor Stefano De Antonellis e il professor Cesare Maria Joppolo per permettermi di vivere un'esperienza così importante per la mia formazione come ricercatore. Vorrei anche ringraziare gli altri dottorandi e lavoratori del Politecnico di Milano che hanno reso il mio soggiorno più piacevole e divertente.

A mi director de Tesis Doctoral, Manuel, por confiar en mí y por su dedicación en la dirección de esta tesis. Por sus consejos que me han permitido crecer profesionalmente.

A mis amigos, por tantas alegrías compartidas, por estar siempre ahí.

A Manuela, que con tu amor, apoyo y comprensión has sido capaz de darme ánimos en los momentos más difíciles, espero que sigamos consiguiendo juntos todos los objetivos que nos propongamos.

Y, por supuesto, a mi familia, en especial a mis padres y hermanas, los cuales merecen mi más sentido agradecimiento. Sin vosotros todo esto no hubiera sido posible. Con todo vuestro apoyo, ánimo y alegría, y por siempre creer en mí, todo ha sido mucho más fácil.

A todos vosotros…muchas gracias.

Francisco Comino Montilla

Córdoba, 18 de septiembre de 2017

Preface

The thesis ***"Experimental and numerical study on hybrid HVAC systems activated at low temperature based on desiccant wheels and indirect evaporative coolers"*** was written as a part of a PhD study during the past four years in the Department of Physical Chemistry and Applied Thermodynamics at University of Cordoba, Spain. The thesis is presented as a collection of the following research papers: four international papers and five national and international conferences.

Paper I F. Comino, M. Ruiz de Adana, F. Peci, First and second order simplified models for the performance evaluation of low temperature activated desiccant wheels, Energy and Buildings. 116 (2016) 574–582. doi:10.1016/j.enbuild.2016.02.005. Journal Impact Factor 2016: 4.067. Quartile: Q1 (Civil engineering category)

Paper II F. Comino, M. Ruiz de Adana, Experimental and numerical analysis of desiccant wheels activated at low temperatures, Energy and Buildings. 133 (2016) 529–540. doi:10.1016/j.enbuild.2016.10.021. Journal Impact Factor 2016: 4.067. Quartile: Q1 (Civil engineering category)

Paper III F. Comino, S. Milani, S. De Antonellis, C.M. Joppolo, M. Ruiz de Adana, Simplified performance correlation of an indirect evaporative cooling system: development and validation, International Journal of Refrigeration. Submitted to the journal. Journal Impact Factor 2016: 2.779. Quartile: Q1 (Thermodynamics category)

Paper IV F. Comino, M. Ruiz de Adana, F. Peci, Energy saving potential of a hybrid HVAC system with a desiccant wheel activated at low temperatures and an indirect evaporative cooler in buildings with high latent load, Applied Thermal Engineering. Submitted to the journal. Journal Impact Factor 2016: 3.356. Quartile: Q1 (Thermodynamics category)

Congress I F. Comino, A. Cerezuela, M. Ruiz de Adana, M. Zamora, F. Peci, Numerical study of hybrid HVAC systems with desiccant wheel, in: V Ibero-American Congress of sciences and techniques of the cold., Tarragona, Spain, 2014: pp. 433–443.

Congress II F. Comino, M. Ruiz de Adana, Application of the DOE technique to the modelling of desiccant wheels for hybrid HVAC systems, in: Scientific Congress of researchers in training., Cordoba, Spain, 2014.

Congress III F. Comino, M. Ruiz de Adana, A. Cerezuela, M. Zamora, F. Peci, Design and building of a test facility for experimentation of desiccant wheels, in: IX National Congress Engineering Thermodynamics, Cartagena, Spain, 2015: pp. 295–302.

Congress IV F. Comino, M. Ruiz de Adana, F. Peci, Experimental study of the moisture removal capacity of a desiccant wheel activated at low and high temperature, in: CLIMA 2016 - 12th REHVA World Congress. Aalborg, Denmark, 2016.

Congress V F. Comino, M. Ruiz de Adana, Experimental analysis of the desiccant capacity of hybrid HVAC systems based on desiccant wheels activated at low temperature by vapor compression refrigeration systems, in: X National Congress Engineering Thermodynamics, Lleida, Spain, 2017

Summary

Air handling in buildings with high latent loads usually requires a high-energy cost to satisfy the user's thermal comfort needs. Indoor swimming pools or spas are some examples of this type of buildings, which have high internal latent gains, due to the great amount of evaporated water from the wet areas. Excessive air humidity can cause discomfort for the occupants and problems related to the indoor air quality of the building due to fungus and rot.

Conventional HVAC systems based on direct expansion units are widely used in dehumidifying air. However, conventional HVAC systems present some limitations in the combined treatment of sensible and latent loads. These systems usually only control sensible loads, air temperature, or latent loads, air humidity, but not both loads. Moreover, the supply air flow rates required by conventional HVAC systems are sometimes very high, in order to obtain high desiccant capacities. Excessive air flow rate can also cause discomfort to the occupants.

Hybrid HVAC systems composed of desiccant wheels and indirect evaporative coolers could be an alternative to conventional HVAC systems, due to their high desiccant and cooling capacity, respectively. The main objective of this thesis was to analyse experimentally and numerically the performance of a novel hybrid HVAC system activated at low temperature based on desiccant wheels and indirect evaporative coolers for use in small buildings with high latent load.

Firstly, a desiccant wheel and an indirect evaporative cooler were analysed experimentally, where the influence input variables on the devices were obtained and several empirical simplified models were fitted. Then, a sensible and latent heat control strategy was developed in order to independently control the supply air temperature and humidity ratio. A decoupling of the supply air temperature and humidity ratio can be obtained when the process air flow rate and air regeneration temperature in the desiccant wheel, and the water flow rate in the indirect evaporative cooler were varied.

Finally, a novel hybrid HVAC system activated at low temperature based on desiccant wheels and indirect evaporative coolers was analysed and compared to a conventional HVAC system. Both HVAC systems were designed to serve air in a

small building with high latent loads, such as spas. Several annual energy simulations for different climatic conditions were performed, which were based on the experimentally simplified models of the desiccant wheel and the indirect evaporative cooler, analysing energy efficiency of each HVAC system.

The hybrid HVAC system achieved higher energy efficiency than the conventional HVAC system when both HVAC systems served air to a small building with high latent loads, regardless of the climatic conditions. Furthermore, the hybrid HVAC system suitably controlled the sensible and latent loads of the building, using reduced supply air flow rates. Therefore, these results suggest that the proposed hybrid HVAC system could be a serious alternative to conventional HVAC systems to handle air in small buildings with high latent loads and where reduced supply air flow rates are required.

Resumen

El tratamiento de aire en edificios con altas cargas latentes habitualmente requiere un alto coste energético para satisfacer las necesidades de confort térmico de los usuarios. Piscinas climatizadas o spas son algunos ejemplos de este tipo de edificios, los cuales tienen altas ganancias latentes internas, debido a la gran cantidad de agua evaporada en las áreas húmedas. Excesiva humedad del aire podría causar disconfort para los ocupantes y problemas relacionados a la calidad del aire interior de los edificios, debido a hongos y podredumbre.

Los sistemas de climatización convencionales, basados en unidades de expansión directa, son ampliamente usados en la deshumectación del aire. Sin embargo, los sistemas de climatización convencionales presentan algunas limitaciones en el tratamiento combinado de las cargas sensibles y latentes. Estos sistemas usualmente solo controlan las cargas sensibles, temperatura del aire, o las cargas latentes, humedad del aire, pero no ambas cargas. Además, los caudales de aire de impulsión requeridos por los sistemas de climatización convencionales a veces son muy altos, con el fin de obtener altas capacidades desecantes. Excesivo caudal de aire también puede causar disconfort a los ocupantes.

Los sistemas de climatización híbridos compuestos de ruedas desecantes y enfriadores evaporadores indirectos podrían ser una alternativa a los sistemas convencionales, debido a su alta capacidad desecante y de enfriamiento, respectivamente. El objetivo principal de esta tesis fue analizar experimentalmente y numéricamente el rendimiento de un novedoso sistema de climatización híbrido activado a baja temperatura y basado en ruedas desecantes y enfriadores evaporativos indirectos, para su uso en pequeños edificios con altas cargas latentes.

En primer lugar, se analizaron experimentalmente una rueda desecante y un enfriador evaporativo indirecto, donde se obtuvieron las variables influyentes sobre los dispositivos fueron obtenidas y diversos modelos simplificados empíricos fueron ajustados. A continuación, se desarrolló una estrategia de control del calor sensible y latente, con el objetivo de controlar independientemente la temperatura y humedad del aire de impulsión. Un desacoplamiento de la temperatura y humedad del aire de impulsión pudo ser obtenido cuando el caudal del aire de proceso y la

temperatura del aire de regeneración en la rueda desecante, y el caudal de agua en el enfriador evaporativo indirecto fueron variados.

Finalmente, se analizó un novedoso sistema de climatización híbrido activado a baja temperatura y basado en ruedas desecantes y enfriadores evaporativos indirectos, y se comparó con un sistema de climatización convencional. Ambos sistemas de climatización fueron diseñados para servir aire en un pequeño edificio con altas cargas latentes, tales como spas. Se realizaron diversas simulaciones energéticas anuales para diferentes condiciones climáticas, las cuales estuvieron basadas en los modelos simplificados experimentales de la rueda desecante y el enfriador evaporativo indirecto., analizando la eficiencia energética de cada sistema de climatización.

El sistema de climatización híbrido alcanzó mayor eficiencia energética que el sistema de climatización convencional cuando ambos sistemas servían aire a un pequeño edificio con altas cargas latentes, independientemente de las condiciones climáticas. Además, el sistema de climatización híbrido controló adecuadamente las cargas sensibles y latentes del edificio, usando reducidos caudales de aire de impulsión. Por lo tanto, esos resultados sugieren que el sistema de climatización híbrido podría ser una seria alternativa a los sistemas de climatización convencional para tratar aire en pequeños edificios con altas cargas latentes y donde reducidos caudales de aire de impulsión son requeridos.

NOMENCLATURE

A	area of psychrometric chart [ºC g kg^{-1}]
AR	area ratio
ACH	air change rates per hour [h^{-1}]
b	estimated parameter
C	capacity rate of air [kJ h^{-1} K^{-1}]
CC	cooling coil
c_p	specific heat of air [kJ kg^{-1} K^{-1}]
CDD	cooling degree-day [ºC]
CO	condenser
COP	coefficient of performance
DEC	direct evaporative cooler
DOE	design of experiments
DW	desiccant wheel
DX	direct expansion
EA	exhaust air
E_{cons}	energy consumption per unit of dehumidified water [Wh kg^{-1}]
EH	electric heater
EIR	electrical input ratio
EV	evaporator
F	centrifugal fan
FC	flow conditioner
IEC	indirect evaporative cooler
h	air specific enthalpy [kJ kg^{-1}]
HDD	heating degree-day [ºC]
HC	heating coil
k	number of parameters
MA	mixed air
MB	mixing box
MRC	moisture removal capacity [kg h^{-1}]
$\dot{m}$	mass air flow rate [kg h^{-1}]
$\dot{M}_{pool}$	evaporated water flow of the pool [kg h^{-1}]
N	number of experimental test
Np	number of people
OA	outdoor air
P	static pressure [mmca]
PLF	partial load factor
PT	pitot tube
q	variation of air specific enthalpy [kJ kg^{-1}]

$\dot{Q}$	heat transfer [kW]
RA	return air
RH	relative humidity [%]
S	area [m^2]
SCOP	seasonal mean coefficient of performance
SH	steam humidifier
SHE	sensible heat exchanger
SHR	sensible heat ratio
T	dry bulb temperature [ºC]
t	time [s]
T_{wb}	wet bulb temperature [ºC]
UA	overall heat transfer coefficient [kJ h^{-1} K^{-1}]
v	air velocity [m s^{-1}]
$\dot{V}$	volumetric air flow rate [m^3 h^{-1}]
$\dot{V}_w$	water flow rate of indirect evaporative cooler [l h^{-1}]
$\dot{W}$	electric power consumption [kW]
X	input variable
$\hat{Y}$	estimated output value

Greek letters

Δ	increase
ε	effectiveness
ρ	density [kg m^{-3}]
∑	sum
ω	humidity ratio [g kg^{-1}]
Ω	specific mass air flow rate [kg s^{-1} m^{-3}]

Subscripts

a	air
c	condenser
d	dew point
e	evaporator
HC	heating coil
i	inlet
IA	indoor air
lat	latent
N	nominal
PLF	partial load factor
o	outlet

OA	outdoor air
p	process air; primary air
s	secondary air
r	regeneration air
sen	sensible
t	total
T	temperature
w	water

Superscripts

'	mixed outlet process air conditions
*	dimensionless value

Contents

Preface ..... **i**

Summary ..... **iii**

Resumen ..... **v**

Nomenclature ..... **vii**

Contents ..... **xi**

Chapter 1. Introduction **1**

1.1 Buildings with high latent loads 1

1.2 Dehumidification systems 4

1.2.1 Desiccant wheel 7

1.2.2 State-of-the-art of influential parameters on desiccant wheels 8

1.2.3 State-of-the-art of desiccant wheel models 9

1.3 Post-cooling systems 10

1.3.1 Indirect evaporative cooler 11

1.3.2 State-of-the-art of influential parameters on indirect evaporative coolers 12

1.3.3 State-of-the-art of indirect evaporative cooler models 13

1.4 State-of-the-art of hybrid HVAC systems for high latent loads 13

1.5 The importance of novel hybrid HVAC systems for high latent loads 17

1.6 Layout of the thesis 18

Chapter 2. Objectives **21**

Chapter 3. Materials and method **23**

3.1 Overview of the methodology....23
3.2 Experimental materials and facilities....25
3.2.1 Facilities to study the desiccant wheel....25
3.2.2 Facilities to study the indirect evaporative cooler....28
3.3 Experimental methodology....31
3.3.1 Design of experiments....31
3.3.2 Latent heat control of the process air in a DW....35
3.3.3 Sensible heat control of the process air in an IEC....38
3.4 Numerical methodology....40
3.4.1 HVAC systems....40
3.4.2 Building model – Spa....45
3.4.3 Components modelling....46
3.4.4 Climate zones....51
3.4.5 Energy simulation....52
Chapter 4. Experimental analysis of a desiccant wheel activated at low temperatures....53
4.1 DW statistical analysis....54
4.2 DW behaviour analysis....57
4.2.1 DW with balanced air flow rates....57
4.2.2 DW with unbalanced air flow rates....59
4.3 Simplified DW models....61
4.4 Analysis of DW control strategy....62
4.4.1 Analysis of experimental case study 5....62
4.4.2 Analysis of numerical case study 6....64
4.4.3 Analysis of numerical case study 7....66
4.5 Conclusions of Chapter 4....67
Chapter 5. Experimental analysis of an indirect evaporative cooler....69

5.1 IEC statistical analysis 69
5.2 IEC behaviour analysis 71
5.3 Simplified IEC model 71
5.4 Analysis of IEC control strategy 73
5.5 Conclusions of Chapter 5 74

Chapter 6. Energy analysis of a hybrid HVAC system and a conventional HVAC system in handling air in buildings with high latent loads 75

6.1 Daily behaviour analysis 75
6.2 Monthly energy analysis 76
6.2.1 Monthly energy analysis of the conventional HVAC system 76
6.2.2 Monthly energy analysis of the hybrid HVAC system 79
6.3 Annual energy analysis 81
6.3.1 Annual energy consumption 81
6.3.2 Seasonal mean coefficient of performance 82
6.3.3 Energy consumption per unit of dehumidified water 83
6.4 Conclusions of Chapter 6 84

Chapter 7. Conclusions and future work 87

7.1 Conclusions 87
7.2 Future work 88

Bibliography 89

Appendix A. First and second order simplified models for the performance evaluation of low temperature activated desiccant wheels 99

Appendix B. Experimental and numerical analysis of desiccant wheels activated at low temperatures 111

Appendix C. Simplified performance correlation of an indirect evaporative cooling system: development and validation 125

Appendix D. Energy saving potential of a hybrid HVAC system with a desiccant wheel activated at low temperatures and an indirect evaporative cooler in buildings with high latent load 141

Appendix E. Numerical study of hybrid HVAC systems with desiccant wheel

.....165

Appendix F. Application of the DOE technique to the modelling of desiccant wheels for hybrid HVAC systems 175

Appendix G. Design and building of a test facility for experimentation of desiccant wheels.....179

Appendix H. Experimental study of the moisture removal capacity of a desiccant wheel activated at low and high temperature.....189

Appendix I. Experimental analysis of the desiccant capacity of hybrid HVAC systems based on desiccant wheels activated at low temperature by vapor compression refrigeration systems.....199

List of figures

Figure 1. Maximum sensible and latent loads in 3 types of buildings. 2

Figure 2. (a) Picture of a room with high latent loads and supply air flow, (b) Psychrometric chart of the supply air process. 3

Figure 3. Dehumidification with an outdoor air flow rate.....4

Figure 4. Dehumidification with a direct expansion system. 5

Figure 5. Dehumidification with a desiccant system.....6

Figure 6. (a) Schematic of a desiccant wheel, (b) Psychrometric chart with the air states. 7

Figure 7. Desiccant dehumidification and post-cooling process. 10

Figure 8. (a) Schematic of an indirect evaporative cooler, (b) psychrometric diagram with the air states. 12

Figure 9. Hybrid HVAC systems with a desiccant wheel combined with different regeneration systems: (a) desiccant wheel with a direct expansion system, (b) desiccant wheel with a solar system, (c) desiccant wheel with an enthalpy wheel, (d) desiccant wheel with a heating coil and a heat pump. 15

Figure 10. Hybrid HVAC systems with a desiccant wheel combined with different post-cooling systems: (a) desiccant wheel whit a direct expansion system, (b) desiccant wheel with an indirect evaporative cooler, (c) desiccant wheel with a cooling coil and a chiller. 16

Figure 11. Overview of the methodology. 24

Figure 12. Layout of the test facility of the desiccant wheel.....26

Figure 13. Picture of the desiccant wheel.....27

Figure 14. Layout of the test facility of the indirect evaporative cooler. 29

Figure 15. Picture of the indirect evaporative cooler. 30

Figure 16. Schematic of a desiccant wheel system with bypass air. 32

Figure 17. Schematic of the investigated indirect evaporative cooler system.....34

Figure 18. (a) An outlet process air state of a desiccant wheel, (b) decoupling of the outlet process air conditions in a desiccant wheel. 36

Figure 19. Schemes of (a) the DW-DX system, (b) the DX-DW system. 40

Figure 20. Schematic of the conventional HVAC system. 41

Figure 21. Schematic of the hybrid HVAC system. 42

Figure 22. Hybrid HVAC system control logic diagram. 44

Figure 23. World representation of the different climate zones with the selected cities 51

Figure 24. Trends of the main effects of the desiccant wheel for the temperature and humidity ratio of the process outlet air-stream for case study 3. 57

Figure 25. Response surfaces and contour line plots for case study 3 (a) $T_{p,o}$ on $T_{p,i}$ and $\omega_{p,i}$, (b) $\omega_{p,o}$ on $T_{p,i}$ and $\omega_{p,i}$, (c) $T_{p,o}$ on $T_{r,i}$ and $\omega_{r,i}$, (d) $\omega_{p,o}$ on $T_{r,i}$ and $\omega_{r,i}$. ... 58

Figure 26. Trends of the main effects of the desiccant wheel for the temperature and humidity ratio of the mixed process outlet air-stream for case study 4. 59

Figure 27. Relations of (a) $T_{r,i}$ on $T'_{p,o}$ and $\omega'_{p,o}$, and (b) $\Omega_{p,i}$ on $T'_{p,o}$ and $\omega'_{p,o}$, for case study 4 60

Figure 28. Outlet process air conditions for case study 5 when $T_{r,i}$ and $\Omega_{p,i}$ were varied, (a) outlet air states, (b) outlet air area. 63

Figure 29. Outlet process air conditions when $T_{r,i}$ and $\omega_{r,i}$ were modified for case study 6. 65

Figure 30. Outlet process air conditions when $T_{r,i}$, $\Omega_{p,i}$ and $\omega_{r,i}$ were modified for case study 6 66

Figure 31. Trends of the main effects of the indirect evaporative cooler on the response variables for case study 8 72

Figure 32. Experimental and simulation results of the ΔT_p, ΔT_s, $\Delta\omega_s$ and ε_{wb} as a function of $\boldsymbol{Vw}$ for case study 10 73

Figure 33. Energy delivered by each element for the conventional HVAC system for the climatic conditions of Barcelona, (a) sensible energy delivered, (b) latent energy delivered. 77

Figure 34. Monthly energy consumption of each element for the conventional HVAC system for the climatic conditions of Barcelona. 78

Figure 35. Energy delivered by each element for the hybrid HVAC system for the climatic conditions of Barcelona, (a) sensible energy delivered and (b) latent energy delivered. 79

Figure 36. Monthly energy consumption for the hybrid HVAC system for the climatic conditions of Barcelona. 81

Figure 37. Comparative analysis of annual energy consumption of the hybrid HVAC system and the conventional HVAC system in each climate zone. 82

Figure 38. SCOP values of the hybrid HVAC system and the conventional HVAC system in each climate zone. 83

Figure 39. E_{cons} values of the hybrid HVAC system and the conventional HVAC system in each climate zone. 84

List of tables

Table 1. Characteristics of the desiccant wheel. 27

Table 2. Specification of measuring devices for the desiccant wheel. 28

Table 3. Characteristics of the indirect evaporative cooler. 30

Table 4. Specification of measuring devices for the indirect evaporative cooler..31

Table 5. Design of experimental case studies 1, 2, 3 and 4 of the desiccant wheel. 33

Table 6. Ranges of validity of the process and regeneration air streams of the desiccant wheel for experimental case studies 1, 2, 3 and 4. 33

Table 7. Design of experimental case study 8 of the indirect evaporative cooler. 35

Table 8. Ranges of validity of the primary and secondary air streams of the indirect evaporative cooler for experimental case study 8. 35

Table 9. Input variables and output variables for case studies 5, 6 and 7. 36

Table 10. Ranges of validity of the process and regeneration air streams of the desiccant wheel for case studies 5, 6 and 7. 38

Table 11. Input variables and output variables for case studies 5, 6 and 7. 38

Table 12. Ranges of validity of the primary and secondary air streams of the indirect evaporative cooler for experimental and numerical case studies 9, 10 and 11. 39

Table 13. Characteristics of the building.....46

Table 14. Estimated parameters of the refrigeration vapour compression model. 47

Table 15. Nominal parameters of the refrigeration vapour compression system. .48

Table 16. Estimated parameters of the air-water heat pump model. 49

Table 17. Pressure drop of each component for the systems analysed. 50

Table 18. Estimated parameters of the fan models. 50

Table 19. Selected cities from each of the climate zone defined by ASHRAE. ...51

Table 20. Effects of input variables on output variables of the desiccant wheel for case study 1. 54

Table 21. Effects of input variables on output variables of the desiccant wheel for case study 2..... 55

Table 22. Effects of input variables on output variables of the desiccant wheel for case study 3..... 55

Table 23. Effects of input variables on output variables of the desiccant wheel for case study 4..... 56

Table 24. Estimated parameters of the desiccant wheel empirical models. 61

Table 25. Outlet process air conditions and MRC and SHR values obtained for case study 5. 64

Table 26. Output area values of each inlet process air state, P1-P5, for case study 6. 66

Table 27. Effects of input variables on output variables of the indirect evaporative cooler for case study 8. 70

Table 28. Estimated parameters of the indirect evaporative cooler empirical model. 72

Chapter 1

Introduction

Characteristics of handling air in buildings with high latent loads are introduced in this chapter. Commonly used heating, ventilation and air conditioning, HVAC, systems for dehumidification and humidity control strategies for these buildings are shown. Also, a state-of-the-art review of dehumidification, post-cooling and hybrid HVAC systems is presented.

1.1 Buildings with high latent loads

The control of the water vapour content in the air is necessary to maintain the required indoor conditions in buildings and certain industrial processes. The external and internal water vapour sources can produce significant latent loads indoors. Excessive air humidity can cause discomfort for the occupants and problems related to the indoor air quality of the building due to fungus and rot. Therefore, it is necessary to use a system to reduce and control the humidity ratio. Restaurants, indoor swimming pools or spas are examples of buildings with high latent loads.

An example on maximum sensible and latent loads in 3 types of buildings is shown in Figure 1. A standard office of 180 m^3 with 10 occupants, a standard indoor swimming pool of 6500 m^3 with 75 occupants and a standard spa of 240 m^3 with 10 occupants, were analysed. It can be observed that the highest latent load was found in the spa, 33.94 kW m^{-3}, then in the indoor swimming pool, 66% less than in the spa, and finally in the office, 99% less than in the spa. Regarding sensible loads, the highest sensible load was obtained in the office, 0.02 kW m^{-3}, 50% more

than in the indoor swimming pool and the spa. It can also be observed that the sensible load in the office was 50% higher than the latent load. Nevertheless, the results of thermal loads in the indoor swimming pool and spa show that their latent loads were much higher than their sensible loads. Conventional HVAC systems can suitably handle air in buildings with sensible loads higher than latent loads. However, conventional HVAC systems present some limitations in the combined treatment of sensible and latent loads, these systems usually only control sensible loads, air temperature, or latent loads, air humidity, but not both loads.

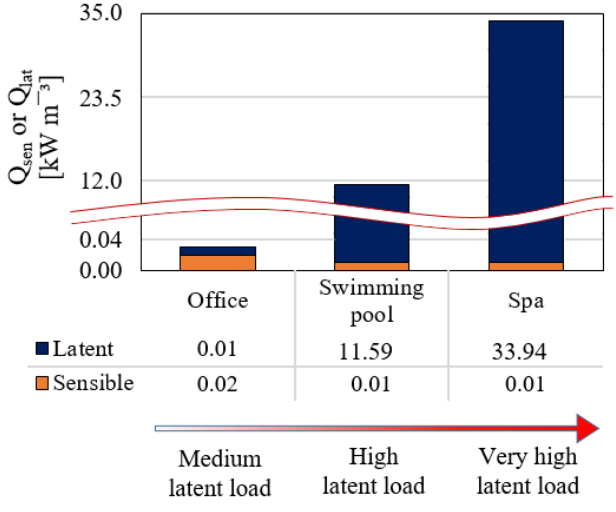

Figure 1. Maximum sensible and latent loads in 3 types of buildings.

Air treatment in buildings with high latent loads is based on supplying a dry air flow to a room. Excess moisture can be controlled from this dry air flow. A room with high latent loads and a psychrometric chart with summer supply air conditions: T_{SA} and ω_{SA}, and indoor air conditions: T_{IA} and ω_{IA}, are represented in Figure 2.

The indoor air conditions, IA, are usually fixed by thermal comfort regulations and standards [1]. The supply air conditions, SA, could be calculated from energy balances, as expressed by Eqs. (1) and (2). Where $\dot{Q}_{lat}$ is the latent load of the room, $\dot{Q}_{sen}$ is the sensible load of the room, ρ is the air density, $\dot{V}_{SA}$ is the supply air flow rate, h_{IA} is the indoor air specific enthalpy, h_{SA} is the supply air specific enthalpy and $h_{SA^*} = f(T_{IA}, \omega_{SA})$.

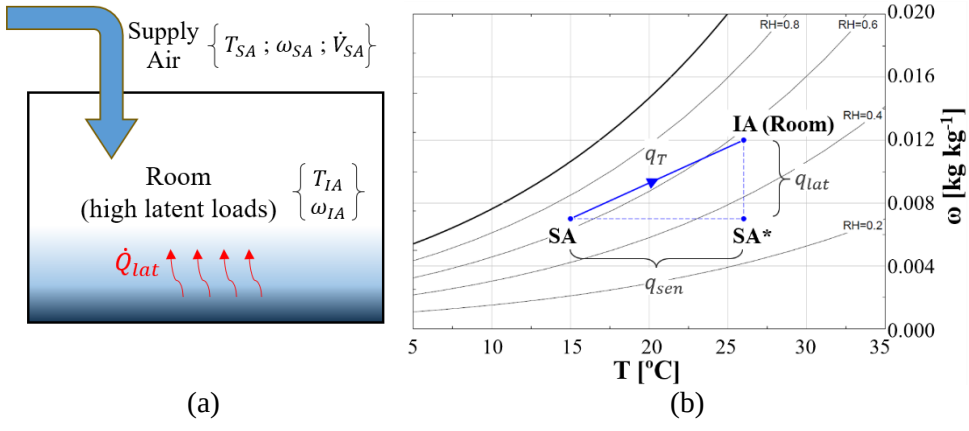

Figure 2. (a) Picture of a room with high latent loads and supply air flow, (b) Psychrometric chart of the supply air process.

$$\dot{Q}_{lat} = \rho \cdot \dot{V}_{SA} \cdot (h_{IA} - h_{SA^*}) \quad (1)$$

$$\dot{Q}_{sen} = \rho \cdot \dot{V}_{SA} \cdot (h_{SA^*} - h_{SA}) \quad (2)$$

The parameters ω_{SA} or $\dot{V}_{SA}$ are commonly used as dehumidification techniques, according to the energy balance expressed by Eq. (1). The lower ω_{SA}, the higher the dehumidification capacity, at a fixed value of $\dot{V}_{SA}$. The higher $\dot{V}_{SA}$, the higher the dehumidification capacity, at a fixed value of ω_{SA}. Conventional HVAC systems usually reduce ω_{SA} to handle latent load. However, these systems sometimes do not achieve the set point humidity ratio in buildings with high latent loads, thus increasing $\dot{V}_{SA}$. This dehumidification technique presents problems in buildings with high latent loads and small volumes, such as spas, where very high air flow rate is required to handle high latent loads. Excessive air flow rate can also cause discomfort to the occupants. The recommended air change rates per hour, ACH, values for indoor swimming pools and spas were shown to vary between 4 h^{-1} and 7 h^{-1} in order to obtain thermal comfort [2]. Therefore, novel dehumidification systems are required to control the moisture content in buildings with high latent loads and small volumes, without the need to use high supply air flow rates, while keeping a low energy consumption.

Previous studies on energy saving in spas with small volumes and high latent loads have been carried out [3,4]. However, these works focused on the hot water system of swimming pools.

1.2 Dehumidification systems

A traditional method of dehumidifying rooms with high latent loads is to introduce a certain air flow rate from outside. This method can only be used when the outdoor humidity ratio is lower than the indoor humidity ratio. This method was studied for indoor swimming pools with large volumes [2]. In this case, the air flow rate required to dehumidify the building was very high. This dehumidification method could cause discomfort to the occupants in small rooms with high latent loads, such as spas, due to the high ACH values required. A schematic of this method of dehumidification is shown in Figure 3.

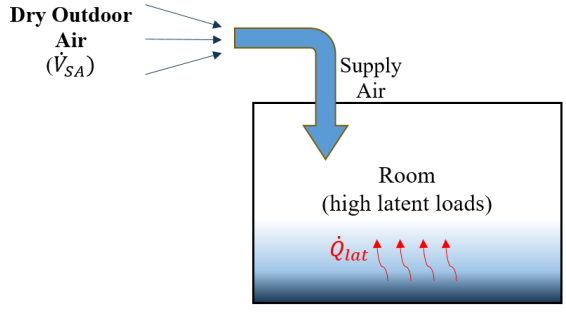

Figure 3. Dehumidification with an outdoor air flow rate.

Another method widely used in dehumidifying air is that of conventional dehumidification systems based on direct expansion units, DX system, which operates according to the vapor-compression cycle. DX systems reduce the air temperature below its dew point in order to condense water. An increase in the cooling power of the DX system usually produces an increase in its desiccant capacity. However, DX systems have a limited cooling capacity when the required dew-point temperature is very low, close to 0°C, the freezing point of water. Moreover, the outlet air temperature of DX systems is usually very low, so it is necessary a post-heating of the supply air flow, before being supplied to the building. Several DX systems have been studied for indoor swimming pools [5,6], where high energy consumption values were required to dehumidify and heat the

supply air flow. A schematic of the method of dehumidification with a DX system is shown in Figure 4.

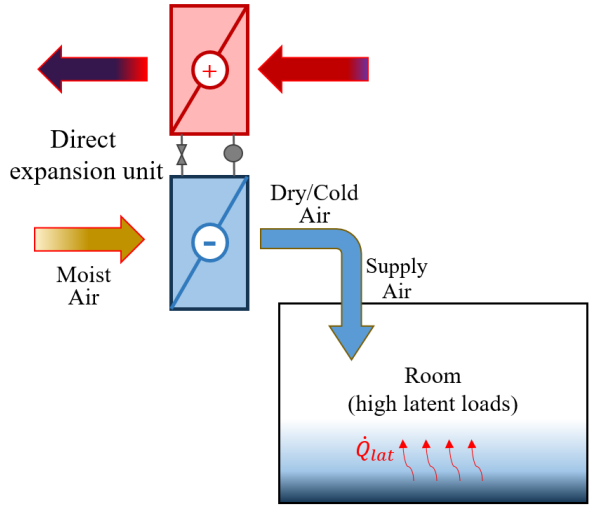

Figure 4. Dehumidification with a direct expansion system.

Desiccant dehumidification systems present an alternative solution to DX systems. These systems differ from cooling-based systems, such as DX systems, in the way of removing moisture from the air. There are two types of desiccants: liquid and solid desiccants. Both types behave the same way, their surface vapor pressure is a function of their temperature and moisture content. One subtle distinction between desiccants is their reaction to moisture [7]. Numerous applications of both desiccant types can be found in the literature [8–11].

The basic working principle of the desiccant systems is to transfer moisture from one air-stream to another by using two processes called as sorption and desorption processes [12]. The sorption process includes the phenomenon of moisture transfer from the air in to desiccant material simply taking in to account the pressure difference of water vapours between the humid air and the desiccant material. The surface vapor pressure of the desiccant material is lower than the pressure of the moist air and therefore the moisture available in the air gets attracted and adsorbed to the desiccant material. However, in the desorption process the captured moisture gets released in to the air-stream increasing the temperature of the desiccant material. Thermal energy is required to derive the desorption process. Renewable energy sources such as solar, biomass, waste heat, or others can be used

for this purpose. The cycle repeats and desiccant material transfer moisture continuously by changing the surface vapor pressure of the desiccant material [13]. A schematic of the method of dehumidification with a desiccant system is shown in Figure 5.

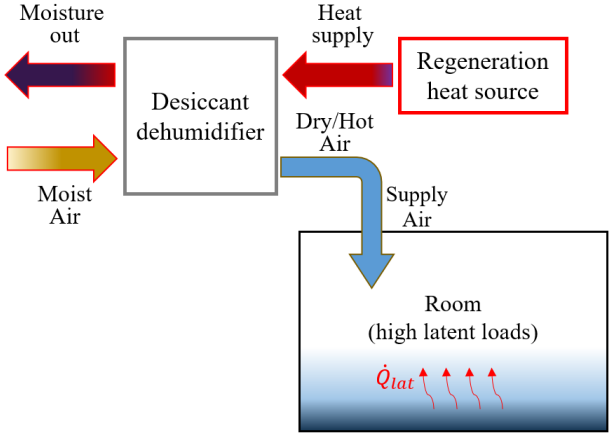

Figure 5. Dehumidification with a desiccant system.

The main advantages of desiccant systems are [14]:

- Only air is required as working fluids. Fluorocarbons and other substances with Global Warning Potential, GWP, are not required; thus, there is no impact on the ozone layer neither the environment.
- The source of thermal energy can be diverse: renewable energy, such as solar, biomass, geothermal, waste heat and non-renewable energy such as natural gas and electrical sources such as heat pumps.
- Since desiccant systems operate near atmospheric pressure, maintenance and construction are simplified compared to DX systems.

However, the main disadvantage of desiccants is the heat transfer generated by the adsorption process [15], which is delivered from the regeneration air flow to the process air flow.

Five typical equipment configurations for desiccant dehumidifiers have been studied [13]: liquid spray-tower, solid packed tower, rotating horizontal bed,

multiple vertical bed and desiccant wheel. This thesis focused on the study of desiccant wheels.

1.2.1 Desiccant wheel

A desiccant wheel, DW, consists of a cylindrical rotating device made of rolled-up corrugated sheets of desiccant material, such as silica gel, in order to get a great number of parallel channels with a typical sinusoidal or triangular cross sectional geometry, see Figure 6.

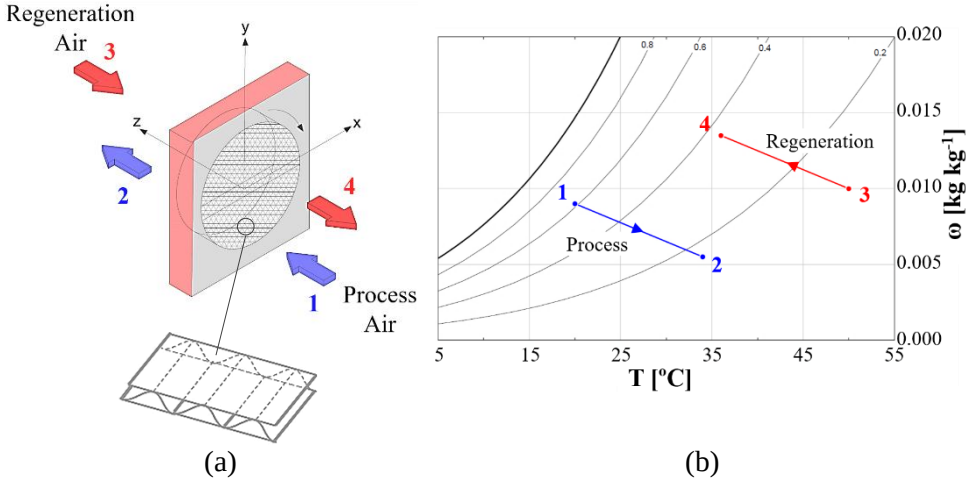

Figure 6. (a) Schematic of a desiccant wheel, (b) Psychrometric chart with the air states.

The wheel rotates slowly, typically between 10 rph and 50 rph, exchanging moisture between the process air stream and regeneration air stream. The process air flows through the channels and the desiccant adsorbs the moisture from the air, which corresponds to states 1 and 2 on the psychrometric chart, see Figure 6. As the desiccant adsorbs moisture it becomes saturated and its surface vapor pressure rises. The air process temperature rise is directly proportional to the amount of moisture removed from the air. The drier the air leaves the dehumidifier, the warmer it is. Then as the wheel rotates into the reactivation air-stream, the desiccant is heated by the regeneration air, and the surface vapor pressure rises, allowing the desiccant to release its moisture into the regeneration air. The regeneration process, state 3 to state 4, is shown in Figure 6 on the psychrometric chart. The higher the air regeneration temperature the greater the increments of the process air states, 1-2, and the regeneration air states, 3-4. Desiccant wheels can also adsorb substances

other than water vapour removing in this way air contaminants and improving indoor air quality [16].

1.2.2 State-of-the-art of influential parameters on desiccant wheels

The performance of DWs can be affected by many parameters, such as:

- Inlet air process temperature
- Inlet air process humidity
- Process air flow rate
- Inlet air regeneration temperature
- Inlet air regeneration humidity
- Regeneration air flow rate
- Wheel rotation speed
- Contact surface between air and desiccant

Previous research studies have analysed the influence of these parameters on the overall performance of the DW [17,18]. The outlet process air conditions of the DW, temperature and humidity, could be suitably controlled by adjusting these parameters. The aim of DW control is to improve the performance of the system, controlling the process air conditions.

Several studies on DW control strategies based on the rotation speed [19–21] were carried out. The control system would be much more energy efficient using the variable air flow rate [22]. The rotation speed and the regeneration temperature were also used as a control strategy [23]. Nevertheless, these works have not satisfactorily clarified the capacity to decouple the temperature and humidity ratio of the outlet process air.

Manufacturers often provide controls inside the system to modulate the regeneration energy of the DW in response to changes in the moisture load. There are three common methods of controlling dehumidification capacity [24]: (i) on-off control of regeneration heat source; (ii) modulated control of regeneration heat source; and (iii) modulated control of the process and regeneration air flow rates by means of variable air bypass. Each of these methods is effective, depending on the degree of precision needed for the humidity control level in the building [24]. In the third method, the DW operates with unbalanced air flow rates to achieve the outlet process air conditions. This method is preferred for industrial process applications, where control within ±1% relative humidity is essential [24]. Previous

results also showed that if the supplied moisture must be very low, such as in spas, the process air flow rate is quite critical and therefore this must be controlled [7].

It has been shown that the variation of process air flow rate allowed the dehumidification capacity of a DW to be modified [25]. However, the air regeneration temperature was more influential on the dehumidification capacity than the air flow rates [17]. The higher the temperature of the desiccant material, the higher the dehumidification capacity, and the easier it is to remove moisture. The air regeneration temperatures usually used range from 60°C to 120°C [26,27]. Therefore, a significant energy consumption is required to regenerate the DW when the required dehumidification capacity is high. Nevertheless, previous studies on DW operated at low regeneration temperatures and found an acceptable dehumidification capacity [28]. A DW activated at low temperatures could be integrated in renewable energy systems in a building or industrial environment [29,30], thus reducing the environmental impact associated with air dehumidification. In this thesis, values below 60°C were considered as low regeneration temperatures.

The performance and the outlet process air conditions of a DW strongly depend on its control strategy. Therefore, it would be interesting to know the behaviour of a DW activated at low temperatures by setting the process air flow rate and air regeneration temperature, in order to control the outlet process air conditions.

1.2.3 State-of-the-art of desiccant wheel models

Different experimental and numerical research works have been carried out in order to study the operational parameters that influence the overall performance of the DW. Some researchers developed detailed mathematical models, considering the heat and mass transfer in the DW [31–33]. These models are not easy to implement and require long computation time. Moreover, some physical characteristics and specific parameters of the DW are not available.

Another mathematical modelling approach is based on simplified models of the DW which requires less computation time. A widely used simplified method to study the behaviour of the DW is one that is based on the effectiveness concept. It is also referred to as the linear analogy method [34] and takes into account two independent potential variables [35]. The effectiveness method has been used previously in several studies [36,37]. These simplified mathematical models are

easy to implement, but many experimental tests are required to fit the effectiveness parameters. Important errors can be introduced when constant values of the effectiveness parameters are assumed in the effectiveness method [38].

Other authors have developed simplified models based on correlations to study the behaviour of the DW [39–41]. The advantage of this approach is that the model fits any physical characteristics and specific materials of one specific DW. However, the obtained simplified model is not valid for any other DW.

A methodology widely used in engineering to obtain a regression model is the design of experiments, DOE [42,43]. DOE is a technique used for exploring new processes, gaining knowledge of the existing processes and optimizing these processes to achieve high performance [44].

1.3 Post-cooling systems

The heat generated by the sorption process of a DW, which is delivered from the regeneration section to the process section, causes the outlet process air temperatures to increase. Therefore, a post-cooling system is needed to reduce the process air temperature before being supplied to a building. The principle of desiccant dehumidification and post-cooling process is shown in Figure 7.

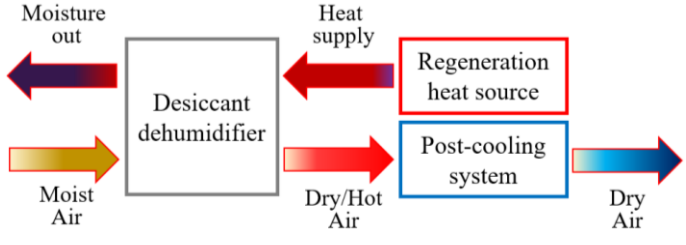

Figure 7. Desiccant dehumidification and post-cooling process.

Cooling systems based on evaporators of a DX system, as shown in Figure 4, are usually combined with a DW [45]. This technology presents some advantages, e.g., good stability in performance, low cost and long life cycle time. However, this type of system normally requires a high electric energy consumption and can have an important environmental impact [46].

Another cooling technology that could be combined with DWs is the evaporative cooler. The evaporative cooling systems are based on heat and mass

transfer between air and cool water [47]. The main advantages of evaporative coolers are their constructive simplicity and energy saving compared to DX systems. There are two types of evaporative coolers: the direct evaporative cooler, DEC, and the indirect evaporative cooler, IEC. DEC is based on direct contact between air and water, while IEC is based on heat and mass transfer between two streams of air, separated by a heat transfer surface with a dry side, where only air is cooling, and a wet side, where water is evaporated into air [47]. Both DEC and IEC are characterised by very high energy efficiency but also by significant water consumption rates. However, DEC adds moisture to the supply air flow, therefore, in humid climates or in building with high latent loads it is not efficient and practical. Another problem of DECs is the possible risk for human health related to Legionella infections. IEC does not present these problems, since it can reduce air temperature without adding moisture to the supply air flow and there is no mix between the two flows intervening in the exchange process, consequently there is no possible risk of contamination from Legionella [48]. The IEC technology can be used in many applications, such as in pre-cooling and energy recovery units [49–51], in two stage indirect/direct evaporative cooling system [52] or in passive cooling unit [53]. In the present thesis, the IEC technology was studied, in order to cool air supplied by a DW.

1.3.1 Indirect evaporative cooler

An indirect evaporative cooler, IEC, consists of a metal cross flow heat exchanger with two unmixed air streams. The working principle and psychometric illustration of the air treatment process relating to an indirect evaporative cooling operation are presented in Figure 8. During operation, the primary air enters into the dry channel while the secondary air enters into the adjacent wet channel. The secondary air flow is humidified with water spray nozzles. As a result, the primary air, state 1, is cooled at the constant moisture content and moves towards the wet-bulb temperature of the inlet secondary air, supplying air in state 2. Whereas the secondary air of state 3 is gradually saturated and changed into state 4' at its earlier flow path. The secondary air is sometimes heated as it moves along the flow path and finally is supplied in saturated air conditions, state 4, [46].

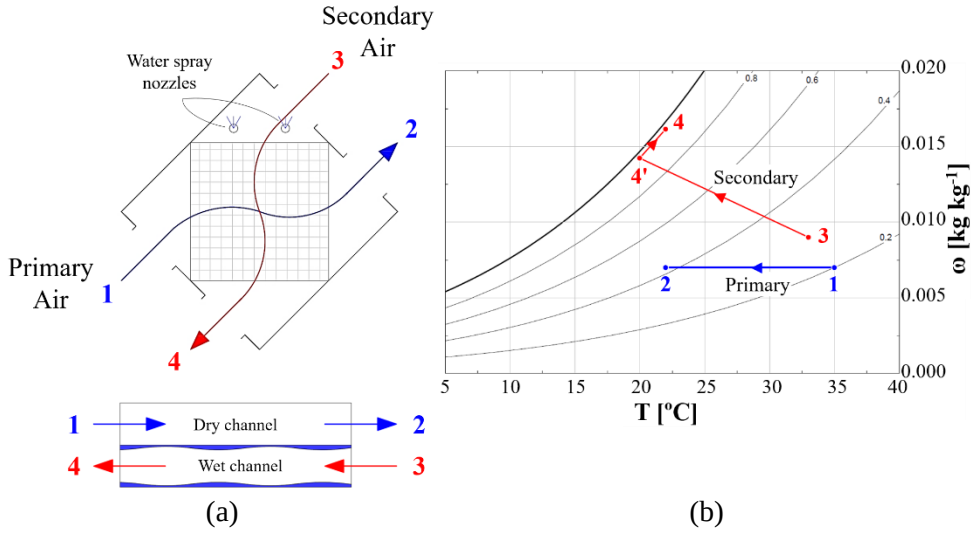

Figure 8. (a) Schematic of an indirect evaporative cooler, (b) psychrometric diagram with the air states.

1.3.2 State-of-the-art of influential parameters on indirect evaporative coolers

IEC systems have been widely analysed by many authors in the available literature, in particular focusing on the optimization of the device and on the analysis of influential parameters on outlet air conditions. The most influential parameters on IEC are:

- Inlet air primary temperature
- Primary air flow rate
- Inlet air secondary temperature
- Inlet air secondary humidity
- Secondary air flow rate
- Water flow rate
- Pressure drops
- Constructive parameters: geometry and materials

The performance of IECs was analysed for different operating conditions, evaluating the effect of variable inlet air velocities [54,55]. Other authors studied the influence of constructive parameters on IEC systems, such as material and

geometry [56,57]. The variation of water flow rate was also analysed [58], which has a significant effect on system performance: the higher the water flow rate, the higher the humidification of the secondary air stream and, consequently, the higher the primary air temperature reduction. Therefore, the amount of evaporated water could be an efficient parameter to control the IEC system.

1.3.3 State-of-the-art of indirect evaporative cooler models

Mathematical models of IECs could also be very useful to optimize the device. Several analytical IEC models were previously developed using a linearized approximate theory for a thin and continuous water layer inside the wet channels [59–61]. Other authors presented a simplified finite volume model [62] starting from Poppe [63] and Merkel [64] models. An analytical model to analyse the thermal performance of wet bulb temperature cooling based on the ε-NTU method for sensible heat exchangers was also developed [65]. A numerical model was carried out to investigate the heat and mass transfer in an IEC under the effect of various parameters as wettability of the plate and air inlet velocity [66]. A mathematical model of an IEC system, taking into account the effect of adiabatic humidification of the secondary air stream and the wettability factor of the heat exchanger surface was obtained [67]. However, most of the aforementioned approaches are not very practical to be implement in energy simulation tools, due to the high computational load.

A methodology recently used to obtain simplified models of IEC systems is based on statistical design [44]. Two simplified models generated by statistical methods were presented [68,69], in order to analyse basic performance characteristics of an IEC. Both statistical models accurately represented the behaviour of an IEC system and they could be easily integrated into HVAC models. However, the influence of a secondary air flow conditions and of the water flow rate has not been analysed. Therefore, it is of interest to obtain a simple correlation of an IEC system based on a cross flow heat exchanger, including the effect of variable water flow rate and secondary air inlet temperature, inlet humidity ratio and flow rate.

1.4 State-of-the-art of hybrid HVAC systems for high latent loads

The combination of novel and promising HVAC elements, such as DWs, IECs, systems based on renewable energy sources such as solar, biomass, heat pumps

systems, etc., could be an alternative to conventional dehumidification units, which are only based on direct expansion units and depend mainly on electrical energy. These combined novel systems are referred to as hybrid HVAC systems. Hybrid HVAC systems proved to be especially useful in the combined treatment of sensible and latent loads in buildings.

Numerous hybrid HVAC systems with a DW combined with different heating systems were analysed in order to regenerate the DW [70,71], see Figure 9. Some authors studied the behaviour of hybrid HVAC systems with DW combined with DX systems [72,73], where the condenser was used to thermally activate the DW, as shown in Figure 9a. However, these systems almost always depend on electrical energy. Energy savings were obtained when the DW was regenerated using waste heat from other processes [74]. However, in some cases waste heat energy is not available or the corresponding temperature level is not adequate. In recent years, some studies have analysed the use of solar energy to regenerate a DW [75,76], see Figure 9b, but the solar thermal system involves a significant increase in the overall economic cost of the system. Other HVAC systems with DW combined with an enthalpy wheel were widely studied [77–79], as shown in Figure 9c. These systems recover sensible heat from the process air flow in order to regenerate the wheel, achieving significant energy savings. Despite this, these require an auxiliary source of heat. Heating coils fed by a hot water produced in a heat pump, combined with a DW were also analysed [80], see Figure 9d. This system obtained higher dehumidifier performance than a system with a DW combined with DX.

The heat generated by the DW dehumidification process causes the outlet process air temperatures to be high, as previously discussed. Therefore, the combination of a DW with a post-cooling system is necessary in most cases, in order to cool the supply air flow. Several hybrid HVAC systems with a DW combined with post-cooling systems were previously studied, as shown in Figure 10. A DW integrated with a DX system was analysed, where the evaporator was used to cool the process air [81], see Figure 10a. An experimental study on a hybrid HVAC system composed of a DW and an IEC was carried out for several summer days in Italy [82], see Figure 10b. This system reduced the electrical consumption significantly compared to one composed of a DW and a cooling coil fed by a conventional vapour compression chiller, see Figure 10c. A numerical simulation study on desiccant units presented a comparative analysis of three different systems with a DW and an IEC [83]. The results of this study showed that all of them were

able to obtain satisfactory supply air temperatures, even when the DW was regenerated at low temperature. Other numerical studies analysed the behaviour of a DW combined with an IEC system [84–88]. They were mainly based on the hybrid HVAC system performance optimization under different steady state air conditions, always using the IEC system to cool the output air stream of the DW.

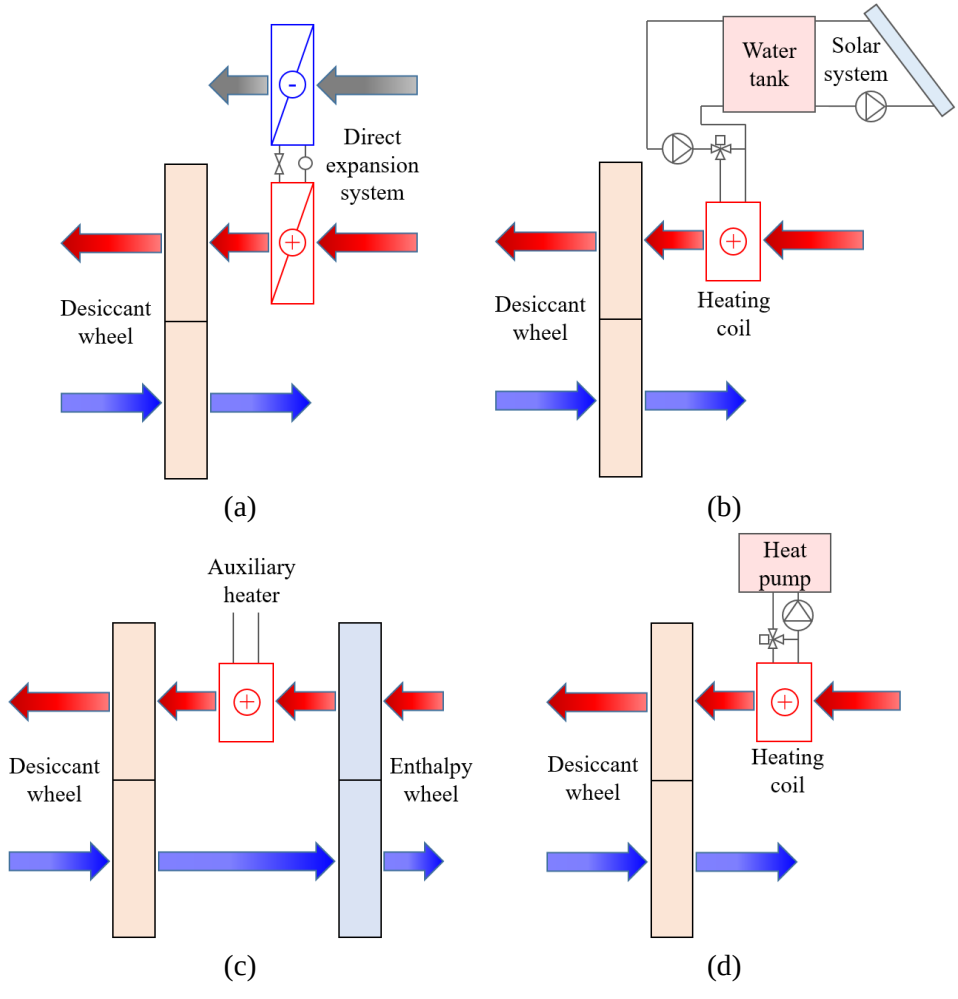

Figure 9. Hybrid HVAC systems with a desiccant wheel combined with different regeneration systems: (a) desiccant wheel with a direct expansion system, (b) desiccant wheel with a solar system, (c) desiccant wheel with an enthalpy wheel, (d) desiccant wheel with a heating coil and a heat pump.

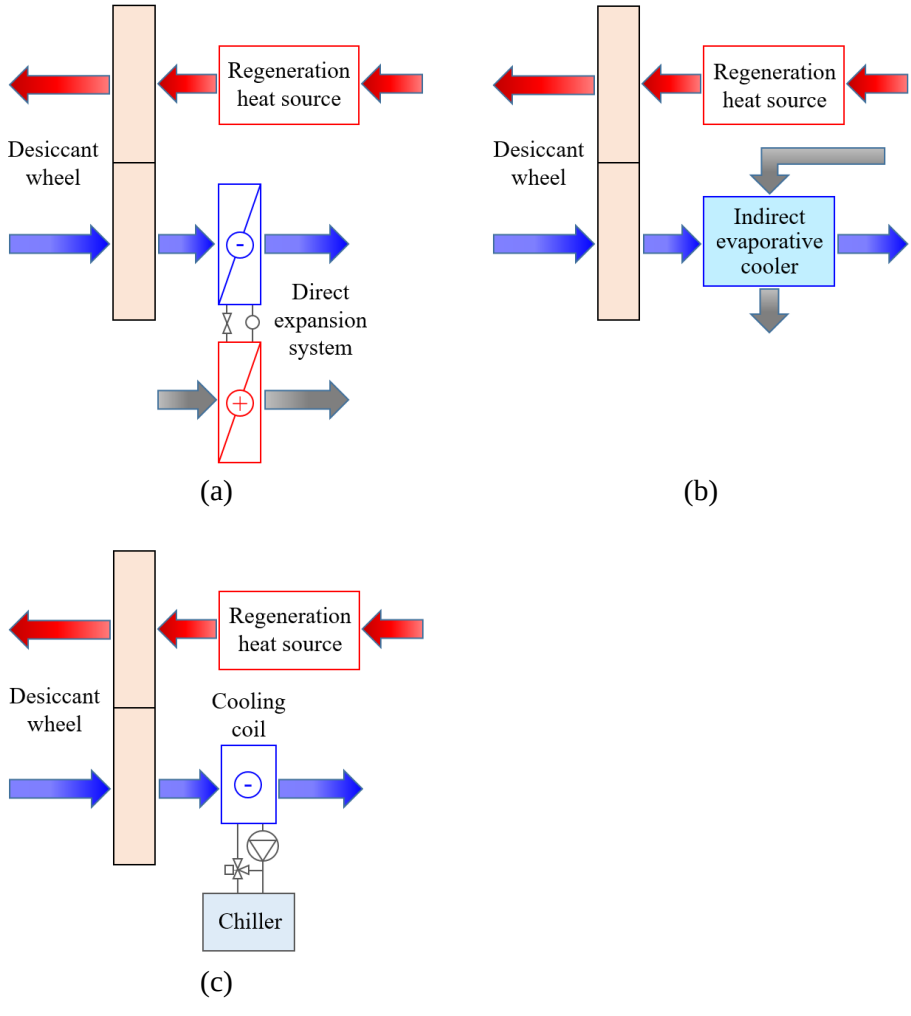

Figure 10. Hybrid HVAC systems with a desiccant wheel combined with different post-cooling systems: (a) desiccant wheel whit a direct expansion system, (b) desiccant wheel with an indirect evaporative cooler, (c) desiccant wheel with a cooling coil and a chiller.

Energy simulation tools are commonly used to study the behaviour of these hybrid HVAC systems throughout a year, such as EES, TRNSYS or EnergyPlus software, [89,90].

1.5 The importance of novel hybrid HVAC systems for high latent loads

The increasing electrical energy consumption and high CO_2 levels in the environment have resulted in the growing need to increase the energy efficiency of the conventional air conditioning systems. In developed countries, conventional HVAC systems needs account for 50% of the energy consumption in buildings and about 20% of the overall national energy use [91]. Moreover, these systems present some problems in the air treatment in buildings with high latent loads and small volumes. To achieve high desiccant capacity, high supply air flow rates and independent control of sensible and latent loads are needed. However, the conventional HVAC systems usually only control the sensible load or latent load, but not both loads.

Some researchers studied new methods to replace conventional HVAC systems. Desiccant technology, such as DWs, has proven to be especially useful for applications with high dehumidification needs, without the requirement of high supply air flow rates. Furthermore, desiccant systems could achieve acceptable dehumidification capacity when activated at low temperature. Therefore, these systems could be activated from thermal energy and integrated with renewable energy sources such as solar, biomass, heat pumps, waste heat or others.

Desiccant systems combined with sensible cooling systems, such as IECs, could independently control the sensible and latent loads in a building, thereby optimizing indoor air conditions. This novel hybrid HVAC configuration could achieve acceptable energy efficiency values when the DW is activated at low temperatures. However, no study on the performance of hybrid HVAC systems has yet been performed.

Based on the limitations in the air treatment with conventional HVAC systems within the framework of air conditioning in buildings with high latent loads, and the few studies on buildings with small volume and high latent loads, such as spas, the present thesis focused on the development of a novel efficient hybrid HVAC system to handle air in small buildings with high latent loads. Accordingly, a research question arises as the starting point of this thesis:

Could a new hybrid HVAC system based on desiccant wheels and indirect evaporative coolers be considered as an alternative for use in small rooms with high latent load in terms of high energy efficiency, decoupling sensible and latent loads by using low temperature energy sources?

Trying to solve this question, this thesis present an experimental and numerical analysis of a hybrid HVAC system based on DW and IEC.

1.6 Layout of the thesis

The thesis has been written using the following chapter structure:

Chapter 1. The overview on the problem of handling air in buildings with high latent loads, commonly used systems to handle and control humidity in these buildings and some alternative HVAC systems are given in this chapter. It also presents a short overview on the state-of-the-art of available technologies, such as desiccant systems and evaporative systems.

Chapter 2. Describes the experimental methodology carried out during the experiments, the laboratory facilities and the measurements devices. Then, it describes the numerical methodology followed and includes the whole description of the energy simulations performed.

Chapter 3. Shows the experimental analysis of a DW activated at low temperatures. Several empirical simplified models obtained of the DW and an air control strategy for DWs.

Chapter 4. Deals with the experimental analysis of an IEC and an empirical simplified model developed for this device. An air control strategy for IECs was also studied.

Chapter 5. Addresses energy simulation results of a hybrid HVAC system composed of a DW and an IEC in order to serve a small building with high latent loads. It also presents a comparative analysis between this hybrid HVAC system and a conventional HVAC system.

Chapter 6. Provides the conclusions achieved in this thesis.

Appendix A. Several empirical models are obtained to evaluate the performance of low temperature activated desiccant wheels.

Appendix B. Addresses the experimental and numerical analysis of a desiccant wheel activated at low temperatures when the process air flow rate and air regeneration temperature are varied.

Appendix C. Shows an empirical simplified model to evaluate the performance of an indirect evaporative cooler and its comparison with a phenomenological model and experimental data.

Appendix D. Discusses the energy saving potential of a hybrid HVAC system with a desiccant wheel activated at low temperatures and an indirect evaporative cooler in buildings with high latent load.

Appendix E. Shows a numerical study on hybrid HVAC systems with desiccant wheel.

Appendix F. Describes the application of the DOE technique to the modelling of desiccant wheels for hybrid HVAC systems.

Appendix G. Deals with the design and building of a test facility for experimentation of desiccant wheels.

Appendix H. Addresses the experimental analysis of the moisture removal capacity of a desiccant wheel activated at low and high temperature.

Appendix I. Shows an empirical study on the desiccant capacity of hybrid HVAC systems based on desiccant wheels activated at low temperature by vapor compression refrigeration systems.

Chapter 2

Objectives

Based on the limitations of conventional air conditioning systems in buildings with high latent loads, the OVERALL OBJECTIVE of this thesis was to analyse experimentally and numerically the performance of a novel hybrid HVAC system activated at low temperature based on desiccant wheels and indirect evaporative coolers for use in small rooms with high latent load.

The overall objective indicated in this thesis was linked to the following SPECIFIC OBJECTIVES:

1 Investigating the desiccant capacity of a desiccant wheel activated at low temperature to identify the most influent parameters on the desiccant wheel and thus develop a latent heat control strategy.
2 Analysing the performance of an indirect evaporative cooler under inlet air conditions of a desiccant wheel to identify the most influent parameters on the indirect evaporative cooler and thus develop a sensible heat control strategy.
3 Evaluating the energy and dehumidification efficiencies of a hybrid HVAC system based on a desiccant wheel and an indirect evaporative cooler in small buildings with high latent load and comparing it with a conventional HVAC system.

Chapter 3

Materials and method

The results of this thesis are based on experimental tests carried out in the HVAC lab at the University of Cordoba and in the HVAC lab at the Politecnico di Milano. Numerical simulations were performed using energy simulation tools. The experimental and numerical methodology used in this thesis is presented in this chapter.

3.1 Overview of the methodology

Three steps were followed to achieve the objectives of this thesis, as shown Figure 11. These were divided mainly in: empirical study of a DW, empirical study of an IEC and finally, numerical simulation study of HVAC systems.

First, the thesis focused on the experimental study of a DW. The design and commissioning of a test rig to analyse DW performance under different working conditions were carried out. Four experimental case studies on the DW were performed, case studies 1, 2, 3 and 4, modifying the input variables in each case. The number of experimental tests performed for each case study was 19, 35, 29 and 46, respectively. Then, a statistical analysis for the four case studies was carried out using the statistical technique of design of experiments, DOE. This technique allowed the influential input variables on output variables to be identified and analysed. The behaviour of the DW activated at low regeneration temperatures was analysed from the influential input variables. In addition, DOE allowed to fit several empirical simplified models which can be used to predict the output

variables in the DW. Three new cases studies on the DW were carried out, one experimental case with a total of 9 tests, case study 5, and two numerical cases with 135 and 216 tests, case studies 6 and 7, respectively, using the obtained DW models, in order to develop a latent heat control strategy, achieving the first specific objective. The results of this analysis are shown in Chapter 4.

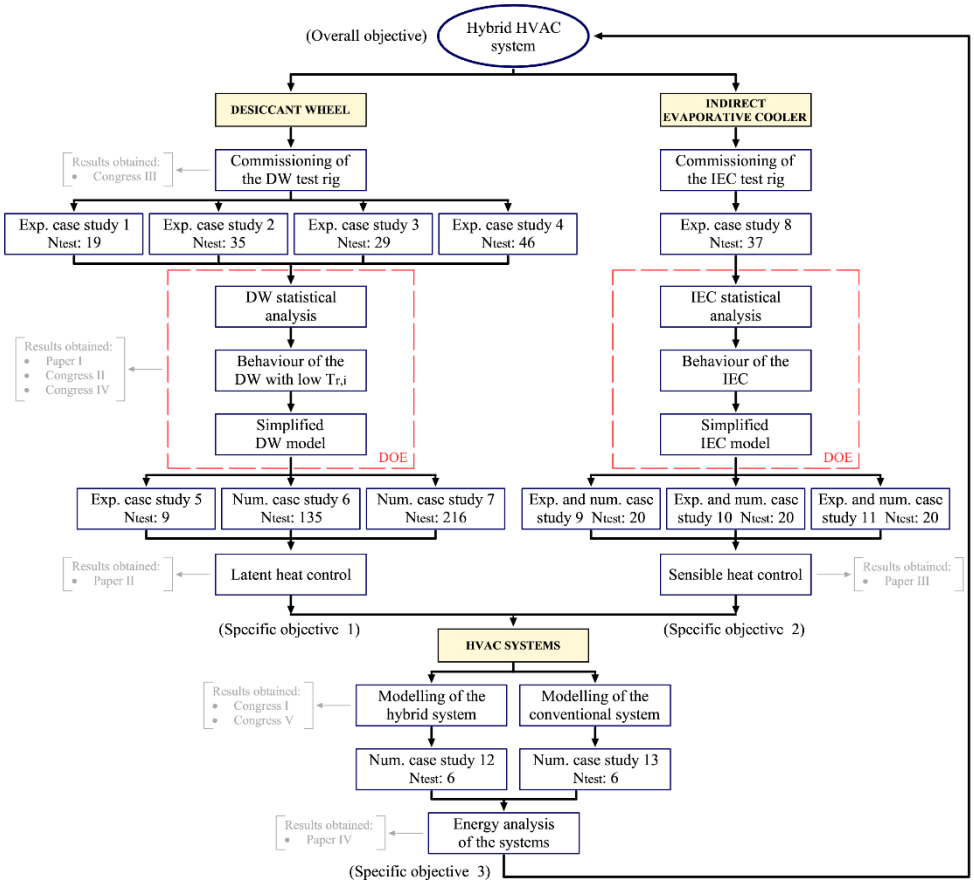

Figure 11. Overview of the methodology.

Second, an experimental study on an IEC was carried out. The methodology followed to study the IEC was similar to that of the DW. A statistical analysis was carried out for an empirical case study, case study 8, identifying the influential input variables on the output variables of the IEC. The behaviour of the IEC was analysed

for the influence input variables and an empirical simplified model was fitted. Then, three experimental and numerical case studies were carried with a total of 20 tests each, case studies 9, 10 and 11, in order to develop a sensible heat control strategy, achieving the second specific objective. The results of this analysis are shown in Chapter 5.

Finally, a hybrid HVAC system and a conventional HVAC system were analysed, case studies 12 and 13. The hybrid HVAC system was composed of a DW and an IEC, and the conventional HVAC system of a DX unit. Both HVAC systems were modelled using the previously developed empirical models of the DW and the IEC, and simulated using an energy simulation tool. An energy analysis of both HVAC systems was carried out for 6 working conditions, 6 climate zones, achieving the third specific objective and the overall objective of the thesis.

3.2 Experimental materials and facilities

3.2.1 Facilities to study the desiccant wheel

An experimental test rig was built to study DW performance under different working conditions. The test rig is located in the HVAC lab at the Department of Physical Chemistry and Applied Thermodynamics, Building Leonardo da Vinci, at the University of Cordoba.

The pilot plant was designed and constructed to carry out the research works of the present thesis and the research project "DESSECA" [92], which was related to desiccant wheels and hybrid HVAC systems

3.2.1.1 Description of the test rig

A schematic representation of the experimental setup is shown in Figure 12. The process and regeneration air streams were configured in a countercurrent flow. The facility was also designed to bypass up to 40% of the process air stream without being treated by the DW. It has a bypass air duct and variable-position dampers for the process side of the DW and for the bypass duct. The DW could operate with unbalanced air flow rates to achieve the outlet process air conditions.

The inlet temperature and humidity ratio of both process and regeneration streams were set using cooling and heating coils (CC, HC), an electric heater (EH) and a steam humidifier (SH), located for each air stream, upstream of the DW. Two refrigeration vapour compression systems were integrated in the test rig, in order to

study the behaviour of the DW combined with conventional HVAC systems. The evaporators (EV) were integrated into the process air stream and the condensers (CO) into the regeneration air stream, both systems were also located upstream of the DW. The process and regeneration air flow rates were set using variable speed fans (F). Two pitot tubes (PT) were used to measure the air flow rate and four flow conditioners (FC) were installed to obtain stable air flow conditions, two upstream of the air flow rate measuring point and two downstream. Furthermore, two mixing boxes (MB), were used either to recirculate the process and regeneration air streams or to mix the exterior air (OA) with the treated air (RA).

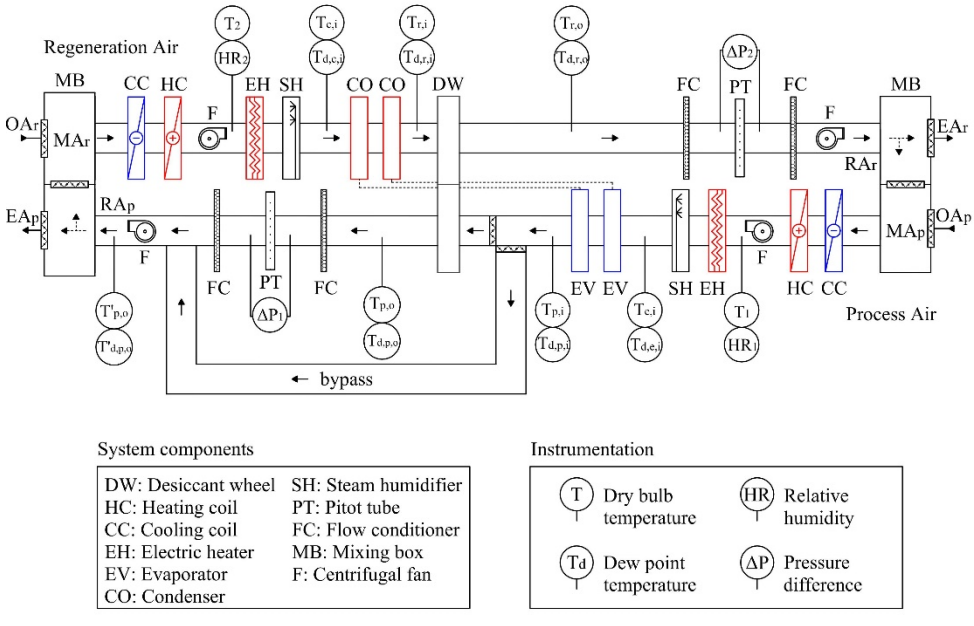

Figure 12. Layout of the test facility of the desiccant wheel.

A picture of the DW of the test rig is shown in Figure 13. The DW is divided into two equal sections and rotates at a constant speed of 42 rph. The matrix of the DW consists of alternate layers of flat and corrugated sheets of silica gel and metal silicates, chemically bonded into a tissue of inorganic fibres. The dimensional sizes and operating parameters of the DW are shown in Table 1.

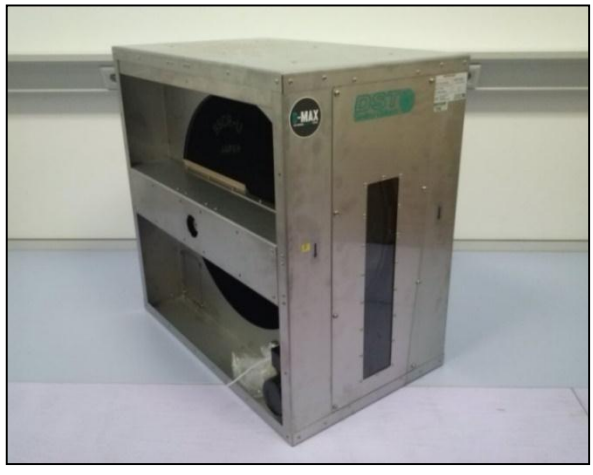

Figure 13. Picture of the desiccant wheel.

Table 1. Characteristics of the desiccant wheel.

Parameters	Value
Rotor diameter	550 mm
Rotor length	200 mm
Desiccant material	Silica gel
Channel shape	Honeycomb
Nominal capacity	15 kg h^{-1}
Nominal air flow	2300 m^3 h^{-1}
Rotation speed	42 rph
Weight	57 kg
Power supply	230 Vac

3.2.1.2 Commissioning of the test rig

In order to build the designed test rig, assembly, installation, set-up and control works were carried out:

1. Installation of the HVAC equipments
2. Assembly of the duct system
3. Installation of the electrical system
4. Installation of the control, monitoring and data recording system
5. Calibration of the equipments
6. Operating tests

A detailed description of the design and construction work is shown in Appendix G.

3.2.1.3 Data processing

The data of temperature, humidity and air flow rate were measured and recorded with BenchLink Data Logger software [93]. These data were post-processed with the corresponding software after each experiment.

The measured parameters in this test rig, the type of sensor and its accuracy are shown in Table 2. The sensor locations are shown in Figure 12. The temperature and humidity at each measuring point were collected at three different points along the horizontal axis, taking the average of the three measurements.

Table 2. Specification of measuring devices for the desiccant wheel.

Measured parameter	Type	Accuracy
T_1, T_2, $T_{e,i}$,$T_{p,i}$, $T_{p,o}$, $T'_{p,o}$, $T_{c,i}$,$T_{r,i}$, $T_{r,o}$	PT 100	± 0.12 ºC
$T_{d,p,i}$, $T_{d,p,o}$, $T'_{d,p,o}$	Chilled mirror hygrometer	± 0.15 ºC
$T_{d,r,i}$, $T_{d,r,o}$, $T_{d,e,i}$, $T_{d,c,i}$	Capacitive	± 0.4 ºC
HR_1, HR_2	Capacitive	± 3%
ΔP_1, ΔP_2	Differential pressure transmitter	± 0.3% (0 to 1 mbar)

Each state point was taken under steady-state conditions and all the measured values were average values over a period of 20 minutes with sampling time steps of 3 seconds.

3.2.2 Facilities to study the indirect evaporative cooler

The experimental tests of the IEC system were carried out in the HVAC lab at the Department of Energy of Politecnico di Milano, working within the AirLab research group.

3.2.2.1 Description of the test rig

An experimental test rig was designed to evaluate the performance of an IEC by controlling the primary and secondary air stream conditions [58]. The design of this experimental setup was similar to the experimental test rig used to study the DW, described in section 3.2.1.1. A schematic diagram of the IEC experimental setup is shown in Figure 14.

The inlet temperature and humidity ratio of both primary and secondary air streams were carefully set by means of heating coils (HC), cooling coils (CC), electric heater (EH), and adiabatic humidifiers (SH), located for each air stream, upstream of the IEC. The primary and secondary air flow rates were set using variable speed fans (F). A mixing box was installed in the system to work in outdoor air mode or in recirculation air mode [58].

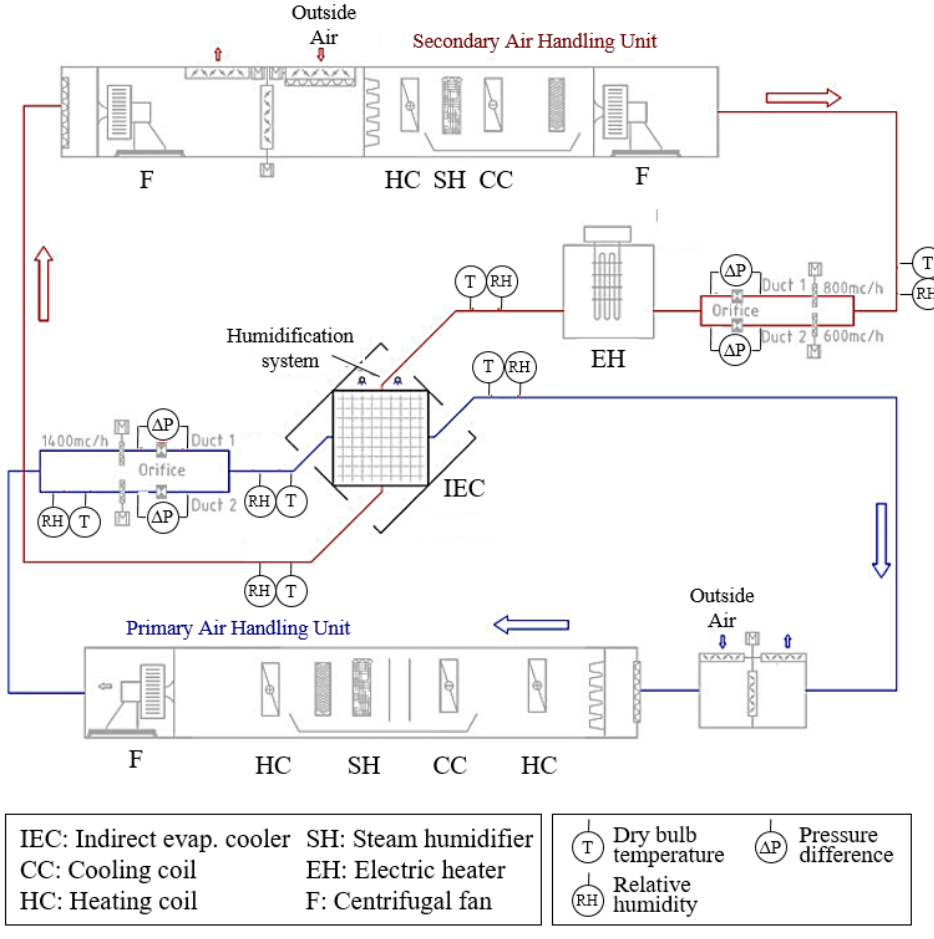

Figure 14. Layout of the test facility of the indirect evaporative cooler.

A picture of the IEC of this test rig is shown in Figure 15. The analysed IEC system consists of a commercial crossflow plate heat exchanger, 8 water spray nozzles installed in the secondary air flow inlet plenum and a water pumping

system. The net face heat exchanger cross area is equal to 0.089 m^2. The plates are made of aluminium with semi spherical dimples, and has a slightly hydrophilic coating. The nominal water flow rate for each axial and full cone type nozzle is 7.50 l h-1 at 9 bar. The distance between nozzles is 8 cm and each manifold is installed 15 cm far from the heat exchanger. The water is supplied in counter current arrangement respect to the secondary air stream through a commercial pumping unit, without any recirculation, at an average temperature around 20°C. Finally, the length of top and side plenums is 42 cm. The characteristics of the IEC system are shown in Table 3.

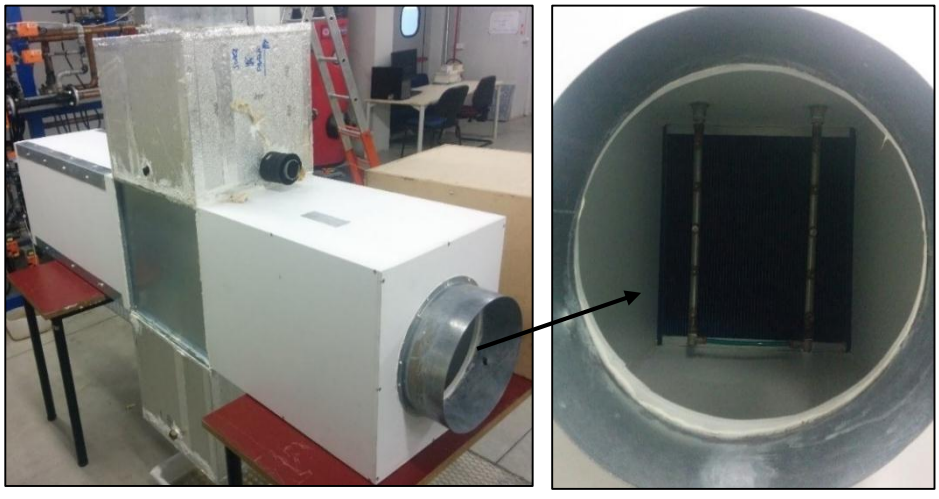

Figure 15. Picture of the indirect evaporative cooler.

Table 3. Characteristics of the indirect evaporative cooler.

Parameter	Value
Number of plates	119
Plate thickness	0.14 mm
Plate pitch	3.35 mm
Net channel height	3.21 mm
Net plate length and width	470 mm
Net face heat exchanger cross area	0.089 m^2

3.2.2.2 Data processing

The data of temperature, humidity and air flow rate were measured, recorded and controlled with LabVIEW software [94]. These data were post-processed with the corresponding software after each experiment.

Each air flow rate was measured using two orifice plates and piezo resistive pressure transmitters placed in two different measurement ducts, constructed according to standards [95]. The water flow rate supplied to the nozzles from the pumping unit was measured using a turbine flow sensor, whose accuracy is 3% of the reading. The data were collected using temperature, humidity and pressure sensors, which characteristics are shown in Table 4.

Table 4. Specification of measuring devices for the indirect evaporative cooler.

Measured parameter	Type	Accuracy
T	PT 100	± 0.2 ºC
HR	Capacitive	± 1% (0 to 90%)
ΔP	Piezoresistive	± 0.5% reading ± 1 Pa

In each experimental session, at least 300 samples for each physical quantity have been collected in steady state conditions and at a frequency of 1 Hz.

3.3 Experimental methodology

3.3.1 Design of experiments

The statistical technique of design of experiments, DOE, was used to empirically study the global behaviour of the DW and the IEC, and obtain simplified mathematical models suitable for integration in simulation tools. This technique was used to achieve specific objectives 1 and 2.

DOE is a methodology for systematically applying statistics to the experimental process [44]. The number of required experimental tests can be reduced if they are optimally designed. Usually, several candidate models can be proposed. The choice between these candidate models is a trade-off between complexity and precision. The statistical analysis and its further fit of the models were supported by the software Statgraphics Centurion XVI [96].

3.3.1.1 Design of experiments of the desiccant wheel

Experimental case studies 1, 2, 3 and 4 on the DW, shown in Figure 11, were carried out using different input and output variables, see Table 5. The input variables were the inlet air process temperature, $T_{p,i}$, inlet air process humidity ratio, $\omega_{p,i}$, process specific mass air flow rate, Ω_p, ratio of inlet mass velocity to the channel length [38], inlet air regeneration temperature, $T_{r,i}$, inlet air regeneration humidity ratio, $\omega_{r,i}$, and regeneration specific mass air flow rate, Ω_r. In case studies 1, 2 and 3, the output variables were the outlet air process temperature, $T_{p,o}$, and outlet air process humidity ratio, $\omega_{p,o}$, see Figure 12. In both air streams were circulated the same air flow rates for these three cases. In case study 4, the output variables were the outlet air process temperature and humidity ratio in the DW system with bypass air, $T'_{p,o}$ and $\omega'_{p,o}$, showing a similar setting to Figure 16. The effects of the input variables on the output variables were studied using a factorial design approach, design at 2-levels, [44] for case studies 1 and 2. However, some previous studies showed nonlinear trend in the adsorption process when the input variables of DW were varied [97].Therefore, a box-Behnken design approach, design at 3-levels, [44] was used for case studies 3 and 4. A total of 19, 35, 27 and 46 experimental tests were performed for case studies 1, 2, 3 and 4, respectively, as shown in Table 5.

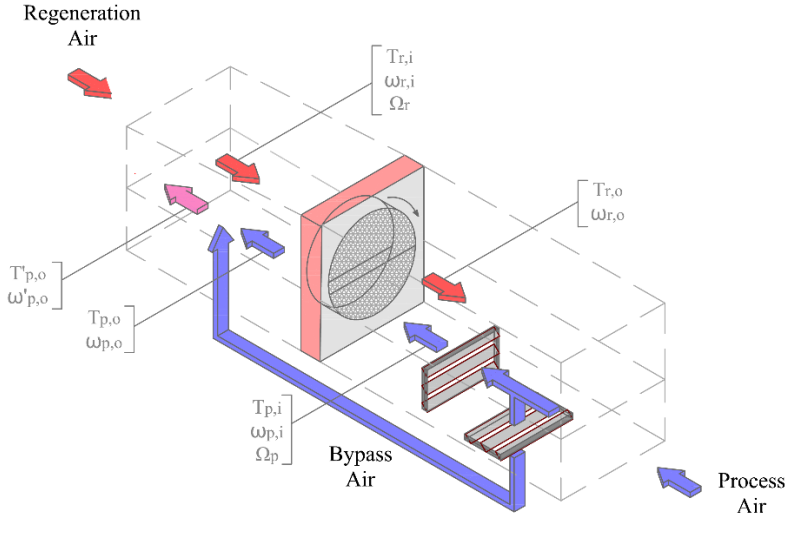

Figure 16. Schematic of a desiccant wheel system with bypass air.

Table 5. Design of experimental case studies 1, 2, 3 and 4 of the desiccant wheel.

Exp. case study	Type	Nº tests	Input variables						Output variables			
			$T_{p,i}$	$\omega_{p,i}$	$T_{r,i}$	$\omega_{r,i}$	Ω_p	Ω_r	$T_{p,o}$	$\omega_{p,o}$	$T'_{p,o}$	$\omega'_{p,o}$
1	Factorial	19	x	x	x	x			x	x		
2	Factorial	35	x	x	x	x	x	x	x	x		
3	Box-behnken	27	x	x	x	x			x	x		
4	Box-behnken	46	x	x	x	x	x				x	x

The set of experimental tests are summarized in Tables 6, 7 and 8 of Appendix A for case studies 1, 2 and 3, respectively, and in Table 6 of Appendix B for case 4.

The ranges of validity of the process and regeneration air streams for case studies 1, 2, 3 and 4 are summarized in Table 6. These ranges were selected to implement the DW model in low temperature activated hybrid system models.

Table 6. Ranges of validity of the process and regeneration air streams of the desiccant wheel for experimental case studies 1, 2, 3 and 4.

Exp. case study	$T_{p,i}$ [ºC]		$\omega_{p,i}$ [g kg^{-1}]		$T_{r,i}$ [ºC]		$\omega_{r,i}$ [g kg^{-1}]		Ω_p [kg s^{-1} m^{-3}]		Ω_r [kg s^{-1} m^{-3}]	
	L	U	L	U	L	U	L	U	L	U	L	U
1	17.5	29.5	12	21.5	34	42.5	13	22.5	30.92	30.92	30.92	30.92
2	17.5	29.5	12	21.5	34	42.5	13	22.5	14.79	30.92	14.79	30.92
3	17.5	29.5	12	21.5	34	42.5	13	22.5	30.92	30.92	30.92	30.92
4	17.5	29.5	12	21.5	34	42.5	13	22.5	13.45	21.51	21.51	21.51

L: Lower value
U: Upper value

The relationship between the output and input variables was examined using first order polynomial equations for the factorial design, expressed by Eq. 3, and second order polynomial equations for the box-Behnken design, expressed by Eq. 4, where $\hat{Y}$ is the estimated output value, X are input variables, b_i, b_{ii}, b_{iii} and b_{ij} are the estimated parameters of linear, quadratic, cubic and the second-order terms, respectively, and b_0 is the average response in the model.

$$\hat{Y} = b_0 + \sum_{i=1}^{k} b_i \cdot X_i + \sum_{i=1}^{k=1} \sum_{\substack{i=2 \\ j>i}}^{k} b_{ij} \cdot X_i \cdot X_j \tag{3}$$

$$\hat{Y} = b_0 + \sum_{i=1}^{k} b_i \cdot X_i + \sum_{i=1}^{k} b_{ii} \cdot X_i^2 + \sum_{i=1}^{k=1} \sum_{\substack{i=2 \\ j>i}}^{k} b_{ij} \cdot X_i \cdot X_j \quad (4)$$

3.3.1.2 Design of experiments of the indirect evaporative cooler

An experimental case study was carried out to study the behaviour of the IEC system, case study 8, see Figure 11, using five input variables and three output variables, as shown in Table 7. The input variables were the inlet air primary temperature, $T_{p,i}$, inlet air secondary temperature, $T_{s,i}$, inlet air secondary humidity ratio, $\omega_{s,i}$, secondary air velocity, v_s and water flow rate, $\dot{V}_w$, see Figure 17. The output process variables were the outlet air primary temperature of system, $T_{p,o}$, outlet air secondary temperature of system, $T_{s,o}$ and outlet air secondary humidity ratio of system, $\omega_{s,o}$, see Figure 17. The effect of the five input variables was studied using the factorial design approach, design at 2-levels [44]. The relationship between the output and input variables was examined using first order polynomial equations, expressed by Eq. 3. A total of 37 experimental tests were carried out, as shown in Table 7.

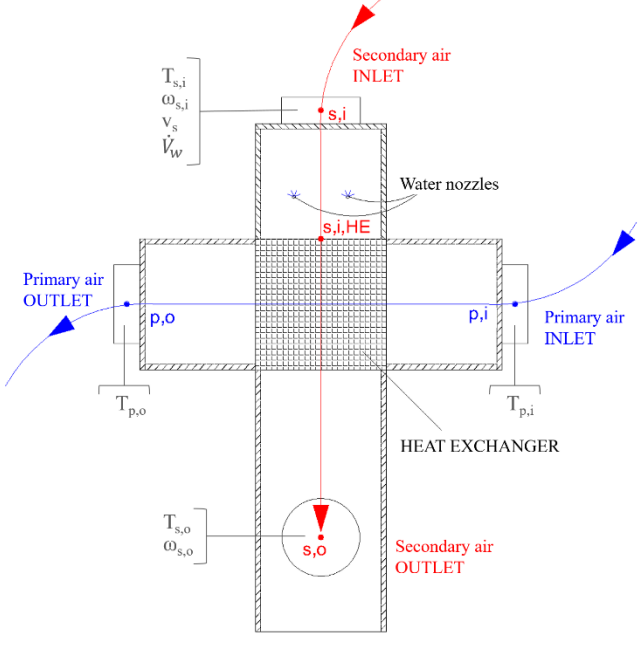

Figure 17. Schematic of the investigated indirect evaporative cooler system.

Table 7. Design of experimental case study 8 of the indirect evaporative cooler.

Exp. case study	Type	Nº tests	Input variables					Output variables		
			$T_{p,i}$	$T_{s,i}$	$\omega_{s,i}$	v_s	$\dot{V}_w$	$T_{p,o}$	$T_{s,o}$	$\omega_{s,o}$
8	Factorial	37	x	x	x	x	x	x	x	x

The combination of experimental tests for case study 8 are summarized in Table 3 of Appendix C.

The ranges of validity of the primary and secondary air streams for case study 8 are shown in Table 8. These ranges were selected to integrate the IEC model into a hybrid HVAC system with a DW.

Table 8. Ranges of validity of the primary and secondary air streams of the indirect evaporative cooler for experimental case study 8.

$T_{p,i}$ [ºC]		$\omega_{p,i}$ [g kg^{-1}]		v_p [m s^{-1}]		$T_{s,i}$ [ºC]		$\omega_{s,i}$ [g kg^{-1}]		v_s [m s^{-1}]		$\dot{V}_w$ [l h^{-1}]	
L	U	L	U	L	U	L	U	L	U	L	U	L	U
28	48	10	10	3.7	3.7	25	38	8	16	3.7	5.7	30	60

L: Lower value
U: Upper value

3.3.1.3 Accuracy of the models

A statistical analysis was performed to obtain the lack of fit test, the R^2 value and the standard error of the estimate. The lack of fit test is designed to determine whether the selected model is adequate to describe the observed data. The R^2 value and the standard error of the estimate is a measure of the accuracy of the predictions.

3.3.2 Latent heat control of the process air in a DW

The inlet air regeneration temperature, $T_{r,i}$, and process air flow rate, $\Omega_{p,i}$, were used to control the latent heat of the process air in the DW, showing a similar setting to Figure 16. These input variables could achieve a fine-tuning of outlet air humidity ratio. The remaining input variables analysed, shown in Table 6, were not considered as latent heat control variables, because they could not have a high influence on the air humidity ratio or could be influenced by outdoor air.

Three case studies were carried out, case studies 5, 6 and 7, see Table 9. Case study 5 was tested experimentally and a total of 9 tests were performed. Case studies 6 and 7 were carried out for different inlet air conditions using the empirical model fitted with case study 4, shown in section 3.3.1.1. A total of 135 and 216 numerical simulations were performed for case studies 6 and 7, respectively. The outlet process air conditions of the DW, $T'_{p,o}$ and $\omega'_{p,o}$, were evaluated for each case study.

Table 9. Input variables and output variables for case studies 5, 6 and 7.

Case study	Nº tests	Input variables					Output variables			
		$T_{p,i}$	$\omega_{p,i}$	$T_{r,i}$	$\omega_{r,i}$	$\Omega_{p,i}$	$T'_{p,o}$	$\omega'_{p,o}$	MRC	SHR
5	9			x		x	x	x	x	x
6	135	x	x	x	x	x	x	x	x	x
7	216	x	x	x	x	x	x	x		

The set of experimental tests for case study 5 are summarized in Table 7 of Appendix B and the combination of numerical tests for case studies 6 and 7 are summarized in Tables 8 and 9 of Appendix B.

The air dehumidification process in a DW when a single input variable is varied is shown in Figure 18a, where an outlet air state is achieved from a given inlet air state. Nevertheless, a decoupling of the outlet process air conditions, $T'_{p,o}$ and $\omega'_{p,o}$, could be obtained when the $T_{r,i}$, and $\Omega_{p,i}$ are varied, as shown in Figure 18b.

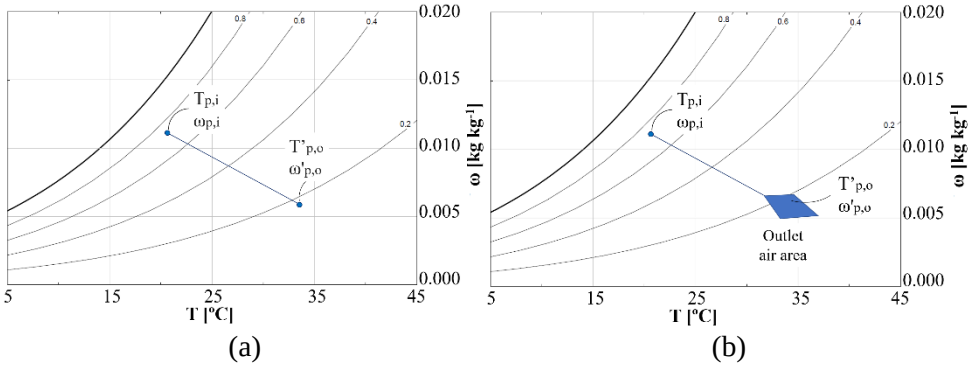

Figure 18. (a) An outlet process air state of a desiccant wheel, (b) decoupling of the outlet process air conditions in a desiccant wheel.

The decoupling potential of the outlet air process temperature and humidity ratio were evaluated in case study 5 by varying three levels of $T_{r,i}$ and three levels of $\Omega_{p,i}$. These three levels are shown in Table 7 of Appendix B. The remaining input variables were fixed at constant values: $T_{p,i}$=25 ºC, $\omega_{p,i}$=17 g kg^{-1}, $\omega_{r,i}$=13 g kg^{-1} and $\Omega_{p,i}$=21.51 kg s^{-1} m^{-3}. In order to quantify the decoupling of the outlet process air conditions of the DW, a psychrometric area, A_o, was obtained. The psychrometric area was calculated from the contour of the outlet process air states, where the main axes of psychrometric chart were considered the dry bulb temperature, horizontal axis, and the humidity ratio, vertical axis.

In case study 6, the decoupling potential was evaluated for five inlet air conditions, shown in Figure 3 of Appendix B. The combination of three levels of $T_{r,i}$, $\omega_{r,i}$ and $\Omega_{p,i}$ was used to analyse $T'_{p,o}$, and $\omega'_{p,o}$, see Table 8 of Appendix B. The remaining input variables were fixed at constant value, as in case study 5.

In practice, inlet process air conditions could vary over time, for example, when these conditions are influenced by outdoor air. In order to analyse the outlet process air conditions of the DW system when inlet process air conditions vary, a third case was performed, case study 7. In this case, three inlet process air areas were selected. These areas are related to three climatic conditions, see Figure 4 of Appendix B:

- Area I: inlet process air conditions with low temperature and low humidity ratio values
- Area II: inlet process air conditions with high temperature values and low humidity ratio values
- Area III: inlet process air conditions with high temperature and high humidity ratio values.

The ranges of validity of the process and regeneration air streams for case studies 5, 6 and 7 are summarized in Table 10.

The experimental and numerical results were also evaluated using the moisture removal capacity, MRC, and the sensible heat ratio, SHR, as shown in Table 9. MRC of the DW was defined according to ASHRAE [98]:

$$MRC = \rho \cdot \dot{V} \cdot \left(\omega_{p,i} - \omega'_{p,o}\right) \quad (5)$$

Similar desiccant capacities in a DW are possible, so MRC was analysed regarding SHR, expressed by Eq. (6). Where $\dot{Q}_{sen}$ is the sensible heat transfer of the process air stream and $\dot{Q}_{lat}$ is the latent heat transfer of the process air stream. SHR values range between 0 and 1.

$$SHR = \frac{\dot{Q}_{sen}}{\dot{Q}_{sem} + \dot{Q}_{lat}} \quad (6)$$

Table 10. Ranges of validity of the process and regeneration air streams of the desiccant wheel for case studies 5, 6 and 7.

Case study	$T_{p,i}$ [ºC]		$\omega_{p,i}$ [g kg^{-1}]		$T_{r,i}$ [ºC]		$\omega_{r,i}$ [g kg^{-1}]		Ω_p [kg s^{-1} m^{-3}]		Ω_r [kg s^{-1} m^{-3}]	
	L	U	L	U	L	U	L	U	L	U	L	U
5	25.0	25.0	17.0	17.0	34.0	42.5	13.0	13.0	13.45	21.51	30.92	30.92
6	17.5	29.5	12.0	21.5	34.0	42.5	13.0	22.5	13.45	21.51	30.92	30.92
7	17.5	29.5	12.0	21.5	34.0	42.5	13.0	22.5	13.45	21.51	30.92	30.92

L: Lower value
U: Upper value

3.3.3 Sensible heat control of the process air in an IEC

The water flow rate supplied on an IEC system was used to control the sensible heat of the primary air, showing a similar setting to Figure 17. The remaining input variables analysed, shown in Table 7, were not considered as sensible heat control variables, because they could not have a high influence on the air temperature or could be influenced by outdoor air.

Three case studies were carried out, case studies 9,10 and 11, see Table 11.

Table 11. Input variables and output variables for case studies 5, 6 and 7.

Case study	Nº tests	Input variables	Output variables			
		$\dot{V}_w$	ε_{wb}	ΔT_p	ΔT_s	$\Delta\omega_s$
9- Data center	20	x	x	x	x	x
10- DW	20	x	x	x	x	x
11- Residential	20	x	x	x	x	x

Case study 9 is related to a data center application, case study 10 to a configuration with DW and case study 11 to a residential application. The three case studies were tested experimentally and numerically with a total of 20 tests each case, 10 experimental tests and 10 numerical tests. The numerical tests were carried out using the empirical model fitted with case study 4, shown in section 3.3.1.1.

Experimental and numerical results were evaluated in terms of wet bulb effectiveness ε_{wb}, of variation of air primary temperature ΔT_p, air secondary temperature ΔT_s, and air secondary humidity ratio $\Delta\omega_s$. These indexes are defined through the following equations:

$$\varepsilon_{wb} = \frac{(T_{p,i} - T_{p,o})}{(T_{p,i} - T_{wb,s,i})} \tag{7}$$

$$\Delta T_p = T_{p,i} - T_{p,o} \tag{8}$$

$$\Delta T_s = T_{s,i} - T_{s,o} \tag{9}$$

$$\Delta \omega_s = \omega_{s,i} - \omega_{s,o} \tag{10}$$

The set of experimental and numerical tests for case study 9, 10 and 11 are summarized in Table 3 of Appendix C.

Table 12. Ranges of validity of the primary and secondary air streams of the indirect evaporative cooler for experimental and numerical case studies 9, 10 and 11.

Case study	$T_{p,i}$ [°C]		$\omega_{p,i}$ [g kg^{-1}]		v_p [m s^{-1}]		$T_{s,i}$ [°C]		$\omega_{s,i}$ [g kg^{-1}]		v_s [m s^{-1}]		$\dot{V}_w$ [l h^{-1}]	
	L	U	L	U	L	U	L	L	U	L	U	L	U	L
9	35	35	10	10	3.7	3.7	30	30	13.3	13.3	4.7	4.7	30	65
10	60	60	10	10	3.7	3.7	26	26	12.7	12.7	3.7	3.7	30	65
11	30	30	10	10	3.7	3.7	26	26	12.7	12.7	3.7	3.7	30	65

L: Lower value
U: Upper value

The ranges of validity of the primary and secondary air streams for case studies 9, 10 and 11 are shown in Table 12.

3.4 Numerical methodology

Several annual energy simulations on a building with high latent loads treated with hybrid and conventional HVAC systems were carried out under different climatic conditions.

3.4.1 HVAC systems

3.4.1.1 Approach to hybrid HVAC systems

A previous study on two hybrid HVAC systems was carried out. Both hybrid HVAC systems were composed of a DW and a DX unit, see Figure 19. The two HVAC systems were analysed under different steady state air conditions. However, these two systems were excluded for a detailed energy analysis, because their efficiency was lower than that of other hybrid HVAC systems, such as a hybrid HVAC system composed of a DW and an IEC. All results obtained of these two hybrid HVAC systems are shown in appendices E and I.

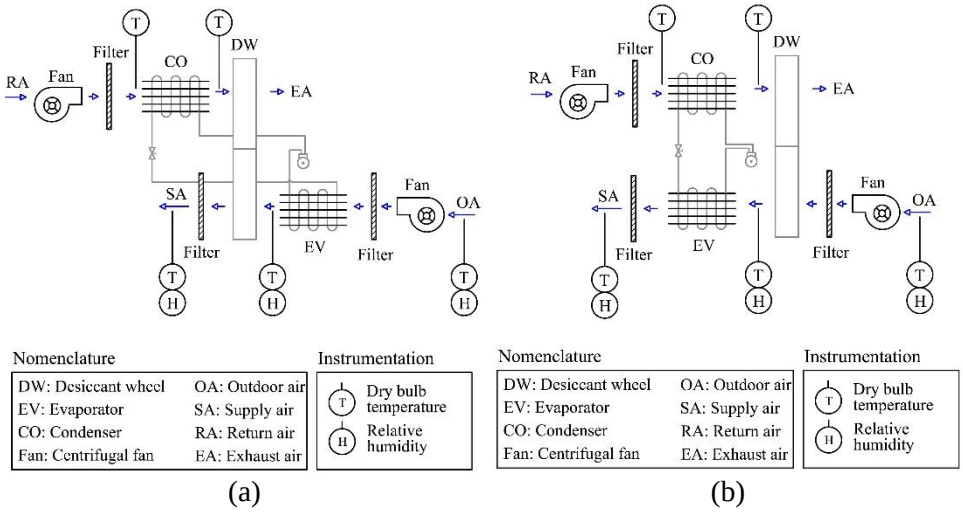

Figure 19. Schemes of (a) the DW-DX system, (b) the DX-DW system.

A hybrid HVAC system composed of a DW and an IEC was analysed and compared with a conventional HVAC system composed of a DX unit, case studies 12 and 13, shown in Figure 11. Both HVAC systems are described below.

A criterion commonly used by manufacturers to select dehumidification units, is their moisture removal capacity, MRC, as defined in Eq. (5), [6]. In this study, this criterion was used. The same nominal MRC value for the systems was considered, 15.2 kg h^{-1}. The selected DX unit was specifically designed to maintain indoor conditions in swimming pools and other high latent loads buildings, such as spas [99]. The HVAC systems studied were not equipped with any humidifier element, since they were designed to handle very humid indoor air.

3.4.1.2 Conventional HVAC system

The conventional HVAC system was composed of an air-mixing box, a direct expansion unit, DX, and a heating coil, HC, see Figure 20. The HC was fed by a constant water flow, which was heated using an air-water heat pump. The evaporator, EV, and the condenser, CO, of the vapor-compression cycle were installed in a parallel arrangement. The supply air humidity ratio was controlled with the EV and the supply air temperature was controlled with the HC.

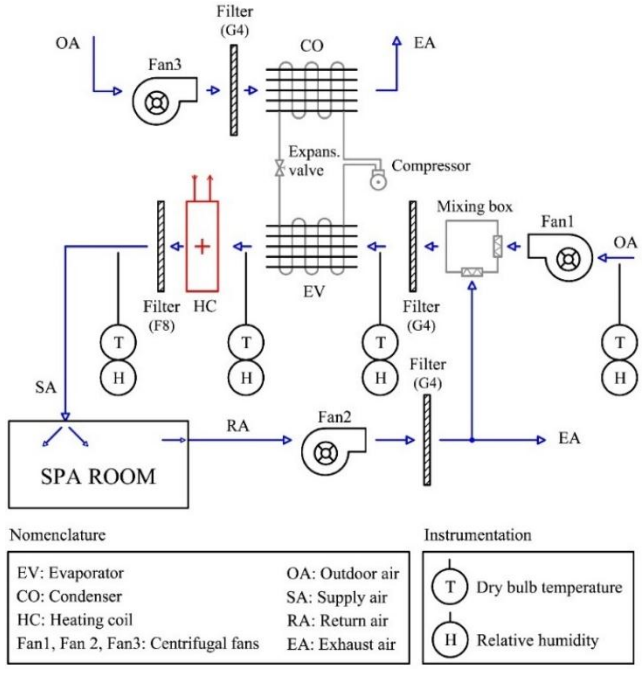

Figure 20. Schematic of the conventional HVAC system.

Air handling by the conventional HVAC system is described below. Firstly, the outdoor air, OA, stream was mixed with the return air, RA, stream. Secondly,

the mixed air stream was dehumidified and cooled by the evaporator, EV. Finally, the air stream was heated by the HC until the supply air temperature equalled the set point temperature. The outdoor air flow rate of this system was 1600 $m^3 h^{-1}$, and the total air flow rate handled and supplied by the conventional HVAC system was 3680 $m^3 h^{-1}$. The condenser, CO, of the direct expansion refrigeration unit handled 100% outdoor air, 3680 $m^3 h^{-1}$.

3.4.1.3 Hybrid HVAC system

An alternative hybrid HVAC system was proposed in this work in order to maintain the required indoor conditions in buildings. A schematic of the proposed hybrid HVAC system is shown in Figure 21.

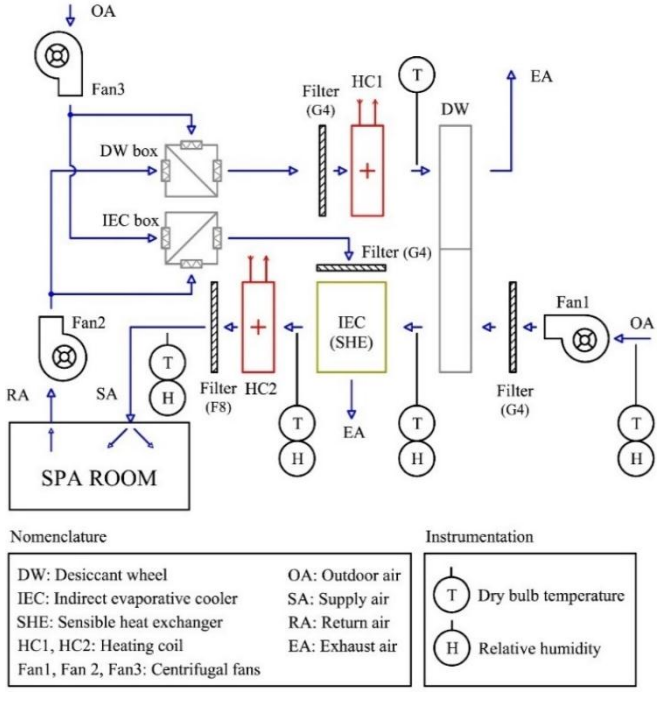

Figure 21. Schematic of the hybrid HVAC system.

The hybrid HVAC system is composed of a DW to handle latent heat loads in the room, and an IEC and a heating coil, HC2, to handle sensible heat loads. The DW was activated by means of a heating coil, HC1. Alternatively, the IEC was used as a sensible heat exchanger, SHE, recovering sensible heat from the return air stream,

when it was necessary to heat the process air stream. In addition, two air boxes were integrated into the system to increase the desiccant and cooling capacity of the DW and the IEC, respectively. DW box and IEC box have two air inlet dampers and one outlet. Depending on outdoor air conditions, the exhaust air stream is the outside, OA, air or return air, RA, as shown in Figure 21. A constant air flow rate of 1600 $m^3\ h^{-1}$ was considered for the three air streams. The outdoor air flow rate of this system was equal to that of the conventional HVAC system. Furthermore, this study was performed for relatively low regeneration air temperatures (40–60 ºC), which can be obtained using a commercial heat pump or other renewable energy sources.

3.4.1.3.1 System operation modes

Two independent main control loops were considered in the proposed hybrid HVAC system. The first one was an indoor air humidity control loop and the second one an indoor air temperature control loop. A diagram of the control logic of the hybrid HVAC system is represented in Figure 22. The air humidity control loop was divided into two specific modes of operation, Mode 1-H and 2-H. This loop modulated the water flow rate of the regeneration heating coil, HC1, activated the rotation of the DW and set the position of the dampers in the DW and IEC boxes. The air temperature control loop was divided into three specific modes of operation, Mode 1-T, 2-T and 3-T. This loop modulated the water flow rate of the IEC and the post-heating coil, HC2. These modes of operation are described below.

- **Air humidity control**

The operating mode of the selected humidity control was based on the outdoor air humidity ratio, ω_{OA}. The hybrid HVAC system did not dehumidify when the outdoor air humidity was lower than the set point air humidity. Mode 1-H was activated, see Figure 21 and Figure 22. For this operating mode, the DW, HC1 and Fan3 elements were disabled, and as a result the supply air humidity ratio was equal to the outdoor air humidity ratio. On the contrary, the hybrid HVAC system dehumidified when the outdoor air humidity was higher than the set point air humidity, and Mode 2-H was activated. For this control mode, the system dehumidified the outdoor air until the outlet process air humidity ratio of the DW, $\omega_{p,o,}$ was equal to or lower than the set point humidity. The DW, HC1 and Fan3 elements were activated and the dampers of the two air boxes were set to the correct position, see Figure 21 and Figure 22. The outdoor air, OA, passed through DW damper and the return air, RA, passed through IEC damper when the outdoor air temperature was higher than the set point air temperature. On the contrary, the

outdoor air, OA, passed through IEC damper and the return air, RA, passed through DW damper.

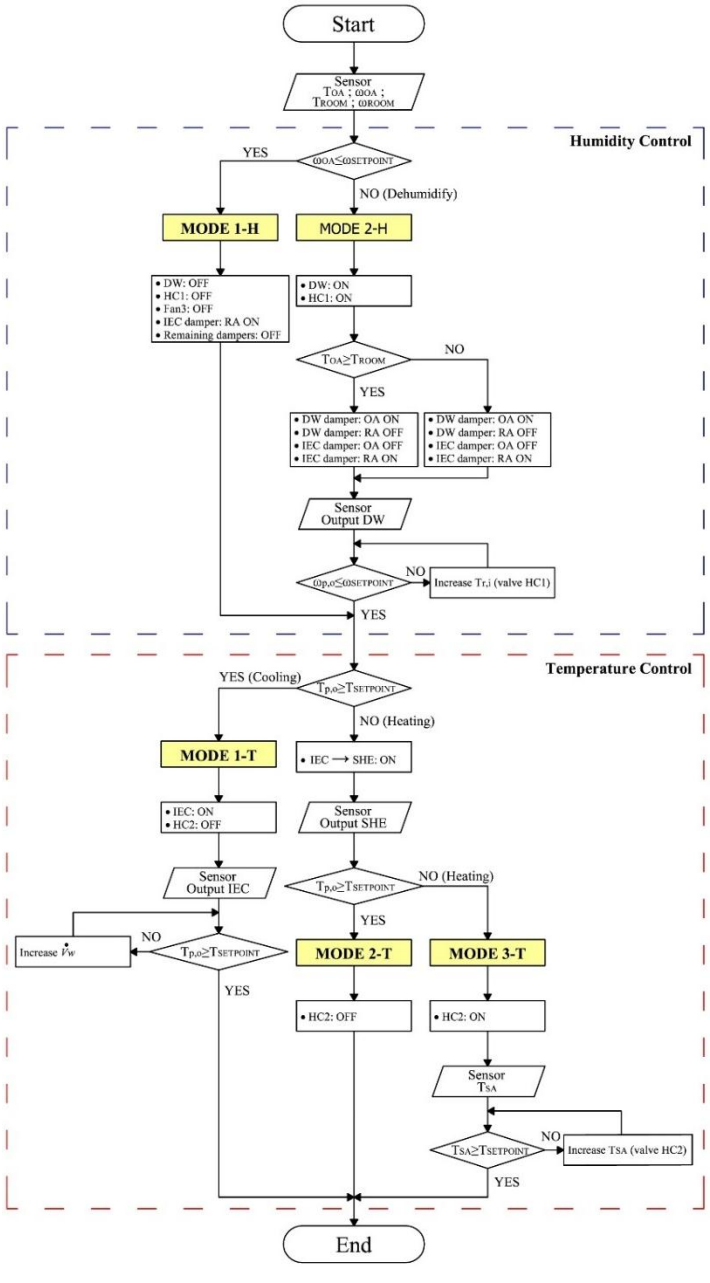

Figure 22. Hybrid HVAC system control logic diagram.

- **Air temperature control**

The operating mode of the selected temperature control was based on the DW outlet process air temperature, $T_{p,o}$. Mode 1-T was activated when $T_{p,o}$ was higher than the set point air temperature, see Figure 21 and Figure 22. The IEC system was activated until the set point temperature of the process air steam was achieved. The process air stream was heated when $T_{p,o}$ of the DW was lower than the set point air temperature. The outlet process air stream of the DW can be heated by the sensible heat exchanger, SHE. The IEC was only used as SHE when the rotation of the DW was disabled and the secondary air stream was return air. In this situation, no water was evaporated in the SHE. Then, the air temperature was measured again at the output of the IEC unit, see Figure 21 and Figure 22. The primary air stream of the IEC was supplied to the building when $T_{p,o}$ was higher than the set point air temperature, and the HC2 was off, Mode 2-T. However, HC2 was activated when $T_{p,o}$ was lower than the set point air temperature and the air stream was heated until the supply air temperature was equal to the set point temperature, Mode 3-T.

3.4.2 Building model – Spa

Both HVAC systems were designed to serve air in a building with high latent loads. A building model was designed to simulate the thermal behaviour of a spa. This was modelled and simulated using TRNSYS package tool [100]. The building consisted of a room with a surface area of 64 m^2 and a height of 3.9 m, where a south-oriented was, and the roof were exterior. The characteristics of the building are summarized in Table 13.

The building was composed of a swimming pool of 32 m^2 and a daily maximum number of 8 people in the pool. The evaporated water flow rate from the pool was calculated using Eq. (11), according to that established in [6]. Where S is the pool area, ω_w is the saturated air humidity ratio at the pool water temperature, ω_{IA} is the indoor air humidity ratio and Np is the number of people.

$$\dot{M}_{pool} = S \cdot \left(16 + 133 \cdot \frac{Np}{S}\right) \cdot (\omega_w - \omega_{IA}) + 0{,}1 \cdot Np \qquad (11)$$

Other internal energy gains due to people and lighting were considered, as shown in Table 13.

Based on the Spanish regulations on thermal installations in buildings [1], the indoor air temperature set for swimming pools should be between 1°C and 2°C above the pool water temperature, with a maximum of 30°C, and the indoor relative humidity should be maintained below 65%. In this paper, the indoor conditions were set at 27°C for the air temperature and 60% for the relative humidity. The building was simulated for a daily operating schedule from 09:00 am to 24:00 pm.

Table 13. Characteristics of the building.

Building	Floor area	64 m^2
	Height	3.9 m
	Exterior wall area	31.2 m^2
	Exterior roof area	64 m^2
	Indoor air temperature	27 ºC
	Indoor relative humidity	60%
Pool	Area	32 m^2
	Water temperature	25 ºC
U-value	Exterior wall	0.339 W m^{-2} K^{-1}
	Roof	0.313 W m^{-2} K^{-1}
Heat gain	Pool	Latent: 6662 W ($\dot{M}_{pool}$=9.6 kg h^{-1})
	Lighting	55 W m^{-2} (50% convective part)
	People	8 persons Sensible: 75 W/person Latent: 75 W/person
Daily schedule	09:00 am to 24:00 pm	

3.4.3 Components modelling

The empirical models of the DW and the IEC developed in case studies 4 and 8 with the DOE technique were used to model the proposed hybrid HVAC system. The remaining components that compose the hybrid HVAC system and the conventional HVAC system, were modelled as described below. The models of the refrigeration vapour compression unit, the heat pump and the fans were validated experimentally. Each of the component models was combined and integrated into TRNSYS [100]. These models were fitted by first, second and third order polynomial equations, expressed by Eqs. (3), (4) and (12), respectively.

$$\hat{Y} = b_0 + \sum_{i=1}^{k} b_i \cdot X_i + \sum_{i=1}^{k} b_{ii} \cdot X_i^2 + \sum_{i=1}^{k=1} b_{iii} \cdot X_i^3 \qquad (12)$$

3.4.3.1 Refrigeration vapour compression model

The considered refrigeration vapour compression unit of the conventional HVAC system was specially designed to dehumidify indoor swimming pools and other dehumidification applications. This unit was modelled using experimental data available from the manufacturer [99]. The unit works for balanced air flow rates in both coils, with a value of 3680 $m^3\ h^{-1}$.

A simplified experimental model based on correlations was obtained to study its behaviour. The relationship between the output and input variables was expressed by second order polynomial equations, as shown in Eq. (4). The input variables of this model were the inlet evaporator dry bulb air temperature, $T_{e,i}$, the inlet evaporator wet bulb air temperature, $T_{wb,e,i}$, the inlet condenser dry bulb air temperature, $T_{c,i}$, and the volumetric air flow rate ratio, $\dot{V}^* = \dot{V}/\dot{V}_N$. The output variables were calculated using the following ratios: evaporator total heat transfer ratio $\dot{Q}^*_{e,t} = \dot{Q}_{e,t}/\dot{Q}_{e,t,N}$; evaporator sensible heat transfer ratio $\dot{Q}^*_{e,sen} = \dot{Q}_{e,sen}/\dot{Q}_{e,sen,N}$; condenser total heat transfer ratio $\dot{Q}^*_{c,t} = \dot{Q}_{c,t}/\dot{Q}_{c,t,N}$; electric power consumption ratio $\dot{W}^* = \dot{W}/\dot{W}_N$. Where $\dot{Q}_{e,t}$ is the evaporator total heat transfer, $\dot{Q}_{e,sen}$ is the evaporator sensible heat transfer, $\dot{Q}_{c,t}$ is the condenser total heat transfer and $\dot{W}$ is the electric power consumption of the compressor. The estimated parameters of the output variables are shown in Table 14.

Table 14. Estimated parameters of the refrigeration vapour compression model.

b_x	X_i	$\dot{Q}^*_{e,t}$ x10^3	$\dot{Q}^*_{e,sen}$ x10^3	$\dot{Q}^*_{c,t}$ x10^3	$\dot{W}^*$ x10^3	b_x	X_i	$\dot{Q}^*_{e,t}$ x10^3	$\dot{Q}^*_{e,sen}$ x10^3	$\dot{Q}^*_{c,t}$ x10^3	$\dot{W}^*$ x10^3
b_0	-	145.2	202.4	264.3	622.1	b_8	$\dot{V}^{*2}$	-185.2	-249.6	-89.8	221.3
b_1	$T_{e,i}$	-1.8	33.9	-1.7	-1.0	b_9	$T_{e,i}\cdot T_{c,i}$	0.1	-0.3	0.1	0.1
b_2	$T_{c,i}$	8.5	8.9	7.8	7.3	b_{10}	$T_{e,i}\cdot T_{wb,e,i}$	-0.7	2.3	-0.6	-0.3
b_3	$T_{wb,e,i}$	17.7	-35.5	16.4	11.8	b_{11}	$T_{e,i}\cdot \dot{V}^*$	3.6	57.6	2.8	0.2
b_4	$\dot{V}^*$	475.3	610.5	280.2	-345.7	b_{12}	$T_{c,i}\cdot T_{wb,e,i}$	-0.3	0.5	-0.2	0.1
b_5	$T_{e,i}^2$	0.2	-0.0	0.2	0.1	b_{13}	$T_{c,i}\cdot \dot{V}^*$	-0.3	-2.4	-1.2	-4.9
b_6	$T_{c,i}^2$	-0.2	-0.3	-0.1	0.3	b_{14}	$T_{wb,e,i}\cdot \dot{V}^*$	1.0	-49.7	0.2	-11.9
b_7	$T_{wb,e,i}^2$	0.8	-1.8	0.7	0.4	-	-	-	-	-	-

The nominal characteristics of the vapour compression system are summarized in Table 15.

Table 15. Nominal parameters of the refrigeration vapour compression system.

Parameters	Value	
$\dot{Q}_{e,t,N}$	23.06	[kW]
$\dot{Q}_{e,sen,N}$	13.00	[kW]
$\dot{Q}_{c,t,N}$	30.32	[kW]
$\dot{W}_N$	7.53	[kW]
$\dot{V}_N$	4600	[m^3 h^{-1}]

3.4.3.2 Heating coil with heat pump model

The heating coils of both systems studied, Figure 20 and Figure 21, were fed by a constant water flow, which was heated by an air-water heat pump. The thermal power exchanged by the heating coil was obtained by Eq. (13).

$$\dot{Q}_{HC} = \dot{V}_{a,i} \cdot \rho_{a,i} \cdot \left(h_{a,o} - h_{a,i}\right) \tag{13}$$

The selected air-water heat pump covered all the required sensible heat. This heat pump is fitted with a scroll inverter compressor. The technical characteristics of the heat pump were: a nominal heating capacity of 28.1 kW, a nominal electric power consumption 9.6 kW and a nominal COP of 2.93 [99].

In order to obtain the electric power consumption of the heat pump, the simplified experimental model obtained by the manufacturer was used [99]. The output variable of the model was the heating electrical input ratio, EIR, which is the inverse of COP. The estimate EIR value was calculated from Eq. (14), where EIR_N is its nominal value, EIR_T is a second order polynomial equation based on the outdoor air temperature and outlet water temperature, as shown in Eq. (4), and EIR_{PLF} is a third order polynomial based on the partial load factor, expressed by Eq. (12).

$$EIR = EIR_N \cdot EIR_T \cdot EIR_{PLF} \tag{14}$$

The estimated parameters of the estimate EIR value are shown in Table 16.

Table 16. Estimated parameters of the air-water heat pump model.

b_x	X_i	EIR_T x10^3	b_x	X_i	EIR_{PLF} x10^3
b_0	-	805.57	b_0	-	30.39
b_1	$T_{w,o}$	-4.20	b_1	PLF	1518.51
b_2	$T_{w,o}^2$	0.11	b_2	PLF^2	-1323.27
b_3	T_{OA}	-5.68	b_3	PLF^3	774.38
b_4	T_{OA}^2	0.11	-	-	-
b_5	$T_{w,o}{\cdot}T_{OA}$	-0.15	-	-	-

3.4.3.3 Sensible heat exchanger model

The IEC was used as a SHE when it was necessary to heat the process air stream and not to cool it, as was mentioned previously. For this reason, a cross flow sensible heat exchanger with both hot and cold sides unmixed, was modelled. The physical design characteristics of SHE were similar to those of the IEC. The effectiveness of the SHE at each time step was calculated by Eq. (15), where UA is the overall heat transfer coefficient of the exchanger, C_p is the capacity rate of air on primary side ($C_p = \dot{m}_p \cdot c_{p,p}$) and C_s is the capacity rate of air on secondary side ($C_s = \dot{m}_s \cdot c_{p,s}$). In this work, the effectiveness of the SHE was calculated for a fixed value of UA, given the inlet temperatures and air flow rates. The UA value of the cross-flow heat exchanger was measured experimentally for a wide range of input conditions, obtaining an average value of 1440 kJ h^{-1} K^{-1}.

$$\varepsilon = \frac{1 - \exp(-\frac{UA}{C_s} \cdot \left(1 + \frac{C_s}{C_p}\right))}{1 + \frac{C_s}{C_p}} \tag{15}$$

3.4.3.4 Filter

Filters were characterized by a constant pressure drop in the air circuit. Several filters with F8 or G4 protection were considered, as shown in Figure 20 and Figure 21. The pressure drop of these filters are shown in Table 17. However, the increase of their pressure drop due to dust accumulation was not considered.

3.4.3.5 Fan model

The fans were sized to maintain the design air flow rate given the estimated system pressure drop. The air pressure drop of each component is shown in Table

17. The fans were modelled using manufacturer data from Sodeca QuickFan software [101]. Three centrifugal fans were selected for the conventional HVAC system and another three for the hybrid HVAC system, as shown in Figure 20 and Figure 21. The return and exhaust fans of the conventional HVAC systems were the same. These fans were also the same for the hybrid HVAC systems, but different from those of the conventional HVAC system. The estimated parameters of the fan models are shown in

Table 18, where the output variables were static pressure, P, and electric power consumption of the fans, $\dot{W}$. The relationship between the output and input variables was expressed by second order polynomials, according to Eq. (4).

Table 17. Pressure drop of each component for the systems analysed.

Component	Pressure drop [Pa]
Desiccant wheel (process side)	350
Desiccant wheel (regeneration side)	380
Indirect evaporative cooler (primary and secondary sides)	146
Evaporator	40
Condenser	27
Heating coil	35
Air box with dampers	40
Filter (G4 protection)	60
Filter (F8 protection)	100
Air duct	40

Table 18. Estimated parameters of the fan models.

	Conventional HVAC system				Hybrid HVAC system			
	Fan1		Fan2 and Fan3		Fan1		Fan2 and Fan3	
b_x X_i	P x10^3 [mmca]	$\dot{W}$ x10^3 [kW]	P x10^3 [mmca]	$\dot{W}$ x10^3 [kW]	P x10^3 [mmca]	$\dot{W}$ x10^3 [kW]	P x10^3 [mmca]	$\dot{W}$ x10^3 [kW]
b_0 -	35478.6	339.9	8824.7	162.2	191371	463.03	76510.9	194.7
b_1 $\dot{V}$	11.653	0.057	14.669	0.039	77.617	0.522	- 4.768	0.192
b_2 $\dot{V}^2$	0.004	-	- 0.004	-	-0.077	-	- 0.005	-

3.4.4 Climate zones

The performance of the conventional and hybrid HVAC systems under several climatic conditions was evaluated according to ASHRAE climate classification [102]. This classification consists of 8 climate zones, depending on the cooling degrees-day, CDD, and heating degrees-day, HDD. In this study, both systems were simulated for the climate zones 1 to 6, from very hot to cold. Climate zones 7 and 8, very cold and subarctic, respectively, were not used in this study because they are very dry, and therefore, do not require a dehumidification system. The simulations were performed using the Meteonorm weather data library [103]. One city from each of the 6 selected climate zones was chosen, see Table 19. A world representation of the different climate zones with the selected cities is shown in Figure 23.

Table 19. Selected cities from each of the climate zone defined by ASHRAE.

Climate zone[a]	City	Thermal criteria[b] [ºC]
1	Singapore	5000 < CDD
2	Taipei	3500 < CDD ≤ 5000
3	Tunis	CDD ≤ 2500 and HDD ≤ 2000
4	Barcelona	CDD ≤ 2500 and HDD ≤ 3000
5	Budapest	3000 < HDD≤ 4000
6	Ottawa	4000 < HDD ≤ 5000

[a] 1- Very hot, 2- hot, 3- warm, 4- mixed, 5- cool, 6- cold
[b] T_{base}= 10ºC for CDD; T_{base}= 18ºC for HDD

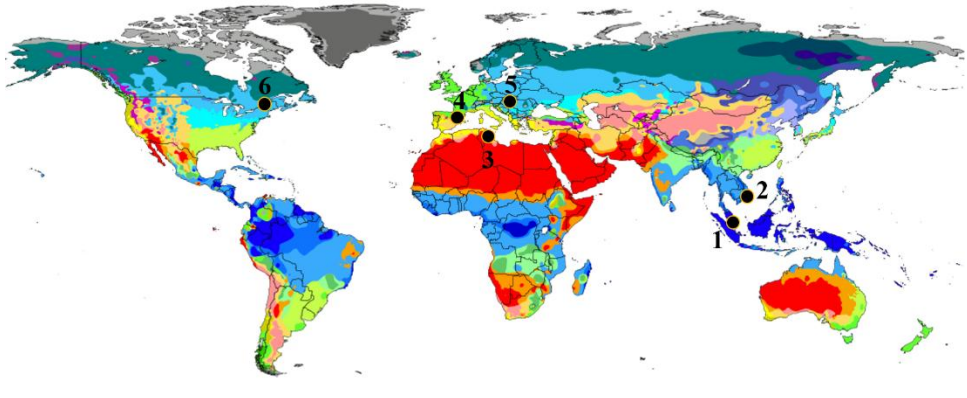

Figure 23. World representation of the different climate zones with the selected cities.

3.4.5 Energy simulation

Several detailed energy simulations were carried out with the assumption that both HVAC systems served a spa with high latent loads. All the energy simulations were carried out with the TRNSYS 17 software [100], using a time step of 15 minutes. The control system of the hybrid HVAC system, described in section 3.4.1.3.1, was used in these energy simulations. The simulations were performed for the selected six climate zones throughout the whole year.

The conventional and hybrid HVAC systems were evaluated according to the parameters: SCOP and E_{cons}. The seasonal mean coefficient of performance, SCOP, is defined as the ratio between the sensible and latent energy delivered, $\dot{Q}_{sen}$ and $\dot{Q}_{lat}$, respectively, and the electric power consumption, $\dot{W}$, expressed by Eq. (16). The energy consumption per unit of dehumidified water, E_{cons}, is the ratio between $\dot{W}$ and MRC, expressed by Eq. (17). E_{cons} was calculated only when the HVAC system was in dehumidification mode, i.e. when air dehumidification was demanded by the system.

$$SCOP = \frac{\int \left(\dot{Q}_{sen} + \dot{Q}_{lat}\right) dt}{\int \dot{W}\, dt} \tag{16}$$

$$E_{cons} = \frac{\int \dot{W}\, dt}{\int MRC\, dt} \tag{17}$$

Chapter 4

Experimental analysis of a desiccant wheel activated at low temperatures

In this chapter, five empirical and two numerical case studies on a DW were carried. The influential input variables on output variables, the behaviour of the DW activated at low regeneration temperatures and several simplified models were obtained following the DOE methodology. A latent heat control strategy was also analysed using the variable air flow rates and the air regeneration temperature. Papers I and II and Congress II and IV, shown in appendices A, B, F and H, respectively, address the results of this chapter.

A previous study on the feasibility of using the DOE technique to analyse the global behaviour of a DW was performed, see Appendix F. Satisfactory results were obtained compared to other methodologies used in the literature [38,39]. Another previous study on the regeneration temperature of DW was carried out, see Appendix H. The purpose of this was to empirically determine the moisture removal capacity, MRC, of a DW activated at low and high temperatures. Using high regeneration temperatures, the MRC values were found 61% higher than using low regeneration temperatures. Nevertheless, with low temperatures MRC acceptable values were achieved compared to MRC nominal value, see Table 1. Moreover, the DW activated at high temperature required higher cooling energy, due to the high air process outlet temperatures derived from the higher heat rejection in the adsorption process.

4.1 DW statistical analysis

Four case studies were performed using the DOE statistical technique, case studies 1, 2, 3 and 4, shown in Figure 11. The input variables set in each case study are shown in Tables 6, 7 and 8 of Appendix A for case studies 1, 2 and 3, respectively, and in Table 6 of Appendix B for case 4. The test rig described in section 3.2.1.1 was used to carry out the four cases. The results of the analyses of variance, ANOVA, for the four case studies are summarized in Table 20-Table 23. These tables show each of the main estimated effects, the standard error of each of the effects, the statistical parameter F-Ratio, and the statistical parameter P-value. All variables were found significant at 95% confidence level, as the P-values were lower than 0.05 in all cases. Therefore, a variation of the output variables with the input variables was expected. The designs were found to be suitable for the observed data at 95% confidence level, as the P-values for lack-of-fit tests were greater than 0.05 in all cases.

The results for case studies 1, 2 and 3, cases where the DW operated with balanced air flow rates, showed that the most influential variables on $T_{p,o}$, ordered from most to least influential, were: $T_{r,i}$, $T_{p,i}$, $\omega_{r,i}$, and $\omega_{p,i}$, as a result of the parameter F-Ratio, see Table 20-Table 22. Regarding $\omega_{p,o}$, the most influential variables, ordered from most to least influential, were: $\omega_{p,i}$, $\omega_{r,i}$, $T_{r,i}$, and $T_{p,i}$, as a result of the parameter F-ratio. This suggested that, if extremely dry process air outlet conditions were necessary, $\omega_{r,i}$ should not be very high, and if low temperature air outlet conditions were necessary, $T_{r,i}$ should not be high.

Table 20. Effects of input variables on output variables of the desiccant wheel for case study 1.

Case study 1								
	$T_{p,o}$				$\omega_{p,o}$			
Effect	Estimate	Stnd. Error	F-Ratio	P-value	Estimate	Stnd. Error	F-Ratio	P-value
Average	29.96	0.12			14.21	0.05		
$T_{p,i}$	4.05	0.28	594.24	0.0017	-0.69	0.17	22.12	0.0450
$\omega_{p,i}$	1.44	0.23	38.74	0.0249	7.64	0.16	2326.64	0.0004
$T_{r,i}$	6.87	0.12	997.45	0.0010	0.78	0.1	23.20	0.0405
$\omega_{r,i}$	-1.81	0.12	198.85	0.0050	1.58	0.1	248.43	0.0040
Lack-of-fit				0.1020				0.0970
	R^2=98.77				R^2=98.56			

In case study 2, the specific mass air flow rate, Ω, was also analysed, which was influential on the output variables, see Table 21. However, to achieve greater dehumidification with a DW with balanced air flow rates, the specific mass air flow rates were less influential than the inlet process and regeneration air temperatures and humidity ratios, according to the parameter F-Ratio.

Table 21. Effects of input variables on output variables of the desiccant wheel for case study 2.

Case study 2								
	$T_{p,o}$				$\omega_{p,o}$			
Effect	Estimate	Stnd. Error	F-Ratio	Effect	Estimate	Stnd. Error	F-Ratio	Effect
Average	31.33	0.04			14.64	0.04		
$T_{p,i}$	4.53	0.08	4542.12	0.0002	-1.01	0.08	161.79	0.0061
$\omega_{p,i}$	1.96	0.07	1935.40	0.0006	7.64	0.07	11789.5	0.0001
$T_{r,i}$	5.89	0.04	13011.2	0.0001	1.08	0.04	688.45	0.0014
$\omega_{r,i}$	-2.01	0.04	2559.92	0.0004	1.88	0.04	2357.63	0.0004
Ω	-1.45	0.04	744.94	0.0013	0.24	0.04	40.54	0.0238
Lack-of-fit				0.0720				0.1020
	R^2=97.46				R^2=95.14			

Table 22. Effects of input variables on output variables of the desiccant wheel for case study 3.

Case study 3								
	$T_{p,o}$				$\omega_{p,o}$			
Effect	Estimate	Stnd. Error	F-Ratio	Effect	Estimate	Stnd. Error	F-Ratio	Effect
Average	29.47	0.07			14.97	0.07		
$T_{p,i}$	2.99	0.49	203.35	0.0049	-1.51	0.19	99.48	0.0099
$\omega_{p,i}$	1.24	0.23	29.31	0.0325	3.75	0.10	1416.55	0.0007
$T_{r,i}$	7.05	0.17	310.53	0.0032	1.98	0.12	170.63	0.0058
$\omega_{r,i}$	-1.78	0.17	110.22	0.0090	2.36	0.12	417.13	0.0024
Lack-of-fit				0.0850				0.0990
	R^2=98.68				R^2=96.62			

The results of case study 4, case where the DW operated with unbalanced air flow rates, showed that the most influential variables on $T'_{p,o}$ were $T_{p,i}$, $T_{r,i}$ and $\Omega_{p,i}$, and on $\omega'_{p,o}$ were $\omega_{p,i}$, $\Omega_{p,i}$, and $\omega_{r,i}$, see Table 23. These results suggested that if a fine tuning of outlet process air conditions was necessary, $\Omega_{p,i}$ should be controlled, opposed to those obtained in case study 2, see Table 21, where the influence of the air flow rate presented low.

Table 23. Effects of input variables on output variables of the desiccant wheel for case study 4.

Case study 4								
	$T'_{p,o}$				$\omega'_{p,o}$			
Effect	Estimate	Stnd. Error	F-Ratio	Effect	Estimate	Stnd. Error	F-Ratio	Effect
Average	30.37	0.09			13.27	0.17		
$T_{p,i}$	6.12	0.35	299.24	0.0000	3.04	0.63	23.07	0.0049
$\omega_{p,i}$	2.46	0.36	46.21	0.0010	5.44	0.65	70.06	0.0004
$T_{r,i}$	3.54	0.21	281.66	0.0000	-1.12	0.38	8.95	0.0304
$\omega_{r,i}$	-1.39	0.21	43.66	0.0012	1.81	0.38	23.14	0.0048
$\Omega_{p,i}$	1.85	0.21	77.37	0.0003	-2.60	0.38	47.71	0.0010
Lack-of-fit				0.0600				0.0590
	R^2=98.23%				R^2=95.54%			

The R^2 values for the four DOE are also presented in Table 20-Table 23. R^2 values obtained were always greater than 97.4% for outlet temperature and 95.1% for outlet humidity ratio. Lower R^2 values, 97% for $T_{p,o}$ and 95% for $\omega_{p,o}$, were obtained in a widely used simplified model to study the behaviour of the DW with balanced air flow rates [39]. Modifications of this model were carried out to work with unbalanced air flow rates [40]. However, model accuracy decreased, with R^2 values equal to 90% for $T'_{p,o}$ and 92% for $\omega'_{p,o}$ [40].

Based on these results, designs of experiments at 2-levels, as factorial design, could be sufficiently precise to study the behaviour of a DW. However, previous studies showed nonlinear trend in the adsorption process when the input variables of DW were varied [97]. The designs at 3-levels, used in case studies 3 and 4, could allow to study nonlinear processes [44].

4.2 DW behaviour analysis

The effects of the input variables on the output variables were analysed, in order to obtain a deeper understanding of the behaviour of the air outlet conditions in a DW operated with balanced and unbalanced air flow rates. Case study 3 was used to analyse the DW with balanced air flow rates and case study 4 to analyse the DW with unbalanced air flow rates.

4.2.1 DW with balanced air flow rates

The main effects of the input variables on the output variables when the DW operated with balanced air flow rates are shown in Figure 24. It can be observed that $T_{p,o}$ increased as $T_{p,i}$, $\omega_{p,i}$ and $T_{r,i}$ increased. However, an increase of $\omega_{r,i}$ caused the opposite effect. It was also observed that an increase of $T_{p,i}$, $\omega_{p,i}$ and $\omega_{r,i}$, produced an increase of the value of $\omega_{p,o}$. The opposite was true for variable $T_{r,i}$. Similar results were obtained in previous studies [7,97].

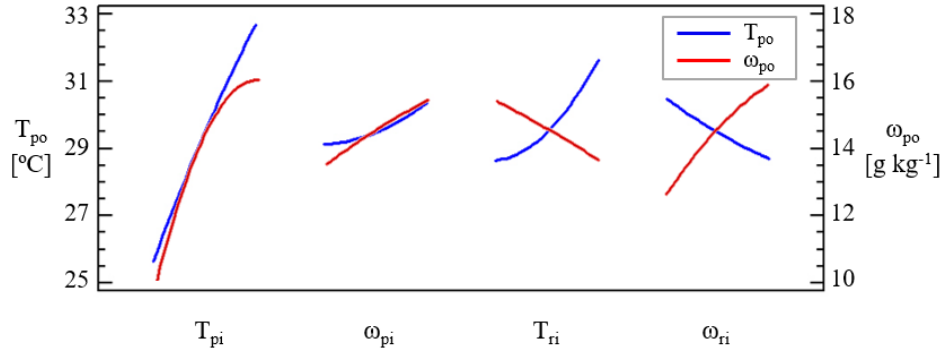

Figure 24. Trends of the main effects of the desiccant wheel for the temperature and humidity ratio of the process outlet air-stream for case study 3.

The cross effects of two input variables on each of the output variables were analysed. Four response surfaces and contour line plots for $T_{p,o}$ and $\omega_{p,o}$ are represented in Figure 25. First, $T_{p,i}$ and $\omega_{p,i}$ were considered variables and $T_{r,i}$ and $\omega_{r,i}$ were fixed at constant values of 40°C and 15 g kg^{-1}, respectively, see Figure 25a and Figure 25b. The trends of the treated air by the DW were similar for different values of $T_{r,i}$ and $\omega_{r,i}$. It can be observed that $T_{p,o}$ increased as $T_{p,i}$ was increased, when $\omega_{p,i}$ remained constant. For example, an increase of approximately 1.5 ºC for $T_{p,i}$, yielded an increase of 1 ºC for $T_{p,o}$. However, $T_{p,o}$ values exhibited

a minimal variation with $\omega_{p,i}$, representing low gradient, when $T_{p,i}$ remained constant, see Figure 25a. Regarding $\omega_{p,o}$, low values of $T_{p,i}$ and $\omega_{p,i}$ were achieved when the inlet air was near saturation. As $\omega_{p,i}$ was higher, $\omega_{p,o}$, increased when $T_{p,i}$ remained constant, see Figure 25b.

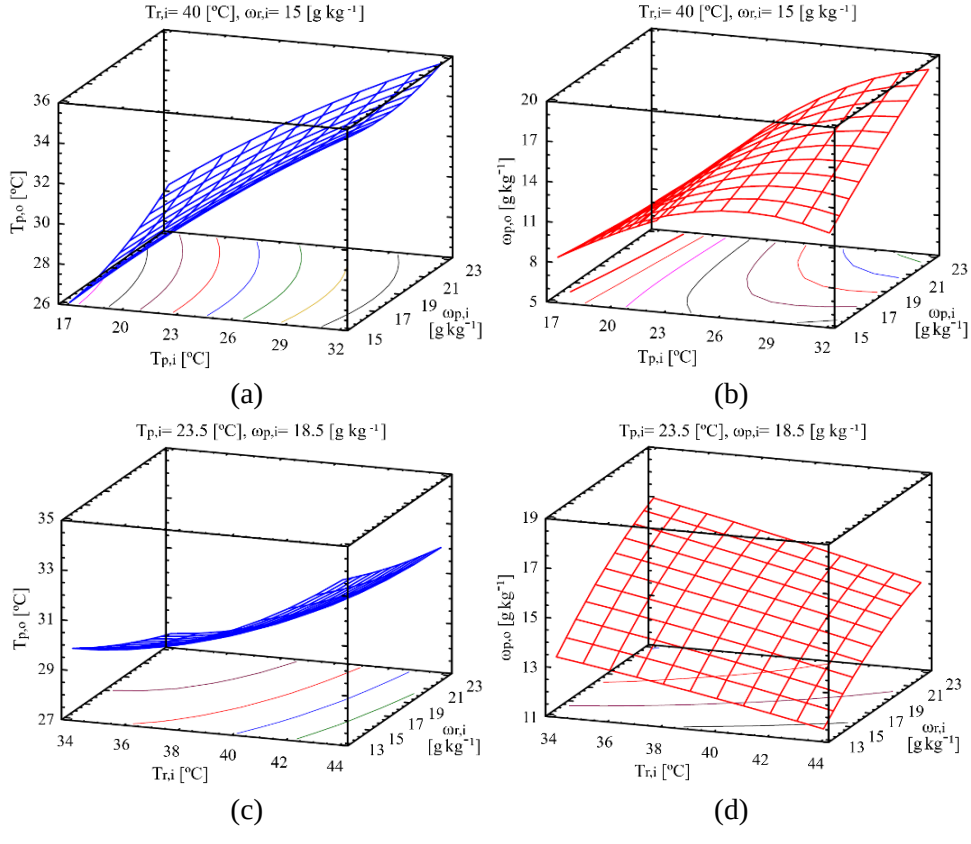

Figure 25. Response surfaces and contour line plots for case study 3 (a) $T_{p,o}$ on $T_{p,i}$ and $\omega_{p,i}$, (b) $\omega_{p,o}$ on $T_{p,i}$ and $\omega_{p,i}$, (c) $T_{p,o}$ on $T_{r,i}$ and $\omega_{r,i}$, (d) $\omega_{p,o}$ on $T_{r,i}$ and $\omega_{r,i}$.

Figure 25c and Figure 25d shows the response surfaces and contour line plots for $T_{p,o}$ and $\omega_{p,o}$ when $T_{r,i}$ and $\omega_{r,i}$ were variables and $T_{p,i}$ and $\omega_{p,i}$ were fixed at constant values of 23.5°C and 18.5 g kg^{-1}, respectively. The trends of the treated air by the DW were similar for different values of $T_{p,i}$ and $\omega_{p,i}$. Regarding $T_{p,o}$, significant dependence on $T_{r,i}$ was observed, as a portion of regeneration heat was transferred to the air flow process stream, see Figure 25c. However, the influence was reduced as $T_{r,i}$ decreased. Conversely, the influence of $\omega_{r,i}$ on the output

variable, $T_{p,o}$ was weak, see Figure 25c. The effect on $\omega_{p,o}$ was quite predictable. An increase of $T_{r,i}$ and a decrease of $\omega_{r,i}$ resulted in a decrease of $\omega_{p,o}$, see Figure 25d. This effect was discussed in section 4.1.

4.2.2 DW with unbalanced air flow rates

The trends of the main effects on the output variables when the DW operated with unbalanced air flow rates are shown in Figure 26, corresponding to case study 4. It can be observed that $T'_{p,o}$ increased as $T_{p,i}$, $\omega_{p,i}$, $T_{r,i}$ and $\Omega_{p,i}$ increased and $\omega_{r,i}$ decreased. Regarding $\omega'_{p,o}$, its value increased as $T_{p,i}$, $\omega_{p,i}$ and $\omega_{r,i}$ increased. The opposite was true for variables $T_{r,i}$ and $\Omega_{p,i}$. Similar trends of the output variables with regard to $T_{p,i}$, $\omega_{p,i}$, $T_{r,i}$ and $\omega_{r,i}$ were obtained when the DW operated with balanced air flow rates, see Figure 24. However, inverse trends of the output process variables with regard to $\Omega_{p,i}$ were achieved in previous studies, where $\omega'_{p,o}$ values increased [7] and $T'_{p,o}$ values decreased [97], as process air flow rates were increased. These trends are caused by the fact that the outlet process air conditions of the current DW system, were mixed with the bypass air flow and also, the regeneration and process air flow rates were unbalanced.

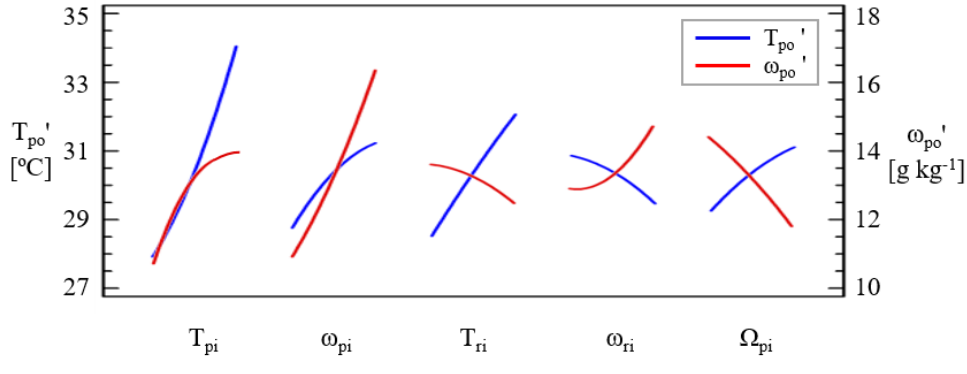

Figure 26. Trends of the main effects of the desiccant wheel for the temperature and humidity ratio of the mixed process outlet air-stream for case study 4.

The effects of interaction between $T_{r,i}$ and $\Omega_{p,i}$, and $T'_{p,o}$ and $\omega'_{p,o}$, were studied for three levels of $T_{r,i}$ and three levels of $\Omega_{p,i}$, in order to find the relationships between $T_{r,i}$ and $\Omega_{p,i}$ on the outlet process air conditions. Both effects are represented in Figure 27. Low increments of $T'_{p,o}$ can be observed when $\Omega_{p,i}$ was increased and $T_{r,i}$ was fixed at a constant value, see Figure 27a. For example,

an increase of $\Omega_{p,i}$ from 13.45 kg s^{-1} m^{-3} to 17.48 kg s^{-1} m^{-3}, and $T_{r,i}$=34 ºC, yielded a lower increase of 1 ºC for $T'_{p,o}$. With respect to $\omega'_{p,o}$, it can be observed that this output variable increased when $\Omega_{p,i}$ decreased and $T_{r,i}$ was fixed at a constant value, see Figure 27a. An increment of 1.4 g kg^{-1} for $\omega'_{p,o}$ was achieved when $\Omega_{p,i}$ decreased from 17.48 kg s^{-1} m^{-3} to 21.51 kg s^{-1} m^{-3}, and $T_{r,i}$=34 ºC.

Greater increments of $T'_{p,o}$ were obtained when $T_{r,i}$ was increased and $\Omega_{p,i}$ was fixed at a constant value, see Figure 27b. A rise of approximately 2 ºC of $T'_{p,o}$ was achieved for each level of $T_{r,i}$ and $\Omega_{p,i}$= 13.45 kg s^{-1} m^{-3}. Regarding $\omega'_{p,o}$, lower increments of this output variable were found after fixing the $\Omega_{p,i}$ at a constant value and varying $T_{r,i}$, see Figure 27b. For example, an increase of $T_{r,i}$ from 38.25 ºC to 42.5 ºC, and $\Omega_{p,i}$=13.45 kg s^{-1} m^{-3}, yielded a lower increase of 1 g kg^{-1} for $\omega'_{p,o}$. The maximum and minimum values of $T'_{p,o}$ achieved were 35.5 ºC and 29.8 ºC, respectively, and the maximum and minimum values of $\omega'_{p,o}$ achieved were 15.4 g kg^{-1} and 11.3 g kg^{-1}, respectively. Similar trends of $T'_{p,o}$ and $\omega'_{p,o}$ on $T_{r,i}$ and $\Omega_{p,i}$ were obtained for different values of $T_{p,i}$, $\omega_{p,i}$ and $\omega_{r,i}$.

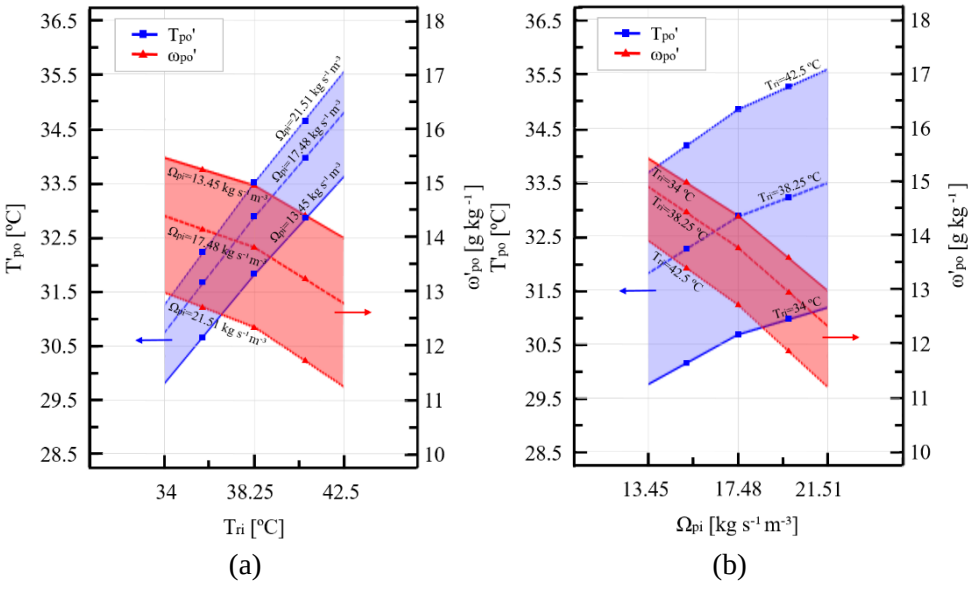

Figure 27. Relations of (a) $T_{r,i}$ on $T'_{p,o}$ and $\omega'_{p,o}$, and (b) $\Omega_{p,i}$ on $T'_{p,o}$ and $\omega'_{p,o}$, for case study 4.

These results suggested that the influence of $\Omega_{p,i}$ on $T'_{p,o}$ was less than that of $T_{r,i}$. Also, the influence of $T_{r,i}$ on $\omega'_{p,o}$ was less than that of $\Omega_{p,i}$. Therefore, a wider

range of outlet process air conditions can be achieved if the outlet air temperature, $T'_{p,o}$, is controlled by the inlet air regeneration temperature, $T_{r,i}$, and the outlet air humidity ratio, $\omega'_{p,o}$, is controlled by the process specific mass air flow rate, $\Omega_{p,i}$. This strategy can be used to ensure independent control of outlet air temperature and humidity ratio.

4.3 Simplified DW models

Four new empirical simplified models were developed to predict the behaviour of the air outlet conditions of the DW. The relationships between the input variables and output variables, $T_{p,o}$, $\omega_{p,o}$, $T'_{p,o}$ and $\omega'_{p,o}$, were expressed by Eqs. (3) and (4). The corresponding estimated parameters are shown in Table 24, where X_i are linear variables, quadratic variables or their interactions, $b_1 \ldots b_{20}$ are the regression coefficients, showing the weight each one has in the equation, and b_0 is the average response in the design of experiments. Case study 2 was tested for balanced specific mass air flow, therefore, the input variable Ω corresponds to the specific mass air flow process, Ω_p, and the specific mass air flow regeneration, Ω_r.

Table 24. Estimated parameters of the desiccant wheel empirical models.

b_x	Case study 1			Case study 2		
	X_i	$T_{p,o}x10^3$ [ºC]	$\omega_{p,o}x10^3$ [g kg^{-1}]	X_i	$T_{p,o}x10^3$ [ºC]	$\omega_{p,o}x10^3$ [g kg^{-1}]
b_0	-	6081.84	-16707.70	-	9012.70	-4828.58
b_1	$T_{p,i}$	328.15	144.14	$T_{p,i}$	-25.41	-16.01
b_2	$\omega_{p,i}$	-400.65	1786.87	$\omega_{p,i}$	23.17	1783.16
b_3	$T_{r,i}$	438.02	82.74	$T_{r,i}$	543.06	-189.88
b_4	$\omega_{r,i}$	-49.42	505.68	$\omega_{r,i}$	-291.07	485.12
b_5	$T_{p,i} \cdot \omega_{p,i}$	8.64	-19.08	Ω	-26.53	-337.70
b_6	$T_{p,i} \cdot T_{r,i}$	3.49	3.80	$T_{p,i} \cdot \omega_{p,i}$	6.38	-7.31
b_7	$T_{p,i} \cdot \omega_{r,i}$	-1.91	2.16	$T_{p,i} \cdot T_{r,i}$	7.34	7.44
b_8	$\omega_{p,i} \cdot T_{r,i}$	4.62	-6.52	$T_{p,i} \cdot \omega_{r,i}$	-2.36	8.74
b_9	$\omega_{p,i} \cdot \omega_{r,i}$	9.73	-13.22	$T_{p,i} \cdot \Omega$	8.41	-8.42
b_{10}	$T_{r,i} \cdot \omega_{r,i}$	-6.78	-4.24	$\omega_{p,i} \cdot T_{r,i}$	-0.21	-20.09
b_{11}	-	-	-	$\omega_{p,i} \cdot \omega_{r,i}$	4.78	-11.79
b_{12}	-	-	-	$\omega_{p,i} \cdot \Omega$	3.04	6.25
b_{13}	-	-	-	$T_{r,i} \cdot \omega_{r,i}$	-0.51	-4.71
b_{14}	-	-	-	$T_{r,i} \cdot \Omega$	-7.56	14.04
b_{15}	-	-	-	$\omega_{r,i} \cdot \Omega$	3.31	-5.11

b_x	Case study 3			Case study 4		
	X_i	$T_{p,o}x10^3$ [ºC]	$\omega_{p,o}x10^3$ [g kg^{-1}]	X_i	$T'_{p,o}x10^3$ [ºC]	$\omega'_{p,o}x10^3$ [g kg^{-1}]
b_0	-	93985.40	-9448.80	-	-6736.67	-15366.80
b_1	$T_{p,i}$	-177.97	1277.70	$T_{p,i}$	72.10	1277.57
b_2	$\omega_{p,i}$	-392.09	-1217.59	$\omega_{p,i}$	772.28	-785.18
b_3	$T_{r,i}$	-3168.40	82.29	$T_{r,i}$	410.38	1310.33
b_4	$\omega_{r,i}$	-1361.45	1188.94	$\omega_{r,i}$	224.17	-916.88
b_5	$T_{p,i}^2$	-8.35	-44.00	$\Omega_{p,i}$	357.36	-94.71
b_6	$T_{p,i}\cdot\omega_{p,i}$	-17.27	78.95	$T_{p,i}^2$	16.58	-28.38
b_7	$T_{p,i}\cdot T_{r,i}$	28.64	9.202	$T_{p,i}\cdot\omega_{p,i}$	-14.35	29.84
b_8	$T_{p,i}\cdot\omega_{r,i}$	21.52	-28.54	$T_{p,i}\cdot T_{r,i}$	7.35	-10.61
b_9	$\omega_{p,i}^2$	30.12	-10.47	$T_{p,i}\cdot\omega_{r,i}$	-12.93	6.35
b_{10}	$\omega_{p,i}\cdot T_{r,i}$	-8.06	-11.85	$T_{p,i}\cdot\Omega_{p,i}$	-8.71	5.89
b_{11}	$\omega_{p,i}\cdot\omega_{r,i}$	11.17	29.96	$\omega_{p,i}^2$	-17.23	16.76
b_{12}	T_{ri}^2	37.53	-2.63	$\omega_{p,i}\cdot T_{r,i}$	-1.49	-2.23
b_{13}	$T_{r,i}\cdot\omega_{r,i}$	7.06	-5.08	$\omega_{p,i}\cdot\omega_{r,i}$	5.65	16.84
b_{14}	$\omega_{r,i}^2$	5.39	-14.74	$\omega_{p,i}\cdot\Omega_{p,i}$	20.50	-6.79
b_{15}	-	-	-	T_{ri}^2	-5.09	-11.90
b_{16}	-	-	-	$T_{r,i}\cdot\omega_{r,i}$	7.31	-10.40
b_{17}	-	-	-	$T_{r,i}\cdot\Omega_{p,i}$	6.71	-3.50
b_{18}	-	-	-	$\omega_{r,i}^2$	-9.72	24.41
b_{19}	-	-	-	$\omega_{r,i}\cdot\Omega_{p,i}$	-5.49	11.88
b_{20}	-	-	-	$\Omega_{p,i}^2$	-12.17	-9.44

4.4 Analysis of DW control strategy

Three empirical and numerical case studies were carried out in this work, case studies 5, 6 and 7, shown in Figure 11, in order to obtain a strategy to control latent heat of the air process of a DW activated at low temperatures when $\Omega_{p,i}$ and $T_{r,i}$ were varied. The parameters MRC and SHR were also analysed in case studies 5 and 6.

4.4.1 Analysis of experimental case study 5

Experimental tests were carried out to analyse the variation of outlet process air conditions in a DW controlling $T_{r,i}$ and $\Omega_{p,i}$. The results of the outlet process air conditions of the DW for case study 5 are shown in Figure 28. States 1 to 3 show the outlet air states when $T_{r,i}$ was varied from 34 ºC to 42.5 ºC, and the remaining input variables were fixed at constant values, see Figure 28a. States 3 to 5 show the outlet air states when $\Omega_{p,i}$ was varied from 21.51 kg s^{-1} m^{-3} to 13.45 kg s^{-1} m^{-3}, and

the remaining input variables were fixed at constant values, see Figure 28a. These outlet process air states are shown in Table 25. It can be observed that $T'_{p,o}$ increased and $\omega'_{p,o}$ decreased when $T_{r,i}$ and $\Omega_{p,i}$ were increased, although different slopes were obtained.

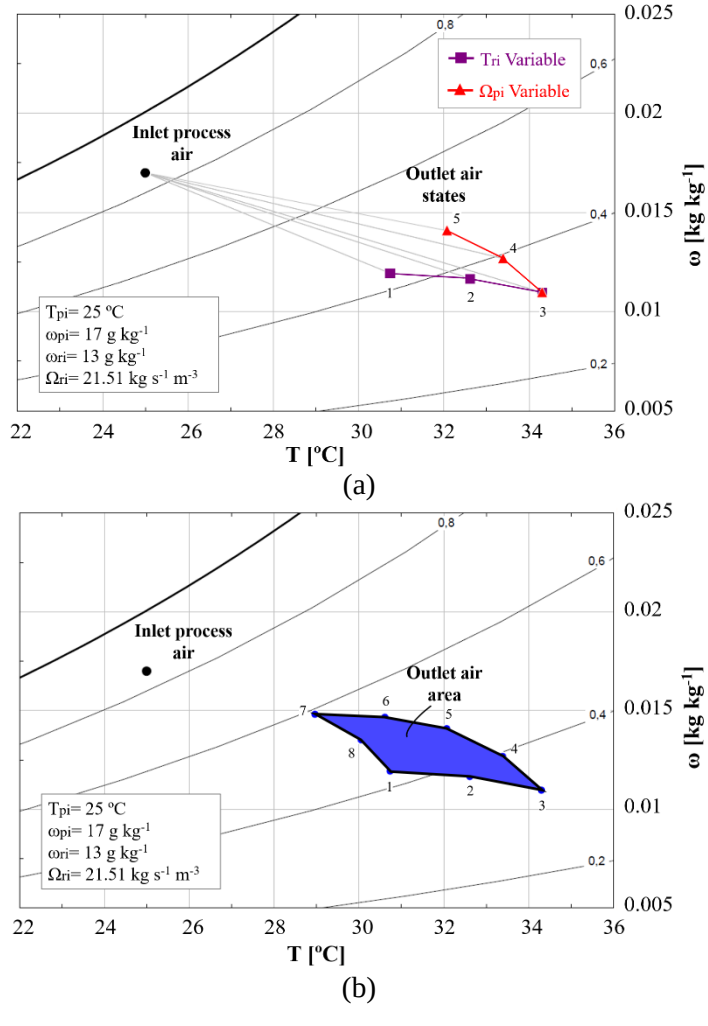

Figure 28. Outlet process air conditions for case study 5 when $T_{r,i}$ and $\Omega_{p,i}$ were varied, (a) outlet air states, (b) outlet air area.

The combination between the values of $T_{r,i}$ and $\Omega_{p,i}$ defined in Table 7 of Appendix B, resulted in an area of outlet process air, see Figure 28b. The area

obtained is equal to 8.26 ºC g kg^{-1}. Any air state within the shaded area can be obtained by setting the $T_{r,i}$ and $\Omega_{p,i}$ values in the specified range and fixing $T_{p,i}$, $\omega_{p,i}$, $\omega_{r,i}$ and $\Omega_{r,i}$ at constant values. The variations of the outlet air process temperature and humidity ratio from a fixed inlet state were 5.33 ºC and 3.85 g kg^{-1}, respectively, see Table 25. These results show that this strategy allows the outlet process air conditions to be controlled in a DW setting $T_{r,i}$ and $\Omega_{p,i}$. Similar results can be obtained experimentally from different inlet process air states. In general, it is possible to vary the outlet process air conditions in a DW activated at low temperatures controlling $T_{r,i}$ and $\Omega_{p,i}$.

Table 25. Outlet process air conditions and MRC and SHR values obtained for case study 5.

N	$T'_{p,o}$ [ºC]	$\omega'_{p,o}$ [g kg^{-1}]	MRC [kg h^{-1}]	SHR
1	30.74	11.93	9.37	0.70
2	32.61	11.66	9.81	0.68
3	34.30	10.97	11.04	0.64
4	33.38	12.68	7.92	0.74
5	32.07	14.09	5.36	0.82
6	30.61	14.67	4.31	0.86
7	28.97	14.82	4.06	0.87
8	30.05	13.53	6.43	0.79

4.4.2 Analysis of numerical case study 6

The empirical model developed with case study 4 was used to analyse the variation of outlet process air conditions in the DW system for five inlet air states, states P1-P5. First, the outlet process air conditions were studied when $T_{r,i}$ and $\omega_{r,i}$ were varied. The combination of these two input variables are shown in Table 8 of Appendix B. $\Omega_{p,i}$ and $\Omega_{r,i}$ were fixed at a constant value, 21.51 kg s^{-1} m^{-3}. The results of the outlet process air conditions are represented in Figure 29. States P1 to P5 indicate the inlet process air conditions and the lines represent the outlet process air states. Three outlet process air lines for each inlet air state were obtained by varying $\omega_{r,i}$, and three outlet process air states were obtained in each outlet process air line by varying $T_{r,i}$. Therefore, a decoupling of the outlet air process temperature and humidity was not completely achieved. Regarding $\omega_{r,i}$, $\omega'_{p,o}$ values were increased and $T'_{p,o}$ values were reduced when $\omega_{r,i}$ increased. These results were in agreement

with those in section 4.1, if extremely dry outlet process air conditions were necessary, $\omega_{r,i}$ should not be very high.

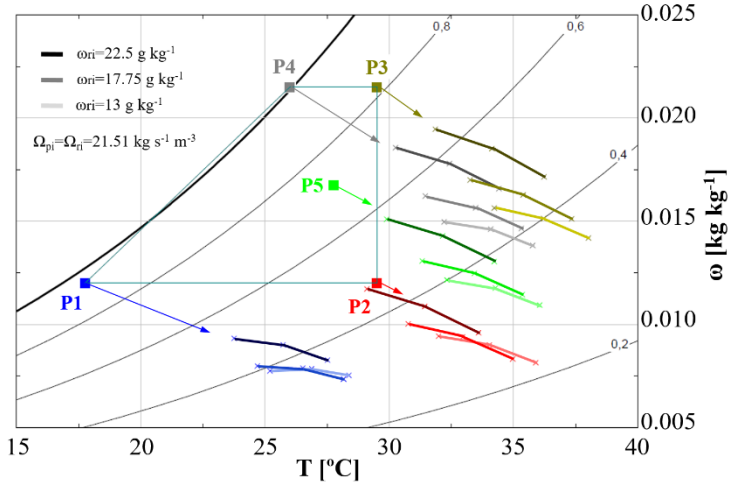

Figure 29. Outlet process air conditions when $T_{r,i}$ and $\omega_{r,i}$ were modified for case study 6.

Second, in this case study, the outlet process air conditions were analysed when $T_{r,i}$, $\Omega_{p,i}$ and $\omega_{r,i}$ were varied. The combination of these three input variables is shown in Table 8 of Appendix B. The results of the outlet process air conditions are represented in Figure 30. Three outlet process air areas were obtained for each inlet process air state by varying $\omega_{r,i}$. The decoupling of the temperature and humidity is shown by setting the $T_{r,i}$ and $\Omega_{p,i}$. Area values obtained from the contour of the outlet process air states, for each inlet process air state, P1-P5, are shown in Table 26. It can be observed that the greatest areas were achieved for inlet process air states with low $\omega_{p,i}$ values, states P1 and P2. The areas were reduced when $\omega_{p,i}$ increased, from states P1 and P2 to states P3 and P4, and the inlet process air conditions are located away from the saturation conditions, states P4 to P3 or states P1 to P2. Furthermore, the areas were reduced for all inlet process air states when $\omega_{r,i}$ increased, from 13 to 22.5 g kg^{-1}, see Table 26.

Regarding the outlet process air area of state P2 with $\omega_{r,i}$=22.5 g kg^{-1}, some outlet process air states with lower $T'_{p,o}$ values and higher $\omega'_{p,o}$ values than the inlet air state, P2, were achieved, see Figure 30. The proximity of $T_{p,i}$ to $T_{r,i}$, and the relative high $\omega_{r,i}$ values compared to the $\omega_{p,i}$ values, caused this process.

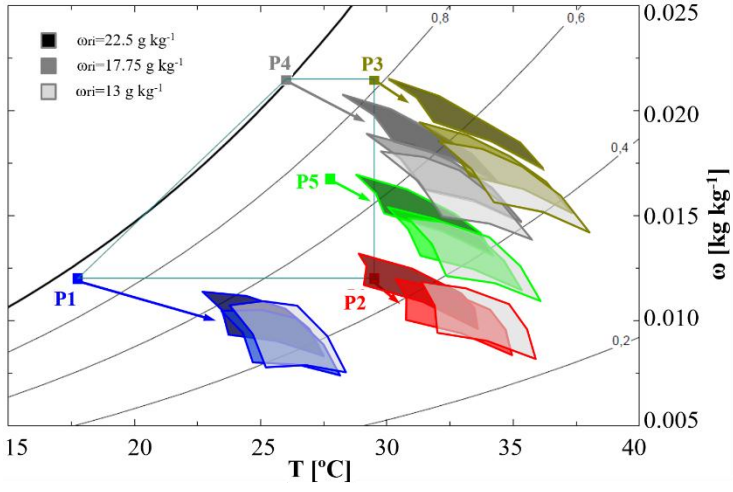

Figure 30. Outlet process air conditions when $T_{r,i}$, $\Omega_{p,i}$ and $\omega_{r,i}$ were modified for case study 6.

Table 26. Output area values of each inlet process air state, P1-P5, for case study 6.

$\omega_{r,i}$ [g kg^{-1}]	P1 Area [ºC g kg^{-1}]	P2 Area [ºC g kg^{-1}]	P3 Area [ºC g kg^{-1}]	P4 Area [ºC g kg^{-1}]	P5 Area [ºC g kg^{-1}]
13.00	8.80	8.25	7.45	7.96	8.10
17.75	7.53	7.17	6.06	6.24	7.00
22.50	6.46	6.09	4.37	4.72	5.28

4.4.3 Analysis of numerical case study 7

The results of case study 7 were in agreement with those of case studies 5 and 6. These results are shown in Appendix B.

The results of MRC and SHR for the case studies and a complete discussion of these, are also shown in Appendix B. The variation of the outlet process air conditions from a given inlet process air state, by setting the $T_{r,i}$ and $\Omega_{p,i}$, caused MRC and SHR values to be modified. The MRC maximum value was achieved for high $\omega_{p,i}$ values and inlet air conditions close to saturation, 14 kg h^{-1}. This MRC value was acceptable compared to the MRC nominal value, 15 kg h^{-1}, see Table 1, where the DW was activated at high regeneration temperatures.

4.5 Conclusions of Chapter 4

The results of this chapter showed the most influential psychrometric factors in the behaviour of a DW activated at low temperatures. A significant influence on the inlet humidity ratio of the air process and the air regeneration was found to achieve greater dehumidification.

Four different empirical models of a DW were fitted by conducting a limited number of experimental tests. The four models can be used to predict the air process outlet conditions in the DW especially for low regeneration temperature activated systems. These models considered the influence of the air inlet temperature, air inlet humidity ratio and/or the air flow rates of the process and regeneration air on the DW. The accuracy of the numerical results of the models has been found to be acceptable in all models, with R^2 values greater than 97.4% for outlet temperature and 95.1% for outlet humidity ratio. Therefore, these simplified mathematical models are suitable for their integration in simulation tools.

The experimental and numerical results of this chapter also showed that a decoupling of the outlet process air conditions, temperature and humidity ratio, can be obtained when the process air flow rate and air regeneration temperature are varied. This decoupling resulted in a psychrometric area of the outlet process air. These results suggest that if a fine tuning of outlet process air conditions was necessary, the process air flow rate and the air regeneration temperature should be controlled. Therefore, these input variables could be used as a latent heat control strategy in a DW activated at low temperatures.

Chapter 5

Experimental analysis of an indirect evaporative cooler

At present, there is an increasing interest in indirect evaporative coolers, IEC, which are an effective alternative to conventional cooling systems, due to their high efficiency and reduced primary energy consumption. Performance of such systems significantly depends on inlet air conditions and water flow rate and, therefore, it should be properly evaluated through experimental tests or appropriate models.

In this chapter, an experimental study on an IEC was carried out. The methodology followed to study the IEC was similar to that of the DW, the DOE statistical technique. This allowed to obtain the influential input variables on the IEC performance, its behaviour and a simplified predictive model. Then, three experimental and numerical case studies were carried, in order to develop a sensible heat control strategy. Paper III, shown in Appendix C, address the results of this chapter.

5.1 IEC statistical analysis

An experimental case study of an IEC system was performed, case study 8 shown in Figure 11. The input variables set in each experimental test are shown in Table 3 of Appendix C. The test rig described in section 3.2.2.1 was used to carry out the cases study. The significance of the input factors and their interactions was evaluated. The ANOVA results are summarized in Table 27. This table shows the main estimated effects, the standard error of each of these effects and the statistical parameters F-Ratio and P-value.

Table 27. Effects of input variables on output variables of the indirect evaporative cooler for case study 8.

	$T_{p,o}$			
Effect	Estimate	Stnd. Error	F-Ratio	P-value
Average	24.24	0.02		
$T_{p,i}$	2.87	0.04	4156.24	0.0000
$T_{s,i}$	3.93	0.04	7827.72	0.0000
$\omega_{s,i}$	4.00	0.04	8103.67	0.0000
v_s	-0.27	0.04	35.68	0.0039
$\dot{V}_w$	-1.35	0.04	915.65	0.0000
Lack-of-fit			5.66	0.0526
	R^2=99.54%			
	$T_{s,o}$			
Effect	Estimate	Stnd. Error	F-Ratio	P-value
Average	26.15	0.02		
$T_{p,i}$	5.17	0.04	18036.21	0.0000
$T_{s,i}$	3.54	0.04	8448.88	0.0000
$\omega_{s,i}$	2.97	0.04	5927.50	0.0000
v_s	-0.81	0.04	441.51	0.0000
$\dot{V}_w$	-1.47	0.04	1455.14	0.0000
Lack-of-fit			4.36	0.0820
	R^2=99.78%			
	$\omega_{s,o}$			
Effect	Estimate	Stnd. Error	F-Ratio	P-value
Average	18.34	0.01		
$T_{p,i}$	3.04	0.02	16217.79	0.0000
$T_{s,i}$	2.53	0.02	11194.01	0.0000
$\omega_{s,i}$	5.63	0.02	55511.56	0.0000
v_s	-1.18	0.02	2447.80	0.0000
$\dot{V}_w$	0.80	0.02	1127.36	0.0000
Lack-of-fit			5.37	0.0576
	R^2=99.89%			

The results indicated that all input variables were found significant at 95% confidence level, as the P-values were lower than 0.05 in all cases. The input variables most influential on the responses can be analysed by the statistical parameter F-Ratio. It can be observed than the most influential input variable on $T_{p,o}$ and $\omega_{s,o}$ was $\omega_{s,i}$, and on $T_{s,o}$ was $T_{p,i}$, within the studied ranges, see Table 27. The least influential input variable on $T_{p,o}$ and $T_{s,o}$ was v_s, and on $\omega_{s,o}$ was $\dot{V}_w$. Therefore, v_s is not recommended as a sensible heat control variable. Regarding the

lack-of-fit test, all the P-values obtained were greater than 0.05. These results, determine that the selected design is suitable to describe the observed data at the 95% confidence level and a more complex design is not necessary to represent the relationship between the input variables and $T_{p,o}$, $T_{s,o}$ and $\omega_{s,o}$. The accuracy of the design was also shown by the R^2 values, which were found to be close to 100%. The R^2 values obtained were 99.54% for $T_{p,o}$, 99.78% for $T_{s,o}$ and 99.89% for $\omega_{s,o}$.

5.2 IEC behaviour analysis

The behaviour of the IEC system was analysed when $T_{p,i}$, $T_{s,i}$, $\omega_{s,i}$, v_s and $\dot{V}_w$ were varied. The trends of the main effects on output variables are shown in Figure 31. It can be observed that values of $T_{p,o}$ and $T_{s,o}$ were increased when $T_{p,i}$, $T_{s,i}$ and $\omega_{s,i}$ increased and v_s and $\dot{V}_w$ decreased. These results suggested that, if low air temperature values in both streams were necessary, the secondary air flow rate value, v_s, and water flow rate value, $\dot{V}_w$, should be high.

In Figure 31, it can also be observed that an increase of $T_{p,i}$, $T_{s,i}$, $\omega_{s,i}$ and $\dot{V}_w$ and a reduction of v_s, produced higher values of $\omega_{s,o}$. These trends were found consistent with the positive and negative estimated effects in Table 27. In previous studies on IEC systems, similar trends of the output variables with regard to the input variables were obtained [104–106].

5.3 Simplified IEC model

An empirical simplified model was developed to predict the behaviour of the air outlet conditions of the IEC system. The estimated regression coefficients corresponding to Eq. (3) are shown in Table 28, coefficients $b_1 \ldots b_{15}$. The regression coefficients show the relationship the variables and the weight each one has in the equation. It can be observed that the coefficients with the highest weight were b_3 for $T_{p,o}$ and b_4 for $T_{s,o}$ and $\omega_{s,o}$.

This simplified model was also compared with results of a detailed one, based on heat and mass transfer equations, shown in Appendix C. Both models behaved in a similar way. Therefore, the first-order approach adopted in the simplified model can be assumed satisfactory to estimate the behaviour of the IEC system.

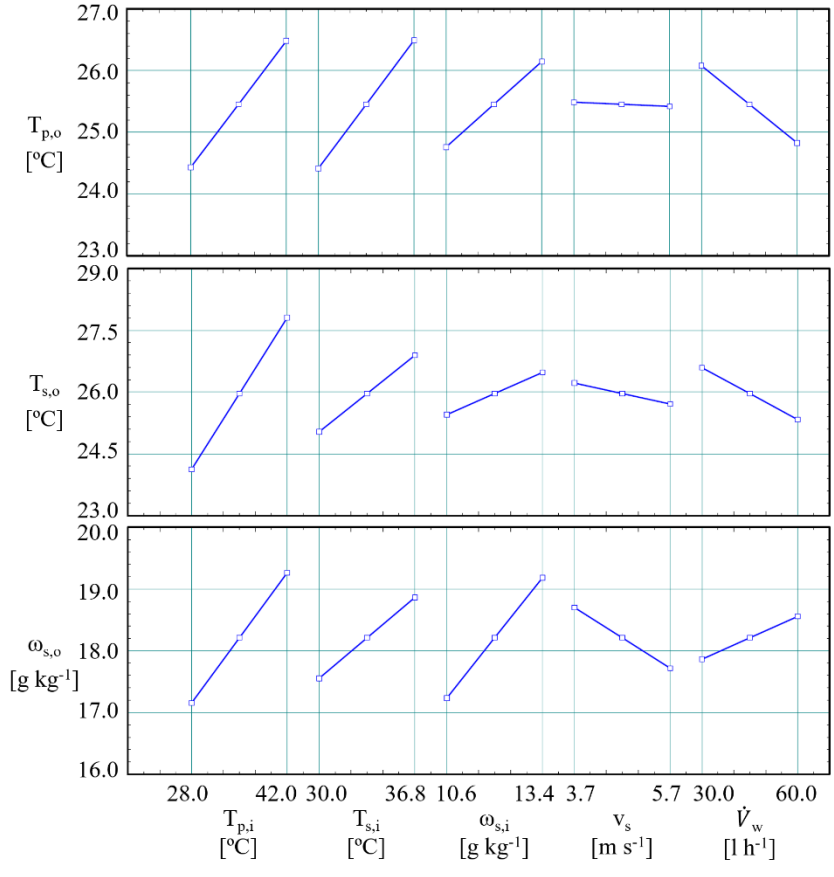

Figure 31. Trends of the main effects of the indirect evaporative cooler on the response variables for case study 8.

Table 28. Estimated parameters of the indirect evaporative cooler empirical model.

b_x	X_i	$T_{p,o}x10^3$ [ºC]	$T_{s,o}x10^3$ [ºC]	$\omega_{s,o}x10^3$ [g kg^{-1}]	b_x	X_i	$T_{p,o}x10^3$ [ºC]	$T_{s,o}x10^3$ [ºC]	$\omega_{s,o}x10^3$ [g kg^{-1}]
b_0	-	-1313.8	3801.7	-379.6	b_8	$T_{p,i}\cdot v_s$	-15.7	-25.3	-35.1
b_1	$T_{p,i}$	322.4	500.5	183.2	b_9	$T_{p,i}\cdot\dot{V}_w$	-1.2	-2.0	1.1
b_2	$T_{s,i}$	364.1	191.6	135.7	b_{10}	$T_{s,i}\cdot\omega_{s,i}$	-8.5	-5.9	3.3
b_3	$\omega_{s,i}$	766.5	455.4	313.3	b_{11}	$T_{s,i}\cdot v_s$	26.1	42.6	-6.6
b_4	v_s	-467.1	-1199.6	755.4	b_{12}	$T_{s,i}\cdot\dot{V}_w$	-2.1	-1.5	0.9
b_5	$\dot{V}_w$	41.9	21.0	3.3	b_{13}	$\omega_{s,i}\cdot v_s$	12.6	19.5	33.9
b_6	$T_{p,i}\cdot T_{s,i}$	0.4	0.6	0.2	b_{14}	$\omega_{s,i}\cdot\dot{V}_w$	2.9	3.4	-2.4
b_7	$T_{p,i}\cdot\omega_{s,i}$	-5.1	-3.9	6.3	b_{15}	$v_s\cdot\dot{V}_w$	-0.9	3.9	-4.5

5.4 Analysis of IEC control strategy

Three empirical and numerical case studies were carried out, case studies 9, 10 and 11 of Figure 11, in order to obtain a strategy to control outlet air primary temperature of the IEC system when $\dot{V}_w$ was varied. The results of case study 10, which is related to a configuration of an IEC with DW, are shown in Figure 32. The results of the remaining cases, case studies 9 and 11, are summarized in Appendix C. It is highlighted that in the three case studies, the higher $\dot{V}_w$, the higher ΔT_p, ΔT_s, $\Delta\omega_s$ and ε_{wb}.

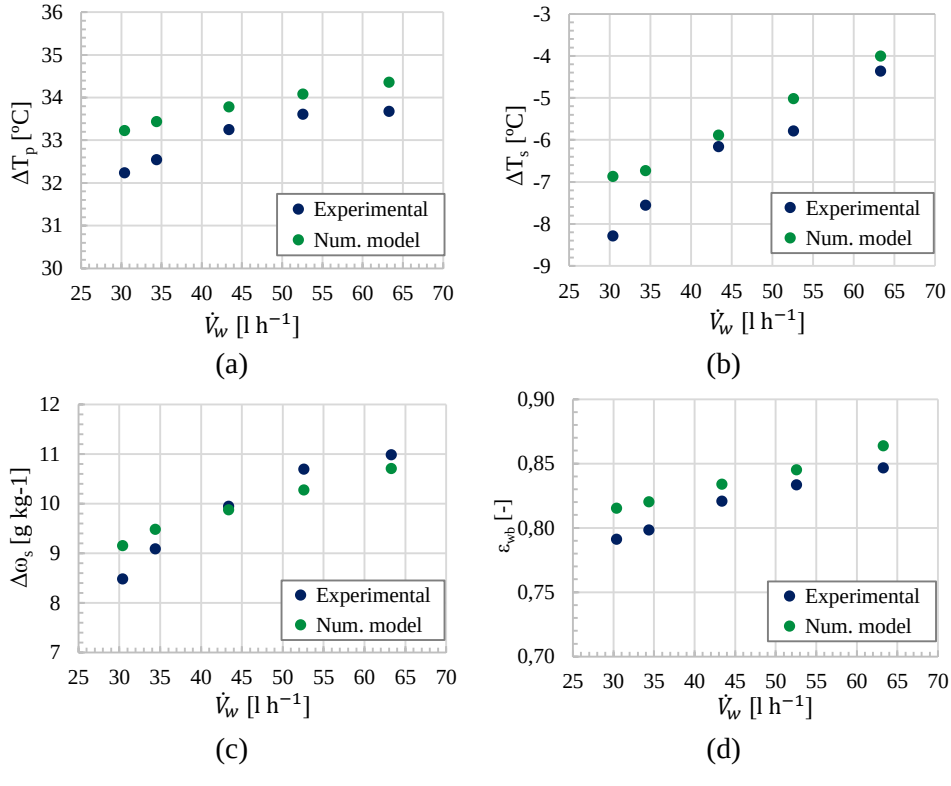

Figure 32. Experimental and simulation results of the ΔT_p, ΔT_s, $\Delta\omega_s$ and ε_{wb} as a function of $\dot{V}_w$ for case study 10.

It can be observed that the experimental maximum values of ΔT_p, ΔT_s, $\Delta\omega_s$ and ε_{wb} obtained for case 10 were 33.67 ºC, -4.37 ºC, 10.98 g kg^{-1} and 0.85, respectively, while the minimum values are 32.23 ºC, -8.29 ºC, 8.47 g kg^{-1} and 0.79,

see Figure 32. Therefore, in the investigated range, the output values depend significantly on $\dot{V}_w$. Negative values of ΔT_s were experienced because the inlet primary air temperature is significantly hotter than the secondary air one. As a consequence, measured ΔT_p increased significantly, reaching 33.66 ºC at the maximum water flow rate, with a wet bulb effectiveness of 84%. Figure 32 also shows that the simplified model correctly predicted the behaviour of the IEC, although its operating conditions are far from the models calibration range, see Table 8. The deviation between the experimental and numerical values were always below 5%, as shown in Table 6 of Appendix C. Previous studies showed similar trends in these four parameters when the water flow rate of an IEC was varied [58].

5.5 Conclusions of Chapter 5

The results of this chapter showed the most influential input variables on the IEC system. A significant influence on the inlet air secondary humidity ratio was found to achieve greater cooling in the primary air flow.

A simplified IEC model, based on a first order linear regression approach, was developed. This model can be used to predict the influence of $T_{p,i}$, $T_{s,i}$, $\omega_{s,i}$, v_s and $\dot{V}_w$ on the output variables $T_{p,o}$, $T_{s,o}$ and $\omega_{s,o}$, in the IEC. The model effectively correlated experimental data, with R^2 values equal to 99.54% for $T_{p,o}$, 99.78% for $T_{s,o}$ and 99.89% for $\omega_{s,o}$. Therefore, it is possible to state that the simplified IEC model can be effectively integrated in energy simulation tools, due to its low computational load and good accuracy.

The experimental and numerical results also showed that a significant variation of the outlet air primary temperature can be obtained when the water flow rate is varied. Therefore, it could be used as a sensible heat control variable.

Chapter 6

Energy analysis of a hybrid HVAC system and a conventional HVAC system in handling air in buildings with high latent loads

The previous detailed experimental studies allowed to improve the understanding of how a DW activated at low temperatures and an IEC behave. In addition, several simplified predictive models of the DW and the IEC were developed, which could be effectively integrated in energy simulation tools.

In this chapter, two simulated case studies on a conventional HVAC systems and a proposed hybrid HVAC system were carried out, case studies 12 and 13, shown in Figure 11. Both HVAC systems were designed to serve air in a spa. The component models used for the simulations of the HVAC systems were those obtained in Chapter 4 and Chapter 5 for the DW and the IEC, respectively, and those described in section 3.4.3 for remaining components. The energy analysis of the results is presented in daily, monthly and annual analysis to correctly understand the behaviour of the HVAC systems. All the results are addressed in Paper IV, shown in Appendix D.

6.1 Daily behaviour analysis

The daily analysis was performed for the climatic conditions of Barcelona. A typical winter day, January 10th, and a typical summer day, July 10th, were

selected. The thermal behaviour and energy consumption of the conventional and hybrid HVAC systems for both days are shown in Appendix D.

The highest energy consumption values for the hybrid HVAC system were those of Fan 1, due to the process side pressure losses, see Figure 6 of Appendix D, and for the conventional HVAC system were those of the compressor, due to the dehumidification demand, see Figure 5 of Appendix D.

The supply air humidity ratio of the hybrid HVAC system, see Figure 6 of Appendix D, was lower than the supply air humidity of the conventional HVAC system, see Figure 5 of Appendix D, because the process air flow rate of the hybrid HVAC system was lower than that of the conventional HVAC system. Thus, the latent energy delivered to the building with both systems was similar.

6.2 Monthly energy analysis

A monthly energy analysis for both HVAC systems for the climatic conditions of Barcelona was performed. Monthly sensible and latent energy delivered and monthly energy consumption by the conventional and hybrid HVAC systems were obtained.

6.2.1 Monthly energy analysis of the conventional HVAC system

The sensible and latent energy delivered of the conventional HVAC system for the climatic conditions of Barcelona, climate zone 4, are represented in Figure 33. This figure shows energy delivered of each element and the total monthly energy. The negative energy values indicate that the elements reduced the air temperature and humidity ratio, and the positive energy values indicate that the elements increased the air temperature and humidity ratio. It can be observed that the process of mixing air slightly increased the sensible energy delivered, see Figure 33a, thus increasing the outlet air temperature of the mixing box. This process caused the sensible energy required by the HC to decrease, especially in January and December, where the sensible energy delivered in the process of mixing air is greater than in the remaining months, 7.2 kWh m^{-2} and 7.5 kWh m^{-2}, respectively. However, the mixing air also increased the latent energy delivered, see Figure 33b, thus increasing the outlet air humidity of the mixing box. For example, the latent energy values delivered in January and December were 15.2 kWh m^{-2} and 16.2 kWh m^{-2}, respectively. Therefore, the mixing air did not improve the dehumidification system performance for the climate conditions of Barcelona.

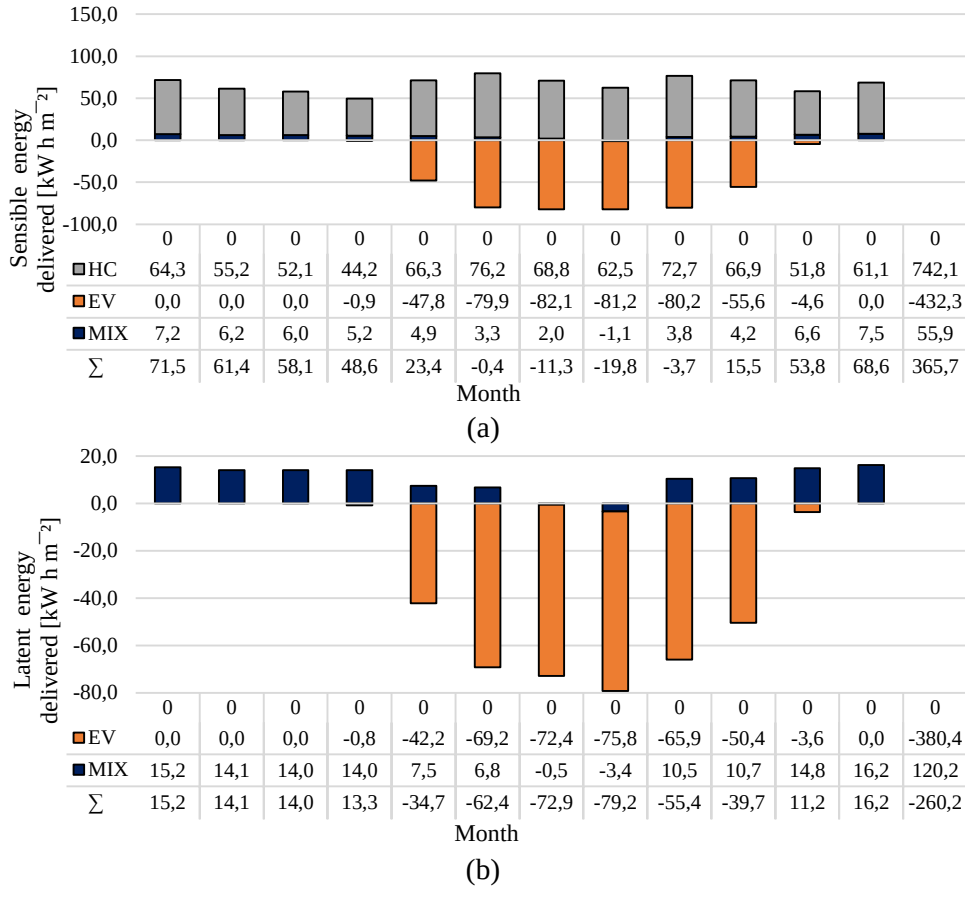

Figure 33. Energy delivered by each element for the conventional HVAC system for the climatic conditions of Barcelona, (a) sensible energy delivered, (b) latent energy delivered.

The EV delivered sensible and latent energy during the months with dehumidification demand, i.e. when the mixed air humidity ratio was higher than the set point air humidity ratio, from April to November. The maximum sensible and latent energy values delivered by the EV were obtained in July and August. The building did not require dehumidification from December to March, therefore, the sensible and latent energy delivered by the EV was zero.

The sensible energy delivered by the HC was maintained throughout the year, due to the heating demand, i.e. when the inlet air temperature to the HC was

lower than the set point air temperature. This temperature was lower the set point air temperature from November to April, due mainly to the outdoor air, and from May to October, due to the low outlet air temperature of the EV.

Finally, it can be observed that the annual sensible and latent energy values delivered by the conventional HVAC system were 365.7 kWh m^{-2} $year^{-1}$ and -260.2 kWh m^{-2} $year^{-1}$, respectively.

The monthly energy consumption of the conventional HVAC system is represented in Figure 34. This figure shows the monthly energy consumption of each element and the total monthly consumption.

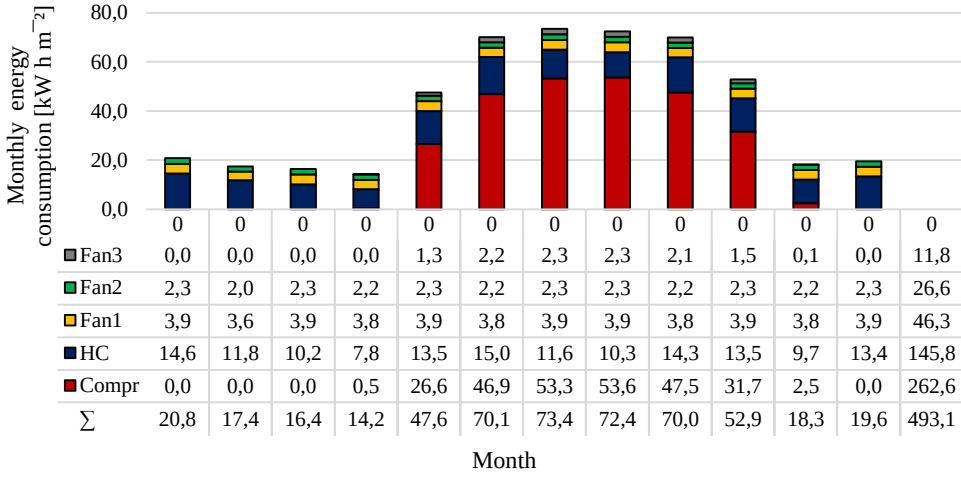

	0	0	0	0	0	0	0	0	0	0	0	0	0
Fan3	0,0	0,0	0,0	0,0	1,3	2,2	2,3	2,3	2,1	1,5	0,1	0,0	11,8
Fan2	2,3	2,0	2,3	2,2	2,3	2,2	2,3	2,3	2,2	2,3	2,2	2,3	26,6
Fan1	3,9	3,6	3,9	3,8	3,9	3,8	3,9	3,9	3,8	3,9	3,8	3,9	46,3
HC	14,6	11,8	10,2	7,8	13,5	15,0	11,6	10,3	14,3	13,5	9,7	13,4	145,8
Compr	0,0	0,0	0,0	0,5	26,6	46,9	53,3	53,6	47,5	31,7	2,5	0,0	262,6
∑	20,8	17,4	16,4	14,2	47,6	70,1	73,4	72,4	70,0	52,9	18,3	19,6	493,1

Figure 34. Monthly energy consumption of each element for the conventional HVAC system for the climatic conditions of Barcelona.

It can be observed that the highest energy consumption values were those for the compressor, which was activated during the months with dehumidification demand. The operation Fan3 was linked to that of the compressor, see Figure 20, therefore, the energy consumption of Fan3 was zero during the months that the compressor was not in operation, from December to March. The energy consumption of the HC was maintained throughout the year, due to its sensible energy demand, as shown in Figure 33a. The energy consumption of the HC was that of the heat pump. Regarding the monthly energy consumption, the maximum values were found from May to October, due mainly to the high dehumidification demand. The energy consumption was less during cold months with high heating

demand, from November to February, and warm months, such as March and April. It can also be observed that the annual energy consumption for the climatic conditions of Barcelona with the conventional HVAC system was 493.1 kWh m^{-2} $year^{-1}$, see Figure 34.

6.2.2 Monthly energy analysis of the hybrid HVAC system

The sensible and latent energy delivered of the hybrid HVAC system for the climatic conditions of Barcelona is shown in Figure 35, broken down by the elements.

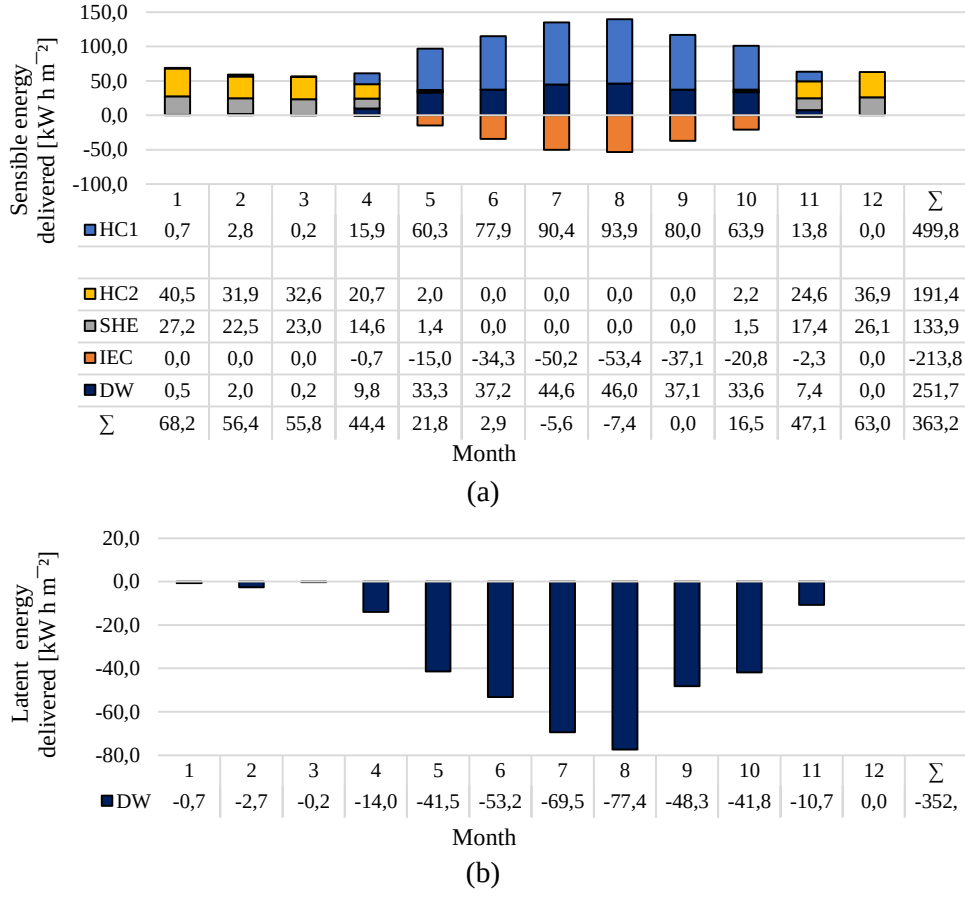

	1	2	3	4	5	6	7	8	9	10	11	12	∑
HC1	0,7	2,8	0,2	15,9	60,3	77,9	90,4	93,9	80,0	63,9	13,8	0,0	499,8
HC2	40,5	31,9	32,6	20,7	2,0	0,0	0,0	0,0	0,0	2,2	24,6	36,9	191,4
SHE	27,2	22,5	23,0	14,6	1,4	0,0	0,0	0,0	0,0	1,5	17,4	26,1	133,9
IEC	0,0	0,0	0,0	-0,7	-15,0	-34,3	-50,2	-53,4	-37,1	-20,8	-2,3	0,0	-213,8
DW	0,5	2,0	0,2	9,8	33,3	37,2	44,6	46,0	37,1	33,6	7,4	0,0	251,7
∑	68,2	56,4	55,8	44,4	21,8	2,9	-5,6	-7,4	0,0	16,5	47,1	63,0	363,2

	1	2	3	4	5	6	7	8	9	10	11	12	∑
DW	-0,7	-2,7	-0,2	-14,0	-41,5	-53,2	-69,5	-77,4	-48,3	-41,8	-10,7	0,0	-352,

Figure 35. Energy delivered by each element for the hybrid HVAC system for the climatic conditions of Barcelona, (a) sensible energy delivered and (b) latent energy delivered.

It can be observed that the DW delivered high latent energy values from April to November, as shown in Figure 35b, due to the dehumidification demand. The peak values, corresponding to July and August, are due to the high outdoor air humidity. The operation of HC1 was linked to that of the DW, in order to regenerate it, see Figure 21 and Figure 22.The sensible energy of HC1 was not delivered to the building, but outside. The activation of the IEC was caused by the sensible energy delivered during the dehumidification process of the DW. As a consequence, sensible energy delivered by the IEC is obtained from April to November, in order to reduce the process air temperature, see Figure 35a. The SHE recovered a large amount of energy during the months with heating demand and the DW was not in operation, thus reducing the energy required by HC2. The highest sensible energy values delivered by HC2 was found during the months with high heating demand, from November to March, months with low outdoor temperatures. Nevertheless, the sensible energy delivered by HC2 was zero from June to September, as shown in Figure 35a.

After analysing these monthly results and those obtained with the conventional HVAC system, it can be observed that the monthly sensible and latent energy delivered to the building by each system was similar, see Figure 33 and Figure 35. The slight variations in the energy values delivered between both systems were mainly due to the different control systems used.

The monthly energy consumption by each element of the hybrid HVAC system are shown in Figure 36. It can be observed that the element with the highest energy consumption values throughout the year was Fan1, 119.1 kWh m^{-2}, due to the high pressure drop of the proposed system. High energy consumption values by HC1 were found during the months with high dehumidification demand, from April to November. However, very low dehumidification demand was obtained from December to March, so the monthly energy consumption values by HC1 were very low or zero, see Figure 36. The energy consumption of HC1 and HC2 were those of the heat pump. It can also be observed that the trend of energy consumption by HC2 was contrary to that of HC1. The highest energy consumption values by HC2 were found November to April, due to the heating demand, and the lowest values from May to October, because the outlet process air temperature of the DW was usually higher than the set point air temperature. The energy consumption of Fan3 was very low during the months that the DW was not in operation, since the operation of Fan2 was linked to that of the DW, see Figure 21 and Figure 22. The maximum monthly energy consumption values were found from May to October,

due mainly to the high dehumidification demand, and then, as with the conventional HVAC system. Finally, the annual energy consumption for the climatic conditions of Barcelona with the proposed hybrid HVAC system was 314.7 kWh m^{-2} $year^{-1}$, as shown in Figure 36. Therefore, the annual energy consumption of the hybrid HVAC system was 36.2% lower than that of the conventional HVAC system for the climatic conditions of Barcelona, see Figure 34 and Figure 36.

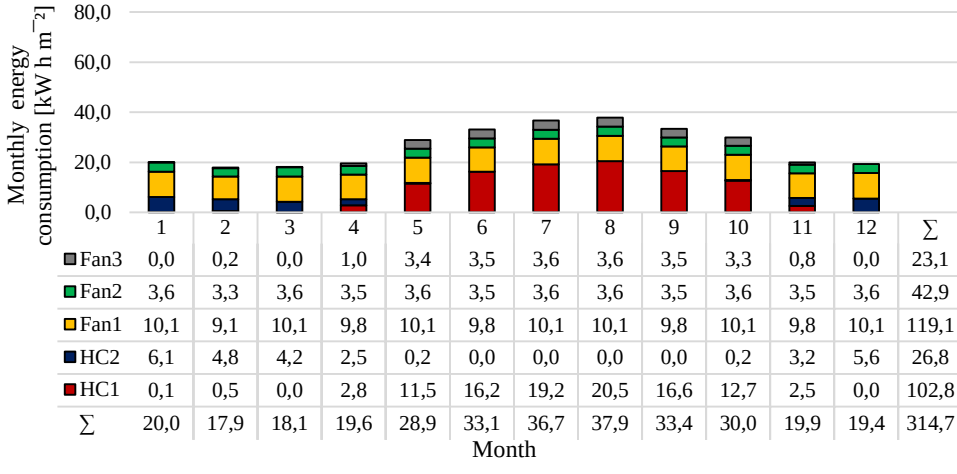

	1	2	3	4	5	6	7	8	9	10	11	12	∑
Fan3	0,0	0,2	0,0	1,0	3,4	3,5	3,6	3,6	3,5	3,3	0,8	0,0	23,1
Fan2	3,6	3,3	3,6	3,5	3,6	3,5	3,6	3,6	3,5	3,6	3,5	3,6	42,9
Fan1	10,1	9,1	10,1	9,8	10,1	9,8	10,1	10,1	9,8	10,1	9,8	10,1	119,1
HC2	6,1	4,8	4,2	2,5	0,2	0,0	0,0	0,0	0,0	0,2	3,2	5,6	26,8
HC1	0,1	0,5	0,0	2,8	11,5	16,2	19,2	20,5	16,6	12,7	2,5	0,0	102,8
∑	20,0	17,9	18,1	19,6	28,9	33,1	36,7	37,9	33,4	30,0	19,9	19,4	314,7

Figure 36. Monthly energy consumption for the hybrid HVAC system for the climatic conditions of Barcelona.

6.3 Annual energy analysis

In this section, the annual energy consumption of the proposed hybrid HVAC system was compared with those of the conventional HVAC system. The comparative analysis was carried out for the 6 climate zones, as shown in Table 19.

6.3.1 Annual energy consumption

The operating annual energy consumption of both systems for the 6 climate zones is shown in Figure 37. It can be observed that the maximum annual consumption values for both systems were obtained for the climate zone 1, a very hot climate zone, due to the high dehumidification demand. The energy consumption values were significantly reduced for cool climatic conditions, such as in climate zone 5. The consumption decreased by 51% and 37% between the climate zone 1 and 5 for

the conventional HVAC system and the hybrid HVAC system, respectively. However, the annual energy consumption values increased for climate zone 6, a cold climate zone, compared to those of zones 3, 4 and 5. This increase was caused mainly by the high heating demand. This trend of annual energy consumption was also obtained for the monthly energy consumption analysed in section 6.2, where the highest monthly consumption values were found for the months with high dehumidification demand, then, the months with high heating demand and finally, the remaining months.

It can be observed that the annual energy consumption of the hybrid HVAC system was always lower than that of the conventional HVAC system, obtaining significant energy savings, always over 27.8%, see Figure 37. The highest energy savings were found for the climate zones with the highest annual energy consumption and the highest dehumidification demand, zones 1 and 2, with 43.5% and 46.8%, respectively.

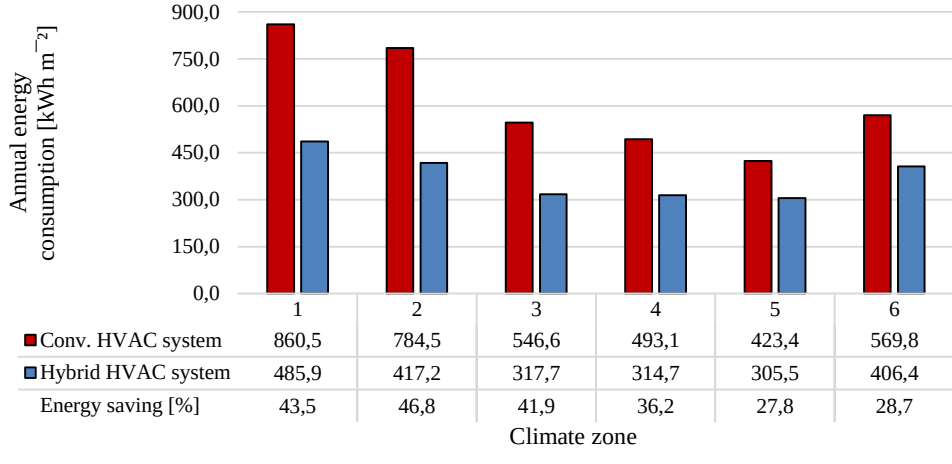

	1	2	3	4	5	6
Conv. HVAC system	860,5	784,5	546,6	493,1	423,4	569,8
Hybrid HVAC system	485,9	417,2	317,7	314,7	305,5	406,4
Energy saving [%]	43,5	46,8	41,9	36,2	27,8	28,7

Figure 37. Comparative analysis of annual energy consumption of the hybrid HVAC system and the conventional HVAC system in each climate zone.

6.3.2 Seasonal mean coefficient of performance

The seasonal mean coefficient of performance, SCOP, of both systems, was calculated using Eq. (16). The SCOP values for the 6 climate zones are represented in Figure 38. It can be observed that the maximum SCOP value for the conventional HVAC system was 1.9, obtained from a cool climate zone, zone 5. Nevertheless,

the maximum SCOP value for the hybrid HVAC system was 2.8, obtained from a very hot climate zone, zone 1.

The SCOP values of the hybrid HVAC system were always higher than that of the conventional HVAC system, always over 27%, as shown in Figure 38. The greatest differences in SCOP between both systems, ΔSCOP, were found for climate zones 1 and 2, and the lowest for climate zones 5 and 6. The trend of ΔSCOP was similar to the trend of annual energy saving, as shown in Figure 37, since the sensible and latent energy delivered to the building by each system were the same, so ΔSCOP depended exclusively on energy consumption.

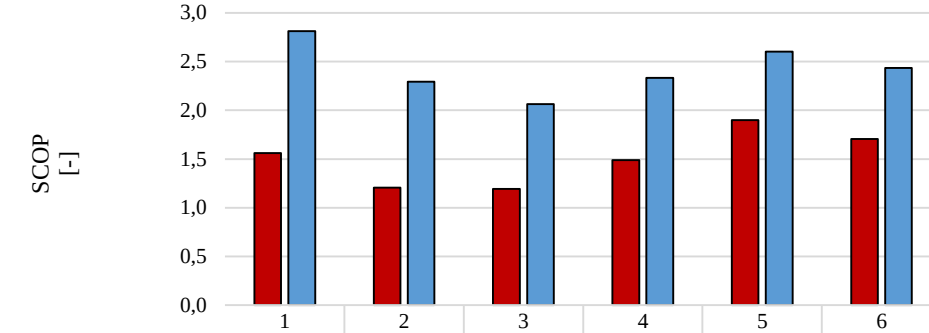

	1	2	3	4	5	6
Conv. HVAC system	1,6	1,2	1,2	1,5	1,9	1,7
Hybrid HVAC system	2,8	2,3	2,1	2,3	2,6	2,4
ΔSCOP [%]	44,5	47,4	42,1	36,1	27,0	29,9

Climate zone

Figure 38. SCOP values of the hybrid HVAC system and the conventional HVAC system in each climate zone.

6.3.3 Energy consumption per unit of dehumidified water

The energy consumption per unit of dehumidified water, E_{cons}, was obtained for both system, in order to know the energy used only when the dehumidification demand was required. The E_{cons} results for each system and climate zone, are shown in Figure 39. It can be observed that the lowest E_{cons} values were obtained for very hot climatic conditions, such as in climate zone 1 and the highest E_{cons} values for cool conditions, such as in climate zone 5. The trend of E_{cons} is contrary to that obtained for annual energy consumption, see Figure 37.Comparing both systems studied, it can be observed that the E_{cons} values from the conventional HVAC

system were always higher than those from the hybrid HVAC system. The highest energy saving, ΔE_{cons}, was obtained for zone 1, 34.6%. However, small energy savings were found for zones 5 and 6, 4.4% and 1.7%, respectively, climate zones with low dehumidification demand.

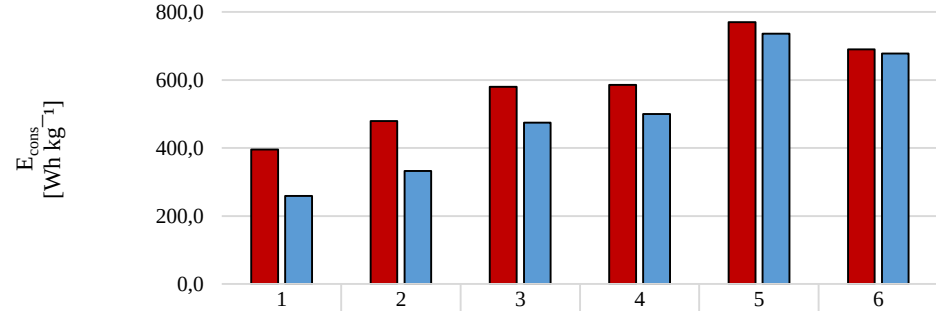

	1	2	3	4	5	6
Conv. HVAC system	395,9	478,9	580,0	585,9	770,0	690,0
Hybrid HVAC system	259,1	332,8	474,5	500,1	736,2	678,0
ΔEcons [%]	34,6	30,5	18,2	14,6	4,4	1,7

Climate zone

Figure 39. E_{cons} values of the hybrid HVAC system and the conventional HVAC system in each climate zone.

6.4 Conclusions of Chapter 6

The results of this chapter showed that the conventional and hybrid HVAC systems satisfactorily achieved the set point air conditions. Both systems delivered similar sensible and latent energy values to the building.

The annual energy consumption of the hybrid HVAC system was lower than that of the conventional HVAC system for the 6 climate zones, achieving significant energy savings, especially for hot climate zones with high dehumidification demand, where a 46.8 % annual energy saving was obtained. The lowest energy saving was achieved for a cool climate zone, 27.8 %. These energy savings resulted in better SCOP values for the hybrid HVAC system. The highest SCOP value was 2.8, obtained for a very hot climatic zone. The difference in SCOP between both systems was always greater than 25% for all climate zones.

The energy consumption per unit of dehumidified water, E_{cons}, of both systems was analysed for the 6 climate zones. Significant energy savings were

obtained with the proposed hybrid HVAC system for very hot climate zone, due to the high dehumidification demand, achieving up to 34.6% savings. However, the energy savings of the hybrid HVAC system were lower for cool and cold climate zones, 4.4 % and 1.7 %, respectively, climate zones with low dehumidification demand and high heating demand.

Chapter 7

Conclusions and future work

Following are the conclusions and proposals for future work that are deduced from the research work developed in the frame of this thesis.

7.1 Conclusions

A novel hybrid HVAC system activated at low temperature based on desiccant wheels and indirect evaporative coolers was proposed as an alternative to conventional HVAC systems based on direct expansion units.

The hybrid HVAC system activated at low temperature achieved a suitable desiccant capacity to dehumidify air in a small building with high latent loads. A fine-tuned control of the latent heat of the process air of the hybrid HVAC system could be obtained when the process air flow rate and air regeneration temperature of the desiccant wheel were varied.

A proper adjustment of the water flow rate of the indirect evaporative cooler reduced the high air temperatures generated by the adsorption process of the desiccant wheel and controlled the sensible heat of the process air of the hybrid HVAC system.

The control strategies of the desiccant wheel and the indirect evaporative cooler allowed to decouple sensible and latent heat of the hybrid HVAC system.

The hybrid HVAC system achieved higher energy efficiency than the conventional HVAC system when both HVAC systems served air to a small building with high latent loads, regardless of the climatic conditions. Furthermore, the hybrid HVAC system independently controlled the sensible and latent loads of the building, using reduced supply air flow rates.

The results suggest that the proposed hybrid HVAC system could be a serious alternative to conventional HVAC systems composed of direct expansion units to handle air in small buildings with high latent loads and where reduced supply air flow rates are required.

7.2 Future work

The present thesis focused on the performance of a hybrid HVAC system composed of a desiccant wheel and an indirect evaporative cooler and a conventional HVAC system composed of a direct expansion unit, under different thermodynamic conditions. It would be interesting to know the life-cycle costs, LCC, of both HVAC systems, as an auxiliary analysis, in order to evaluate the viability of this hybrid HVAC system.

The proposed hybrid HVAC system achieved good thermal performance when it was activated at low temperature. Therefore, this hybrid HVAC system could be activated with waste heat or renewable energy systems, such as solar thermal, biomass or other energy sources. This offers many possibilities for the study of the performance of the hybrid HVAC system using renewable energy sources.

Some elements that compose the proposed hybrid HVAC system could have a relative economic cost, such as the desiccant wheel. Therefore, it would be interesting to investigate new desiccant materials and other matrix shapes other than rotating wheels, such as packed beds using desiccant materials, in order to reduce economic costs of the hybrid HVAC system.

Bibliography

[1] RITE 2007. Regulation of thermal installations in buildings, Real Decreto. (2007) 35931–35984.

[2] P. Torrero, DTIE 10.04. Covered swimming pools air-conditioned only with outdoor air, ATECYR, 2008.

[3] J.L. Míguez Tabarés, M. Gándara Alvarez, L.M. López González, P. Fernández Viar, Feasibility study for the installation of HVAC for a spa by means of energy recovery from thermal water - Part I: Energy analysis, Renew. Energy. 23 (2001) 135–149. doi:10.1016/S0960-1481(00)00162-2.

[4] J.L. Míguez Tabarés, M. Gándara Alvarez, L.M. López González, P. Fernández Viar, Feasibility study for the installation of HVAC for a spa by means of energy recovery from thermal water - Part II: Energy analysis, Renew. Energy. 23 (2001) 135–149. doi:10.1016/S0960-1481(00)00162-2.

[5] P. Sun, J.Y. Wu, R.Z. Wang, Y.X. Xu, Analysis of indoor environmental conditions and heat pump energy supply systems in indoor swimming pools, Energy Build. 43 (2011) 1071–1080. doi:10.1016/j.enbuild.2010.08.004.

[6] R. Tubío, N. Molero, M. Zamora, DTIE 10.06. Covered swimming pools. Systems of air conditioning, dehumidification and energy saving using heat pumps, ATECYR, 2013.

[7] L.G. Harriman III, The dehumidification handbook, second edition., Munters Corp. Amesbury, MA. (2003).

[8] ASHRAE, Fundamentals Handbook, Chapter 32: Sorbents and Desiccants, American Society of Heating, Refrigerating and Air-Conditioning Engineers, Atlanta, 2009.

[9] ASHRAE, Refrigeration Handbook, Chapters 7, 17, 44, 18, and 8, American Society of Heating, Refrigerating and Air-Conditioning Engineers, Atlanta, 2010.

[10] ASHRAE, HVAC Applications Handbook, Chapters 1, 2, 6, 10, 18, 20, 23, 30, and 46, American Society of Heating, Refrigerating and Air-Conditioning Engineers, Atlanta, 2011.

[11] ASHRAE, HVAC Systems and Equipment Handbook, Chapters 24 and 26,

American Society of Heating, Refrigerating and Air-Conditioning Engineers, Atlanta, 2012.

[12] I. Sarbu, C. Sebarchievici, Review of solar refrigeration and cooling systems, Energy Build. 67 (2013) 286–297. doi:10.1016/j.enbuild.2013.08.022.

[13] Harriman L., 20 Years of commercial desiccant systems, HPAC Engineering, June, 2003, 43–54.

[14] L.Z. Zhang, J.L. Niu, A pre-cooling Munters environmental control desiccant cooling cycle in combination with chilled-ceiling panels, Energy. 28 (2003) 275–292. doi:10.1016/S0360-5442(02)00114-7.

[15] C. Aprea, A. Greco, A. Maiorino, The application of a desiccant wheel to increase the energetic performances of a transcritical cycle, Energy Convers. Manag. 89 (2015) 222–230. doi:10.1016/j.enconman.2014.09.066.

[16] Hines, A.J., T.K. Ghosh, S.K. Loyalka, and R.C. Warder, Jr. 1991. Investigation of co-sorption of gases and vapors as a means to enhance indoor air quality. ASHRAE Research Project 475-RP and Gas Research Institute Project GRI-90/0194. Gas Research Instit.

[17] G. Angrisani, F. Minichiello, C. Roselli, M. Sasso, Experimental analysis on the dehumidification and thermal performance of a desiccant wheel, Appl. Energy. 92 (2012) 563–572. doi:10.1016/j.apenergy.2011.11.071.

[18] G. Panaras, E. Mathioulakis, V. Belessiotis, Solid desiccant air-conditioning systems - Design parameters, Energy. 36 (2011) 2399–2406. doi:10.1016/j.energy.2011.01.022.

[19] U. Eicker, U. Schürger, M. Köhler, T. Ge, Y. Dai, H. Li, et al., Experimental investigations on desiccant wheels, Appl. Therm. Eng. 42 (2012) 71–80. doi:10.1016/j.applthermaleng.2012.03.005.

[20] G. Angrisani, C. Roselli, M. Sasso, Effect of rotational speed on the performances of a desiccant wheel, Appl. Energy. 104 (2013) 268–275. doi:10.1016/j.apenergy.2012.10.051.

[21] L. Yadav, A. Yadav, Mathematical investigation of purge sector angle for clockwise and anticlockwise rotation of desiccant wheel, Appl. Therm. Eng. 93 (2016) 839–848. doi:10.1016/j.applthermaleng.2015.10.062.

[22] S. De Antonellis, M. Intini, C.M. Joppolo, F. Romano, On the control of desiccant wheels in low temperature drying processes, Int. J. Refrig. 70 (2016) 171–182. doi:10.1016/j.ijrefrig.2016.06.026.

[23] M. Aprile, M. Motta, Grey-box modelling and in situ experimental identification of desiccant rotors, Appl. Therm. Eng. 51 (2013) 55–64.

doi:10.1016/j.applthermaleng.2012.08.065.

[24] American Gas Cooling Center. Applications Engineering Manual for Desiccant Systems, Arlington, 1996.

[25] C.R. Ruivo, A. Carrillo-Andres, J.J. Costa, F. Dominguez-Munoz, Exponential correlations to predict the dependence of effectiveness parameters of a desiccant wheel on the airflow rates and on the rotation speed, Appl. Therm. Eng. 51 (2013) 442–450. doi:10.1016/j.applthermaleng.2012.08.037.

[26] C.R. Ruivo, A. Carrillo-Andrés, J.J. Costa, F. Domínguez-Muñoz, Interpolation procedures for the effectiveness method to account for the influence of the inlet airflow states on the desiccant wheels performance, Energy Build. 55 (2012) 380–388. doi:10.1016/j.enbuild.2012.08.028.

[27] A.M. Baniyounes, M.G. Rasul, M.M.K. Khan, Experimental assessment of a solar desiccant cooling system for an institutional building in subtropical Queensland, Australia, Energy Build. 62 (2013) 78–86. doi:10.1016/j.enbuild.2013.02.062.

[28] C.E.L. Nóbrega, N.C.L. Brum, An analysis of the heat and mass transfer roles in air dehumidification by solid desiccants, Energy Build. 50 (2012) 251–258. doi:10.1016/j.enbuild.2012.03.049.

[29] J. Wrobel, P. Morgenstern, G. Schmitz, Modeling and experimental validation of the desiccant wheel in a hybrid desiccant air conditioning system, Appl. Therm. Eng. 51 (2013) 1082–1091. doi:10.1016/j.applthermaleng.2012.09.033.

[30] A. Al-Alili, Y. Hwang, R. Radermacher, A hybrid solar air conditioner: Experimental investigation, Int. J. Refrig. 39 (2014) 117–124. doi:10.1016/j.ijrefrig.2013.10.006.

[31] J.Y. San, S.C. Hsiau, Effect of axial solid heta-conduction and mass diffusion in a rotary heat and mass regenerator, Int. J. Heat Mass Transf. 36 (1993) 2051–2059. doi:10.1016/s0017-9310(05)80136.

[32] E. Vandenbulck, J.W. Mitchell, S.A. Klein, Design theory for rotary heat and mass exchangers .1. Wave analysis of rotary heat and mass exchangers with infinite transfer-coefficients, Int. J. Heat Mass Transf. 28 (1985) 1575–1586. doi:10.1016/0017-9310(85)90259-5.

[33] C.R. Ruivo, J.J. Costa, A.R. Figueiredo, On the behaviour of hygroscopic wheels: Part I - channel modelling, Int. J. Heat Mass Transf. 50 (2007) 4812–4822. doi:10.1016/j.ijheatmasstransfer.2007.03.003.

[34] Maclaine.Il, P.J. Banks, Coupled heat and mass-transfer in regenerators -

prediction using an analogy with heat-transfer, Int. J. Heat Mass Transf. 15 (1972) 1225–1242. doi:10.1016/0017-9310(72)90187-1.

[35] J.J. Jurinak, Open cycle desiccant cooling and Component models and system simulations, PhD thesis, University of Wisconsin, Madison, USA, 1982.

[36] G. Angrisani, C. Roselli, M. Sasso, Experimental validation of constant efficiency models for the subsystems of an unconventional desiccant-based Air Handling Unit and investigation of its performance, Appl. Therm. Eng. 33–34 (2012) 100–108. doi:10.1016/j.applthermaleng.2011.09.018.

[37] G. Panaras, E. Mathioulakis, V. Belessiotis, N. Kyriakis, Experimental validation of a simplified approach for a desiccant wheel model, Energy Build. 42 (2010) 1719–1725. doi:10.1016/j.enbuild.2010.05.006.

[38] C.R. Ruivo, A. Carrillo-Andres, J.J. Costa, F. Dominguez-Munoz, A new approach to the effectiveness method for the simulation of desiccant wheels with variable inlet states and airflows rates, Appl. Therm. Eng. 58 (2013) 670–678. doi:10.1016/j.applthermaleng.2011.12.052.

[39] M. Beccali, F. Butera, R. Guanella, R.S. Adhikari, Simplified models for the performance evaluation of desiccant wheel dehumidification, Int. J. Energy Res. 27 (2003) 17–29. doi:10.1002/er.856.

[40] M. Beccali, R.S. Adhikari, F. Butera, V. Franzitta, Update on desiccant wheel model, Int. J. Energy Res. 28 (2004) 1043–1049. doi:10.1002/er.1011.

[41] F.E. Nia, D. van Paassen, M.H. Saidi, Modeling and simulation of desiccant wheel for air conditioning, Energy Build. 38 (2006) 1230–1239. doi:10.1016/j.enbuild.2006.03.020.

[42] A.N. Sadeghifam, S.M. Zahraee, M.M. Meynagh, I. Kiani, Combined use of design of experiment and dynamic building simulation in assessment of energy efficiency in tropical residential buildings, Energy Build. 86 (2015) 525–533. doi:10.1016/j.enbuild.2014.10.052.

[43] I. Jaffal, C. Inard, C. Ghiaus, Fast method to predict building heating demand based on the design of experiments, Energy Build. 41 (2009) 669–677. doi:10.1016/j.enbuild.2009.01.006.

[44] D.C. Montgomery, Design and analysis of experiments, 6th Edition, Wiley, 2004.

[45] D. Kosar, Dehumidification System Enhancement, ASHRAE J. 48 (2006) 48–58.

[46] Z. Duan, C. Zhan, X. Zhang, M. Mustafa, X. Zhao, B.

Alimohammadisagvand, et al., Indirect evaporative cooling: Past, present and future potentials, Renew. Sustain. Energy Rev. 16 (2012) 6823–6850. doi:10.1016/j.rser.2012.07.007.

[47] B. Porumb, P. Ungureşan, L.F. Tutunaru, A. Şerban, M. BĂlan, A Review of Indirect Evaporative Cooling Technology, Energy Procedia. 85 (2016) 461–471. doi:10.1016/j.egypro.2015.12.228.

[48] F.J.R. Martínez, E.V. Gómez, R.H. Martín, J.M. Gutiérrez, F.V. Diez, Comparative study of two different evaporative systems: An indirect evaporative cooler and a semi-indirect ceramic evaporative cooler, Energy Build. 36 (2004) 696–708. doi:10.1016/j.enbuild.2003.10.010.

[49] S. Delfani, J. Esmaeelian, H. Pasdarshahri, M. Karami, Energy saving potential of an indirect evaporative cooler as a pre-cooling unit for mechanical cooling systems in Iran, Energy Build. 42 (2010) 2169–2176. doi:10.1016/j.enbuild.2010.07.009.

[50] Y. Chen, Y. Luo, H. Yang, Fresh air pre-cooling and energy recovery by using indirect evaporative cooling in hot and humid region - A case study in Hong Kong, Energy Procedia. 61 (2014) 126–130. doi:10.1016/j.egypro.2014.11.922.

[51] X. Cui, K.J. Chua, M.R. Islam, K.C. Ng, Performance evaluation of an indirect pre-cooling evaporative heat exchanger operating in hot and humid climate, Energy Convers. Manag. 102 (2015) 140–150. doi:10.1016/j.enconman.2015.02.025.

[52] G. Heidarinejad, M. Bozorgmehr, S. Delfani, J. Esmaeelian, Experimental investigation of two-stage indirect/direct evaporative cooling system in various climatic conditions, Build. Environ. 44 (2009) 2073–2079. doi:10.1016/j.buildenv.2009.02.017.

[53] E. González Cruz, E. Krüger, Evaluating the potential of an indirect evaporative passive cooling system for Brazilian dwellings, Build. Environ. 87 (2015) 265–273. doi:10.1016/j.buildenv.2015.01.020.

[54] E. Velasco Gómez, A. Tejero González, F.J. Rey Martínez, Experimental characterisation of an indirect evaporative cooling prototype in two operating modes, Appl. Energy. 97 (2012) 340–346. doi:10.1016/j.apenergy.2011.12.065.

[55] A. Ahmad, S. Rehman, L.M. Al-Hadhrami, Performance evaluation of an indirect evaporative cooler under controlled environmental conditions, Energy Build. 62 (2013) 278–285. doi:10.1016/j.enbuild.2013.03.013.

[56] A. Tejero-González, M. Andrés-Chicote, E. Velasco-Gómez, F.J. Rey-Martínez, Influence of constructive parameters on the performance of two

indirect evaporative cooler prototypes, Appl. Therm. Eng. 51 (2013) 1017–1025. doi:10.1016/j.applthermaleng.2012.10.054.

[57] E.V. Gómez, F.J.R. Martínez, F.V. Diez, M.J.M. Leyva, R.H. Martín, Description and experimental results of a semi-indirect ceramic evaporative cooler, Int. J. Refrig. 28 (2005) 654–662. doi:10.1016/j.ijrefrig.2005.01.004.

[58] S. De Antonellis, C.M. Joppolo, P. Liberati, S. Milani, L. Molinaroli, Experimental analysis of a cross flow indirect evaporative cooling system, Energy Build. 121 (2016) 130–138. doi:10.1016/j.enbuild.2016.03.076.

[59] I.L. Maclaine-cross, P.J. Banks, A General Theory of Wet Surface Heat Exchangers and its Application to Regenerative Evaporative Cooling, J. Heat Transfer. 103 (1981) 579–585. http://dx.doi.org/10.1115/1.3244505.

[60] C. Ren, H. Yang, An analytical model for the heat and mass transfer processes in indirect evaporative cooling with parallel/counter flow configurations, Int. J. Heat Mass Transf. 49 (2006) 617–627. doi:10.1016/j.ijheatmasstransfer.2005.08.019.

[61] J.F.S. José Alonso, F.J.R. Martínez, E.V. Gómez, M. a. A.-G. Plasencia, Simulation model of an indirect evaporative cooler, Energy Build. 29 (1998) 23–27. doi:10.1016/S0378-7788(98)00014-0.

[62] P.J. Erens, A.A. Dreyer, Modelling of indirect evaporative air coolers, Int. J. Heat Mass Transf. 36 (1993) 17–26. doi:10.1016/0017-9310(93)80062-Y.

[63] M. Poppe, H. Rögener, Evaporative cooling systems, VDI-Warmeatlas, Sect. Mh. (1984).

[64] F. Merkel, Verdunstungskühlung, VDI-Zeitchrift. (1925) 123–8.

[65] A. Hasan, Going below the wet-bulb temperature by indirect evaporative cooling: Analysis using a modified ε-NTU method, Appl. Energy. 89 (2012) 237–245. doi:10.1016/j.apenergy.2011.07.005.

[66] X.C. Guo, T.S. Zhao, A parametric study of an indirect evaporative air cooler, Int. Commun. Heat Mass Transf. 25 (1998) 217–226. doi:10.1016/S0735-1933(98)00008-6.

[67] S. De Antonellis, C.M. Joppolo, P. Liberati, S. Milani, F. Romano, Modeling and experimental study of an indirect evaporative cooler, Energy Build. 142 (2017) 147–157. doi:10.1016/j.enbuild.2017.02.057.

[68] D. Pandelidis, S. Anisimov, Application of a statistical design for analyzing basic performance characteristics of the cross-flow Maisotsenko cycle heat exchanger, Int. J. Heat Mass Transf. 95 (2016) 45–61. doi:10.1016/j.ijheatmasstransfer.2015.11.060.

[69] A. Sohani, H. Sayyaadi, S. Hoseinpoori, Modeling and multi-objective optimization of an M-cycle cross-flow indirect evaporative cooler using the GMDH type neural network, Int. J. Refrig. 69 (2016) 186–204. doi:10.1016/j.ijrefrig.2016.05.011.

[70] P. Mazzei, F. Minichiello, D. Palma, HVAC dehumidification systems for thermal comfort: A critical review, Appl. Therm. Eng. 25 (2005) 677–707. doi:10.1016/j.applthermaleng.2004.07.014.

[71] H. Parmar, D. Hindoliya, Desiccant cooling system for thermal comfort: a review, Int. J. Eng. Sci. 3 (2011) 4218–4227. http://www.ijest.info/docs/IJEST11-03-05-256.pdf.

[72] Y. Sheng, Y. Zhang, N. Deng, L. Fang, J. Nie, L. Ma, Experimental analysis on performance of high temperature heat pump and desiccant wheel system, Energy Build. 66 (2013) 505–513. doi:http://dx.doi.org/10.1016/j.enbuild.2013.07.058.

[73] D. La, Y.J. Dai, Y. Li, R.Z. Wang, T.S. Ge, Technical development of rotary desiccant dehumidification and air conditioning: A review, Renew. Sustain. Energy Rev. 14 (2010) 130–147. doi:10.1016/j.rser.2009.07.016.

[74] Y. Guan, Y. Zhang, Y. Sheng, X. Kong, S. Du, Feasibility and economic analysis of solid desiccant wheel used for dehumidification and preheating in blast furnace: A case study of steel plant, Nanjing, China, Appl. Therm. Eng. 81 (2015) 426–435. doi:10.1016/j.applthermaleng.2015.02.006.

[75] K.F. Fong, T.T. Chow, C.K. Lee, Z. Lin, L.S. Chan, Advancement of solar desiccant cooling system for building use in subtropical Hong Kong, Energy Build. 42 (2010) 2386–2399. doi:10.1016/j.enbuild.2010.08.008.

[76] K.F. Fong, C.K. Lee, T.T. Chow, a. M.L. Fong, Investigation on solar hybrid desiccant cooling system for commercial premises with high latent cooling load in subtropical Hong Kong, Appl. Therm. Eng. 31 (2011) 3393–3401. doi:10.1016/j.applthermaleng.2011.06.024.

[77] C.R. Ruivo, F. Fernández Hernández, J.M. Cejudo López, Influence of the desiccant wheel effectiveness method approaches, with fix and variable effectiveness parameters, on the performance results of an airport air-conditioning system, Energy Convers. Manag. 94 (2015) 458–471. doi:10.1016/j.enconman.2015.01.090.

[78] M. El Hourani, K. Ghali, N. Ghaddar, Effective desiccant dehumidification system with two-stage evaporative cooling for hot and humid climates, Energy Build. 68 (2014) 329–338. doi:10.1016/j.enbuild.2013.09.040.

[79] J.L. Niu, L.Z. Zhang, H.G. Zuo, Energy savings potential of chilled-ceiling combined with desiccant cooling in hot and humid climates, Energy Build.

34 (2002) 487–495. doi:10.1016/S0378-7788(01)00132-3.

[80] K.J. Chua, S.K. Chou, W.M. Yang, Advances in heat pump systems: A review, Appl. Energy. 87 (2010) 3611–3624. doi:10.1016/j.apenergy.2010.06.014.

[81] D.B. Jani, M. Mishra, P.K. Sahoo, Performance studies of hybrid solid desiccant-vapor compression air-conditioning system for hot and humid climates, Energy Build. 102 (2015) 284–292. doi:10.1016/j.enbuild.2015.05.055.

[82] P. Finocchiaro, M. Beccali, B. Nocke, Advanced solar assisted desiccant and evaporative cooling system equipped with wet heat exchangers, Sol. Energy. 86 (2012) 608–618. doi:10.1016/j.solener.2011.11.003.

[83] D. Pandelidis, S. Anisimov, W.M. Worek, P. Drag, Comparison of desiccant air conditioning systems with different indirect evaporative air coolers, Energy Convers. Manag. 117 (2016) 375–392. doi:10.1016/j.enconman.2016.02.085.

[84] M. Goldsworthy, S. White, Optimisation of a desiccant cooling system design with indirect evaporative cooler, Int. J. Refrig. 34 (2011) 148–158. doi:10.1016/j.ijrefrig.2010.07.005.

[85] W. Gao, W. Worek, V. Konduru, K. Adensin, Numerical study on performance of a desiccant cooling system with indirect evaporative cooler, Energy Build. 86 (2015) 16–24. doi:10.1016/j.enbuild.2014.09.049.

[86] E. Elgendy, A. Mostafa, M. Fatouh, Performance enhancement of a desiccant evaporative cooling system using direct/indirect evaporative cooler, Int. J. Refrig. 51 (2015) 77–87. doi:10.1016/j.ijrefrig.2014.12.009.

[87] J.D. Chung, D.Y. Lee, Contributions of system components and operating conditions to the performance of desiccant cooling systems, Int. J. Refrig. 34 (2011) 922–927. doi:10.1016/j.ijrefrig.2011.03.003.

[88] S.D. White, P. Kohlenbach, C. Bongs, Indoor temperature variations resulting from solar desiccant cooling in a building without thermal backup, Int. J. Refrig. 32 (2009) 695–704. doi:10.1016/j.ijrefrig.2009.01.019.

[89] K.F. Fong, T.T. Chow, C.K. Lee, Z. Lin, L.S. Chan, Comparative study of different solar cooling systems for buildings in subtropical city, Sol. Energy. 84 (2010) 227–244. doi:10.1016/j.solener.2009.11.002.

[90] S.W. Ham, S.J. Lee, J.W. Jeong, Operating energy savings in a liquid desiccant and dew point evaporative cooling-assisted 100% outdoor air system, Energy Build. 116 (2016) 535–552. doi:10.1016/j.enbuild.2016.02.011.

[91] M. Jradi, S. Riffat, Experimental and numerical investigation of a dew-point cooling system for thermal comfort in buildings, Appl. Energy. 132 (2014) 524–535. doi:10.1016/j.apenergy.2014.07.040.

[92] Dehumidification and Air Drying, DESSECA, promoted by the company CIAT and co-funded by the Agency for Innovation and Development of Andalusia, expedient IDEA 360097, and by the Technological Corporation of Andalusia, expedient CTA 12/612, (2012-2014).

[93] Agilent Technologies, http://www.agilent.com, (Accessed 05.07.17).

[94] National Instruments, http://www.ni.com, (Accessed 05.07.17).

[95] DIN EN ISO 5167-2 Standards, Masurement of a fluid flow by means of pressure differential devices inserted in circular cross-section conduits running full - Part 2: Orifice plates (ISO 5167-2:2003).

[96] Statgraphics Centurion XV, (2006). doi:Available from (http://www.statgraphics.com/) (accessed 21.08.17).

[97] F.E. Nia, Sustainable Air Handling by Evaporation and Adsorption, PhD thesis, Deft University of Technology, 2011.

[98] American Society of Heating, Method of Testing for Rating Desiccant Dehumidifiers Utilizing Heat for the Regeneration Process, American Society of Heating, Refrigerating and Air-Conditioning Engineers, Incorporated, 2007.

[99] CIAT, http://www.grupociat.es/, (Accessed 05.07.17).

[100] Klein, S.A. 2006. TRNSYS 17: A Transient System Simulation Program, SEL, University of Wisconsin, Madison USA.

[101] SODECA, http://www.sodeca.es/, (Accessed 05.07.17).

[102] Ashrae, ASHRAE STANDARD 90.1 Energy Standard for Buildings Except Low-Rise Residential Buildings, Society. 8400 (2007) 404–636. doi:http://dx.doi.org/10.1108/17506200710779521.

[103] Meteotest (2003). Meteonorm handbook, Parts I, II and III. Meteotest, Bern, Switzerland. http://www.meteotest.ch, (accessed 05.07.17).

[104] B. Riangvilaikul, S. Kumar, An experimental study of a novel dew point evaporative cooling system, Energy Build. 42 (2010) 637–644. doi:10.1016/j.enbuild.2009.10.034.

[105] S. Anisimov, D. Pandelidis, A. Jedlikowski, V. Polushkin, Performance investigation of a M (Maisotsenko)-cycle cross-flow heat exchanger used for indirect evaporative cooling, Energy. 76 (2014) 593–606. doi:10.1016/j.energy.2014.08.055.

[106] X. Cui, K.J. Chua, M.R. Islam, W.M. Yang, Fundamental formulation of a modified LMTD method to study indirect evaporative heat exchangers, Energy Convers. Manag. 88 (2014) 372–381. doi:10.1016/j.enconman.2014.08.056.

Appendix A

First and second order simplified models for the performance evaluation of low temperature activated desiccant wheels

The paper presented in this appendix is published in *Energy and Buildings* (doi: 10.1016/j.enbuild.2016.02.005)

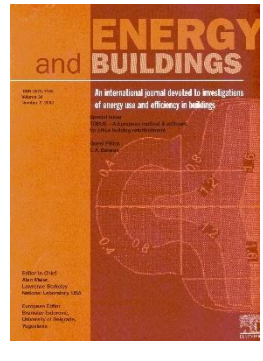

Energy and Buildings 116 (2016) 574–582

Contents lists available at ScienceDirect

Energy and Buildings

journal homepage: www.elsevier.com/locate/enbuild

First and second order simplified models for the performance evaluation of low temperature activated desiccant wheels

F. Comino*, M. Ruiz de Adana, F. Peci

Departamento de Química-Física y Termodinámica Aplicada, Escuela Politécnica Superior, Universidad de Córdoba, Campus de Rabanales, Antigua Carretera Nacional IV, km 396, 14072 Córdoba, Spain

ARTICLE INFO

Article history:
Received 9 September 2015
Received in revised form
17 December 2015
Accepted 1 February 2016
Available online 2 February 2016

Keywords:
Desiccant wheel
Low temperature activated systems
Design of experiments

ABSTRACT

Hybrid systems with a desiccant wheel, DW, are an alternative to heating, ventilation and air conditioning, HVAC, commonly used systems for dehumidification and humidity control in rooms with high latent loads.

Currently, the experimental methodology used to study the behaviour of a DW requires a high number of tests. The aim of this study is to obtain a DW empirical model which accurately represents the behaviour of a DW activated at low temperature, values below 60 °C, by conducting a reduced number of experimental tests. For this study, the statistical Design of Experiments technique, DOE, is used.

The proposed models can be used to predict the influence of the inlet process air and inlet regeneration air, on the air process outlet temperature and humidity ratio. The accuracy obtained of the experimental models is more than acceptable, with R^2 values greater than 97.4% for outlet temperature and 95.1% for outlet humidity ratio. The first order model was considered to be a good option due to the balance between accuracy and the low number of experimental tests required. However, the second order model allowed a deeper understanding of the behaviour of the air outlet conditions in the DW.

1. Introduction

The control of the water vapour content in the air is necessary to maintain the required indoor conditions in buildings and certain industrial processes. The external and internal water vapour sources can produce significant latent loads indoors, so it is necessary to use a system to reduce and control the humidity ratio. Restaurants, indoor swimming pools or spas are examples of premises with high latent loads. There are two techniques of removing moisture from air under ambient pressure conditions: cooling-based and desiccant dehumidification. Cooling-based systems reduce the air temperature to condense its moisture. Desiccant dehumidifier systems differ from cooling-based systems in the way of removing moisture from the air. Desiccant dehumidifier systems adsorb water vapour from the air reaching an area of low vapour pressure at the surface of the desiccant [1]. Furthermore, desiccants can adsorb substances other than water vapour removing in this way air contaminants and improving indoor air quality [2].

Desiccant dehumidifiers can be combined with cooling systems, solar systems or waste heat systems. These combined systems are referred to as hybrid systems. Many studies about hybrid systems with desiccant wheels, DW, have been carried out [3,4]. Energy savings were obtained only when the DW was regenerated using waste heat from another process. Some authors studied the behaviour of hybrid systems using waste energy to regenerate the DW, obtaining significant economic savings [5,6]. However, in some cases waste heat energy is not available or the corresponding temperature level is not adequate. In recent years, some studies have analysed the use of solar energy to regenerate a DW [7,8]. However, these systems require an auxiliary source of heat. The solar thermal system also involves a significant increase in the overall economic cost of the system.

A DW integrated into a hybrid system can be operated at low regeneration temperatures. Hybrid systems with air regeneration temperatures of 55 °C and 46 °C [6,9] has been analysed, showing acceptable desiccant capacity. Values below 60 °C were considered low regeneration temperatures in this study, which correspond to the outlet air temperature in an air-cooled condenser of a refrigeration vapour compression system.

Two low temperature activated systems with DW are shown in Fig. 1. The first system is composed of a solar thermal heating system and a low temperature boiler that supplies hot water to the

* Corresponding author. Tel.: +34 626285994.
E-mail address: francisco.comino@uco.es (F. Comino).

http://dx.doi.org/10.1016/j.enbuild.2016.02.005
0378-7788/

Nomenclature

a estimated parameter
CC cooling coil
DOE design of experiments
DW desiccant wheel
EA exhaust air
F centrifugal fan
FC flow conditioner
EH electric heater
HC heating coil
HR relative humidity [%]
k number of parameters
MA mixed air
MB mixing box
N number of experimental test
OA outdoor air
PT pitot tube
RA recirculated air
SH steam humidifier
T temperature [°C]
X input variable
$\hat{Y}$ estimated output value

Greek letters
ΔP pressure difference [Pa]
ω humidity ratio [g kg^{-1}]
Ω specific mass airflow rate [kg s^{-1} m^{-3}]

Subscripts
d dew point
i inlet
o outlet
p process
r regeneration

heating coil, HC. The HC heats up the regeneration air upstream of the DW, see Fig. 1a. Fig. 1b shows a low regeneration temperature hybrid system composed of a refrigeration vapour compression system and a DW. This hybrid system allows the regeneration of the DW using the heat from the condenser. In addition, the evaporator cooling effect is used to cool and dehumidify the process air.

A numerical model of a DW is very convenient for parametric optimization analysis of hybrid systems. Different experimental and numerical research works have been carried out in order to study the operational parameters that influence the overall performance of the DW. Some researchers developed detailed mathematical models, considering the heat and mass transfer in the DW [10–14]. These models are not easy to implement and require long computation time. Moreover, some physical characteristics and specific materials of the DW are not normally available.

Another mathematical modelling approach is based on simplified models of the DW which requires less computation time. A widely used simplified method to study the behaviour of the DW is one that is based on the effectiveness concept. It is also referred to as the linear analogy method [15] and takes into account two independent potential variables [16]. The effectiveness method based on constant values has been used previously in several studies [17,18]. These simplified mathematical models are easy to implement, but many experimental tests are required to fit the effectiveness parameters. Important errors can be introduced when constant values of the effectiveness parameters are assumed in the effectiveness method [19]. Simplified mathematical models can be improved by using variable parameters of effectiveness. However, the accuracy of simplified models is reduced when variable effectiveness parameters are obtained by means of interpolation [19].

Other authors have developed simplified models based on correlations to study the behaviour of the DW [20–22]. The advantage of this approach is that the model fits any physical characteristics and specific materials of one specific DW. However, the obtained simplified model is not valid for any other DW.

A methodology widely used in engineering to obtain a regression model is the design of experiments, DOE [23,24]. DOE is a technique used for exploring new processes, gaining knowledge of the existing processes and optimizing these processes to achieve high performance [25].

The objective of this work is to obtain a DW empirical model which accurately represents the behaviour of a DW activated at low temperature by conducting a reduced number of experimental tests. The methodology used is based on the statistical technique of DOE. The secondary aim of this work is to identify the most influential factors in the behaviour of a DW activated at low regeneration temperatures.

2. Methodology

2.1. Experimental setup

In order to analyse DW performance under different working conditions, a test facility has been designed. A schematic diagram of the DW experimental setup is shown in Fig. 2. Process and regeneration air streams flow across the DW in counter-current arrangement. Inlet process air and regeneration air temperature and humidity are carefully controlled by means of a cooling coil (CC), heating coil (HC), electric heater (EH), and a steam humidifier (SH), located, for each air stream, upstream of the DW [26,27].

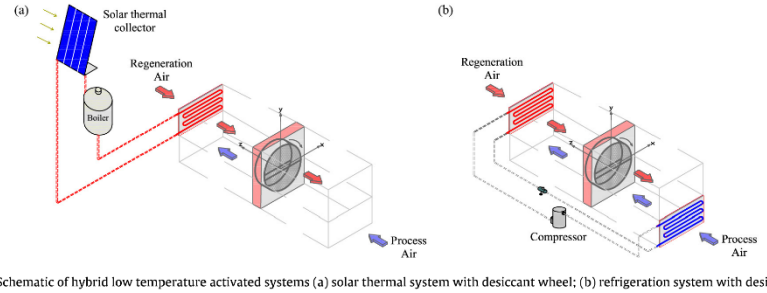

Fig. 1. Schematic of hybrid low temperature activated systems (a) solar thermal system with desiccant wheel; (b) refrigeration system with desiccant wheel.

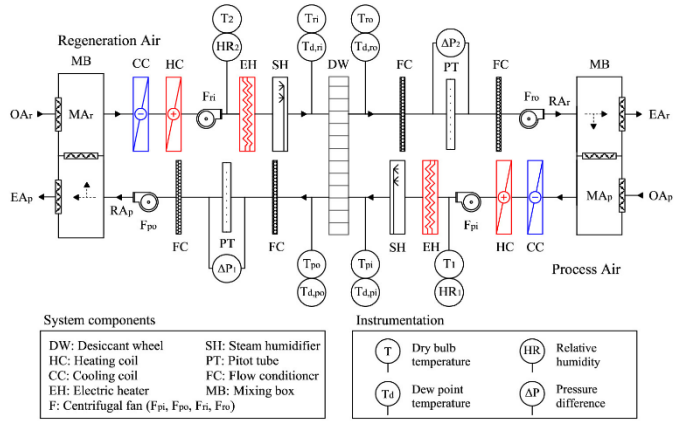

Fig. 2. Layout of test facility.

The process and regeneration airflow rates are controlled by means of variable speed fans (*F*). Two mixing boxes (MB), are used to recirculate the process and regeneration air streams or to mix the exterior air with the treated air. Characteristic of the equipment of the experimental test rig setup are shown in Table 1.

The DW is divided into two equal partitions and rotates at a constant speed of 42 rph. The matrix of the DW consists of alternate layers of flat and corrugated sheets of silica gel and metal silicates, chemically bonded into a tissue of inorganic fibres. The nominal process air flow and nominal regeneration air flow is 2300 $m^3 h^{-1}$. Other physical and operational characteristics of the DW are shown in Table 2.

Two Pitot tubes (PT) are used to measure the airflow rate. Four flow conditioners (FC) are installed in the ducts, two upstream of the airflow rate measuring point and two downstream, in order to obtain stable airflow conditions.

The measured variables in the test rig, the type of sensor and its accuracy are shown in Table 3. The locations of the sensors are shown in Fig. 2. The temperature and humidity at the inlet and outlet of the DW are measured at three different points along the horizontal axis, averaging the three measurements [28]. All the experimental tests are carried out under steady-state conditions. The maximum values of standard deviations of the mean are ±0.32 °C for the temperature, ±1.2 g kg^{-1} for the humidity ratio and ±22 $m^3 h^{-1}$ for the airflow rate. The sampling time was 3 s and the values are averaged every 20 min.

Table 1
Characteristics of equipment.

Equipment	Value
Cooling coil (CC)	
Total cooling capacity	15.8 kW
Sensible cooling capacity	12.2 kW
Nominal water flow	2.7 $m^3 h^{-1}$
Nominal pressure drop	5.1 m
Heating coil (HC)	
Heating capacity	18.8 kW
Nominal water flow	2.7 $m^3 h^{-1}$
Nominal pressure drop	5.1 m
Electric heater (EH)	
Electric power	7.2 kW
Fan (F)	
Nominal airflow	3100 $m^3 h^{-1}$
Available static pressure	0.007 m
Nominal motor power	0.6 kW
Speed	1125 rpm
Steam humidifier (SH)	
Steam flow	45 kg h^{-1}
Max. power	33.75 kW

Table 2
Characteristics of desiccant wheel.

Parameters	Value
Rotor diameter	550 mm
Rotor length	200 mm
Desiccant material	Silica gel
Channel shape	Honeycomb
Nominal capacity	15 kg h^{-1}
Nominal air flow	2300 $m^3 h^{-1}$
Rotation speed	42 rph
Weight	57 kg
Power supply	230 V

Table 3
Specification of measuring devices.

Measured parameter	Type	Accuracy
T_1, T_2, T_{pi}, T_{po}, T_{ri}, T_{ro} $T_{d,pi}$, $T_{d,po}$	PT 100 Chilled mirror hygrometer	±0.12 °C ±0.15 °C
$T_{d,ri}$, $T_{d,ro}$	Capacitive	±0.4 °C
HR_1, HR_2	Capacitive	±3%
ΔP_1, ΔP_2	Differential pressure transmitter	±0.3% (0 to 1 mbar)

2.2. Design of experiment

The statistical technique DOE is used to fit different models with the experimental data. DOE is a methodology for systematically applying statistics to the experimental process [25,29]. The number of required experimental tests can be reduced if they are

Table 4
Design of case studies.

Case study	Type	Order	Input variables						Output variables	
			T_{pi}	ω_{pi}	T_{ri}	ω_{ri}	Ω_p	Ω_r	T_{po}	ω_{po}
1	2 level factorial	First	x	x	x	x			x	x
2	2 level factorial	First	x	x	x	x	x	x	x	x
3	3 level Box–Behnken	Second	x	x	x	x			x	x

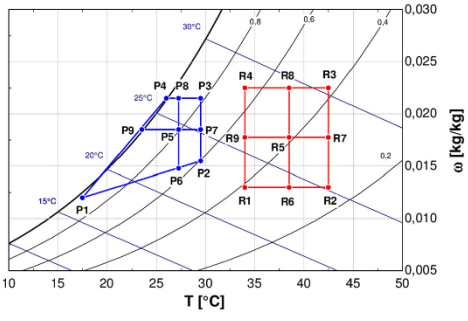

Fig. 3. Grid for the inlet states of the process and regeneration airflow for case studies 1, 2 and 3.

optimally designed. Usually, several candidate models can be proposed. The choice between these candidate models is a trade-off between complexity and precision.

In this study, the statistical technique DOE is used to obtain simplified mathematical models by means of a reduced number of experimental tests. Three cases were studied using different input and output variables, as shown in Table 4. The input variables were the inlet air process temperature, T_{pi}, inlet air process humidity ratio, ω_{pi}, process specific mass airflow rate, Ω_p, ratio of inlet mass velocity to the channel length [19], inlet air regeneration temperature, T_{ri}, inlet air regeneration humidity ratio, ω_{ri}, and regeneration specific mass airflow rate, Ω_r. The output variables were the outlet air process temperature, T_{po}, and outlet air process humidity ratio, ω_{po}. In case studies 1 and 3, the effect of four input variables, T_{pi}, ω_{pi}, T_{ri}, ω_{ri}, were studied applying a two level factorial design [25] and a three level Box–Behnken design [25], respectively. In case study 2, the effect of five input variables, T_{pi}, ω_{pi}, T_{ri}, ω_{ri}, Ω_p, Ω_r, was studied using a two level factorial design. In both air streams were circulated the same air flow rates for all cases.

2.2.1. Case study 1

Two grids were defined to cover the range of validity of the process and regeneration air streams, as shown in Fig. 3. The ranges were selected to implement the DW model in low temperature activated hybrid models. The process air flow ranges were from 17.5 °C to 29.5 °C for temperature and from 12 g kg^{-1} to 21.5 g kg^{-1} for humidity ratio. The regeneration air flow ranges were from 34 °C to 42.5 °C for temperature and from 13 g kg^{-1} to 22.5 g kg^{-1} for humidity ratio, see Table 5. The process grid was defined as: (i) four inlet limit states for the process airflow were selected, *P*1 to *P*4, as shown in the psychrometric chart of Fig. 3, covering the range of interest and (ii) a fifth inlet state *P*5 was added, located inside the four-sided polygon previously defined. The regeneration inlet conditions were defined introducing another set of five points *R*1 to *R*5, see Fig. 3. The resulting process grid was not rectangular, in order to obtain the widest range of validity. The combination of tests was

Table 5
Inlet states airflow for case studies 1, 2 and 3.

Point	T_{pi} [°C]	ω_{pi} [g kg^{-1}]	Point	T_{ri} [°C]	ω_{ri} [g kg^{-1}]
*P*1	17.50	12.00	*R*1	34.00	13.00
*P*2	29.50	15.50	*R*2	42.50	13.00
*P*3	29.50	21.50	*R*3	42.50	22.50
*P*4	26.00	21.50	*R*4	34.00	22.50
*P*5	27.25	18.50	*R*5	38.50	17.75
*P*6	27.25	14.60	*R*6	38.50	13.00
*P*7	29.50	18.50	*R*7	42.50	17.75
*P*8	27.25	21.50	*R*8	38.50	22.50
*P*9	24.00	18.50	*R*9	34.00	17.75

Table 6
Experimental tests defined for case study 1 based on the factorial design approach.

N	Process	Regeneration	*N*	Process	Regeneration
1	*P*2	*R*2	11	*P*3	*R*2
2	*P*1	*R*3	12	*P*4	*R*4
3	*P*3	*R*3	13	*P*1	*R*1
4	*P*1	*R*4	14	*P*5	*R*5
5	*P*2	*R*1	15	*P*3	*R*4
6	*P*3	*R*1	16	*P*1	*R*2
7	*P*2	*R*3	17	*P*4	*R*3
8	*P*5	*R*5	18	*P*4	*R*1
9	*P*4	*R*2	19	*P*5	*R*5
10	*P*2	*R*4	–	–	–

based on a factorial design approach [25]. Table 6 illustrates the experimental tests for case study 1.

All the tests were performed using the nominal airflow rate of the DW. The study consists of 19 experimental tests, including 3 repetitions of the tests combining the interior points, *P*5 and *R*5, and 8 degrees of freedom. The results of this set of experiments were used to fit the parameters of a first order model expressed by the following equation:

$$\hat{Y} = a_0 + \sum_{i=1}^{k} a_i \cdot X_i + \sum_{i=1}^{k=1} \sum_{\substack{i=2 \\ j>i}}^{k} a_{ij} \cdot X_i \cdot X_j \quad (1)$$

where k is the number of parameters, a_0 and a_i are the estimated parameters, X are input variables and $\hat{Y}$ is the estimated output value.

2.2.2. Case study 2

The same grids as in case 1 are used in case study 2, see Fig. 3. The values of temperature and humidity ratio are the same as in case 1, as shown in Table 5. The specific mass airflow rate range considered varies from 14.79 kg s^{-1} m^{-3} (Ω_1) to 30.92 kg s^{-1} m^{-3} (Ω_3). A total of 35 experimental tests were carried out, based on a factorial design approach [25], including 3 repetitions of the tests combining the interior points, *P*5, *R*5 and Ω_2, and 16 degrees of freedom, see Table 7. The results of this set of experiments were used to fit the parameters of a model expressed by Eq. (1).

Table 7
Experimental tests defined for case study 2 based on the factorial design approach.

N	Process	Regeneration	Ω	N	Process	Regeneration	Ω
1	P2	R2	Ω_3	19	P2	R4	Ω_3
2	P1	R3	Ω_3	20	P2	R2	Ω_1
3	P3	R3	Ω_1	21	P1	R1	Ω_1
4	P4	R4	Ω_1	22	P3	R2	Ω_3
5	P2	R4	Ω_1	23	P2	R3	Ω_1
6	P3	R4	Ω_1	24	P4	R4	Ω_3
7	P3	R3	Ω_3	25	P3	R2	Ω_1
8	P3	R1	Ω_1	26	P5	R5	Ω_2
9	P1	R4	Ω_3	27	P3	R4	Ω_3
10	P1	R4	Ω_1	28	P5	R5	Ω_2
11	P1	R3	Ω_1	29	P1	R2	Ω_1
12	P4	R1	Ω_1	30	P1	R2	Ω_3
13	P2	R1	Ω_3	31	P4	R3	Ω_3
14	P3	R1	Ω_3	32	P4	R1	Ω_3
15	P2	R1	Ω_1	33	P4	R2	Ω_3
16	P2	R3	Ω_3	34	P5	R5	Ω_2
17	P4	R2	Ω_3	35	P1	R1	Ω_3
18	P4	R3	Ω_1	–	–	–	–

Table 8
Experimental tests defined for case study 3 based on the Box–Behnken design approach.

N	Process	Regeneration	N	Process	Regeneration
1	P2	R5	15	P3	R5
2	P6	R6	16	P8	R8
3	P4	R5	17	P6	R8
4	P8	R6	18	P5	R5
5	P7	R7	19	P7	R6
6	P8	R9	20	P5	R1
7	P9	R9	21	P5	R4
8	P8	R7	22	P6	R9
9	P5	R3	23	P1	R5
10	P6	R7	24	P5	R5
11	P7	R8	25	P5	R5
12	P9	R6	26	P7	R9
13	P5	R2	27	P9	R7
14	P9	R8	–	–	–

2.2.3. Case study 3

The third case was used to study nonlinear response surfaces with a limited number of tests. Two grids were defined, to cover the same range of validity as in cases 1 and 2, see Table 5, but with additional inlet states, see Table 8. Both grids were defined by inlet states for process air, P1–P9, and inlet states for regeneration air, R1–R9, see Fig. 3. The combination of tests was based on a Box–Behnken design approach [25]. Table 8 illustrates the set of generated tests, which were obtained by implementing all of these inputs. All the tests were performed for the nominal airflow rate of the DW. A total of 27 experimental tests were carried out, including 3 repetitions of the tests combining the interior points, and 12 degrees of freedom. The results of this set of experiments were used to fit the parameters of a second order model expressed by the following equation:

$$\hat{Y} = a_0 + \sum_{i=1}^{k} a_i \cdot X_i + \sum_{i=1}^{k} a_{ii} \cdot X_i^2 + \sum_{i=1}^{k=1} \sum_{\substack{i=2 \\ j>i}}^{k} a_{ij} \cdot X_i \cdot X_j \quad (2)$$

where k is number of parameters, a_0 and a_i are the estimated parameters, X are input variables and $\hat{Y}$ is the estimated output value.

2.3. Accuracy of the models

A statistical analysis was performed to obtain the lack of fit test, the R^2 value and the standard error of the estimate. The lack of fit test is designed to determine whether the selected model is adequate to describe the observed data. The R^2 value and the standard error of the estimate is a measure of the accuracy of the predictions.

3. Results and analysis

3.1. First and second order models

The models given in Eqs. (1) and (2) were adjusted by regression of the data obtained from the experimental tests. The corresponding estimated parameters are shown in Table 9, where $a_1 \ldots a_{15}$ are the regression coefficients, showing the weight each one has in the equation, and a_0 is the average response in the design of experiments, and X_i are the single input variables or their interactions. $\hat{Y}$ is the output variable, corresponds to the outlet process temperature, T_{po}, or the outlet process humidity ratio, ω_{po}.

Case study 2 was tested for balanced specific mass airflow, therefore, the input variable Ω corresponds to the specific mass airflow process, Ω_p, and the specific mass airflow regeneration, Ω_r.

The results for all case studies showed that the parameter with the highest value for T_{po} was a_3, see Table 9, being positive for first order models, case studies 1 and 2, and negative for second order model, case study 3. The parameter with the lowest weight for T_{po} was different in each case: a_7 for case study 1, a_{10} for case study 2, and a_{14} for case study 3. Regarding ω_{po}, the estimated parameter a_2 had the highest weight for the first order models, cases 1 and

Table 9
Estimated parameters for case studies.

Estimated parameters	Case study 1			Case study 2			Case study 3		
	T_{po} ($\times 10^3$) [°C]	ω_{po} ($\times 10^3$) [g kg^{-1}]	X_i	T_{po} ($\times 10^3$) [°C]	ω_{po} ($\times 10^3$) [g kg^{-1}]	X_i	T_{po} ($\times 10^3$) [°C]	ω_{po} ($\times 10^3$) [g kg^{-1}]	X_i
a_0	6081.84	−16,707.70	–	9012.70	−4828.58	–	93,985.40	−9448.80	–
a_1	328.15	144.14	T_{pi}	−25.41	−16.01	T_{pi}	−177.97	1277.70	T_{pi}
a_2	−400.65	1786.87	ω_{pi}	23.17	1783.16	ω_{pi}	−392.09	−1217.59	ω_{pi}
a_3	438.02	82.74	T_{ri}	543.06	−189.88	T_{ri}	−3168.40	82.29	T_{ri}
a_4	−49.42	505.68	ω_{ri}	−291.07	485.12	ω_{ri}	−1361.45	1188.94	ω_{ri}
a_5	8.64	−19.08	$T_{pi}\cdot\omega_{pi}$	−26.53	−337.70	Ω	−8.35	−44.00	T_{pi}^2
a_6	3.49	3.80	$T_{pi}\cdot T_{ri}$	6.38	−7.31	$T_{pi}\cdot\omega_{pi}$	−17.27	78.95	$T_{pi}\cdot\omega_{pi}$
a_7	−1.91	2.16	$T_{pi}\cdot\omega_{ri}$	7.34	7.44	$T_{pi}\cdot T_{ri}$	28.64	9.202	$T_{pi}\cdot T_{ri}$
a_8	4.62	−6.52	$\omega_{pi}\cdot T_{ri}$	−2.36	8.74	$T_{pi}\cdot\omega_{ri}$	21.52	−28.54	$T_{pi}\cdot\omega_{ri}$
a_9	9.73	−13.22	$\omega_{pi}\cdot\omega_{ri}$	8.41	−8.42	$T_{pi}\cdot\Omega$	30.12	−10.47	ω_{pi}^2
a_{10}	−6.78	−4.24	$T_{ri}\cdot\omega_{ri}$	−0.21	−20.09	$\omega_{pi}\cdot T_{ri}$	−8.06	−11.85	$\omega_{pi}\cdot T_{ri}$
a_{11}	–	–	–	4.78	−11.79	$\omega_{pi}\cdot\omega_{ri}$	11.17	29.96	$\omega_{pi}\cdot\omega_{ri}$
a_{12}	–	–	–	3.04	6.25	$\omega_{pi}\cdot\Omega$	37.53	−2.63	T_{ri}^2
a_{13}	–	–	–	−0.51	−4.71	$T_{ri}\cdot\omega_{ri}$	7.06	−5.08	$T_{ri}\cdot\omega_{ri}$
a_{14}	–	–	–	−7.56	14.04	$T_{ri}\cdot\Omega$	5.39	−14.74	ω_{ri}^2
a_{15}	–	–	–	3.31	−5.11	$\omega_{ri}\cdot\Omega$			–

Table 10
Effects of input variables on output variables of the DW.

Case study 1

	T_{po}				ω_{po}			
Effect	Estimate	Stnd. error	*F*-ratio	*P*-value	Estimate	Stnd. error	*F*-ratio	*P*-value
Average	29.96	0.12			14.21	0.05		
T_{pi}	4.05	0.28	594.24	0.0017	−0.69	0.17	22.12	0.0450
ω_{pi}	1.44	0.23	38.74	0.0249	7.64	0.16	2326.64	0.0004
T_{ri}	6.87	0.12	997.45	0.0010	0.78	0.1	23.20	0.0405
ω_{ri}	−1.81	0.12	198.85	0.0050	1.58	0.1	248.43	0.0040
	Lack-of-fit *P*-value: 0.102				Lack-of-fit *P*-value: 0.097			

Case study 2

	T_{po}				ω_{po}			
Effect	Estimate	Stnd. error	*F*-ratio	*P*-value	Estimate	Stnd. error	*F*-ratio	*P*-value
Average	31.33	0.04			14.64	0.04		
T_{pi}	4.53	0.08	4542.12	0.0002	−1.01	0.08	161.79	0.0061
ω_{pi}	1.96	0.07	1935.40	0.0006	7.64	0.07	11,789.5	0.0001
T_{ri}	5.89	0.04	13,011.2	0.0001	1.08	0.04	688.45	0.0014
ω_{ri}	−2.01	0.04	2559.92	0.0004	1.88	0.04	2357.63	0.0004
$\Omega 2$	−1.45	0.04	744.94	0.0013	0.24	0.04	40.54	0.0238
	Lack-of-fit *P*-value: 0.072				Lack-of-fit *P*-value: 0.102			

Case study 3

	T_{po}				ω_{po}			
Effect	Estimate	Stnd. error	*F*-ratio	*P*-value	Estimate	Stnd. error	*F*-ratio	*P*-value
Average	29.47	0.07			14.97	0.07		
T_{pi}	2.99	0.49	203.35	0.0049	−1.51	0.19	99.48	0.0099
ω_{pi}	1.24	0.23	29.31	0.0325	3.75	0.10	1416.55	0.0007
T_{ri}	7.05	0.17	310.53	0.0032	1.98	0.12	170.63	0.0058
ω_{ri}	−1.78	0.17	110.22	0.0090	2.36	0.12	417.13	0.0024
	Lack-of-fit *P*-value: 0.085				Lack-of-fit *P*-value:0.099			

2, see Table 9. However, for the second order model, case study 3, the estimated parameter with the highest weight was a_1. The estimated parameters with lower weights for ω_{po} were: a_7 for case study 1, a_{13} for case study 2, and a_{12} for case study 3.

3.2. Statistical analysis

The results of the analyses of variance, ANOVA, for the three case studies are summarized in Table 10. This table shows each of the main estimated effects, the standard error of each of the effects, which measures their sampling error, the statistical parameter *F*-ratio, the statistical parameter *P*-value and the lack-of-fit test. All variables were found significant at 95% confidence level. Therefore, a variation of the output variables with the input variables was expected. The models were found to be suitable for the observed data at 95% confidence level, as the *P*-values for lack-of-fit tests were greater than 0.05 in all cases.

The results for case studies 1 and 3 showed that the most influential variables on the outlet process temperature, T_{po}, ordered from most to least influential, were: regeneration inlet air temperature, T_{ri}, process inlet air temperature, T_{pi}, inlet regeneration humidity ratio, ω_{ri}, and inlet process humidity ration, ω_{pi}, as a result of the parameter *P*-value. Regarding outlet process humidity ratio, ω_{po}, the most influential variables, ordered from most to least influential, were: inlet process humidity ratio, ω_{pi}, inlet regeneration humidity ratio, ω_{ri}, inlet regeneration air temperature, T_{ri}, and inlet process air temperature, T_{pi}, as a result of the parameter *P*-value. This suggested that, if extremely dry process air outlet conditions were necessary, the inlet regeneration humidity ratio, ω_{ri}, should not be very high, and if low temperature air outlet conditions were necessary, the regeneration temperature, T_{ri}, should not be high.

The results for case study 2 showed that the temperature, humidity ratio and specific mass airflow rate of the process air and regeneration air influenced the output variables. This indicated that, if the moisture of the desiccant increased, it would be important to keep the process and regeneration airflow proportional to the moisture being absorbed by the desiccant on the process air side. However, to achieve greater dehumidification, the specific mass airflow rates were less influential than the inlet process and regeneration air temperatures and humidity ratios, according to the parameter *P*-value.

The R^2 values and standard errors of the estimate for the three models are presented in Table 11. It can be observed that the accuracy of the regression models was guaranteed with a limited amount of tests. R^2 values obtained were greater than 97.4% for outlet temperature and 95.1% for outlet humidity ratio for all 3 cases. The R^2 coefficients for ω_{po} obtained were lower than the R^2 coefficients for T_{po}. R^2 values in very good agreement, 98% for T_{po} and 99% for ω_{po}, were obtained in the first model proposed by Beccali, called Model 54 [20]. The methodology of model development was complex and 54 experimental tests were required to fit the model. To overcome the complexities of Model 54, further

Table 11
Results of the accuracy of the models.

Model	*N* (design exp. tests)	R^2 (T_{po}) [%]	R^2 (ω_{po}) [%]	Stnd. Error of Est. (T_{po})	Stnd. Error of Est. (ω_{po})
Case study 1	19	98.77	98.56	0.23	0.21
Case study 2	35	97.46	95.14	0.10	0.1
Case study 3	27	98.68	96.62	0.12	0.3

simplifications were made [20]. However, model accuracy decreased, with R^2 values equal to 97% for T_{po} and 95% for ω_{po}.

The standard errors of the estimate obtained were acceptable, lower than 0.3 for all the cases. Based on these results, a first order model could be sufficiently precise to estimate T_{po} and ω_{po}. However, previous studies showed nonlinear trend in the adsorption process when the input variables of DW were varied [30]. Second order models, as case study 3, allow to study nonlinear processes [25].

3.3. Response surfaces for case study 3

The main cross effects of the input variables on the output variables corresponding to the second order model, case study 3, are shown in Fig. 4. It can be observed that T_{po} increased as T_{pi}, ω_{pi} and T_{ri} increased. However, an increase of ω_{ri} caused the opposite effect. It was also observed that an increase of T_{pi}, ω_{pi} and ω_{ri}, produced an increase of the value of ω_{po}. The opposite was true for variable T_{ri}. Similar results were obtained in previous studies [1,30].

The response surfaces and contour line plots for outlet process temperature and outlet process humidity ratio were obtained from the second order model, corresponding to case study 3. T_{pi} and ω_{pi} were considered variables and T_{ri} and ω_{ri} were fixed at constant values of 40 °C and 15 g kg^{-1}, respectively. The trends of the treated air by the DW were similar for different values of T_{ri} and ω_{ri}, as shown in Fig. 5. It can be observed that T_{po} increased as T_{pi} was increased,

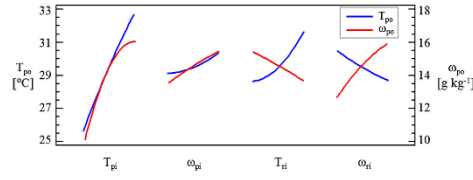

Fig. 4. Trends of the main cross effects for the temperature and humidity ratio of the process outlet air-stream for case study 3.

when ω_{pi} remained constant. For example, an increase of approximately 1.5 °C for T_{pi}, yielded an increase of 1 °C for T_{po}. However, T_{po} values exhibited a minimal variation with ω_{pi}, representing low gradient, when T_{pi} remained constant, see Fig. 5a and b.

Regarding ω_{po}, low values of T_{pi} and ω_{pi} were achieved when the inlet air was near saturation. As ω_{pi} was higher, the outlet air process humidity ratio, ω_{po}, increased when T_{pi} remained constant, see Fig. 5c and d.

Fig. 6 shows the response surfaces and contour line plots for outlet process temperature, T_{po}, and outlet process humidity ratio, ω_{po}, when T_{ri} and ω_{ri} were variables and T_{pi} and ω_{pi} were fixed at constant values of 23.5 °C and 18.5 g kg^{-1}, respectively. The trends of the treated air by the DW were similar for different values of T_{pi} and ω_{pi}. Regarding T_{po}, significant dependence on T_{ri} was observed,

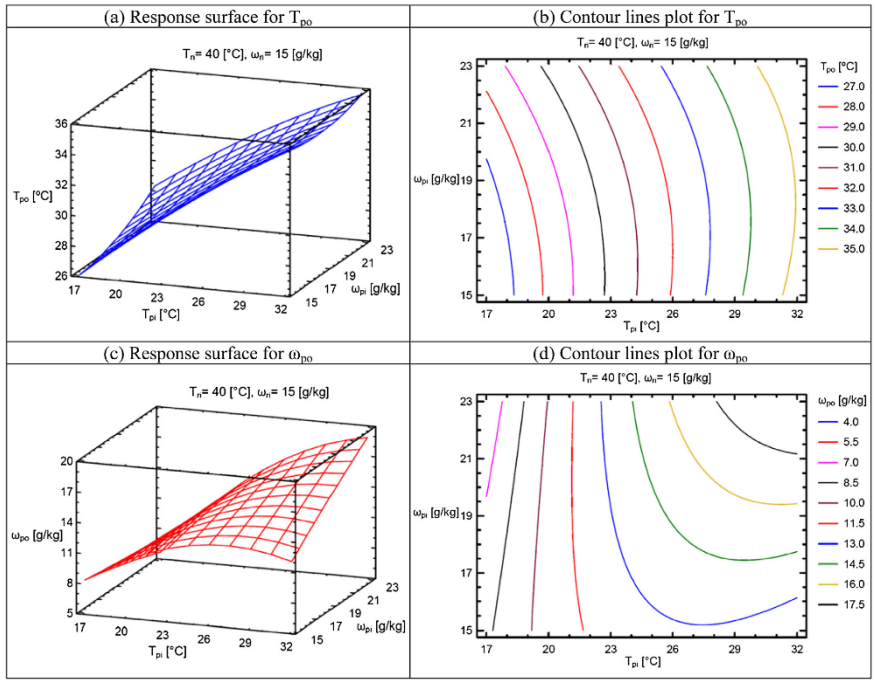

Fig. 5. Response surfaces and contour line plots for case study 3 when the input variables T_{ri} and ω_{ri} remain constant.

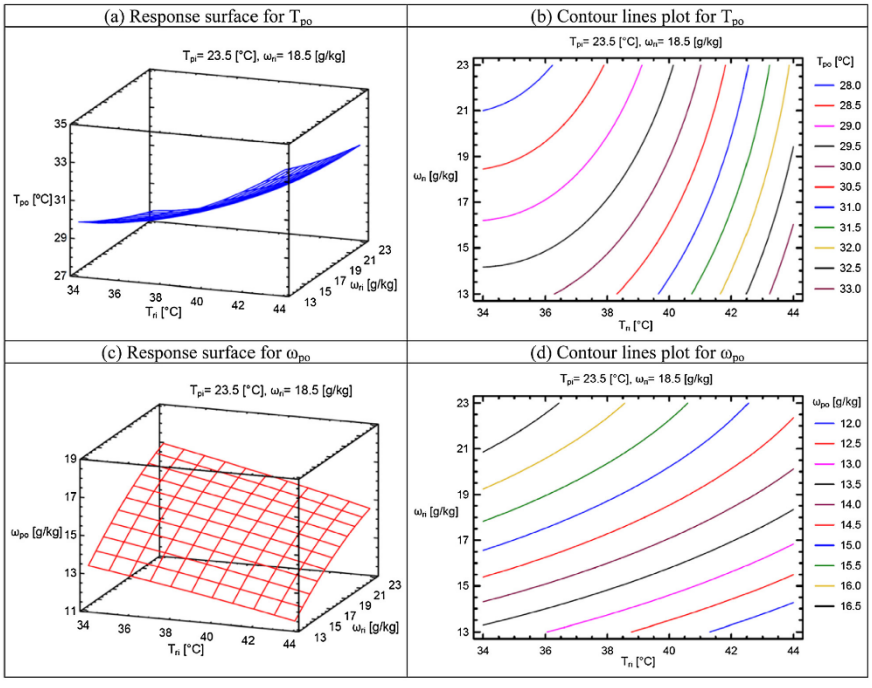

Fig. 6. Response surfaces and contour line plots for case study 3 when the input variables T_{pi} and ω_{pi} remain constant.

as a portion of regeneration heat was transferred to the airflow process stream see Fig. 6a and b. However, the influence was reduced as T_{ri} decreased. Conversely, the influence of ω_{ri} on the output variable, T_{po} was weak, see Fig. 6a and b. The effect on ω_{po} was quite predictable. An increase of T_{ri} and a decrease of ω_{ri} resulted in a decrease of ω_{po}, see Fig. 6c and d. This effect was discussed in Section 3.2.

4. Conclusions

In this work, three different empirical models of a DW were fitted by conducting a limited number of experimental tests using a methodology based on the statistical technique of design of experiments, DOE. The three models can be used to predict the air process outlet temperature and air process outlet humidity ratio in the DW especially for low regeneration temperature activated systems. Two first order models with 19 and 35 experimental tests, case studies 1 and 2 respectively, and one second order model with 27 experimental tests, case study 3, were carried out. These three models considered the influence of the air inlet temperature and air inlet humidity ratio of the process and regeneration air on the DW. The influence of the process and regeneration airflow rate was also considered in the first order model for case study 2.

The accuracy of the numerical results of the models has been found to be acceptable in all models, with R^2 values greater than 97.4% for outlet temperature and 95.1% for outlet humidity ratio. First order models show are in good agreement with the experimental tests. However, the second order model, case study 3, allows to study nonlinear processes.

The methodology of DOE has also allowed the identification of the most influential psychrometric factors in the behaviour of a DW. The results show a significant influence on the inlet humidity ratio of the air process and the air regeneration to achieve greater dehumidification.

The results suggest that the proposed approach is a valid methodology to study the global behaviour of a DW. This methodology uses a limited number of experimental tests and the simplified mathematical models obtained are suitable for integration in simulation tools.

Acknowledgements

This work is related to the research project dehumidification and air drying, DESSECA, promoted by the company CIAT and co-funded by the Agency for Innovation and Development of Andalusia, expedient IDEA 360097, and by the Technological Corporation of Andalusia, expedient CTA 12/612, (2012-2014). The authors are grateful for the collaboration of Adoración Cerezuela Parish and Dr. Miguel Zamora García from CIAT Spain R&I Department.

References

[1] L.G. Harriman III, The Dehumidification Handbook, second ed., Munters Corp, Amesbury, MA, 2003.

[2] A.J. Hines, T.K. Ghosh, S.K. Loyalka, R.C. Warder Jr., Investigation of co-sorption of gases and vapors as a means to enhance indoor air quality, in: ASHRAE Research Project 475-RP and Gas Research Institute Project GRI-90/0194, Gas Research Instit, 1991.
[3] A.G.C.C.American Gas Cooling Center, Applications Engineering Manual for Desiccant Systems, Arlington, TX, 1996.
[4] Y. Sheng, Y. Zhang, N. Deng, L. Fang, J. Nie, L. Ma, Experimental analysis on performance of high temperature heat pump and desiccant wheel system, Energy Build. 66 (2013) 505–513.
[5] Y. Guan, Y. Zhang, Y. Sheng, X. Kong, S. Du, Feasibility and economic analysis of solid desiccant wheel used for dehumidification and preheating in blast furnace: a case study of steel plant, Nanjing, China, Appl. Therm. Eng. 81 (2015) 426–435.
[6] D. Kosar, Dehumidification system enhancement, ASHRAE J. 48 (2006) 48–58.
[7] K.F. Fong, T.T. Chow, C.K. Lee, Z. Lin, L.S. Chan, Advancement of solar desiccant cooling system for building use in subtropical Hong Kong, Energy Build. 42 (2010) 2386–2399.
[8] M. El Hourani, K. Ghali, N. Ghaddar, Effective desiccant dehumidification system with two-stage evaporative cooling for hot and humid climates, Energy Build. 68 (2014) 329–338.
[9] A. Al-Alili, Y. Hwang, R. Radermacher, A hybrid solar air conditioner: experimental investigation, Int. J. Refrig. 39 (2014) 117–124.
[10] J.Y. San, S.C. Hsiau, Effect of axial solid heta-conduction and mass diffusion in a rotary heat and mass regenerator, Int. J. Heat Mass Transfer 36 (1993) 2051–2059.
[11] E. Vandenbulck, J.W. Mitchell, S.A. Klein, Design theory for rotary heat and mass exchangers. 1. Wave analysis of rotary heat and mass exchangers with infinite transfer-coefficients, Int. J. Heat Mass Transfer 28 (1985) 1575–1586.
[12] E. Vandenbulck, J.W. Mitchell, S.A. Klein, Design theory for rotary heat and mass exchangers. 2. Effectiveness-number-of-transfer-units method for rotary heat and mass exchangers, Int. J. Heat Mass Transfer 28 (1985) 1587–1595.
[13] C.R. Ruivo, J.J. Costa, A.R. Figueiredo, On the behaviour of hygroscopic wheels: Part I—Channel modelling, Int. J. Heat Mass Transfer 50 (2007) 4812–4822.
[14] C.R. Ruivo, J.J. Costa, A.R. Figueiredo, On the behaviour of hygroscopic wheels: Part II—Rotor performance, Int. J. Heat Mass Transfer 50 (2007) 4823–4832.
[15] Maclaine, P.J. II, Banks, coupled heat and mass-transfer in regenerators—prediction using an analogy with heat-transfer, Int. J. Heat Mass Transfer 15 (1972) 1225–1242.
[16] J.J. Jurinak, Open cycle Desiccant Cooling and Component Models and System Simulations, University of Wisconsin, Madison, USA, 1982, PhD Thesis.
[17] G. Angrisani, C. Roselli, M. Sasso, Experimental validation of constant efficiency models for the subsystems of an unconventional desiccant-based air handling unit and investigation of its performance, Appl. Therm. Eng. 33–34 (2012) 100–108.
[18] G. Panaras, E. Mathioulakis, V. Belessiotis, N. Kyriakis, Experimental validation of a simplified approach for a desiccant wheel model, Energy Build. 42 (2010) 1719–1725.
[19] C.R. Ruivo, A. Carrillo-Andres, J.J. Costa, F. Dominguez-Munoz, A new approach to the effectiveness method for the simulation of desiccant wheels with variable inlet states and airflows rates, Appl. Therm. Eng. 58 (2013) 670–678.
[20] M. Beccali, F. Butera, R. Guanella, R.S. Adhikari, Simplified models for the performance evaluation of desiccant wheel dehumidification, Int. J. Energy Res. 27 (2003) 17–29.
[21] M. Beccali, R.S. Adhikari, F. Butera, V. Franzitta, Update on desiccant wheel model, Int. J. Energy Res. 28 (2004) 1043–1049.
[22] F.E. Nia, D. van Paassen, M.H. Saidi, Modeling and simulation of desiccant wheel for air conditioning, Energy Build. 38 (2006) 1230–1239.
[23] A.N. Sadeghifam, S.M. Zahraee, M.M. Meynagh, I. Kiani, Combined use of design of experiment and dynamic building simulation in assessment of energy efficiency in tropical residential buildings, Energy Build. 86 (2015) 525–533.
[24] I. Jaffal, C. Inard, C. Ghiaus, Fast method to predict building heating demand based on the design of experiments, Energy Build. 41 (2009) 669–677.
[25] D.C. Montgomery, Design and Analysis of Experiments, sixth ed., Wiley, New York, 2004.
[26] F. Comino Montilla, M. Ruiz de Adana Santiago, A. Cerezuela Parish, M. Zamora García, F. Peci López, Design and building of a test facility for experimentation of desiccant wheels, in: The Minutes Book of the National Congress Engineering Thermodynamics, Cartagena, 2015, pp. 295–302.
[27] S. De Antonellis, M. Intini, C.M. Joppolo, F. Pedranzini, Experimental analysis and practical effectiveness correlations of enthalpy wheels, Energy Build. 84 (2014) 316–323.
[28] M. Aprile, M. Motta, Grey-box modelling and in situ experimental identification of desiccant rotors, Appl. Therm. Eng. 51 (2013) 55–64.
[29] Statgraphics, Statgraphics Centurion XV, 2006, Available from ⟨http://www.statgraphics.com/⟩ (accessed 10.12.15).
[30] F.E. Nia, Sustainable Air Handling by Evaporation and Adsorption, Deft University of Technology, 2011, PhD Thesis.

Appendix B

Experimental and numerical analysis of desiccant wheels activated at low temperatures

The paper presented in this appendix is published in *Energy and Buildings* (doi: 10.1016/j.enbuild.2016.10.021)

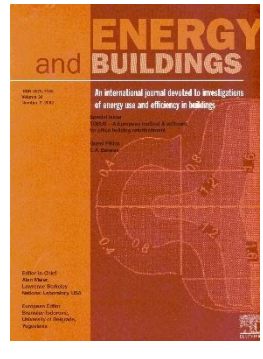

Energy and Buildings 133 (2016) 529–540

Contents lists available at ScienceDirect

Energy and Buildings

journal homepage: www.elsevier.com/locate/enbuild

Experimental and numerical analysis of desiccant wheels activated at low temperatures

F. Comino*, M. Ruiz de Adana

Departamento de Química-Física y Termodinámica Aplicada, Escuela Politécnica Superior, Universidad de Córdoba, Campus de Rabanales, Antigua Carretera Nacional IV, km 396, 14072 Córdoba, Spain

ARTICLE INFO

Article history:
Received 5 July 2016
Received in revised form 13 October 2016
Accepted 14 October 2016
Available online 14 October 2016

Keywords:
Desiccant wheel
Low temperature activated systems
Moisture removal capacity
Sensible heat ratio
Design of experiments

ABSTRACT

Desiccant wheels, DW, can be used to control the indoor air conditions in buildings and industrials environments. The control of the outlet process air conditions of a DW can be obtained by controlling the moisture removal capacity, MRC, and sensible heat ratio, SHR. The objective of this work is to obtain MRC and SHR of a DW activated at low temperatures when the process airflow rate and air regeneration temperature are varied. Two secondary objectives are to obtain the influence of the variation of the process airflow rate and air regeneration temperature on the outlet process air conditions and the relationship between MRC and SHR. Three empirical and simulated case studies are carried out.

The results show that a decoupling of the outlet air temperature and humidity ratio can be obtained when the process airflow rate and air regeneration temperature are varied. This decoupling allows several MRC values for a constant SHR value, and vice versa, to be obtained, achieving ranges of 7 kg h^{-1} and 0.25, respectively. These results suggest that a control strategy for DW activated at low temperatures, would allow MRC and SHR to be controlled by setting the process airflow rate and air regeneration temperature.

1. Introduction

Desiccant systems present an alternative solution to refrigeration vapour compression systems, commonly used for dehumidification and humidity control in rooms with high latent loads. Refrigeration vapour compression systems reduce the air temperature to condense its moisture, although these systems present some problems in the combined treatment of sensible and latent loads in rooms [1]. Furthermore, refrigeration vapour compression systems working under partial load conditions, presented a reduced latent capacity compared to nominal latent capacity [2]. Desiccant dehumidifier systems differ from refrigeration vapour compression systems in the way moisture is removed from the air. Desiccant dehumidifier systems adsorb water vapour from the air reaching an area of low vapour pressure at the surface of the desiccant [1]. These systems combined with refrigeration vapour compression systems, called hybrid HVAC systems, proved to be especially useful in the decoupling of sensible and latent loads in buildings [3,4].

In HVAC systems, control strategies are required to achieve the independent control of temperature and humidity. The aim of a control strategy is to improve the performance of the system, while satisfying user's thermal comfort [5]. Many HVAC systems based on DW using two-stage dehumidification achieved a fine tuning of humidity ratio [6–8]. However, this control would not guarantee independent control of temperature and humidity. Other HVAC systems with DW combined with a enthalpy wheel were studied to control indoor conditions [9]. This system did not have capacity to control indoor humidity during some critical periods.

Previous research studies on DW control strategies were carried out with the aim of saving energy by setting the regeneration section with a purge sector [10]. Another control strategy approach is based on the rotation speed of a DW [11,12]. The control system would be much more energy efficient using the variable airflow rate [13]. The rotation speed and the regeneration temperature were also used as a control strategy [14]. Nevertheless, these works have not satisfactorily clarified the capacity to decouple the outlet process air conditions, temperature and humidity ratio, especially as regards the quantitative effect of both variables.

Manufacturers often provide controls inside the system to modulate the reactivation energy of the DW in response to changes in the moisture load. There are three common methods of controlling dehumidification capacity [15]: (i) on-off reactivation control; (ii) reactivation energy modulation; and (iii) variable air bypass. Each of these methods is effective, depending on the degree of precision needed for the humidity control level in the building [15].

A schematic of a DW system with an air bypass is shown in Fig. 1. It requires a bypass air duct and variable-position dampers for the face of the DW and for the bypass duct. The DW would oper-

* Corresponding author.
E-mail address: francisco.comino@uco.es (F. Comino).

http://dx.doi.org/10.1016/j.enbuild.2016.10.021
0378-7788/

Nomenclature

A	Area [°C g kg^{-1}]
AR	Area ratio
b	Estimated parameter
CC	Cooling coil
DOE	Design of experiments
DW	Desiccant wheel
EA	Exhaust air
F	Centrifugal fan
FC	Flow conditioner
EH	Electric heater
HC	Heating coil
HR	Relative humidity [%]
K	Number of parameters
MA	Mixed air
MB	Mixing box
MRC	Moisture removal capacity [kg h^{-1}]
N	Number of experimental tests
OA	Outdoor air
P	Pressure [Pa]
PT	Pitot tube
$\dot{Q}$	Heat transfer [kW]
RA	Recirculated air
SH	Steam humidifier
SHR	Sensible heat ratio
T	Temperature [°C]
t	Time [s]
$\dot{V}$	Volumetric airflow rate [m^3 h^{-1}]
X	Input variable
$\hat{Y}$	Estimated output value

Greek letters

Δ	Increase
ρ	Density [kg m^{-3}]
ω	Humidity ratio [g kg^{-1}]
Ω	Specific mass airflow rate [kg s^{-1} m^{-3}]

Subscripts

d	Dew point
i	Inlet
L	Latent
o	Outlet
p	Process
r	Regeneration
S	Sensible

Superscripts

'	Mixed outlet process air conditions

ate with unbalanced airflow rates to achieve the outlet process air conditions. This method is preferred for industrial process applications, where control within ±1 or 2% relative humidity is essential [15]. Previous results also showed that if the outlet moisture must be very low, the process airflow rate is quite critical and therefore this must be controlled [1].

Different experimental works have been carried out in order to study the influence of unbalanced airflow rates in DW [16,17]. Other authors developed mathematical models of DW which allowed its behaviour with unbalanced airflow rates to be analysed [18,19]. However, the methodology used to fit these models requires a high number of experimental tests. Some physical characteristics of the DW required by these models are not usually available.

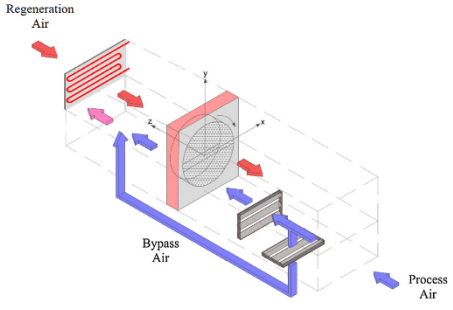

Fig. 1. Schematic of a DW system with bypass air.

It has been shown that the variation of process airflow rate allowed the psychrometric trend of the process air stream and moisture removal capacity, MRC, to be modified [20]. The psychrometric trend of the process air stream can be studied by sensible heat ratio, SHR, [21]. Several studies on HVAC systems with DW analysed SHR [22,23]. Nevertheless, to modify MRC the air regeneration temperature was more influential than the airflow rates [24].

MRC was considered to be the most appropriate parameter to analyse the performance of a DW with unbalanced airflow rates [25]. The higher the temperature of the desiccant material, the higher the MRC, and the easier it is to remove moisture. Thus, the regeneration air temperature has a strong effect on MRC [26,27]. Therefore, a significant energy consumption is required to regenerate the DW to obtain high MRC values. Energy savings are usually obtained when the DW is regenerated using waste heat from other processes [28]. However, in some cases waste heat energy is not available or the corresponding temperature level is not adequate. On the other hand, previous studies on DW operated at low regeneration temperatures and reached acceptable MRC values [29,30]. A DW activated at low temperatures could be integrated in refrigeration vapour compression systems in a building or industrial environment [31,32]. In this paper, values below 60 °C were considered as low regeneration temperatures. The regeneration temperatures usually used range from 60 °C to 120 °C [33,34].

The performance and the outlet process air conditions of a DW strongly depend on its control strategy. Therefore, it would be interesting to know the behaviour of a DW activated at low temperatures by setting the process airflow rate and air regeneration temperature, in order to control MRC and SHR.

The objective of this work was to obtain empirically MRC and SHR of a DW activated at low temperatures when the process airflow rate and air regeneration temperature were varied. To obtain this, two secondary objectives were carried out: first, to study the influence of the variation of the process airflow rate and air regeneration temperature on the outlet process air conditions, and then to obtain the relationship between MRC and SHR.

2. Methodology

2.1. Experimental setup

An experimental test rig was built to analyse the performance of DW under different working conditions. A schematic representation of the experimental setup is shown in Fig. 2. The process and regeneration air streams were configured in a countercurrent flow. The facility is also designed to bypass up to 40% of the process air

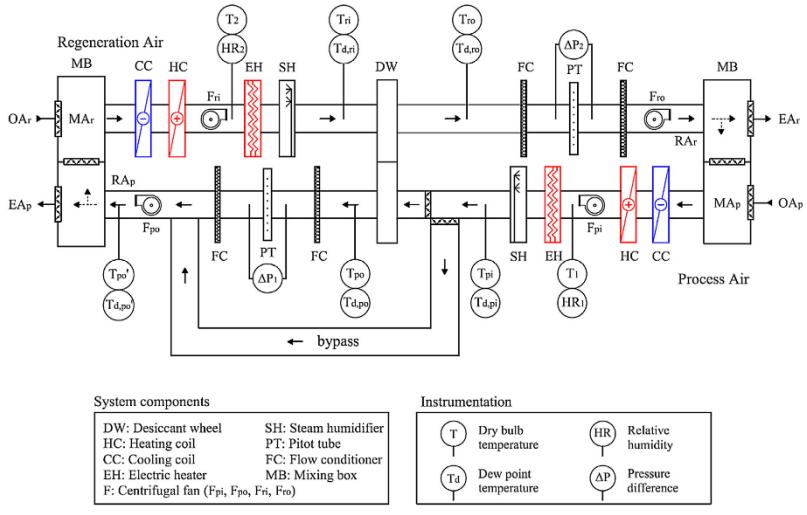

Fig. 2. Layout of the test facility.

stream without being treated by the DW. It has a bypass air duct and variable-position dampers for the face of the DW and for the bypass duct. The DW could operate with unbalanced airflow rates to achieve the outlet process air conditions.

The inlet temperature and humidity ratio of both process and regeneration streams were set using cooling and heating coils (CC, HC), an electric heater (EH) and a steam humidifier (SH), located for each air stream, upstream of the DW [35]. The process and regeneration airflow rates were set using variable speed fans (F). Two Pitot tubes (PT) were used to measure the airflow rate and four flow conditioners (FC) were installed to obtain stable airflow conditions, two upstream of the airflow rate measuring point and two downstream. Furthermore, two mixing boxes (MB), were used either to recirculate the process and regeneration air streams or to mix the exterior air with the treated air. The characteristics of the equipment of the test facility setup are shown in Table 1.

The DW is divided into two equal sections and rotates at a constant speed of 42 rph. The matrix of the DW consists of alternate layers of flat and corrugated sheets of silica gel and metal silicates, chemically bonded into a tissue of inorganic fibres. The dimensional sizes and operating parameters of the DW are shown in Table 2.

The measured variables in this test rig, the type of sensor and its accuracy are shown in Table 3. The sensor locations are shown in Fig. 2. The temperature and humidity at each measuring point were collected at three different points along the horizontal axis, taking the average of the three measurements [14].

Each state point was taken under steady-state conditions and all the measured values were average values over a period of 20 min with sampling time steps of 3 s [35]. The maximum values of standard deviations of the mean are shown in Table 4.

2.2. Design of experiments

The statistical technique of design of experiments, DOE, was used to fit an empirical regression model which was used to predict the outlet air process temperature and humidity ratio in the DW system with bypass air, T_{po}' and ω_{po}', showing a similar setting to Fig. 1. In addition, DOE allowed the influential variables on T_{po}' and ω_{po}' to be identified and analysed [36]. The number of required experimental tests can be reduced if they are optimally designed. Usually, several candidate models can be proposed. The choice between these candidate models is a trade-off between complexity and precision. The fit of the model and its further statistical analysis were supported by the software Statgraphics Centurion XVI [37].

In this work, a DOE was carried out with five input variables: inlet air process temperature, T_{pi}, inlet air process humidity ratio, ω_{pi}, process specific mass airflow rate, Ω_{pi}, ratio of inlet mass velocity to the channel length [38], inlet air regeneration temperature, T_{ri} and inlet air regeneration humidity ratio, ω_{ri}. The output process

Table 1
Characteristics of the equipment.

Equipment	Value
Cooling coil (CC)	
Total cooling capacity	15.8 kW
Sensible cooling capacity	12.2 kW
Nominal water flow	2.7 $m^3 h^{-1}$
Nominal pressure drop	5.1 m
Heating coil (HC)	
Heating capacity	18.8 kW
Nominal water flow	2.7 $m^3 h^{-1}$
Nominal pressure drop	5.1 m
Electric heater (EH)	
Electric power	7.2 kW
Fan (F)	
Nominal airflow	3100 $m^3 h^{-1}$
Available static pressure	0.007 m
Nominal motor power	0.6 kW
Speed	1125 rpm
Steam humidifier (SH)	
Steam flow	45 kg h^{-1}
Max. power	33.75 kW

Table 2
Characteristics of the desiccant wheel.

Parameters	Value
Rotor diameter	550 mm
Rotor length	200 mm
Desiccant material	Silica gel
Channel shape	Honeycomb
Nominal capacity	15 kg h^{-1}
Nominal air flow	2300 m^3 h^{-1}
Rotation speed	42 rph
Weight	57 kg
Power supply	230 Vac

Table 3
Specification of measuring devices.

Measured parameter	Type	Accuracy
T_1, T_2, T_{pi}, T_{po}, $T_{po'}$, T_{ri}, T_{ro}	PT 100	±0.12 °C
$T_{d,pi}$, $T_{d,po}$, $T_{d,po'}$	Chilled mirror hygrometer	±0.15 °C
$T_{d,ri}$, $T_{d,ro}$	Capacitive	±0.4 °C
HR_1, HR_2	Capacitive	±3%
ΔP_1, ΔP_2	Differential pressure transmitter	±0.3% (0–1 mbar)

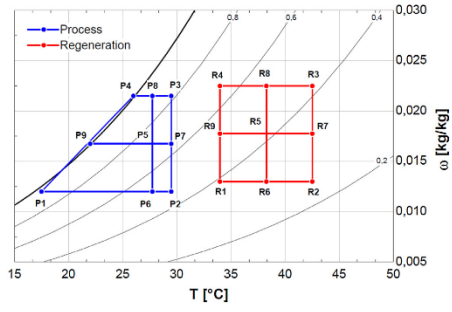

Fig. 3. Grid for the inlet states of the process and regeneration airflow.

variables were the outlet air process temperature of system, T_{po}', and outlet air process humidity ratio of system, ω_{po}'. The effect of the five input variables was studied using a Box-Behnken design approach [36]. This design was carried out at low air regeneration temperatures defining two grids to cover the range of validity of the process and regeneration air streams, as shown in Fig. 3. Nine inlet states for the process airflow, P1 to P9, and nine inlet states for the regeneration airflow, R1 to R9, were selected. The resulting process grid was not rectangular, in order to obtain the widest range of validity.

The values of the nine inlet states for the process and regeneration airflow are shown in Table 5. The inlet air process temperature ranged from 17.5 °C to 29.5 °C and the humidity range from 12 g kg^{-1} to 21.5 g kg^{-1}. Furthermore, the process specific mass airflow rate values were varied in three levels, 13.45 kg s^{-1} m^{-3} ($\Omega_{pi,1}$), 17.48 kg s^{-1} m^{-3} ($\Omega_{pi,2}$) and 21.51 kg s^{-1} m^{-3} ($\Omega_{pi,3}$). The inlet air regeneration temperature range was from 34 °C to 42.5 °C and the humidity range from 13 g kg^{-1} to 22.5 g kg^{-1}. The regeneration specific mass airflow rate was fixed at a constant value for all tests, 21.51 kg s^{-1} m^{-3}.

Table 5
Inlet states of the process and regeneration airflow.

Point	T_{pi} [°C]	ω_{pi} [g kg^{-1}]	Point	T_{ri} [°C]	ω_{ri} [g kg^{-1}]
P1	17.50	12.00	R1	34.00	13.00
P2	29.50	12.00	R2	42.50	13.00
P3	29.50	21.50	R3	42.50	22.50
P4	26.00	21.50	R4	34.00	22.50
P5	27.25	16.75	R5	38.25	17.75
P6	27.25	12.00	R6	38.25	13.00
P7	29.50	16.75	R7	42.50	17.75
P8	27.25	21.50	R8	38.25	22.50
P9	22.00	16.75	R9	34.00	17.75

Table 6
Experimental tests defined for DOE based on the Box-Behnken design approach.

N	Process	Regeneration	Ω_{pi}	N	Process	Regeneration	Ω_{pi}
1	P6	R5	$\Omega_{pi,1}$	24	P5	R6	$\Omega_{pi,3}$
2	P5	R2	$\Omega_{pi,2}$	25	P7	R5	$\Omega_{pi,1}$
3	P6	R7	$\Omega_{pi,2}$	26	P5	R8	$\Omega_{pi,3}$
4	P9	R8	$\Omega_{pi,2}$	27	P8	R5	$\Omega_{pi,3}$
5	P6	R6	$\Omega_{pi,2}$	28	P8	R7	$\Omega_{pi,2}$
6	P5	R6	$\Omega_{pi,1}$	29	P6	R9	$\Omega_{pi,2}$
7	P4	R5	$\Omega_{pi,2}$	30	P7	R9	$\Omega_{pi,2}$
8	P9	R7	$\Omega_{pi,2}$	31	P5	R8	$\Omega_{pi,1}$
9	P5	R5	$\Omega_{pi,2}$	32	P8	R9	$\Omega_{pi,2}$
10	P3	R5	$\Omega_{pi,2}$	33	P6	R5	$\Omega_{pi,3}$
11	P5	R5	$\Omega_{pi,2}$	34	P7	R8	$\Omega_{pi,2}$
12	P9	R5	$\Omega_{pi,1}$	35	P5	R5	$\Omega_{pi,2}$
13	P8	R8	$\Omega_{pi,2}$	36	P9	R9	$\Omega_{pi,2}$
14	P5	R4	$\Omega_{pi,2}$	37	P5	R7	$\Omega_{pi,1}$
15	P5	R5	$\Omega_{pi,2}$	38	P5	R9	$\Omega_{pi,3}$
16	P5	R5	$\Omega_{pi,2}$	39	P9	R6	$\Omega_{pi,2}$
17	P6	R8	$\Omega_{pi,2}$	40	P8	R5	$\Omega_{pi,1}$
18	P7	R6	$\Omega_{pi,2}$	41	P5	R5	$\Omega_{pi,2}$
19	P5	R9	$\Omega_{pi,1}$	42	P7	R7	$\Omega_{pi,2}$
20	P8	R6	$\Omega_{pi,2}$	43	P7	R5	$\Omega_{pi,3}$
21	P5	R1	$\Omega_{pi,2}$	44	P1	R5	$\Omega_{pi,2}$
22	P5	R3	$\Omega_{pi,2}$	45	P5	R7	$\Omega_{pi,3}$
23	P9	R5	$\Omega_{pi,3}$	46	P2	R5	$\Omega_{pi,2}$

A total of 46 experimental tests were carried out, including 6 repetitions of the tests combining the interior points, P5, R5 and $\Omega_{pi,2}$, and 25 degrees of freedom. The combination of tests are summarized in Table 6.

The performance of the process was evaluated by analysing the responses (Y), which are dependent on the input variables. The relationship between the responses and the input variables was examined using second order polynomial equations. The generalized second order polynomial equation model is expressed by Eq. (1). Where $\hat{Y}$ is the estimated output value, X are input variables, b_i, b_{ii} and b_{ij} are the estimated parameters of linear, quadratic and the second-order terms, respectively, and b_0 is the average response in the model.

$$\hat{Y} = b_0 + \sum_{i=1}^{k} b_i \cdot X_i + \sum_{i=1}^{k} b_{ii} \cdot X_i^2 + \sum_{i=1}^{k=1} \sum_{\substack{i=2 \\ j>i}}^{k} b_{ij} \cdot X_i \cdot X_j \quad (1)$$

In order to check if the selected model accurately describes the observed data, the R^2 value was obtained, and a lack-of-fit test of the model was carried out. This test was performed by comparing the

Table 4
Maximum values of standard deviations of the mean.

	T_{pi} [°C]	ω_{pi} [g kg^{-1}]	T_{po} [°C]	ω_{po} [g kg^{-1}]	T_{ri} [°C]	ω_{ri} [g kg^{-1}]	T_{ro} [°C]	ω_{ro} [g kg^{-1}]	$\dot{V}_p$ [m^3 h^{-1}]	$\dot{V}_r$ [m^3 h^{-1}]
Σ	0.17	0.46	0.34	0.50	0.31	0.53	0.21	0.42	28.2	24.7

Table 7
Experimental tests for case study I.

N	T_{pi} [°C]	ω_{pi} [g kg^{-1}]	Ω_{pi} [kg s^{-1} m^{-3}]	T_{ri} [°C]	ω_{ri} [g kg^{-1}]	Ω_{ri} [kg s^{-1} m^{-3}]
1	25.00	17.00	21.51	34.00	13.00	21.51
2	25.00	17.00	21.51	38.25	13.00	21.51
3	25.00	17.00	21.51	42.50	13.00	21.51
4	25.00	17.00	17.48	42.50	13.00	21.51
5	25.00	17.00	13.45	42.50	13.00	21.51
6	25.00	17.00	13.45	38.25	13.00	21.51
7	25.00	17.00	13.45	34.00	13.00	21.51
8	25.00	17.00	17.48	34.00	13.00	21.51

Table 8
Inlet air states of Ω_{pi}, T_{ri} and ω_{ri} for case study II.

Ω_{pi} [kg s^{-1} m^{-3}]	T_{ri} [°C]	ω_{ri} [g kg^{-1}]
13.45	34.00	13.00
17.48	38.25	17.75
21.51	42.50	22.50

variability of the current model residuals to the variability between observations at replicate settings of the factors.

2.3. Strategy to control outlet process air conditions

In this work, three case studies were carried out to analyse the outlet process air conditions of a DW when the inlet air regeneration temperature and process airflow rate were controlled. Case study I was tested experimentally and case studies II and III were carried out for different inlet air conditions using the empirical model fitted with the technique DOE. This technique allows to fit the model by using a low number of experimental tests. The analysis of the outlet process air conditions for a wide range of inlet air states was carried out using the empirical model.

2.3.1. Case study I

The decoupling potential of the outlet air process temperature and humidity ratio were evaluated in case study I by varying three levels of T_{ri} and three levels of Ω_{pi}, see Table 7. The remaining input variables were fixed at constant values. In order to quantify the decoupling of the outlet process air conditions of the DW, a psychrometric area, A_o, was obtained. The psychrometric area was calculated from the contour of the outlet process air states, where the main axes of psychrometric chart were considered the dry bulb temperature, horizontal axis, and the humidity ratio, vertical axis.

2.3.2. Case study II

In this case study five inlet process air conditions were defined, states P1-P5, see Fig. 3. The combination of three levels of T_{ri}, ω_{ri} and Ω_{pi} was used to analyse the outlet air process temperature, T_{po}', and the outlet air process humidity ratio, ω_{po}', see Table 8. Ω_{ri} was fixed at a constant value, 21.51 kg s^{-1} m^{-3}. The results of outlet process air conditions were quantified by the aforementioned variable A_o.

2.3.3. Case study III

In practice, inlet process air conditions could vary over time, for example, when these conditions are influenced by outdoor air. In order to analyse the outlet process air conditions of the DW system when inlet process air conditions vary, a third case study was performed. In this case, three inlet process air areas were selected. These areas are related to three climatic conditions, see Fig. 4:

- Area I: inlet process air conditions with low temperature and low humidity ratio values
- Area II: inlet process air conditions with high temperature values and low humidity ratio values

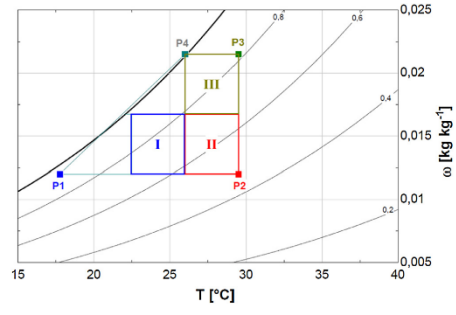

Fig. 4. Inlet process air condition areas considered for case study III.

- Area III: inlet process air conditions with high temperature and high humidity ratio values.

All areas have the same dimensions, 16.6 °C g kg^{-1}. The limit condition values of the process input areas are summarized in Table 9.

The outlet process air conditions of the DW system for variable inlet air conditions were quantified by an area ratio between outlet and inlet air area, AR, expressed by Eq. (2). The inlet and outlet air area values were obtained from the contour of the inlet air states and outlet air states, respectively.

$$AR = \frac{A_o}{A_i} \tag{2}$$

2.4. Moisture removal capacity and sensible heat ratio

In a DW, the variation of outlet air process humidity ratio, ω_{po}', from a given inlet air process humidity ratio, ω_{pi}, causes the desiccant capacity to be modified. Therefore, the moisture removal capacity, MRC, of the DW in the three case studies was obtained. ASHRAE defines MRC as a primary figure of merit for desiccant wheel performance [39]. MRC was defined as:

$$MRC = \rho \cdot \dot{V} \cdot \left(\omega_{pi} - \omega'_{po}\right) \tag{3}$$

Similar desiccant capacities in a DW are possible, so MRC was analysed regarding the sensible heat ratio, SHR, expressed by Eq. (4). Where $\dot{Q}_S$ is the sensible heat transfer of the process air stream and $\dot{Q}_L$ is the latent heat transfer of the process air stream. SHR values range between 0 and 1.

$$SHR = \frac{\dot{Q}_S}{\dot{Q}_S + \dot{Q}_L} \tag{4}$$

Table 9
Limit states of the inlet process air condition areas considered for case study III.

	Area I		Area II		Area III	
	T_{pi} [°C]	ω_{pi} [g kg^{-1}]	T_{pi} [°C]	ω_{pi} [g kg^{-1}]	T_{pi} [°C]	ω_{pi} [g kg^{-1}]
Lower limit	22.5	12	26	12	26	16.75
Upper limit	26	16.75	29.5	16.75	29.5	21.5

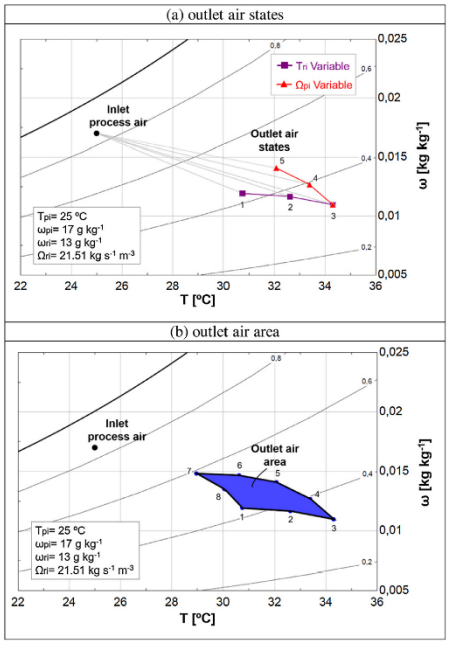

Fig. 5. Outlet process air conditions for case study I when T_{ri} and Ω_{pi} were varied.

3. Results and analysis

3.1. Experimental case study I

Experimental tests were carried out to analyse the variation of outlet process air conditions in a DW controlling T_{ri} and Ω_{pi}. The results of the outlet process air conditions of the DW for case study I are shown in Fig. 5. States 1 to 3 show the outlet air states when T_{ri} was varied from 34 °C to 42.5 °C, tests 1 to 3, see Table 7, and the remaining input variables were fixed at constant values, see Fig. 5a. States 3 to 5 show the outlet air states when Ω_{pi} was varied from 21.51 kg s^{-1} m^{-3} to 13.45 kg s^{-1} m^{-3}, test 3 to 5, see Table 7, and the remaining input variables were fixed at constant values, see Fig. 5a. These outlet process air states are shown in Table 10. It can be observed that T_{po}' increased and ω_{po}' decreased when T_{ri} and Ω_{pi} were increased, although different slopes were obtained.

The combination between the values of T_{ri} and Ω_{pi} defined in Table 7, resulted in an area of outlet process air, see Fig. 5b. The area obtained is equal to 8.26 °C g kg^{-1}. Any air state within the shaded area can be obtained by setting the T_{ri} and Ω_{pi} values in the specified range and fixing T_{pi}, ω_{pi}, ω_{ri} and Ω_{ri} at constant values, as shown in Table 7. The variations of the outlet air process temperature and humidity ratio from a fixed inlet state were 5.33 °C and 3.85 g kg^{-1}, respectively, see Table 10. These results show that this strategy allows the outlet process air conditions to be controlled in a DW setting T_{ri} and Ω_{pi}. Similar results can be obtained experimentally from different inlet process air states. In general, it is possible to vary the outlet process air conditions in a DW activated at low temperatures controlling T_{ri} and Ω_{pi}.

Table 10
Outlet process air conditions and MRC and SHR values obtained for case study I.

N	T_{po}' [°C]	ω_{po}' [g kg^{-1}]	MRC [kg h^{-1}]	SHR
1	30.74	11.93	9.37	0.70
2	32.61	11.66	9.81	0.68
3	34.3	10.97	11.04	0.64
4	33.38	12.68	7.92	0.74
5	32.07	14.09	5.36	0.82
6	30.61	14.67	4.31	0.86
7	28.97	14.82	4.06	0.87
8	30.05	13.53	6.43	0.79

3.2. Correlation model

An empirical model was obtained to predict the outlet air process temperature and humidity ratio, in order to control MRC and SHR in a DW operating at low air-regeneration temperatures.

The results of the set of experiments were used to fit the parameters of a second order model expressed by Eq. (1). The corresponding estimated parameters, which show the relationship between the output process variables, T_{po}' and ω_{po}', and the set of process variables, are shown in Table 11. Where X_i are linear variables, quadratic variables or their interactions, $b_1 \ldots b_{15}$ are the regression coefficients, showing the weight each one has in the equation, and b_0 is the average response in the design of experiments. It can be observed that the coefficients with the highest weight were b_2 for T_{po}', and b_3 for ω_{po}', ω_{pi} and T_{ri} variables, respectively.

3.2.1. Statistical analysis

The ANOVA results of the empirical model obtained are summarized in Table 12. This table shows each of the main estimated effects, the standard error of each of the effects, the statistical parameter F-Ratio, which is the ratio of the mean square error to the pure error obtained from the replicates at the design center, and the statistical parameter P-value, which is used as a tool to check the significance of each effect.

All variables were found significant at 95% confidence level, as the P-values were lower than 0.05 in all cases. The results of the parameter P-value showed that the most influential variables on the outlet temperature, T_{po}', were T_{pi}, T_{ri} and Ω_{pi}. Regarding the outlet humidity ratio, ω_{po}', the most influential variables were ω_{pi}, Ω_{pi}, and ω_{ri}. This suggested that if a fine tuning of outlet process air conditions was necessary, the process specific mass airflow, Ω_{pi}, should be controlled. Previous results of a DW with balanced airflow rates differ from the results obtained in this work [40], where the specific mass airflow presented less influence compared to the inlet air process and regeneration conditions.

Table 11
Estimated parameters of the empirical model.

Estimated parameters	X_i	T_{po}'x10^3 [°C]	ω_{po}'x10^3 [g kg^{-1}]	Estimated parameters	X_i	T_{po}'x10^3 [°C]	ω_{po}'x10^3 [g kg^{-1}]
b_0	–	−6736.67	−15366.80	b_{11}	ω_{pi}^2	−17.23	16.76
b_1	T_{pi}	72.10	1277.57	b_{12}	$\omega_{pi}\cdot T_{ri}$	−1.49	−2.23
b_2	ω_{pi}	772.28	−785.18	b_{13}	$\omega_{pi}\cdot\omega_{ri}$	5.65	16.84
b_3	T_{ri}	410.38	1310.33	b_{14}	$\omega_{pi}\cdot\Omega_{pi}$	20.50	−6.79
b_4	ω_{ri}	224.17	−916.88	b_{15}	T_{ri}^2	−5.09	−11.90
b_5	Ω_{pi}	357.36	−94.71	b_{16}	$T_{ri}\cdot\omega_{ri}$	7.31	−10.40
b_6	T_{pi}^2	16.58	−28.38	b_{17}	$T_{ri}\cdot\Omega_{pi}$	6.71	−3.50
b_7	$T_{pi}\cdot\omega_{pi}$	−14.35	29.84	b_{18}	ω_{ri}^2	−9.72	24.41
b_8	$T_{pi}\cdot T_{ri}$	7.35	−10.61	b_{19}	$\omega_{ri}\cdot\Omega_{pi}$	−5.49	11.88
b_9	$T_{pi}\cdot\omega_{ri}$	−12.93	6.35	b_{20}	Ω_{pi}^2	−12.17	−9.44
b_{10}	$T_{pi}\cdot\Omega_{pi}$	−8.71	5.89	–	–	–	–

Table 12
Effects of input variables on output process variables of the DW.

	T_{po}'				ω_{po}'			
Effect	Estimate	Stnd. Error	F-Ratio	P-value	Estimate	Stnd. Error	F-Ratio	P-value
Average	30.37	0.09			13.27	0.17		
T_{pi}	6.12	0.35	299.24	0.0000	3.04	0.63	23.07	0.0049
ω_{pi}	2.46	0.36	46.21	0.0010	5.44	0.65	70.06	0.0004
T_{ri}	3.54	0.21	281.66	0.0000	−1.12	0.38	8.95	0.0304
ω_{ri}	−1.39	0.21	43.66	0.0012	1.81	0.38	23.14	0.0048
Ω_{pi}	1.85	0.21	77.37	0.0003	−2.60	0.38	47.71	0.0010
Lack-of-fit				0.0600				0.0590
	R^2 = 98.23%				R^2 = 95.54%			

Positive and negative effects for the different input variables were observed, see Table 12. These signs indicate the influential trend of the input variables on the output process variables. T_{po}' can be increased, reducing ω_{ri} and increasing T_{pi}, ω_{pi}, T_{ri} and Ω_{pi}, and ω_{po}' can be increased, reducing T_{ri} and Ω_{pi} and increasing T_{pi}, ω_{pi} and ω_{ri}.

P-values for lack-of-fit test for T_{po}' and ω_{po}' were greater than 0.05, see Table 12. Therefore, the selected design was found suitable for the observed data at 95% confidence level. R^2 values of 98.23% for T_{po}' and 95.54% for ω_{po}' were obtained, which indicates that the final prediction is in agreement with the experimental results. In a previous work, where an empirical model of DW with bypass air was fitted, lower R^2 values were found, 90% for T_{po}' and 92% for ω_{po}' [41].

3.2.2. Effect of input variables on the outlet process air conditions

In order to find the relationships between input and output variables, two response surfaces and contour line plots for the output process variables, T_{po}' and ω_{po}', were analysed using the empirical model obtained, see Fig. 6. Both output process variables are represented as a function of the input variables T_{ri} and Ω_{pi}. The remaining input variables were fixed at constant values: T_{pi} = 27.25 °C, ω_{pi} = 16.75 g kg^{-1} and ω_{ri} = 16.75 g kg^{-1}. Similar trends of T_{po}' and ω_{po}' were obtained for different values of T_{pi}, ω_{pi} and ω_{ri}. It can be observed that T_{po}' increased when T_{ri} was increased and Ω_{pi} remained constant. T_{po}' values also increased when Ω_{pi} was increased and T_{ri} remained constant, see Fig. 6a. Inverse trends of these two input variables were obtained for ω_{po}'. Values of this output variable were increased when T_{ri} and Ω_{pi} decreased. In previous studies on DW with balanced airflow rates, similar trends of the output variables with regard to T_{ri}, were obtained [40,42]. However, inverse trends of the output process variables with regard to Ω_{pi} were achieved, where ω_{po}' values increased [1] and T_{po}' values decreased [42], as process airflow rates were increased. These trends are caused by the fact that the outlet process air conditions of the current DW system, were mixed with the bypass airflow and also, the regeneration and process airflow rates were unbalanced.

The effects of interaction between T_{ri} and Ω_{pi}, and T_{po}' and ω_{po}', using the empirical model obtained, were studied for three levels of T_{ri} and three levels of Ω_{pi}, see Table 8. Both effects are represented in Fig. 7. The same constant values of T_{pi}, ω_{pi} and ω_{ri}, as those shown in Fig. 6, were used. Low increments of T_{po}' can be observed when Ω_{pi} was increased and T_{ri} was fixed at a constant value, see Fig. 7a. For example, an increase of Ω_{pi} from 13.45 kg s^{-1} m^{-3} to 17.48 kg s^{-1} m^{-3}, and T_{ri} = 34 °C, yielded a lower increase of 1 °C for T_{po}'. With respect to ω_{po}', it can be observed that this output variable increased when Ω_{pi} decreased and T_{ri} was fixed at a constant value, see Fig. 7a. An increment of 1.4 g kg^{-1} for ω_{po}' was achieved when Ω_{pi} decreased from 17.48 kg s^{-1} m^{-3} to 21.51 kg s^{-1} m^{-3}, and T_{ri} = 34 °C.

Greater increments of T_{po}' were obtained when T_{ri} was increased and Ω_{pi} was fixed at a constant value, see Fig. 7b. A rise of approximately 2 °C of T_{po}' was achieved for each level of T_{ri} and Ω_{pi} = 13.45 kg s^{-1} m^{-3}. Regarding ω_{po}', lower increments of this output variable were found after fixing the Ω_{pi} at a constant value and varying T_{ri}, see Fig. 7b. For example, an increase of T_{ri} from 38.25 °C to 42.5 °C, and Ω_{pi} = 13.45 kg s^{-1} m^{-3}, yielded a lower increase of 1 g kg^{-1} for ω_{po}'. The maximum and minimum values of T_{po}' achieved were 35.5 °C and 29.8 °C, respectively, and the maximum and minimum values of ω_{po}' achieved were 15.4 g kg^{-1} and 11.3 g kg^{-1}, respectively. Similar trends of T_{po}' and ω_{po}' on T_{ri} and Ω_{pi} were obtained for different values of T_{pi}, ω_{pi} and ω_{ri}.

These results suggested that the influence of Ω_{pi} on T_{po}' was less than that of T_{ri}. Also, the influence of T_{ri} on ω_{po}' was less than that of Ω_{pi}. Therefore, a wider range of outlet process air conditions can be achieved if the outlet air temperature, T_{po}', is controlled by the inlet air regeneration temperature, T_{ri}, and the outlet air humidity ratio, ω_{po}', is controlled by the process specific mass airflow rate, Ω_{pi}. This strategy can be used to ensure independent control of outlet air temperature and humidity ratio.

3.3. Analysis of outlet process air conditions for case study II

The empirical model was used to analyse the variation of outlet process air conditions in the DW system for five inlet air states, states P1-P5. First, the outlet process air conditions were studied

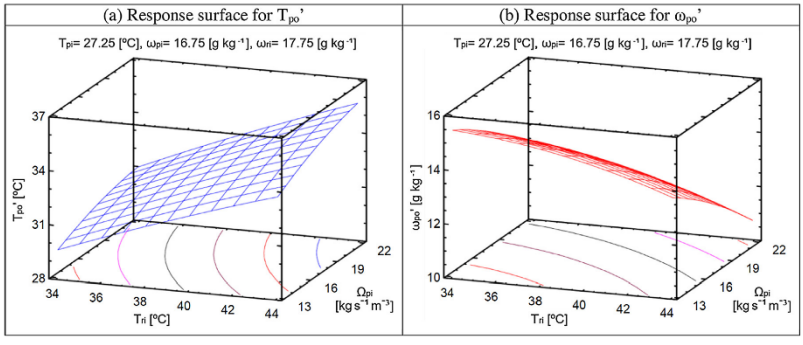

Fig. 6. Response surfaces and contour line plots of the output process variables.

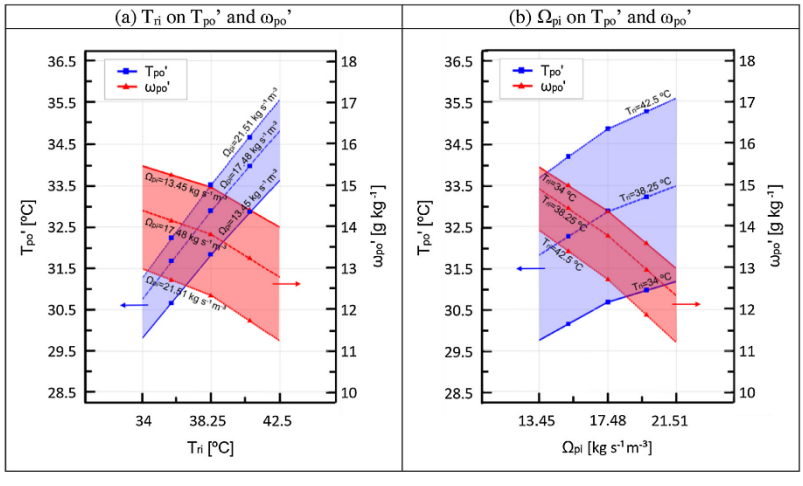

Fig. 7. Relations of T_{ri} and Ω_{pi} on T_{po}' and ω_{po}'.

when T_{ri} and ω_{ri} were varied. The combination of these two input variables are shown in Table 8. Ω_{pi} and Ω_{ri} were fixed at a constant value, 21.51 kg s^{-1} m^{-3}. The results of the outlet process air conditions are represented in Fig. 8. States P1 to P5 indicate the inlet process air conditions and the lines represent the outlet process air states. Three outlet process air lines for each inlet air state were obtained by varying ω_{ri}, and three outlet process air states were obtained in each outlet process air line by varying T_{ri}. Therefore, a decoupling of the outlet air process temperature and humidity was not completely achieved. Regarding ω_{ri}, ω_{po}' values were increased and T_{po}' values were reduced when ω_{ri} increased. Previous works showed that if extremely dry outlet process air conditions were necessary, the inlet air regeneration humidity ratio, ω_{ri}, should not be very high [40].

Second, in this case study, the outlet process air conditions were analysed when T_{ri}, Ω_{pi} and ω_{ri} were varied. The combination of these three input variables is shown in Table 8. The results of the

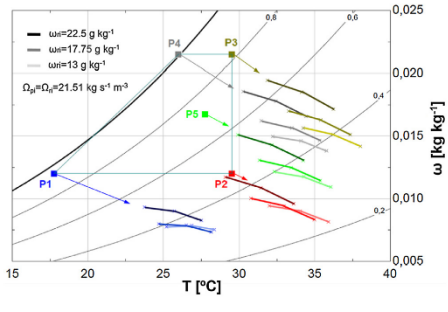

Fig. 8. Outlet process air conditions when T_{ri} and ω_{ri} were modified.

Table 13
Output area values for each inlet process air state, P1-P5.

ω_{ri} [g kg^{-1}]	P1 Area [°C g kg^{-1}]	P2 Area [°C g kg^{-1}]	P3 Area [°C g kg^{-1}]	P4 Area [°C g kg^{-1}]	P5 Area [°C g kg^{-1}]
13.00	8.80	8.25	7.45	7.96	8.10
17.75	7.53	7.17	6.06	6.24	7.00
22.50	6.46	6.09	4.37	4.72	5.28

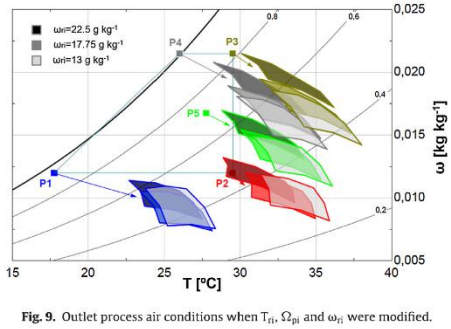

Fig. 9. Outlet process air conditions when T_{ri}, Ω_{pi} and ω_{ri} were modified.

Table 14
Area ratio values for the three input process areas and three levels of ω_{ri}.

ω_{ri} [g kg^{-1}]	Area Ratio I	Area Ratio II	Area Ratio III
13.00	2.35	2.53	2.89
17.75	2.40	2.59	2.95
22.50	2.46	2.63	3.03

outlet process air conditions are represented in Fig. 9. Three outlet process air areas were obtained for each inlet process air state by varying ω_{ri}. The decoupling of the temperature and humidity is shown by setting the T_{ri} and Ω_{pi}. Area values obtained from the contour of the outlet process air states, for each inlet process air state, P1-P5, are shown in Table 13. It can be observed that the greatest areas were achieved for inlet process air states with low ω_{pi} values, states P1 and P2. The areas were reduced when ω_{pi} increased, from states P1 and P2 to states P3 and P4, and the inlet process air conditions are located away from the saturation conditions, states P4 to P3 or states P1 to P2. Furthermore, the areas were reduced for all inlet process air states when ω_{ri} increased, from 13 to 22.5 g kg^{-1}, see Table 13.

Regarding the outlet process air area of state P2 with ω_{ri} = 22.5 g kg^{-1}, some outlet process air states with lower T_{po}' values and higher ω_{po}' values than the inlet air state, P2, were achieved, see Fig. 9. The proximity of T_{pi} to T_{ri}, and the relative high ω_{ri} values compared to the ω_{pi} values, caused this process.

3.4. Analysis of outlet process air conditions for case study III

The results of the outlet process air conditions of the DW system, for the three inlet process air conditions related to climatic conditions selected in Fig. 4, are shown in Fig. 10. Three output process areas were obtained for each input process area by varying ω_{ri}. These output process areas represent the set of individual outlet process air areas obtained from all inlet air states. The area ratio values, AR, for all output process areas, obtained by Eq. (2), are summarized in Table 14 and the increases of outlet air temperature and humidity ratio, ΔT_{po} and $\Delta\omega_{po}$, for each output area, are shown in Table 15. The results show that the AR values were increased when T_{pi} increased, from area I to area II, whose input process

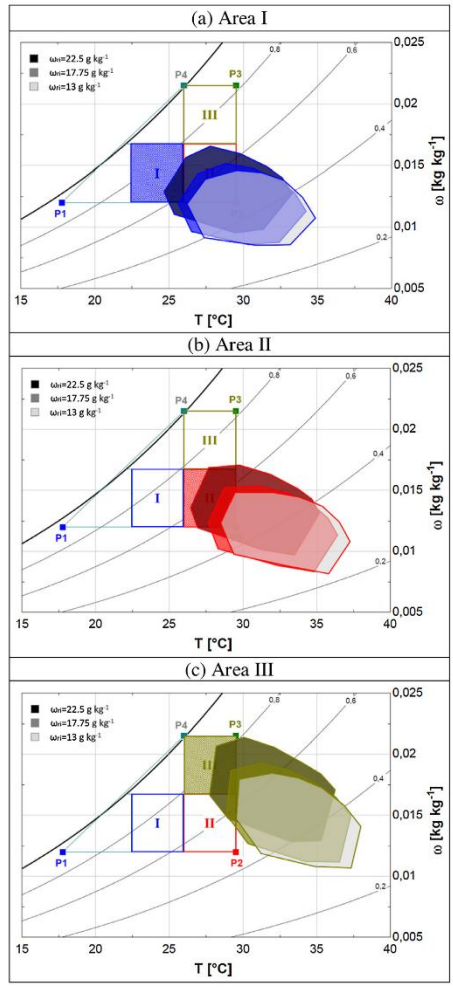

Fig. 10. Outlet process air conditions for the three input process areas when T_{ri}, Ω_{pi} and ω_{ri} were varied.

Table 15
Values of ΔT_{po} and $\Delta\omega_{po}$ for the three output process areas and three levels of ω_{ri}.

ω_{ri} [g kg^{-1}]	Outlet process air conditions					
	Area I		Area II		Area III	
	ΔT_{po} [°C]	$\Delta\omega_{po}$ [g kg^{-1}]	ΔT_{po} [°C]	$\Delta\omega_{po}$ [g kg^{-1}]	ΔT_{po} [°C]	$\Delta\omega_{po}$ [g kg^{-1}]
13.00	8.59	6.07	8.74	6.66	8.53	8.81
17.75	8.59	6.53	8.73	7.00	8.86	9.22
22.50	8.59	6.98	8.73	7.35	9.04	9.63

areas have the same inlet air humidity ratio range but different inlet air temperature range. The difference between area I and area II with respect to ΔT_{po} was 0.15 °C, and with respect to $\Delta\omega_{po}$ was less than 0.6 g kg^{-1}, see Table 15. In addition, the AR values were increased when ω_{pi} increased, from area II to area III, whose input process areas have the same inlet air temperature range but different inlet air humidity ratio range. The differences of ΔT_{po} and $\Delta\omega_{po}$ between area II and area III were less than 0.31 °C and 2.3 g kg^{-1} respectively, see Table 15. Thus, the maximum and minimum AR values were achieved for area III and area I, respectively.

Regarding ω_{ri}, it can be observed that the AR values were increased when ω_{ri} increased, see Table 14. This trend is inverse to that obtained with fixed inlet process air states, case study II. This is caused by the fact that in case study II each outlet process air state corresponds to a single inlet process air state. However, in case study III each outlet process air state corresponds to several inlet process air states.

These results suggest that the higher the T_{pi}, ω_{pi} and ω_{ri} values, the larger the area of outlet process air conditions.

3.5. Analysis of moisture removal capacity and sensible heat ratio

The variation of the outlet process air conditions from a given inlet process air state, by setting the T_{ri} and Ω_{pi}, caused MRC and SHR values to be modified. The MRC and SHR values of the process air stream for case study I were obtained experimentally, see Table 10. MRC ranged from 4.06 to 11.04 kg h^{-1}. The highest MRC value was obtained at the lower part of the outlet process air area, state 3 defined in Table 7, i.e. for the highest T_{ri} and Ω_{pi} value. SHR ranged from 0.64 to 0.87, where the highest SHR value was obtained at the upper part of the outlet process air area, state 7 defined in Table 7, i.e. for the lowest T_{ri} and Ω_{pi} value.

Regarding case study III, MRC and SHR values were not obtained, because for different inlet process air states, several MRC and SHR values exist in the same outlet process air state.

Regarding case study II, the MRC and SHR values of the process air stream for the five inlet air states, P1-P5, were obtained from the empirical model, and the results are represented in Fig. 11. The differences of MRC between the lower and upper part of the outlet air area were approximately 7 kg h^{-1} for all inlet process air states, see Fig. 11a. The highest MRC values were obtained at the lower part of the outlet process air area. These results of MRC are in agreement with those obtained in experimental case study I. On the other hand, the results showed that the increase of MRC was inversely proportional to the increase of outlet process air area, A_o. The MRC maximum value was achieved for P4 outlet air area, approximately 14 kg h^{-1}, where high ω_{pi} values and inlet air conditions close to saturation, were fixed. This moisture removal capacity was acceptable compared to the MRC nominal value, 15 kg h^{-1}, see Table 2, where the DW was activated at high regeneration temperatures.

The differences of SHR between the lower and upper part of the outlet air area were approximately 0.25 for all inlet process air states, see Fig. 11b. The lowest SHR values were obtained at the lower part of the outlet process air area. These results of SHR are in agreement with those obtained in experimental case study I. The SHR minimum value was achieved for P1 outlet air area, approximately 0.62.

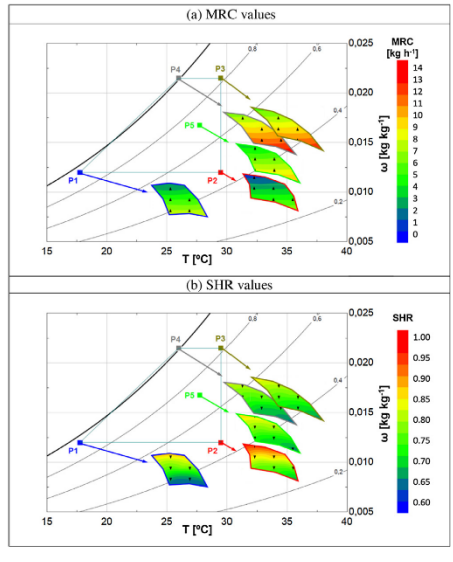

Fig. 11. MRC and SHR values of the five inlet air states for case study II.

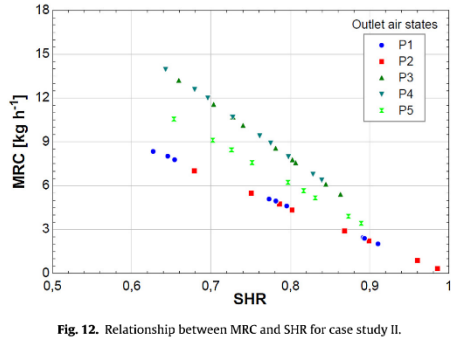

Fig. 12. Relationship between MRC and SHR for case study II.

The relationships between MRC and SHR for the five inlet air states, P1-P5, were obtained using the empirical model, as shown in Fig. 12. Similar slopes were obtained for equal ω_{pi} values, P1-P2

and P3-P4. However, for the same slope angle, the MRC values were increased and the SHR values were reduced when T_{pi} decreased, P2 to P1 and P3 to P4. It can be observed that the slope angle of the MRC-SHR relationship was higher when ω_{pi} increased. Furthermore, for the same MRC values, the SHR values were increased when ω_{pi} increased.

These results suggest that a control strategy by setting T_{ri} and Ω_{pi}, would allow MRC and SHR to be controlled over a wide range of outlet process air conditions of a DW activated at low temperatures. Furthermore, these results show a significant influence of the inlet air process humidity ratio on the MRC-SHR relationship. Therefore, different MRC-SHR relationships can be obtained by adjusting the inlet air process humidity ratio.

4. Conclusions

In the present work, an analysis of MRC and SHR of a DW activated at low temperatures, values below 60 °C, by varying the process airflow rate and air regeneration temperature, was carried out. Case study I was tested experimentally and case studies II and III were carried out using an empirical model fitted with the statistical technique of design of experiments, DOE. This empirical model allowed the analysis of the outlet process air conditions for a wide range of inlet air states.

The experimental and simulated results showed that a decoupling of the outlet process air conditions, temperature and humidity ratio, can be obtained when the process airflow rate and air regeneration temperature are varied. This decoupling resulted in a psychrometric area of the outlet process air. The outlet process air area was increased when inlet process air conditions were located close from saturation and the inlet air process and regeneration humidity ratio values were reduced. The maximum and minimum values of outlet process air area achieved from a given inlet process air state were 8.80 °C g kg^{-1} and 4.37 °C g kg^{-1}, respectively. Furthermore, a wider range of the outlet process air area can be achieved if the outlet air process temperature is controlled by the inlet air regeneration temperature, and the outlet air process humidity ratio is controlled by the process specific mass airflow rate. These results suggest that a control strategy by setting the process airflow rate and air regeneration temperature, would allow MRC and SHR to be controlled over a wide range of outlet process air conditions for a DW activated at low temperatures.

MRC and SHR were obtained experimentally and numerically for the case studies. The differences of MRC and SHR between the lower and upper part of the outlet air area were approximately 7 kg h^{-1} and 0.25, respectively, for all inlet process air states The highest MRC values and the lowest SHR values were obtained for the highest process airflow rate values and the highest inlet air regeneration temperature values, 14 kg h^{-1} and 0.62, respectively. The relationship between MRC and SHR was analysed, where several MRC values were obtained for a constant SHR value and vice versa. A significant influence of the inlet air process humidity ratio on the MRC-SHR relationship was showed. Therefore, different relationships can be obtained by adjusting the inlet air process humidity ratio.

The results show that a DW system activated at low temperatures, by setting the process airflow rate and air regeneration temperature, can obtain an independent control of MRC and SHR.

Acknowledgements

This work is related to the research project dehumidification and air drying, DESSECA, promoted by the company CIAT and co-funded by the Agency for Innovation and Development of Andalusia, expedient IDEA 360097, and by the Technological Corporation of Andalusia, expedient CTA 12/612, (2012-2014). The authors are grateful for the collaboration of Adoración Cerezuela Parish and Dr. Miguel Zamora García from CIAT Spain R&I Department.

References

[1] L.G. Harriman III, The Dehumidification Handbook, 2nd ed., Munters Corp., Amesbury, MA, 2003.
[2] D. Shirey, H. Henderson, R. Raustad, Understanding the Dehumidification Performance of Air-Conditioning Equipment at Part-Load Conditions, 641, 2006, pp. 655–1063.
[3] Y. Sheng, Y. Zhang, N. Deng, L. Fang, J. Nie, L. Ma, Experimental analysis on performance of high temperature heat pump and desiccant wheel system, Energy Build. 66 (2013) 505–513.
[4] D.B. Jani, M. Mishra, P.K. Sahoo, Performance studies of hybrid solid desiccant-vapor compression air-conditioning system for hot and humid climates, Energy Build. 102 (2015) 284–292.
[5] N. Wang, J. Zhang, X. Xia, Desiccant wheel thermal performance modeling for indoor humidity optimal control, Appl. Energy 112 (2013) 999–1005.
[6] R. Tu, X.-H. Liu, Y. Jiang, Performance analysis of a two-stage desiccant cooling system, Appl. Energy 113 (2014) 1562–1574.
[7] D. La, Y.J. Dai, Y. Li, Z.Y. Tang, T.S. Ge, R.Z. Wang, An experimental investigation on the integration of two-stage dehumidification and regenerative evaporative cooling, Appl. Energy 102 (2013) 1218–1228.
[8] H. Li, Y.J. Dai, Y. Li, D. La, R.Z. Wang, Case study of a two-stage rotary desiccant cooling/heating system driven by evacuated glass tube solar air collectors, Energy Build. 47 (2012) 107–112.
[9] C.R. Ruivo, F. Fernández Hernández, J.M. Cejudo López, Influence of the desiccant wheel effectiveness method approaches with fix and variable effectiveness parameters, on the performance results of an airport air-conditioning system, Energy Convers. Manag. 94 (2015) 458–471.
[10] L. Yadav, A. Yadav, Mathematical investigation of purge sector angle for clockwise and anticlockwise rotation of desiccant wheel, Appl. Therm. Eng. 93 (2016) 839–848.
[11] U. Eicker, U. Schürger, M. Köhler, T. Ge, Y. Dai, H. Li, et al., Experimental investigations on desiccant wheels, Appl. Therm. Eng. 42 (2012) 71–80.
[12] G. Angrisani, C. Roselli, M. Sasso, Effect of rotational speed on the performances of a desiccant wheel, Appl. Energy 104 (2013) 268–275.
[13] S. De Antonellis, M. Intini, C.M. Joppolo, F. Romano, On the control of desiccant wheels in low temperature drying processes, Int. J. Refrig. 70 (2016) 171–182.
[14] M. Aprile, M. Motta, Grey-box modelling and in situ experimental identification of desiccant rotors, Appl. Therm. Eng. 51 (2013) 55–64.
[15] A.G.C.C. American Gas Cooling Center, in: Applications Engineering Manual for Desiccant Systems, Arlington, TX, 1996.
[16] M. Intini, S. De Antonellis, C.M. Joppolo, The effect of inlet velocity and unbalanced flows on optimal working conditions of silica gel desiccant wheels, Energy Procedia 48 (2014) 858–864.
[17] S.D. White, M. Goldsworthy, R. Reece, T. Spillmann, A. Gorur, D.Y. Lee, Characterization of desiccant wheels with alternative materials at low regeneration temperatures, Int. J. Refrig. 34 (2011) 1786–1791.
[18] S. De Antonellis, M. Intini, C.M. Joppolo, Desiccant wheels effectiveness parameters: correlations based on experimental data, Energy Build. 103 (2015) 296–306.
[19] C.R. Ruivo, M. Goldsworthy, M. Intini, Interpolation methods to predict the influence of inlet airflow states on desiccant wheel performance at low regeneration temperature, Energy 68 (2014) 765–772.
[20] C.R. Ruivo, A. Carrillo-Andres, J.J. Costa, F. Dominguez-Munoz, Exponential correlations to predict the dependence of effectiveness parameters of a desiccant wheel on the airflow rates and on the rotation speed, Appl. Therm. Eng. 51 (2013) 442–450.
[21] E. Kozubal, J. Woods, J. Burch, A. Boranian, T. Merrigan, Desiccant Enhanced Evaporative Air-Conditioning (DEVap): Evaluation of a New Concept in Ultra Efficient Air Conditioning, Technical Report NREL/TP-5500-49722, 2011.
[22] M.A. Sayegh, M. Hammad, Z. Faraa, Comparison of two methods of improving dehumidification in air conditioning systems: hybrid system (refrigeration cycle – Rotary desiccant) and heat exchanger cycle, Energy Procedia 6 (2011) 759–768.
[23] J. Jeong, S. Yamaguchi, K. Saito, S. Kawai, Performance analysis of four-partition desiccant wheel and hybrid dehumidification air-conditioning system, Int. J. Refrig. 33 (2010) 496–509.
[24] G. Angrisani, F. Minichiello, C. Roselli, M. Sasso, Experimental analysis on the dehumidification and thermal performance of a desiccant wheel, Appl. Energy 92 (2012) 563–572.
[25] J.D. Chung, D.Y. Lee, S.M. Yoon, Optimization of desiccant wheel speed and area ratio of regeneration to dehumidification as a function of regeneration temperature, Sol. Energy 83 (2009) 625–635.
[26] Y. Sheng, Y. Zhang, Y. Sun, L. Fang, J. Nie, L. Ma, Experimental analysis and regression prediction of desiccant wheel behavior in high temperature heat pump and desiccant wheel air-conditioning system, Energy Build. 80 (2014) 358–365.
[27] D.B. Jani, M. Mishra, P.K. Sahoo, Performance prediction of rotary solid desiccant dehumidifierin hybrid air-conditioning system using artificial neural network, Appl. Therm. Eng. 98 (2016) 1091–1103.

[28] Y. Guan, Y. Zhang, Y. Sheng, X. Kong, S. Du, Feasibility and economic analysis of solid desiccant wheel used for dehumidification and preheating in blast furnace: a case study of steel plant Nanjing, China, Appl. Therm. Eng. 81 (2015) 426–435.
[29] C.E.L. Nóbrega, N.C.L. Brum, An analysis of the heat and mass transfer roles in air dehumidification by solid desiccants, Energy Build. 50 (2012) 251–258.
[30] F. Comino, M. Ruiz de Adana, F. Peci, Experimental study of the moisture removal capacity of a desiccant wheel activated at low and high temperature, CLIMA 2016, Aalborg University, Department of Civil Engineering, in: Proc. 12th REHVA World Congress, vol. 9, 2016.
[31] J. Wrobel, P. Morgenstern, G. Schmitz, Modeling and experimental validation of the desiccant wheel in a hybrid desiccant air conditioning system, Appl. Therm. Eng. 51 (2013) 1082–1091.
[32] S. De Antonellis, C.M. Joppolo, L. Molinaroli, A. Pasini, Simulation and energy efficiency analysis of desiccant wheel systems for drying processes, Energy 37 (2012) 336–345.
[33] C.R. Ruivo, A. Carrillo-Andrés, J.J. Costa, F. Domínguez-Muñoz, Interpolation procedures for the effectiveness method to account for the influence of the inlet airflow states on the desiccant wheels performance, Energy Build. 55 (2012) 380–388.
[34] A.M. Baniyounes, M.G. Rasul, M.M.K. Khan, Experimental assessment of a solar desiccant cooling system for an institutional building in subtropical Queensland Australia, Energy Build. 62 (2013) 78–86.
[35] F. Comino Montilla, M. Ruiz de Adana Santiago, A. Cerezuela Parish, M. Zamora García, F. Peci López, Design and building of a test facility for experimentation of desiccant wheels, in: the Minutes Book of the National Congress Engineering Thermodynamics, Cartagena (2015) 295–302.
[36] D.C. Montgomery, Design and Analysis of Experiments, sixth ed., Wiley, New York, 2004.
[37] Statgraphics Centurion XV, 2006, available from http://www.statgraphics.com/(accessed 15.05.16).
[38] C.R. Ruivo, A. Carrillo-Andrés, J.J. Costa, F. Domínguez-Muñoz, A new approach to the effectiveness method for the simulation of desiccant wheels with variable inlet states and airflows rates, Appl. Therm. Eng. (2012) 1–9.
[39] ASHRAE, Method of Testing for Rating Desiccant Dehumidifiers Utilizing Heat for the Regeneration Process, ASHRAE standard, 2007.
[40] F. Comino, M.R. de Adana, F. Peci, First and second order simplified models for the performance evaluation of low temperature activated desiccant wheels, Energy Build. 116 (2016) 574–582.
[41] M. Beccali, R.S. Adhikari, F. Butera, V. Franzitta, Update on desiccant wheel model, Int. J. Energy Res. 28 (2004) 1043–1049.
[42] F.E. Nia, Sustainable Air Handling by Evaporation and Adsorption, Deft University of Technology, PhD thesis, 2011.

Appendix C

Simplified performance correlation of an indirect evaporative cooling system: development and validation

The paper presented in this appendix has been submitted for *International Journal of Refrigeration* (September 2017)

Simplified performance correlation of an indirect evaporative cooling system: development and validation

Authors: Francisco Comino[a*], Samanta Milani[b], Stefano De Antonellis[b], Cesare Maria Joppolo[b], Manuel Ruiz de Adana[a]

* Corresponding author tel. +34 626285994; e-mail: francisco.comino@uco.es

Affiliations

[a] Departamento de Química-Física y Termodinámica Aplicada, Escuela Politécnica Superior, Universidad de Córdoba, Campus de Rabanales, Antigua Carretera Nacional IV, km 396, 14071 Córdoba, Spain

[b] Dipartimento di Energia, Politecnico di Milano, Via Lambruschini, 4, 20156 Milan, Italy

Abstract

At present, there is an increasing interest in indirect evaporative coolers (IEC), which are an effective alternative to conventional cooling systems, due to their high efficiency and reduced primary energy consumption. Performance of such systems significantly depends on inlet air conditions and water flow rate and, therefore, it should be properly evaluated through experimental tests or appropriate models.

Both phenomenological and simplified models to analyse IEC have been proposed in literature. In the first case, numerical results are particularly accurate but a significant computational load is required. In the second case, numeric calculations are limited and the model can be easily implemented in energy simulation tools.

In this study, experimental tests of an IEC, have been carried out and a new simplified model, based on a first order linear regression approach, has been developed. Results of the proposed correlation have been compared with ones of a phenomenological model and with further experiment data of the system. It is shown that deviations of wet bulb effectiveness are always within 3.4% for the simplified model and 2.1% for the detailed one. Therefore, due to its good accuracy and low computational load, the simplified model is suitable to be implemented in simulation tools.

Keywords: Indirect evaporative cooling; correlation; experimental; numerical; model.

1 Introduction

Indirect evaporative cooling (IEC) systems are an effective alternative to conventional technologies, due to their high efficiency and reduced primary energy consumption [1]. In an IEC system, the primary air stream is cooled at constant humidity ratio in a heat exchanger, which is crossed by a secondary air stream humidified with liquid water.

The IEC technology can be used in many applications: in pre-cooling and energy recovery units [2–4], in two stage indirect/direct evaporative cooling system [5], in passive cooling unit [6] or combined with desiccant dehumidifiers [7]. Furthermore, recent studies highlight that the use of IEC systems in data centres leads to significant energy savings [8].

IEC systems have been widely analysed by many authors in the available literature, in particular focusing on the optimization of the device and on the analysis of influential parameters on outlet air conditions. The performance of IECs has been analysed for different operating conditions, evaluating the effect of variable inlet air velocities [9,10]. Tejero Gonzales et al. [11] studied the influence of constructive parameters on IEC systems, such as material and geometry. De Antonellis et al. [12] focused on the variation of water flow rate, which has a significant effect on system performance: the higher the water flow rate, the higher the humidification of the secondary air stream and, therefore, the higher the primary air temperature reduction.

Mathematical models of IECs are very useful to optimize the device as well as to study the behaviour of the system when it is combined with other HVAC components. MacLaine-cross and Banks [13] developed an analytical model using a linearized approximate theory for a thin and continuous water layer inside the wet channels. Erens and Dreyer [14] presented a simplified finite volume model, starting from Poppe and Rögener [15] and Merkel [16] models for the analysis of direct contact cooling towers. Alonso et al. [17] studied a finite difference method using an equivalent temperature at the interface. Ren and Yang [18] elaborated a detailed analytical model for a heat and mass heat exchanger with parallel or counter flow configurations, taking into account

Nomenclature

$A_{HE,net}$	net heat exchanger cross area [m^2]
b_1-b_{15}	correlation parameters of the simplified model
cp	specific heat [J kg^{-1} K^{-1}]
c_1-c_4	correlation parameters of the detailed model
C_W	wettability coefficient
h	net channel height [m]
H_{HE}	heat exchanger height [m]
h_M	convective mass transfer coefficient [kg s^{-1} m^{-2}]
h_T	convective heat transfer coefficient [W m^{-2} K^{-1}]
k	thermal conductivity [W m^{-1} K^{-1}]
k_1-k_4	correlation parameters of the detailed model
L^*	net plate length and width
$\dot{m}$	specific mass flow rate [kg s^{-1} m^{-2}]
$\dot{M}$	mass flow rate [kg s^{-1}]
N_T	number of tests
N_0-N_{43}	reference test
N_{HE}	number of heat exchanger plate [-]
p	pressure [Pa]
pt	plates pitch [m]
RH	relative humidity [%]
$\dot{Q}$	air volumetric flow rate [m^3 h^{-1}]
$\dot{Q}_w$	water volumetric flow rate [l h^{-1}]
T	dry bulb temperature [°C]
T_{wb}	wet bulb temperature [ºC]
U_T	overall heat transfer coefficient [W m^{-2} K^{-1}]
v	air velocity [m s^{-1}]
V	simplified model input
x	primary air flow direction [m]
X	humidity ratio [kg kg^{-1}]
y	secondary air flow direction [m]
Y	experimental or numerical output

Greek letters

Δ	variation
δ	plate thickness [m]
δ_w	water film thickness [m]
ε_{db}	dry bulb effectiveness [-]
ε_h	saturation efficiency [-]
ε_{wb}	wet bulb effectiveness [-]
ρ	density [kg m^{-3}]
σ	wettability factor [-]

Superscripts

N	reference density (ρ=1.2 kg m^{-3})
EXP	experimental
NUM	numerical

Subscripts

a	air
exp	experimental data
HE	heat exchanger
in	inlet
min	minimum
out	outlet
p	primary air
s	secondary air
w	liquid water

Acronyms

DM	detailed model
DOE	design of experiments
EXP	experimental
IEC	indirect evaporative cooler or cooling
MD	maximum deviation
NUM	numerical
RMSD	root mean standard deviation
SM	simplified model

incomplete surface wetting conditions and water temperature variation. Hasan [19] developed a model to analyse the thermal performance of sub-wet bulb temperature cooling based on the ε-NTU method for sensible heat exchangers. Guo and Zhao [20] carried out a numerical analysis to investigate the heat and mass transfer in a cross flow IEC, evaluating the effect of plates wettability and air inlet velocity variation. Hettiarachchi et al. [21] developed a finite difference method that uses the NTU approach to investigate the effect of longitudinal heat conduction in the heat exchanger. Cui et al. [22] developed a computational model to study the effect of main parameters on a counter-flow dew point evaporative cooler. De Antonellis et al. [23] obtained a mathematical model of a IEC system, taking into account the effect of adiabatic humidification of the secondary air stream and the wettability factor of the heat exchanger surface. However, most of the aforementioned approaches, due to the high computational load, are not very practical to be implement in energy simulation tools.

A methodology recently used to obtain simplified models of IEC systems is based on statistical design [24]. Pandelidis and Anisimov [25] presented a simplified model generated by response surface methodology for analysing performance of a device based on the M-cycle. Sohani et al. [26] obtained a mathematical model to determine the performance of a M-cycle crossflow heat exchanger, based on a statistical method known as "group method of data handling-type neural network". Both statistical models accurately represented the behaviour of an IEC M-cycle system and they could be easily integrated into HVAC models. However, the influence of a secondary airflow conditions and of the water flow rate has not been analysed. Therefore, it is of interest to obtain a simple correlation of a IEC system based on a cross flow heat exchanger, including the effect of variable water flow rate and secondary air inlet temperature, inlet humidity ratio and flow rate.

Finally, the aim of this work is to develop a simplified IEC model based on experimental data, which can be easily introduced in HVAC system simulation tools, and to compared obtained results with outputs of a previously developed phenomenological model [23] and with further laboratory tests of the device.

2 Experimental set up

2.1 Description of the evaluated IEC system

The analysed indirect evaporative cooling system is composed of the following elements:

- A commercial crossflow plate heat exchanger.
- N° 8 water nozzles installed in the secondary airflow inlet plenum.
- A water pumping system.

As shown in Fig. 1, two air streams cross the heat exchanger:

- The primary air stream, which is cooled at constant humidity ratio. It enters the system in condition p,in and it leaves the component in condition p,out.
- The secondary air stream, which enters and leaves the system respectively in condition s,in and s,out. It is supplied to the upper part of the system, where spray nozzles are installed, flowing from the top to the bottom of the device. First, due to the evaporation of water droplets in the inlet plenum, the secondary air stream is humidified almost at constant enthalpy and it reaches the heat exchanger face in condition s,in,HE. Then, the secondary air stream passes through the heat exchanger plates, where a further water evaporation occurs.

The net face heat exchanger cross area $A_{net,HE}$ is equal to 0.089 m^2 and it is evaluated as Anet,HE=(HHE - N_{HE} δ) L*/2, where the heat exchanger height is HHE = (N_{HE}-1) pt + δ. Plates are made of aluminium with semi spherical dimples.

The n° 8 water nozzles are installed on two parallel manifolds. The nominal water flow rate for each axial and full cone type nozzle is 7.50 l h^{-1} at 9 bar. The distance between nozzles is 8 cm and each manifold is installed 15 cm far from the heat exchanger. The water is supplied in counter current arrangement respect to the secondary air stream through a commercial pumping unit, without any recirculation, at an average temperature around 20 °C. Finally, the length of top and side plenums is 42 cm.

Table 1. Main characteristics of the IEC system.

Description	Parameter	Value
Number of plates	N_{HE}	119
Plate thickness	δ	0.14 mm
Plate pitch	pt	3.35 mm
Net channel height	$h=pt-\delta$	3.21 mm
Net plate length and width	L^*	470 mm
Net face heat exchanger cross area	$A_{HE,net}$	0.089 m^2

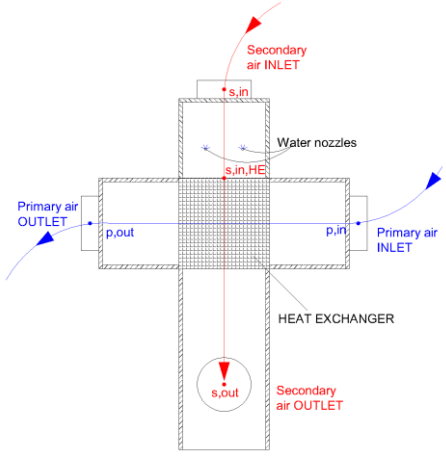

Fig. 1. Scheme of the investigated indirect evaporative cooling system.

2.2 Description of the test rig and experimental methodology

The primary and secondary airflow conditions are controlled by two independent air handling units. Temperature and humidity ratio of each stream are set through heating and cooling coils, evaporative humidifiers and electric heaters. The maximum volumetric flow rates of the primary and secondary air streams are respectively 1400 $m^3 h^{-1}$ and 2000 $m^3 h^{-1}$. Each air flow rate is measured using two orifice plates and piezo resistive pressure transmitters placed in two different measurement ducts, constructed according to standards [27]. The two air handling units can work in outdoor air mode or recirculated air mode, depending on the desired supply air conditions.

Table 2. Specification of measuring devices.

Physical quantity	Type of sensor	Accuracy[a]
T[b]	PT 100 Class A	±0.2 °C
RH[b]	Capacitive	±1% (between 0 and 90%)
p	Piezo resistive	0.5% of reading ±1 Pa

[a] at T=20 °C
[b] Temperature and relative humidity probe

The water flow rate supplied to the nozzles from the pumping unit was measured using a turbine flow sensor, whose accuracy is 3% of the reading. A detailed test rig description has been reported in a previous work of the authors [12], while adopted instruments data are shown in Table 2.

In each experimental session, at least 300 samples for each physical quantity have been collected in steady state conditions and at a frequency of 1 Hz. The experimental uncertainty u_{xi} of each direct monitored variable x_i (T, RH, p) is:

$$u_{x_i} = \pm\sqrt{u_{x_{i,inst}}^2 + \left(t_{95}\,\sigma_{\bar{x}_i}\right)^2} \quad (1)$$

Where $u_{xi,inst}$ $u_{x_{i,inst}}$ is the instrument uncertainty of the measured quantity t_{95} is the student test multiplier al 95% confidence and $\sigma_{\bar{x}_i}$ is the standard deviation of the mean.

The generic combined uncertainty u_y of calculated quantities y, such as ε_{wb}, ΔT_p, ΔT_s and ΔX_s is calculated as:

$$u_{y_i} = \sqrt{\sum_i \left(\frac{\partial y_i}{\partial x_i} u_{x_i,inst}\right)^2 + t_{95}^2 \sum_i \left(\frac{\partial y_i}{\partial x_i}\sigma_{\bar{x}_i}\right)^2} \quad (2)$$

The uncertainty of the evaluated quantities are estimated in accordance with Moffat [28]. The methodology and the assumptions are described in the reference international standard [29].

2.3 Performance indexes and preliminary experimental results

Experimental results have been evaluated in terms of wet bulb effectiveness ε_{wb}, of variation of primary air temperature ΔT_p, secondary air temperature ΔT_s, and secondary air humidity ratio ΔX_s. Such indexes are defined through the following equations:

$$\varepsilon_{wb} = \frac{\left(T_{p,in} - T_{p,out}\right)}{\left(T_{p,in} - T_{wb,s,in}\right)} \quad (3)$$

$$\Delta T_p = T_{p,in} - T_{p,out} \quad (4)$$

$$\Delta T_s = T_{s,in} - T_{s,out} \quad (5)$$

$$\Delta X_s = X_{s,out} - X_{s,in} \quad (6)$$

According to Table 3, 82 tests of the IEC system have been performed for both models calibration and validation. More precisely, 30 tests have been used to calibrate the detailed model [23,30], 37 tests to develop the linear regression correlation and 15 tests to complete the validation and comparison of both the models. In Table 3 the air velocity is referred to reference air density (ρ_a^N=1.2 kg m^{-3}) and calculated as

$v_a^N = \dot{Q}_a^N / (3600\ A_{HE,net})$, where $\dot{Q}_a^N$ is the volumetric airflow rate in the same air condition.

The measured dry bulb effectiveness of the cross flow heat exchanger, which is defined as $\varepsilon_{db} = \dot{M}_p\, cp_p\, (T_{p,in} - T_{p,out}) / [(\dot{M}_a\ cp_a)_{min} (T_{p,in} - T_{s,in})]$, is 62.1 % (at $v_s^N = v_p^N = 3.7$ m s^{-1}, $T_{p,in}$ =31°C and $T_{s,in}$ = 50°C). The nominal pressure drop across the heat exchanger is 100 Pa when v_a = 3.2 m s^{-1} (at T_a= 35°C).

Table 3. Summary of test conditions for calibration and validation of the models.

$N_{1\text{-}26}$[a]	Model	N_T	$T_{s,in}$ [°C]	$X_{s,in}$ [g kg^{-1}]	v_s^N [m s^{-1}]	$T_{p,in}$[b] [°C]	$\dot{Q}_{w,in}$ [l h^{-1}]
N_1	DM	5	30.0	10.6	3.7	35.0	30 - 65
N_2	DM	5	30.0	10.6	5.7	35.0	30 - 65
N_3	DM	5	30.0	13.4	3.7	35.0	30 - 65
N_4	DM	5	30.0	13.4	5.7	35.0	30 - 65
N_5	DM	5	36.8	10.6	3.7	35.0	30 - 65
N_6	DM	5	36.8	10.6	5.7	35.0	30 - 65
N_7	SM	2	25.0	8.0	3.7	28.0	30, 60
N_8	SM	2	25.0	8.0	5.7	28.0	30, 60
N_9	SM	2	25.0	8.0	3.7	48.0	30, 60
N_{10}	SM	2	25.0	8.0	5.7	48.0	30, 60
N_{11}	SM	2	25.0	16.0	3.7	28.0	30, 60
N_{12}	SM	2	25.0	16.0	5.7	28.0	30, 60
N_{13}	SM	2	25.0	16.0	3.7	48.0	30, 60
N_{14}	SM	2	25.0	16.0	5.7	48.0	30, 60
N_{15}	SM	2	38.0	8.0	3.7	28.0	30, 60
N_{16}	SM	2	38.0	8.0	5.7	28.0	30, 60
N_{17}	SM	2	38.0	8.0	3.7	28.0	30, 60
N_{18}	SM	2	38.0	8.0	5.7	28.0	30, 60
N_{19}	SM	2	38.0	16.0	3.7	28.0	30, 60
N_{20}	SM	2	38.0	16.0	5.7	28.0	30, 60
N_{21}	SM	2	38.0	16.0	3.7	28.0	30, 60
N_{22}	SM	2	38.0	16.0	5.7	28.0	30, 60
N_{23}	SM	5	31.5	12.0	4.7	38.0	45
N_{24}	DM, SM	5	30.0	13.3	4.7	35.0	30 - 65
N_{25}	DM, SM	5	26.0	12.6	3.7	60.0	30 - 65
N_{26}	DM, SM	5	26.0	12.6	3.7	30.0	30 - 65

[a] Tests N_1 - N_{22} for models calibration, Tests N_{24} - N_{26} for models validation
[b] v_p^N=3.7 m s^{-1} and $X_{p,in}$ =10.0 g kg^{-1}.

Although a detailed experimental analysis of the investigated IEC system is not the scope of this work, in Fig. 2 typical trends of adopted performance indexes are reported (tests N_1 and N_2 of Table 3). In the investigated conditions, the maximum wet bulb effectiveness is equal to 86% and the maximum primary air temperature difference is close to 13 °C. A detailed analysis of trends of the IEC performance indexes has been discussed in a previous work of the authors [12]. It is highlighted that in the present work, due to the improved setup, system performance is slightly higher than the one obtained in the previous studies [12,23]. In fact, in this case wider air plenums have been adopted, enhancing adiabatic humidification of the secondary air stream and promoting a uniform water distribution in the heat exchanger.

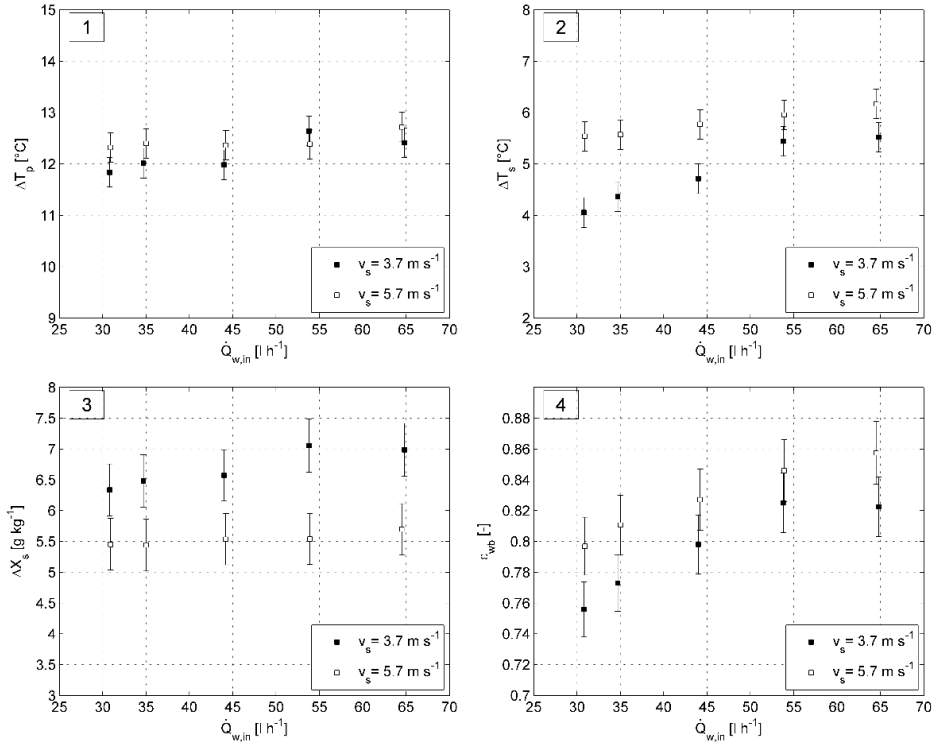

Fig. 2. Experimental data of the investigated IEC system in test N_1 (v_s^N=3.7 m s^{-1}) and N_2 (v_s^N=5.7 m s^{-1}) reported in Table 3.

3 Models description

3.1 Adopted approach

In this work, two indirect evaporative cooling models are discussed: a detailed model (DM), based on heat and mass transfer equations, and a simplified model (SM), based on a first order linear regression approach. As described in detail in sections 3.2 and 3.3, both IEC models have been properly calibrated through specific set of experimental data, summarized in Table 3 and denoted with acronyms DM and SM. Finally, the numerical results obtained with the two models have been analysed and compared with a further set of experimental data, representative of possible operating conditions of the IEC system.

3.2 Detailed model (DM)

The detailed model (DM) is based on the solution of heat and mass transfer equations in the cross flow heat exchanger. It takes into account also the water droplets evaporation in the secondary inlet air plenum and the fraction of wet surface of heat exchanger plates. Assumptions, governing equations and calibration procedure of the model have been discussed in detail in a previous work of the authors [23]. Therefore, in this research only a brief description of the model is reported.

Main adopted assumptions are: i) Steady-state conditions; ii) No heat losses to the surroundings; iii) Negligible axial heat conduction and water diffusion in the air streams; iv) Negligible heat conduction in the heat exchanger plates; v) Uniform air inlet conditions; vi) Interface plate temperature equal to bulk water temperature.

Governing equations applied to the primary air stream, to the secondary air stream and to the heat exchanger surface and water layer are:

$$\frac{dT_p}{dx} = \frac{U_{T,p}\left(T_W - T_p\right)}{v_p cp_p \rho_p \frac{h}{2}} \quad (7)$$

$$\frac{dT_s}{dy} = \frac{h_{T,s}\left(T_W - T_s\right)}{v_s cp_s \rho_s \frac{h}{2}} + \frac{h_{M,s}\left(\lambda + cp_s T_s\right)\left(X_W - X_s\right)\sigma}{v_s cp_s \rho_s \frac{h}{2}} \quad (8)$$

$$\frac{dX_s}{dy} = \frac{h_{M,s}\left(X_W - X_s\right)\sigma}{v_s \rho_s \frac{h}{2}} \quad (9)$$

$$h_{M,s}\left(\lambda + cp_s T_s\right)\left(X_s - X_W\right)\sigma + \\ + h_{T,s}\left(T_s - T_W\right) + U_{T,p}\left(T_p - T_W\right) = 0 \quad (10)$$

$$\frac{d\dot{m}_w}{dy} = \frac{h_{M,s}\left(X_s - X_W\right)\sigma}{h/2} \quad (11)$$

The mass transfer coefficient h_M, assuming $Le=1$, has been calculated as:

$$h_M = \frac{h_T}{cp_a} \quad (12)$$

The heat transfer coefficient h_T was calculated using the following correlation [23]:

$$h_T = \frac{k_a}{2\,h} 0.0185 \,\mathrm{Re}^{0.928} \,\mathrm{Pr}^{1/3} \quad (13)$$

According to the previous research [23], the correlation to predict the wettability factor σ is:

$$\sigma = \dot{m}_w \frac{h}{2\,\delta_w v_w \rho_w} = \dot{m}_w \, C_w \quad (14)$$

Where:

$$C_w = \frac{k_1}{v_S^{N\,k_2} e^{k_3 \,\dot{m}_{w,in,HE}}} \quad (15)$$

And:

$$\dot{m}_{w,in,HE} = \dot{m}_{w,in} - \frac{\left(X_{s,in,HE} - X_{s,in}\right)\dot{Q}_S^N \, \rho^N}{3600 \, A_{HE,net}} \quad (16)$$

$\dot{m}_{w,in,HE}$ is the water specific mass flow rate, net of the water evaporation in the secondary air inlet plenum, and

$$\dot{m}_{w,in} = \frac{\dot{M}_{w,in}}{A_{HE,net}} \quad (17)$$

The correlation to predict the saturation efficiency in the secondary air inlet plenum is [23]:

$$\varepsilon_h = \frac{c_1 \ln\left(T_{s,in} - T_{s,wb,in}\right) + c_2}{\dot{M}_s^{c_3}} \dot{M}_{w,in}^{c_4} \quad (18)$$

As discussed in section 2.3, the experimental setup, more precisely the air plenums, have been improved compared to the previous research work [23]. Therefore, 30 experimental tests have been carried out (N_1 to N_6 in Table 3), in order to fit the wettability factor and saturation efficiency parameters reported in Eq. 15 and Eq. 18 [30]. Tests have been performed adopting the same methodology described in [23] and resulting coefficients are summarized in Table 4 [30].

Table 4. Correlation coefficients for the detailed model (DM) of Eqs. 15 and 18 [30].

Coefficient	Value
k_1	4.82
k_2	0.0114
k_3	4.8192
c_1	6.781
c_2	33.977
c_3	0.9547
c_4	0.9839

As shown in Fig. 3, there is a very good agreement between numerical and experimental primary air

temperature variation, being the deviation always within 0.3 °C.

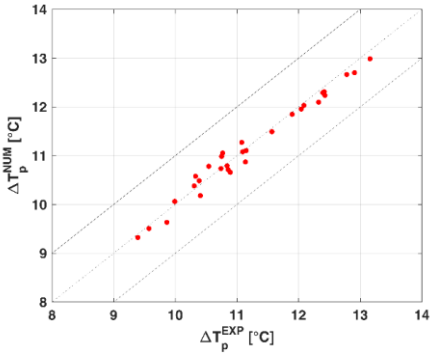

Fig. 3. Parity plot of experimental and numerical ΔT_p of the detailed model (tests N_1 - N_6 reported in Table 3)

3.3 Simplified model (SM)

A new empirical simplified model has been developed in this work to predict the behaviour of the air outlet conditions of the IEC system. The methodology used to fit this model is based on the statistical technique of design of experiments (DOE) [24]. The fit of the model and its further statistical analysis have been carried out through a commercial software [31].

In this work, a DOE with three output variables and five input variables, namely $T_{p,in}$, $T_{s,in}$, $X_{s,in}$, v_s^N and $\dot{Q}_w$, has been developed. The input variables range has been defined in order to have representative operating conditions of actual IEC systems. The primary air velocity has been set constant and equal to typical working conditions, reducing the required number of experimental tests. The output process variables are the outlet primary air temperature $T_{p,out}$, the outlet secondary air temperature $T_{s,out}$ and the outlet secondary air humidity ratio $X_{s,out}$. The effect of the five input variables is studied using the factorial design approach, design at 2-levels [24]. The factorial design method is frequently applied to experimental works when the response is approximately linear within the selected input variables range. The total number of required experimental tests (N_T) to carry out the factorial design is defined as $N_T=2^n+R_c$, where n is the number of input variables and R_c is the replicate number of the centerpoints [24]. In this work, in order to evaluate the repeatability of the measurement system and to estimate whether there are nonlinear processes, 5 replicates of the centerpoints are included, leading to a set of 37 experimental tests, summarized in Table 3 (N_7 - N_{23}).

The relationship between the output and input variables was examined using first order polynomial equations. The resulting polynomial equation model is expressed by Eq. 20, where Y^{NUM} is the predicted output value, V_i is a term equal to each input variable or, in case of correlation, to the product of two input variables and b_i/1000 are the regression coefficients.

$$Y^{NUM} = \frac{b_0 + \sum_{i=1}^{15} b_i V_i}{1000} \qquad (20)$$

The estimated coefficients $b_{0\text{-}15}$ and the terms $V_{1\text{-}15}$ of Eq. 20 are summarized in Table 5. It can be observed that the coefficients with the highest weight were b_3 for $T_{p,out}$ and b_4 for $T_{s,out}$ and $X_{s,out}$.

The accuracy of the model to predict the experimental outlet conditions is reported in terms of the R^2 values. More precisely, the R^2 values, obtained considering all the 37 tests, were 99.54 % for $T_{p,out}$, 99.78 % for $T_{s,out}$ and 99.89 % for $X_{s,out}$.

Table 5. Estimated coefficients of the simplified model (SM) of Eq. 20.

b_x	V_i	$T_{p,out}$ [ºC]	$T_{s,out}$ [ºC]	$X_{s,out}$ [g kg^{-1}]
b_0	-	-1313.76	3801.74	-379.62
b_1	$T_{p,in}$	322.41	500.49	183.23
b_2	$T_{s,in}$	364.07	191.57	135.71
b_3	$X_{s,in}$	766.52	455.43	313.29
b_4	v_s^N	-467.09	-1199.63	755.41
b_5	$\dot{Q}_w$	41.87	20.99	3.33
b_6	$T_{p,in}$·$T_{s,in}$	0.42	0.60	0.19
b_7	$T_{p,in}$·$X_{s,in}$	-5.09	-3.93	6.28
b_8	$T_{p,in}$·v_s^N	-15.66	-25.34	-35.06
b_9	$T_{p,in}$·$\dot{Q}_w$	-1.23	-2.02	1.12
b_{10}	$T_{s,in}$·$X_{s,in}$	-8.45	-5.85	3.32
b_{11}	$T_{s,in}$·v_s^N	26.11	42.55	-6.63
b_{12}	$T_{s,in}$ $\dot{Q}_w$	-2.11	-1.54	0.92
b_{13}	$X_{s,in}$·v_s^N	12.58	19.45	33.91
b_{14}	$X_{s,in}$ $\dot{Q}_w$	2.87	3.37	-2.39
b_{15}	v_s^N $\dot{Q}_w$	-0.94	3.94	-4.54

Finally, in Fig. 4 it is shown that difference of ΔT_p between numerical output and experimental data, which is always below 0.5 °C.

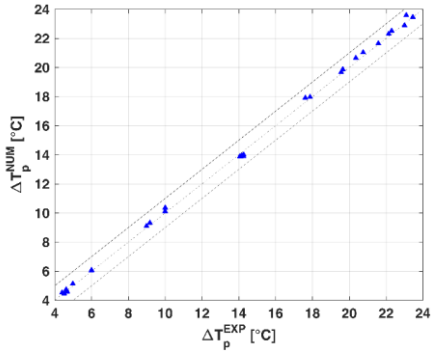

Fig. 4. Parity plot of experimental and numerical ΔT_p of the simplified model (tests N_7 - N_{23} reported in Table 3)

4 Validation of the models: results and analysis

4.1 Preliminary comparison between detailed and simplified models

The results of the detailed and simplified models of the IEC system have been preliminary analysed by varying $T_{p,in}$, $T_{s,in}$, $X_{s,in}$, v_s^N and $\dot{Q}_{w,in}$, as shown in Fig. 5. In the analysis, the average value of each input variable adopted in the detailed model calibration (tests N_1-N_6 reported in Table 3) has been used as reference condition. It can be observed the two models perform similarly and also outputs of the detailed model, in the investigated range, even though based on a phenomenological approach, show an almost linear response. In case of variation of $\dot{Q}_{w,in}$, although outputs response is not fully linear (as shown also by experimental results of Fig. 2), the deviation between the two models is very limited. Therefore, the first-order approach adopted in the simplified model can be assumed satisfactory to estimate the behaviour of the IEC system.

4.2 Case studies

In this section, three case studies have been analysed: experimental tests have been performed (tests N_{24} - N_{27} of Table 3) and compared to results obtained, in the same conditions, with the two models. The first case study is related to a data center application, the second one to a desiccant evaporative cooling (DEC) configuration and the third one to a residential application. In each case, the water flow rate $\dot{Q}_w$ has been varied between 30 and 65 l h^{-1}, while the remaining inputs have been set in this way:

- Case A (Data center application, test N_{24} of Table 3): the primary air stream is at data center ambient conditions ($T_{p,in}$ =35 °C) while the secondary air stream is at summer outdoor conditions ($T_{s,in}$ =30°C, $RH_{s,in}$=50%). This condition is similar to test N_1 and N_2 with a different secondary air flow rate.
- Case B (DEC configuration, test N_{25} of Table 3): the primary air stream is at outlet desiccant wheel conditions ($T_{p,in}$ =60 °C) while the secondary air stream is at indoor conditions (return air from the building $T_{s,in}$ =26°C, $RH_{s,in}$=60%).
- Case C (Residential configuration, test N_{26} of Table 3): the primary air stream is at outdoor conditions ($T_{p,in}$ =30 °C) while the secondary air stream is at indoor conditions (return air from the building $T_{s,in}$ =26°C, $RH_{s,in}$=60%).

The deviation between experimental data and calculated outputs has been evaluated by the Root Mean Standard Deviations, RMSD, and the percentage of the maximum deviation, MD. RMSD of the generic output Y (ΔT_p, ΔT_s, ΔX_s or ε_{wb}) has been calculated as:

$$RMSD_Y = \sqrt{\frac{\sum_{i=1}^{N}\left(Y^{NUM} - Y^{EXP}\right)^2}{N_T}} \qquad (21)$$

Where N_T is the number of adopted tests in each case study. The obtained values of RMSD and of MD are reported in Table 6, while detailed experimental and numerical results are represented in Figs 6-8.

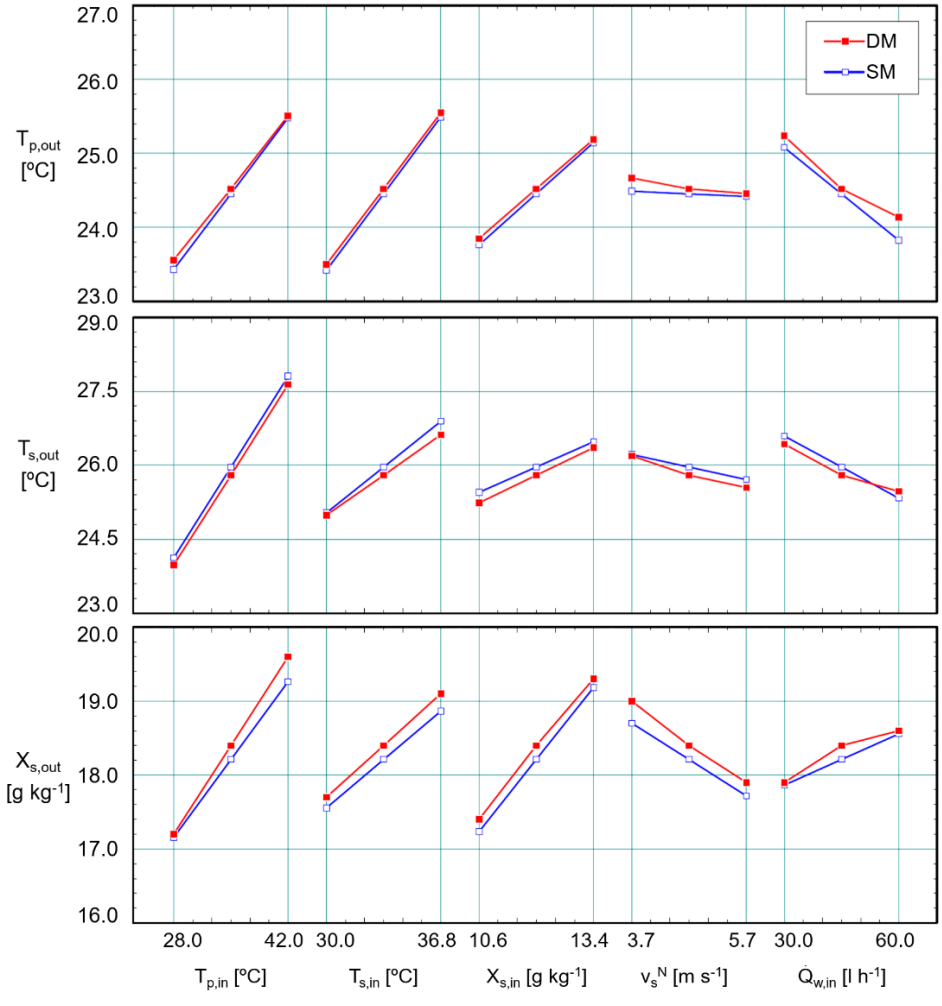

Fig. 5. Effect of inlet conditions on outputs of the simplified and detailed models. Reference inlet conditions: $T_{p,in}$=35.0 °C, $T_{s,in}$=33.4, $X_{s,in}$=12.0 g kg^{-1}, v_s^N = 4.7 m s-1, v_p^N = 3.7 m s^{-1}and $\dot{Q}_{w,in}$= 45 l h^{-1}

Table 6. RMSD values and MD for the three case studies.

Case study	ΔT_p				ΔT_s				ΔX_s				ε_{wb}			
	RMSD [°C]		MD [%]		RMSD [°C]		MD [%]		RMSD [g kg^{-1}]		MD [%]		RMSD [-]		MD [%]	
	DM	SM	DM	SM	DM	SM	DM	SM	DM	SM	DM	SM	DM	SM	DM	SM
A	0.18	0.29	0.85	1.66	0.34	0.39	1.56	1.76	0.18	0.13	1.21	0.90	0.01	0.02	1.85	3.40
B	0.38	0.74	2.36	3.43	0.56	0.83	2.98	4.08	0.62	0.42	4.02	3.13	0.01	0.02	2.05	2.96
C	0.12	0.06	0.68	0.47	0.26	0.33	1.69	1.80	0.24	0.25	1.92	1.85	0.01	0.01	1.93	1.33

It is highlighted that in all cases, the higher $\dot{Q}_{w,in}$, the higher ΔT_p, ΔT_s, ΔX_s and ε_{wb}. Previous studies showed similar trends in these four parameters when the water flow rate of IEC is varied [12]. In case 1, the maximum values of ΔT_p, ΔT_s, ΔX_s and ε_{wb} obtained are 11.55 ºC, 4.01 ºC, 5.24 g kg^{-1} and 0.85, respectively, while the minimum values are 10.85 ºC, 3.60 ºC, 5.04 g kg^{-1} and 0.78. It can be observed that, the in the investigated range, output values don't depend strongly on $\dot{Q}_{w,in}$.

Finally, in Fig. 6 it is shown that numerical results are in very good agreement with experimental data. The results of both models are always within or close to the experimental uncertainty of the measured data, except at high water flow rate for the simplified model. The maximum deviations of εwb is very small and equal to 1.85% and 3.40% respectively for DM and SM.

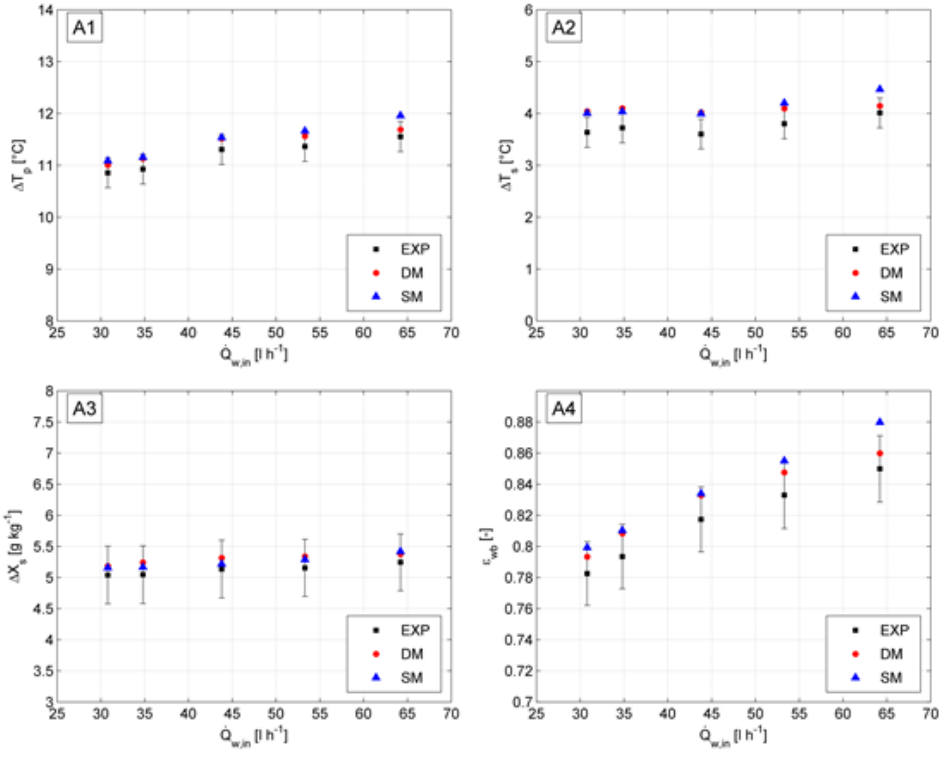

Fig. 6. Experimental and simulation results of ΔT_p, ΔT_s, ΔX_s and ε_{wb} as a function of $\dot{Q}_{w,in}$ for case study A.

Regarding case study B, the trends of outputs as a function of $\dot{Q}_{w,in}$ reported in Fig. 7 are similar those of case study A. However, negative values of ΔT_s have been experienced because the inlet primary air temperature is significantly hotter than the secondary air one. As a consequence, measured ΔT_p increased significantly, reaching 33.66 ºC at the maximum water flow rate, with a wet bulb effectiveness of 84%. Fig. 7 also shows that the models correctly predicted the behaviour of the IEC, although its operating conditions are far from the models calibration range. In this case study the highest values of RMSD and MD of ΔT_p, ΔT_s and ε_{wb} have been calculated for the simplified model and of ΔX_s for the detailed model. Nevertheless, the values of MD are always below 5% for both models.

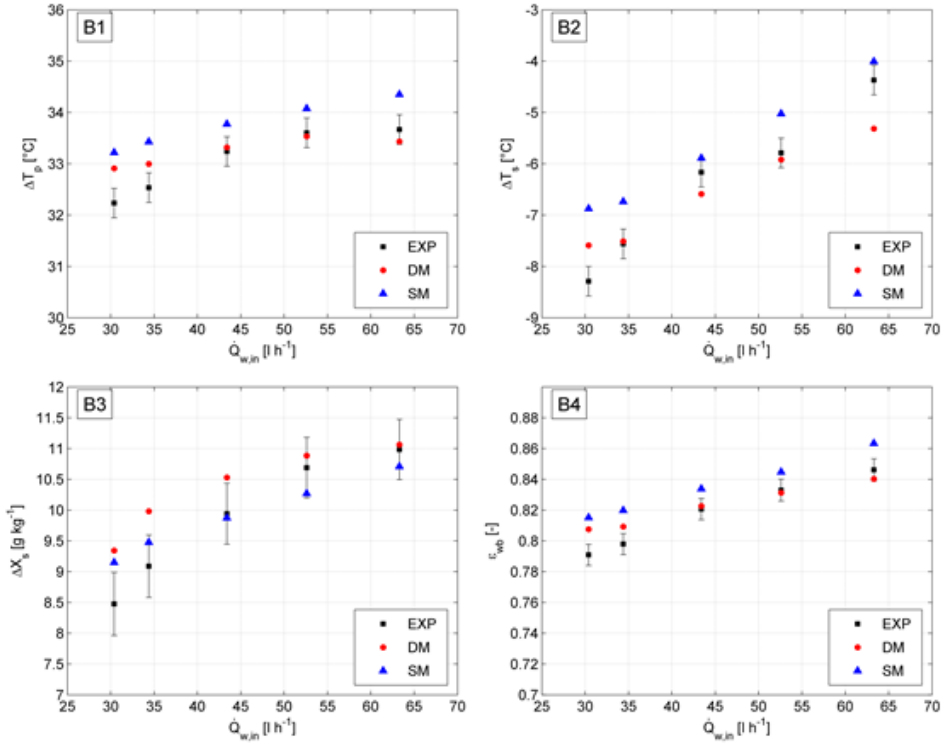

Fig. 7. Experimental and simulation results of ΔT_p, ΔT_s, ΔX_s and ε_{wb} as a function of $\dot{Q}_{w,in}$ for case study B.

Case study C has been carried out in typical residential conditions. Results show similar trends of case study A and B: the higher $\dot{Q}_{w,in}$, the higher the ΔT_p, ΔT_s, ΔX_s and ε_{wb}, as reported in Fig. 8. Also, this case study, the numerical results are in very good agreement with experimental data. The values of MD are always below 2% for the four parameters, highlighting that both models are particularly suitable to accurately predict the behaviour of the IEC.

5 Conclusions

In this work, a simplified IEC model, based on a first order linear regression approach, has been developed. This model can be used to predict the influence of $T_{p,in}$, $T_{s,in}$, $X_{s,in}$, v_p^N and $\dot{Q}_{w,in}$, on the output variables $T_{p,out}$, $T_{s,out}$ and $X_{s,out}$, in the IEC. The model effectively correlates experimental data: R^2 values, obtained considering all the 37 adopted tests, are 99.54 % for $T_{p,out}$, 99.78 % for $T_{s,out}$ and 99.89 % for $X_{s,out}$.

The simplified model (SM) has been compared with results of a detailed one (DM) and with further experimental data. Three cases studies have investigated in order to analyse the IEC system and compare the accuracy of both models. Each case study deals with typical air conditions of actual IEC applications. Numerical results of both models are in agreement with experimental data in all the case studies: the maximum deviations are obtained for the case study 2, whose inlet conditions are outside the calibration range of the two models. Nevertheless, deviations of wet bulb effectiveness are always below 2.05 % for the detailed model and 3.40% for the simplified model.

Finally, it is possible to state that the simplified IEC model can be effectively integrated in energy simulation tools, due to its low computational load and good accuracy. Instead, the detailed model is suitable to design and optimize indirect evaporative coolers, being more accurate than SM and based on a phenomenological approach.

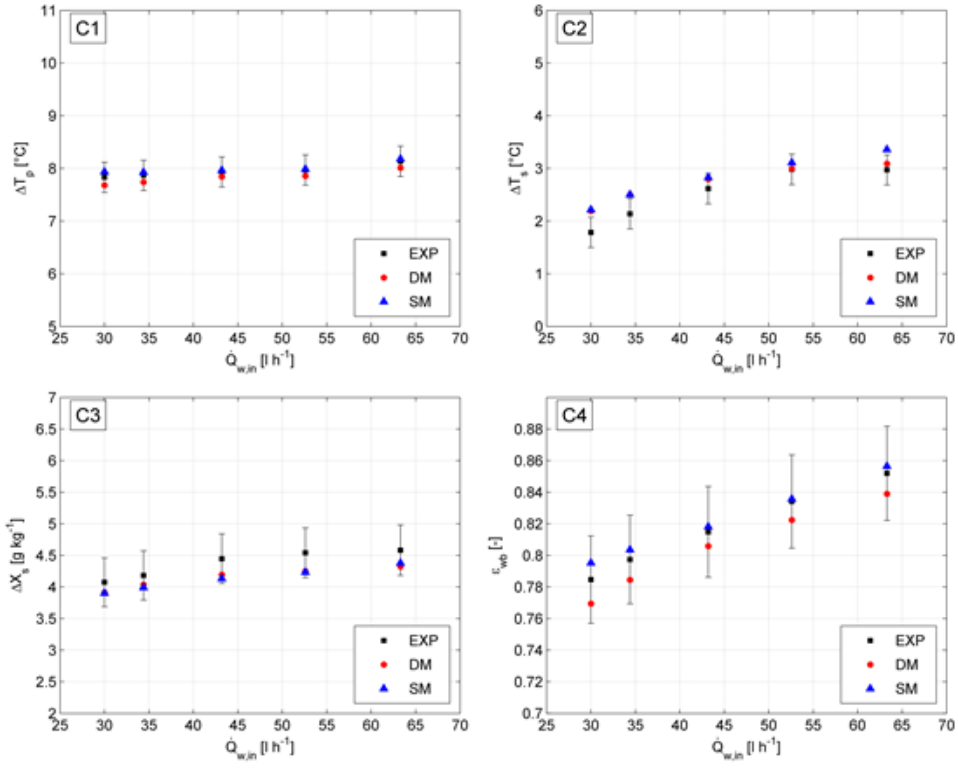

Fig. 8. Experimental and simulation results of ΔT_p, ΔT_s, ΔX_s and ε_{wb} as a function of $\dot{Q}_{w,in}$ for case study C.

Acknowledgements

The authors would like to acknowledge Mr Leone, Mr Bawa and Mr Liberati of Recuperator S.p.A. for their economical and technical support.

References

[1] Z. Duan, C. Zhan, X. Zhang, M. Mustafa, X. Zhao, B. Alimohammadisagvand, et al., Indirect evaporative cooling: Past, present and future potentials, Renew. Sustain. Energy Rev. 16 (2012) 6823–6850. doi:10.1016/j.rser.2012.07.007.

[2] S. Delfani, J. Esmaeelian, H. Pasdarshahri, M. Karami, Energy saving potential of an indirect evaporative cooler as a pre-cooling unit for mechanical cooling systems in Iran, Energy Build. 42 (2010) 2169–2176. doi:10.1016/j.enbuild.2010.07.009.

[3] Y. Chen, Y. Luo, H. Yang, Fresh air pre-cooling and energy recovery by using indirect evaporative cooling in hot and humid region - A case study in Hong Kong, Energy Procedia. 61 (2014) 126–130. doi:10.1016/j.egypro.2014.11.922.

[4] X. Cui, K.J. Chua, M.R. Islam, K.C. Ng, Performance evaluation of an indirect pre-cooling evaporative heat exchanger operating in hot and humid climate, Energy Convers. Manag. 102 (2015) 140–150. doi:10.1016/j.enconman.2015.02.025.

[5] G. Heidarinejad, M. Bozorgmehr, S. Delfani, J. Esmaeelian, Experimental investigation of two-stage indirect/direct evaporative cooling system in various climatic conditions, Build. Environ. 44 (2009) 2073–2079. doi:10.1016/j.buildenv.2009.02.017.

[6] E. González Cruz, E. Krüger, Evaluating the potential of an indirect evaporative passive cooling system for Brazilian dwellings, Build. Environ. 87 (2015) 265–273. doi:10.1016/j.buildenv.2015.01.020.

[7] D. Pandelidis, S. Anisimov, W.M. Worek, P. Drag, Comparison of desiccant air conditioning systems with different indirect evaporative air coolers, Energy Convers. Manag. 117 (2016) 375–392. doi:10.1016/j.enconman.2016.02.085.

[8] A. Agrawal, M. Khichar, S. Jain, Transient simulation of wet cooling strategies for a data center in worldwide climate zones, Energy Build. 127 (2016) 352–359. doi:10.1016/j.enbuild.2016.06.011.

[9] E. Velasco Gómez, A. Tejero González, F.J. Rey Martínez, Experimental characterisation of an indirect evaporative cooling prototype in two operating modes, Appl.

Energy. 97 (2012) 340–346. doi:10.1016/j.apenergy.2011.12.065.

[10] A. Ahmad, S. Rehman, L.M. Al-Hadhrami, Performance evaluation of an indirect evaporative cooler under controlled environmental conditions, Energy Build. 62 (2013) 278–285. doi:10.1016/j.enbuild.2013.03.013.

[11] A. Tejero-González, M. Andrés-Chicote, E. Velasco-Gómez, F.J. Rey-Martínez, Influence of constructive parameters on the performance of two indirect evaporative cooler prototypes, Appl. Therm. Eng. 51 (2013) 1017–1025. doi:10.1016/j.applthermaleng.2012.10.054.

[12] S. De Antonellis, C.M. Joppolo, P. Liberati, S. Milani, L. Molinaroli, Experimental analysis of a cross flow indirect evaporative cooling system, Energy Build. 121 (2016) 130–138. doi:10.1016/j.enbuild.2016.03.076.

[13] I.L. Maclaine-cross, P.J. Banks, A General Theory of Wet Surface Heat Exchangers and its Application to Regenerative Evaporative Cooling, J. Heat Transfer. 103 (1981) 579–585. http://dx.doi.org/10.1115/1.3244505.

[14] P.J. Erens, A.A. Dreyer, Modelling of indirect evaporative air coolers, Int. J. Heat Mass Transf. 36 (1993) 17–26. doi:10.1016/0017-9310(93)80062-Y.

[15] M. Poppe, H. Rögener, Evaporative cooling systems, VDI-Warmeatlas, Sect. Mh. (1984).

[16] F. Merkel, Verdunstungskühlung, VDI-Zeitchrift. (1925) 123–8.

[17] M.H. Kim, J.H. Kim, A.S. Choi, J.W. Jeong, Experimental study on the heat exchange effectiveness of a dry coil indirect evaporation cooler under various operating conditions, Energy. 36 (2011) 6479–6489. doi:10.1016/j.energy.2011.09.018.

[18] C. Ren, H. Yang, An analytical model for the heat and mass transfer processes in indirect evaporative cooling with parallel/counter flow configurations, Int. J. Heat Mass Transf. 49 (2006) 617–627. doi:10.1016/j.ijheatmasstransfer.2005.08.019.

[19] A. Hasan, Going below the wet-bulb temperature by indirect evaporative cooling: Analysis using a modified ε-NTU method, Appl. Energy. 89 (2012) 237–245. doi:10.1016/j.apenergy.2011.07.005.

[20] X.C. Guo, T.S. Zhao, A parametric study of an indirect evaporative air cooler, Int. Commun. Heat Mass Transf. 25 (1998) 217–226. doi:10.1016/S0735-1933(98)00008-6.

[21] H.D.M. Hettiarachchi, M. Golubovic, W.M. Worek, The effect of longitudinal heat conduction in cross flow indirect evaporative air coolers, Appl. Therm. Eng. 27 (2007) 1841–1848. doi:10.1016/j.applthermaleng.2007.01.014.

[22] X. Cui, K.J. Chua, W.M. Yang, Numerical simulation of a novel energy-efficient dew-point evaporative air cooler, Appl. Energy. 136 (2014) 979–988. doi:10.1016/j.apenergy.2014.04.040.

[23] S. De Antonellis, C.M. Joppolo, P. Liberati, S. Milani, F. Romano, Modeling and experimental study of an indirect evaporative cooler, Energy Build. 142 (2017) 147–157. doi:10.1016/j.enbuild.2017.02.057.

[24] D.C. Montgomery, Design and analysis of experiments, 6th Edition, Wiley, 2004.

[25] D. Pandelidis, S. Anisimov, Application of a statistical design for analyzing basic performance characteristics of the cross-flow Maisotsenko cycle heat exchanger, Int. J. Heat Mass Transf. 95 (2016) 45–61. doi:10.1016/j.ijheatmasstransfer.2015.11.060.

[26] A. Sohani, H. Sayyaadi, S. Hoseinpoori, Modeling and multi-objective optimization of an M-cycle cross-flow indirect evaporative cooler using the GMDH type neural network, Int. J. Refrig. 69 (2016) 186–204. doi:10.1016/j.ijrefrig.2016.05.011.

[27] DIN EN ISO 5167-2 Standards, Measurement of a fluid flow by means of pressure differential devices inserted in circular cross-section conduits running full - Part 2: Orifice plates (ISO 5167-2:2003).

[28] R.J. Moffat, Describing the uncertainties in experimental results, Exp. Therm. Fluid Sci. 1 (1988) 3–17. doi:10.1016/0894-1777(88)90043.

[29] ISO, Evaluation of measurement data — Guide to the expression of uncertainty in measurement, Int. Organ. Stand. Geneva ISBN. 50 (2008) 134. doi:10.1373/clinchem.2003.030528.

[30] P. Liberati, S. De Antonellis, C. Leone, C. M. Joppolo, Y. Bawa, Indirect evaporative cooling systems: modelling and performance analysis, Energy Procedia, accepted for pubblication.

[31] Statgraphics Centurion XV, (2006). available from http://www.statgraphics.com/ (accessed 13.06.17).

Appendix D

Energy saving potential of a hybrid HVAC system with a desiccant wheel activated at low temperatures and an indirect evaporative cooler in buildings with high latent load

The paper presented in this appendix has been submitted for *Applied Thermal Engineering* (July 2017)

Energy saving potential of a hybrid HVAC system with a desiccant wheel activated at low temperatures and an indirect evaporative cooler in handling air in buildings with high latent loads

Authors: F. Comino*, M. Ruiz de Adana, F. Peci

Departamento de Química-Física y Termodinámica Aplicada, Escuela Politécnica Superior, Universidad de Córdoba, Campus de Rabanales, Antigua Carretera Nacional IV, km 396, 14071 Córdoba, España

*Corresponding author tel. +34 626285994; e-mail: francisco.comino@uco.es (F. Comino)

Abstract

Air handling in buildings with high latent loads usually requires a high-energy cost to satisfy the user's thermal comfort needs. Hybrid systems composed of desiccant wheels, DW, and indirect evaporative coolers, IEC, could be an alternative to direct expansion conventional systems, DX systems. The main objective of this work was to determine the annual energy consumption of a hybrid system with a DW activated at low temperatures and an IEC, DW-IEC system, compared to a DX system to serve air in a small building with high latent loads, such as spas. Several annual energy simulations for 6 climate zones were performed, analysing electric energy consumption, seasonal mean coefficient of performance, SCOP, and energy consumption per unit of dehumidified water, E_{cons}, of each system. The simulations were based on experimentally validated models.

The annual energy consumption of the DW-IEC system was lower than that of the DX system for the 6 climate zones, achieving significant energy savings, up to 46.8%. These energy savings resulted in better SCOP values for the DW-IEC system. Therefore, the proposed DW-IEC system has high potential to reduce energy costs, achieving the user's thermal comfort.

Keywords: hybrid system; desiccant wheel; indirect evaporative cooler; high latent loads; climate zones

1 Introduction

Air handling in buildings with high latent loads usually requires a high-energy cost to satisfy the user's thermal comfort needs. Indoor swimming pools or spas are some examples of this type of buildings, which have high internal latent gains, due to the great amount of evaporated water from the wet areas [1]. Excessive air humidity can cause discomfort for the occupants and problems related to the indoor air quality of the building due to fungus and rot [2]. Therefore, an air handling system is required to control the indoor moisture content, while keeping a low energy consumption.

A traditional method of dehumidifying rooms with high latent loads is to introduce a certain air flow rate from outside, this method can only be used when the outdoor humidity ratio is lower than the indoor humidity. In this method [3], the air flow rate required to dehumidify the building was very high. The recommended air change rates per hour, ACH, values were shown to vary between 4 h-1 and 7 h-1 in order to obtain thermal comfort [3]. This dehumidification method could cause discomfort to the occupants in small rooms with high latent loads, such as spas, due to the high ACH values.

Another method widely used in dehumidifying air is that of conventional dehumidification systems based on direct expansion units, DX system, which operates according to the vapor-compression cycle. DX systems reduce the air temperature below its dew point in order to condense water. An increase in the cooling power of the DX system usually produces an increase in its desiccant capacity. However, DX systems have a cooling capacity limit when the required dew-point temperature is very low, close to 0 °C, the freezing point of water. Moreover, the outlet air temperature of DX systems is usually very low, so it is necessary a post-heating of air flow, before being supplied to the building. Several DX systems have been studied for indoor swimming pools [4,5], where high energy consumption values were required to dehumidify and heat the air steam. A comparative study between a DX system and an open absorption system to handle air in an indoor swimming pool, was carried out by other authors [6], obtaining significant energy savings with the open absorption system. These studies show the need to search for new HVAC systems in buildings with high latent loads.

Previous studies on energy saving in spas with small volumes and high latent loads have been carried out [7–9]. However, these works focused on the hot water system of swimming pools.

Nomenclature

ACH	air change rates per hour [h^{-1}]
b	estimated parameter
C	capacity rate of air [kJ h^{-1} K^{-1}]
c_p	specific heat of air [kJ kg^{-1} K^{-1}]
CDD	cooling degree-day [ºC]
CO	condenser
COP	coefficient of performance
DEC	direct evaporative cooler
DOE	design of experiments
DW	desiccant wheel
DX	direct expansion
EA	exhaust air
E_{cons}	energy consumption per unit of dehumidified water [Wh kg^{-1}]
EIR	electrical input ratio
EV	evaporator
F	centrifugal fan
IEC	indirect evaporative cooler
h	air specific enthalpy [kJ kg^{-1}]
HDD	heating degree-day [ºC]
HC	heating coil
HR	relative humidity [%]
k	number of parameters
MRC	moisture removal capacity [kg h^{-1}]
$\dot{m}$	mass air flow rate [kg h^{-1}]
$\dot{M}_{pool}$	evaporated water flow of the pool [kg h^{-1}]
Np	number of people
OA	outdoor air
PLF	partial load factor
P	static pressure [mmca]
$\dot{Q}$	heat transfer [kW]
RA	return air
S	area [m^2]
SCOP	seasonal mean coefficient of performance
SHE	sensible heat exchanger
T	dry bulb temperature [ºC]
T_{wb}	wet bulb temperature [ºC]
UA	overall heat transfer coefficient [kJ h^{-1} K^{-1}]
v	air velocity [m s^{-1}]
$\dot{V}$	volumetric air flow rate [m^3 h^{-1}]
$\dot{V}_w$	water flow rate of indirect evaporative cooler [l h^{-1}]
$\dot{W}$	electric power consumption [kW]
X	input variable
$\hat{Y}$	estimated output value
Greek letters	
Δ	increase
ε	effectiveness
ρ	density [kg m^{-3}]
∑	sum
ω	humidity ratio [g kg^{-1}]
Ω	specific mass air flow rate [kg s^{-1} m^{-3}]
Subscripts	
a	air
c	condenser
e	evaporator
HC	heating coil
i	inlet
IA	indoor air

lat	latent
N	nominal
PLF	partial load factor
o	outlet
OA	outdoor air
p	process air; primary air
s	secondary air
r	regeneration air
sen	sensible
t	total
T	temperature
w	water
Superscripts	
'	dimensionless value

Desiccant dehumidification systems present an alternative solution to DX systems. Desiccant dehumidification systems adsorb water from the air in contact with an area of low vapour pressure at the surface of the desiccant [10]. One type of desiccant dehumidification system widely used is the desiccant wheel, DW, [11,12]. The most influential parameter on the desiccant capacity of a DW is the regeneration temperature [13,14]. Usually, DWs are thermally activated at high temperatures, from 60 ºC to 120 ºC [15,16], although other studies also showed acceptable DW performance when their regeneration temperatures were below 60 ºC [17]. The main disadvantage of DWs is the high outlet process air temperatures [18]. This heat is generated by the adsorption process of the DW, which is delivered from the regeneration section to the process section. Therefore, a cooling system is needed to lower the process air temperature before being supplied.

Cooling systems based on evaporators of a DX system are usually combined with a DW [19,20], but these systems normally require a high energy consumption [21]. Another cooling system that is usually combined with DWs is the evaporative cooler. There are two types: the direct evaporative cooler, DEC, and the indirect evaporative cooler, IEC. The IEC system is one of the most promising technologies in reducing the air temperature because of its higher energy saving capacity compared to DX systems [22]. The IEC system requires two separate air flows to operate. The primary air flow which is cooled and supplied to the building without increasing its humidity ratio and the secondary air flow which is humidified with water supplied to the outside [23].

Many studies about IEC integrated into a desiccant system have been carried out [24–26]. An experimental study on a hybrid system composed of a DW and an IEC was carried out for several summer days in Italy [27]. This system reduced the electrical consumption significantly compared to one composed of a DW and two cooling coils fed by a conventional vapour compression chiller. A numerical simulation study on desiccant units presented a comparative analysis of three different systems with a DW and an IEC [28]. The results of this study indicated that all of them were able to obtain satisfactory supply air temperatures, even when the DW was regenerated at low temperature. Other numerical studies analysed the behaviour of a DW combined with an IEC system [29–32]. They were mainly based on the hybrid system performance optimization under different steady state air conditions, always using the IEC system to cool the output air stream of the DW. After analysing the results of the previous studies, it would be interesting to know the energy saving potential and the annual behaviour of a hybrid system with a DW and an IEC in handling air in buildings with high latent loads and low supply air flow rates, such as spas.

The main objective of this work was to determine the annual energy consumption of a hybrid HVAC system composed of a DW activated at low temperatures and an IEC, compared to a DX system composed of a direct expansion unit for a small building with high latent loads. Hence, several annual energy simulations for different climate zones were carried out. Electric energy consumption, $W^{'}$, seasonal mean coefficient of performance, SCOP, and energy consumption per unit of dehumidified water, Econs, of each system were analysed.

2 Methodology

2.1 System description

A criterion commonly used by manufacturers to select dehumidification units, is their moisture removal capacity, MRC [5]. In this study, this criterion was used. The same nominal MRC value for both systems was considered, 15.2 kg h^{-1}. The selected DX system was specifically designed to maintain indoor conditions in swimming pools and other high latent loads buildings, such as spas [33]. Both systems studied were not equipped with any humidifier element, since they were designed to handle very humid indoor air.

2.1.1 DX system

A numerical model of a DX system was created in order to compare its operational behaviour with the proposed DW-IEC system. The DX system was composed of an air-mixing box, a vapor-compression cycle and a heating coil, HC, see Fig. 1. The HC was fed by a constant water flow, which was heated using an air-water heat pump. The evaporator, EV, and the condenser, CO, of the vapor-compression cycle were installed in a parallel arrangement.

Air handling by the DX system is described below. Firstly, the outdoor air stream was mixed with the return air stream. Secondly, the mixed air stream was dehumidified and cooled by the evaporator, EV. Finally, the air stream was heated by the HC until the supply air temperature equalled the set point temperature. The supply air humidity ratio was controlled with the EV and the supply air temperature was controlled with the HC. The outdoor air flow rate of this system was 1600 m^3 h^{-1}, and the total air flow rate handled and supplied by the DX system was 3680 m^3 h^{-1}. The condenser, CO, of the direct expansion refrigeration unit handled 100% outdoor air, 3680 m^3 h^{-1}.

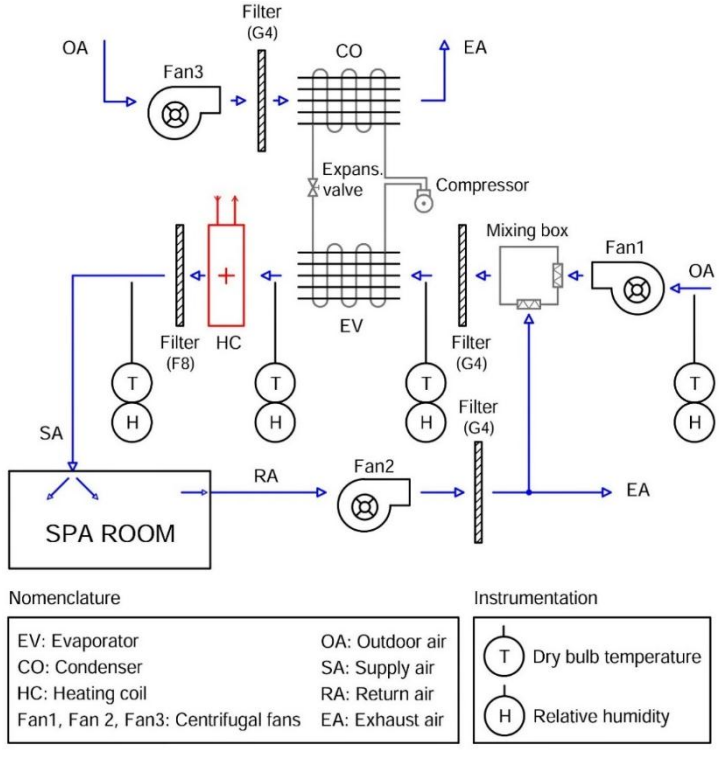

Fig. 1. Schematic of the DX system.

2.1.2 DW-IEC system

An alternative DW-IEC system was proposed in this piece of work in order to maintain the required indoor conditions in buildings with high latent loads. A schematic of the DW-IEC system is shown in Fig. 2. It is composed of a DW to handle latent heat loads in the room, and an IEC and a heating coil, HC2, to handle sensible heat loads. The DW was activated by means of a heating coil, HC1. Alternatively, the IEC was used as a sensible heat exchanger, SHE, recovering sensible heat from the return air stream, when it was necessary to heat the process air stream. In addition, two air boxes were integrated into the system to increase the desiccant and cooling capacity of the DW and the IEC, respectively. Both boxes have two air inlet dampers and one outlet. Depending on outdoor air conditions, the exhaust air stream is the outside, OA, air or return air, RA, as shown in Fig. 2. A constant air flow rate of 1600 $m^3 h^{-1}$ was considered for the three air streams. The outdoor air flow rate of this system was equal to that of the DX system. Furthermore, this study was performed for relatively low regeneration air temperatures (40–60 ºC), which can be obtained using a commercial heat pump.

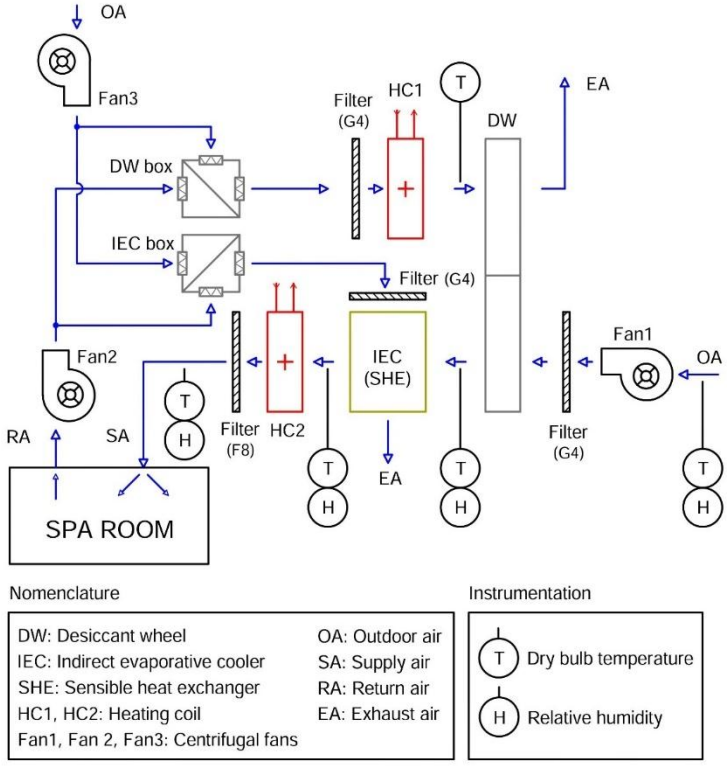

Fig. 2. Schematic of the DW-IEC system.

2.1.2.1 System operation modes

Two independent main control loops were considered in the DW-IEC system. The first one was an indoor air humidity control loop and the second one an indoor air temperature control loop. A diagram of the control logic of the DW-IEC system is represented in Fig. 3. The air humidity control loop was divided into two specific modes of operation, Mode 1-H and 2-H. This loop modulated the water flow rate of the regeneration heating coil, HC1, activated the rotation of the DW and set the position of the dampers in the DW and IEC boxes. The air temperature control loop was divided into three specific modes of operation, Mode 1-T, 2-T and 3-T. This loop modulated the water flow rate of the IEC and the post-heating coil, HC2. These modes of operation are described below.

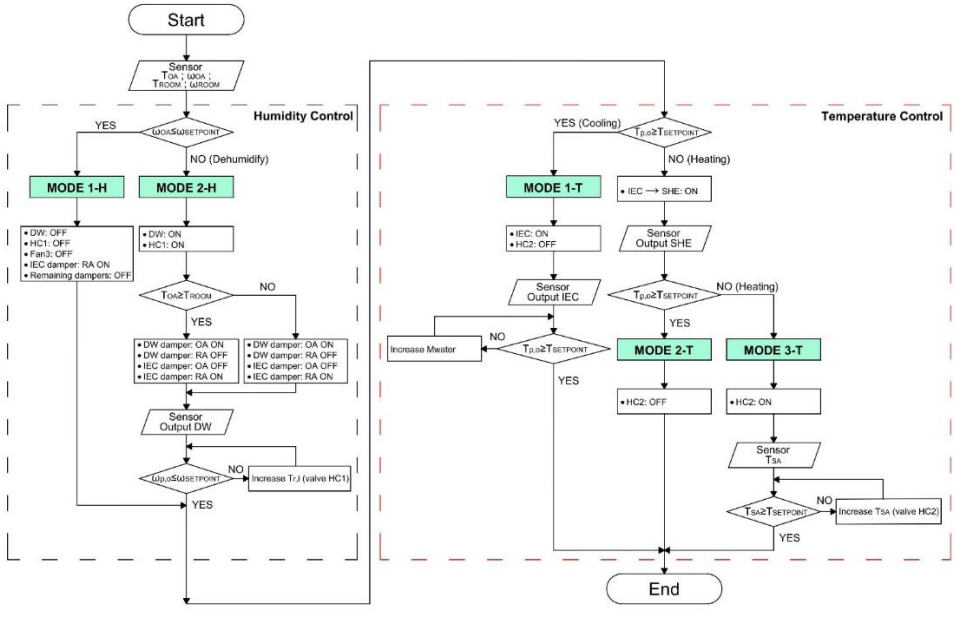

Fig. 3. DW-IEC system control logic diagram.

- **Air humidity control**

The operating mode of the selected humidity control was based on the outdoor air humidity ratio, ω_{OA}. The DW-IEC system did not dehumidify when the outdoor air humidity was lower than the set point air humidity. Mode 1-H was activated, see Fig. 2 and Fig. 3. For this operating mode, the DW, HC1 and Fan3 elements were disabled, and as a result the supply air humidity ratio was equal to the outdoor air humidity ratio. On the contrary, the DW-IEC system dehumidified when the outdoor air humidity was higher than the set point air humidity, and Mode 2-H was activated. For this control mode, the system dehumidified the outdoor air until the outlet process air humidity ratio of the DW, $\omega_{p,o,}$ was equal to or lower than the set point humidity. The DW, HC1 and Fan3 elements were activated and the dampers of the two air boxes were set to the correct position, see Fig. 2 and Fig. 3. The outdoor air, OA, passed through DW damper and the return air, RA, passed through IEC damper when the outdoor air temperature was higher than the set point air temperature. On the contrary, the outdoor air, OA, passed through IEC damper and the return air, RA, passed through DW damper.

- **Air temperature control**

The operating mode of the selected temperature control was based on the DW outlet process air temperature, $T_{p,o}$. Mode 1-T was activated when $T_{p,o}$ was higher than the set point air temperature, see Fig. 2 and Fig. 3. The IEC system was activated until the set point temperature of the process air steam was achieved. The process air stream was heated when $T_{p,o}$ of the DW was lower than the set point air temperature. The outlet process air stream of the DW can be heated by the sensible heat exchanger, SHE. The IEC was only used as SHE when the rotation of the DW was disabled and the secondary air stream was return air. In this situation, no water was evaporated in the SHE. Then, the air temperature was measured again at the output of the IEC unit, see Fig. 2 and Fig. 3. The primary air stream of the IEC was supplied to the building when $T_{p,o}$ was higher than the set point air temperature, and the HC2 was off, Mode 2-T. However, HC2 was activated when $T_{p,o}$ was lower than the set point air temperature and the air stream was heated until the supply air temperature was equal to the set point temperature, Mode 3-T.

2.2 Building model – Spa

Both HVAC systems were designed to serve air in a building with high latent loads. A building model was designed to simulate the thermal behaviour of a spa.

This was modelled and simulated using TRNSYS package tool [34]. The building consisted of a single surface of 64 m^2 and a height of 3.9 m, where a wall, south orientation, and the roof were exterior. The characteristics of the building are summarized in Table 1.

The building was composed of a swimming pool of 32 m^2 and a daily maximum number of 8 people in the pool. The evaporated water flow rate from the pool was calculated using Eq. (1), according to that established in [5]. Other internal energy gains due to people and lighting were considered, as shown in Table 1.

$$\dot{M}_{pool} = S \cdot \left(16 + 133 \cdot \frac{Np}{S}\right) \cdot (\omega_w - \omega_{IA}) + 0{,}1 \cdot Np \quad (1)$$

Table 1. Characteristics of the building.

Building	Floor area	64 m^2
	Height	3.9 m
	Exterior wall area	31.2 m^2
	Exterior roof area	64 m^2
	Indoor air temperature	27 ºC
	Indoor relative humidity	60 %
Pool	Area	32 m^2
	Water temperature	25 ºC
U-value	Exterior wall	0.339 W m^{-2} K^{-1}
	Roof	0.313 W m^{-2} K^{-1}
Heat gain	Pool	Latent: 6662 W ($\dot{M}_{pool}$=9.6 kg h^{-1})
	Lighting	55 W m^{-2} (50 % convective part)
	People	8 persons Sensible: 75 W/person Latent: 75 W/person
Daily schedule	09:00 am to 24:00 pm	

where S is the pool area, ω_w is the saturated air humidity ratio at the pool water temperature, ω_{IA} is the indoor air humidity ratio and Np is the number of people.

Based on the Spanish regulations on thermal installations in buildings [35], the indoor air temperature set for swimming pools should be between 1 and 2 ºC above the pool water temperature, with a maximum of 30 ºC, and the indoor relative humidity should be maintained below 65 %. In this paper, the indoor conditions were set at 27 ºC for the air temperature and 60 % for the relative humidity. The building was simulated for a daily operating schedule from 09:00 am to 24:00 pm.

2.3 Components modelling

The components that compose the proposed DW-IEC system and the DX system, were modelled as described below. Each of the component models was combined and integrated into TRNSYS [34]. The models of the DW, the IEC, the refrigeration vapour compression unit, the heat pump and the fans were validated experimentally. These models were fitted by first, second and third order polynomial equations, expressed by Eqs. (2)-(4), respectively, where $\hat{Y}$ is the estimated output value, X are input variables, b_i, b_{ii}, b_{iii} and b_{ij} are the estimated parameters of linear, quadratic, cubic and the second-order terms, respectively, and b_0 is the average response in the model.

$$\hat{Y} = b_0 + \sum_{i=1}^{k} b_i \cdot X_i + \sum_{i=1}^{k=1} \sum_{\substack{i=2 \\ j>i}}^{k} b_{ij} \cdot X_i \cdot X_j \quad (2)$$

$$\hat{Y} = b_0 + \sum_{i=1}^{k} b_i \cdot X_i + \sum_{i=1}^{k} b_{ii} \cdot X_i^2 + \sum_{i=1}^{k=1} \sum_{\substack{i=2 \\ j>i}}^{k} b_{ij} \cdot X_i \cdot X_j \quad (3)$$

$$\hat{Y} = b_0 + \sum_{i=1}^{k} b_i \cdot X_i + \sum_{i=1}^{k} b_{ii} \cdot X_i^2 + \sum_{i=1}^{k=1} b_{iii} \cdot X_i^3 \quad (4)$$

2.3.1 Desiccant wheel model

The desiccant wheel model behaviour was studied in a previous paper [17]. This model was based on the statistical technique of design of experiments, DOE. The model was adjusted to obtain the outlet process air temperature and humidity ratio in the DW, $T_{p,o}$ and $\omega_{p,o}$, especially for low regeneration temperature activated systems. The input variables of the model

were the inlet process air temperature and humidity ratio, $T_{p,i}$ and $\omega_{p,i}$, the inlet regeneration air temperature and humidity ratio, $T_{r,i}$ and $\omega_{r,i}$, and the process specific mass air flow rate, $\Omega_{p,i}$. In this study, the process and regeneration specific mass air flow rates were always maintained constant, 21.51 kg s^{-1} m^{-3}. The relationship between the output and input variables was examined using second order polynomial equations, expressed by Eq. (3). The corresponding estimated parameters of the DW model are shown in Table 2.

Table 2. Estimated parameters of the DW empirical model.

b_x	X_i	$T_{p,o}x10^3$ [ºC]	$\omega_{p,o}10^3$ [g kg^{-1}]	b_x	X_i	$T_{p,o}x10^3$ [ºC]	$\omega_{p,o}x10^3$ [g kg^{-1}]
b_0	-	-6736.67	-15366.80	b_{11}	$\omega_{p,i}^2$	-17.23	16.76
b_1	$T_{p,i}$	72.10	1277.57	b_{12}	$\omega_{p,i}\cdot T_{r,i}$	-1.49	-2.23
b_2	$\omega_{p,i}$	772.28	-785.18	b_{13}	$\omega_{p,i}\cdot\omega_{r,i}$	5.65	16.84
b_3	$T_{r,i}$	410.38	1310.33	b_{14}	$\omega_{p,i}\cdot\Omega_{p,i}$	20.50	-6.79
b_4	$\omega_{r,i}$	224.17	-916.88	b_{15}	$T_{r,i}^2$	-5.09	-11.90
b_5	$\Omega_{p,i}$	357.36	-94.71	b_{16}	$T_{r,i}\cdot\omega_{r,i}$	7.31	-10.40
b_6	$T_{p,i}^2$	16.58	-28.38	b_{17}	$T_{r,i}\cdot\Omega_{p,i}$	6.71	-3.50
b_7	$T_{p,i}\cdot\omega_{p,i}$	-14.35	29.84	b_{18}	$\omega_{r,i}^2$	-9.72	24.41
b_8	$T_{p,i}\cdot T_{r,i}$	7.35	-10.61	b_{19}	$\omega_{r,i}\cdot\Omega_{p,i}$	-5.49	11.88
b_9	$T_{p,i}\cdot\omega_{r,i}$	-12.93	6.35	b_{20}	$\Omega_{p,i}^2$	-12.17	-9.44
b_{10}	$T_{p,i}\cdot\Omega_{p,i}$	-8.71	5.89	-	-	-	-

2.3.2 Indirect evaporative cooler model

The model used to study the behaviour of the IEC was studied in a previous paper [36] and was based on the DOE technique, as well as the model used for the DW. The IEC empirical model was able to accurately predict the outlet primary air temperature, $T_{p,o}$, the outlet secondary air temperature, $T_{s,o}$, and the outlet secondary air humidity ratio of the system, $\omega_{s,o}$, under different operating conditions. The input variables were the inlet primary air temperature, $T_{p,i}$, the inlet secondary air temperature, $T_{s,i}$, the inlet secondary air humidity ratio, $\omega_{s,i}$, the secondary air velocity, v_s, and the water flow rate, $\dot{V}_w$. The relationship between the input and output variables was expressed by Eq. (2). The corresponding estimated parameters of the IEC model are shown in Table 3.

Table 3. Estimated parameters of the IEC empirical model.

b_x	X_i	$T_{p,o}x10^3$ [ºC]	$T_{s,o}x10^3$ [ºC]	$\omega_{s,o}x10^3$ [g kg^{-1}]	b_x	X_i	$T_{p,o}x10^3$ [ºC]	$T_{s,o}x10^3$ [ºC]	$\omega_{s,o}x10^3$ [g kg^{-1}]
b_0	-	-1313.76	3801.74	-379.62	b_8	$T_{p,i}\cdot v_s$	-15.66	-25.34	-35.06
b_1	$T_{p,i}$	322.41	500.49	183.23	b_9	$T_{p,i}\cdot\dot{V}_w$	-1.23	-2.02	1.12
b_2	$T_{s,i}$	364.07	191.57	135.71	b_{10}	$T_{s,i}\cdot\omega_{s,i}$	-8.45	-5.85	3.32
b_3	$\omega_{s,i}$	766.52	455.43	313.29	b_{11}	$T_{s,i}\cdot v_s$	26.11	42.55	-6.63
b_4	v_s	-467.09	-1199.63	755.41	b_{12}	$T_{s,i}\cdot\dot{V}_w$	-2.11	-1.54	0.92
b_5	$\dot{V}_w$	41.87	20.99	3.33	b_{13}	$\omega_{s,i}\cdot v_s$	12.58	19.45	33.91
b_6	$T_{p,i}\cdot T_{s,i}$	0.42	0.60	0.19	b_{14}	$\omega_{s,i}\cdot\dot{V}_w$	2.87	3.37	-2.39
b_7	$T_{p,i}\cdot\omega_{s,i}$	-5.09	-3.93	6.28	b_{15}	$v_s\cdot\dot{V}_w$	-0.94	3.94	-4.54

The IEC was used as a SHE when it was necessary to heat the process air stream and not to cool it, as was mentioned previously. For this reason, a cross flow sensible heat exchanger with both hot and cold sides unmixed, was modelled. The physical design characteristics of SHE were similar to those of the IEC [36]. The effectiveness of the SHE at each time step was calculated by Eq. (5), where UA is the overall heat

transfer coefficient of the exchanger, C_p is the capacity rate of air on primary side ($C_p = \dot{m}_p \cdot c_{p,p}$) and C_s is the capacity rate of air on secondary side ($C_s = \dot{m}_s \cdot c_{p,s}$). In this work, the effectiveness of the SHE was calculated for a fixed value of UA, given the inlet temperatures and air flow rates. The UA value of the cross-flow heat exchanger was measured experimentally for a wide range of input conditions, obtaining an average value of 1440 kJ h^{-1} K^{-1}.

$$\varepsilon = \frac{1 - \exp(-\frac{UA}{C_s} \cdot \left(1 + \frac{C_s}{C_p}\right))}{1 + \frac{C_s}{C_p}} \quad (5)$$

2.3.3 Refrigeration vapour compression model

The considered refrigeration vapour compression unit of the DX system was specially designed to dehumidify indoor swimming pools and other dehumidification applications. This unit was modelled using experimental data available from the manufacturer [33]. The unit works for balanced air flow rates in both coils, with a value of 3680 m^3 h^{-1}.

A simplified experimental model based on correlations was obtained to study its behaviour [37]. The relationship between the output and input variables was expressed by second order polynomial equations, as shown in Eq. (3). The input variables of this model were the inlet evaporator dry bulb air temperature, $T_{e,i}$, the inlet evaporator wet bulb air temperature, $T_{wb,e,i}$, the inlet condenser dry bulb air temperature, $T_{c,i}$, and the volumetric air flow rate ratio, $\dot{V}' = \dot{V}/\dot{V}_N$. The output variables were calculated using the following ratios: evaporator total heat transfer ratio $\dot{Q}'_{e,t} = \dot{Q}_{e,t}/\dot{Q}_{e,t,N}$; evaporator sensible heat transfer ratio $\dot{Q}'_{e,sen} = \dot{Q}_{e,sen}/\dot{Q}_{e,sen,N}$; condenser total heat transfer ratio $\dot{Q}'_{c,t} = \dot{Q}_{c,t}/\dot{Q}_{c,t,N}$; electric power consumption ratio $\dot{W}' = \dot{W}/\dot{W}_N$. Where $\dot{Q}_{e,t}$ is the evaporator total heat transfer, $\dot{Q}_{e,sen}$ is the evaporator sensible heat transfer, $\dot{Q}_{c,t}$ is the condenser total heat transfer and $\dot{W}$ is the electric power consumption of the compressor. The estimated parameters of the output variables are show n in Table 4. The nominal characteristics of the vapour compression system are summarized in Table 5.

Table 4. Estimated parameters of the refrigeration vapour compression model.

b_x	X_i	$\dot{Q}'_{e,t}$ x10^3	$\dot{Q}'_{e,sen}$ x10^3	$\dot{Q}'_{c,t}$ x10^3	$\dot{W}'$ x10^3	b_x	X_i	$\dot{Q}'_{e,t}$ x10^3	$\dot{Q}'_{e,sen}$ x10^3	$\dot{Q}'_{c,t}$ x10^3	$\dot{W}'$ x10^3
b_0	-	145.20	202.46	264.37	622.12	b_8	$\dot{V}'^2$	-185.21	-249.68	-89.82	221.34
b_1	$T_{e,i}$	-1.79	33.88	-1.70	-1.00	b_9	$T_{e,i}\cdot T_{c,i}$	0.08	-0.28	0.09	0.09
b_2	$T_{c,i}$	8.45	8.93	7.82	7.34	b_{10}	$T_{e,i}\cdot T_{wb,e,i}$	-0.65	2.32	-0.56	-0.29
b_3	$T_{wb,e,i}$	17.71	-35.46	16.36	11.82	b_{11}	$T_{e,i}\cdot \dot{V}'$	3.55	57.59	2.77	0.18
b_4	$\dot{V}'$	475.27	610.50	280.22	-345.74	b_{12}	$T_{c,i}\cdot T_{wb,e,i}$	-0.34	0.46	-0.23	0.14
b_5	$T_{e,i}^2$	0.20	-0.95	0.18	0.09	b_{13}	$T_{c,i}\cdot \dot{V}'$	-0.29	-2.39	-1.24	-4.92
b_6	$T_{c,i}^2$	-0.24	-0.29	-0.12	0.27	b_{14}	$T_{wb,e,i}\cdot \dot{V}'$	3.97	-49.65	0.17	-11.94
b_7	$T_{wb,e,i}^2$	0.75	-1.81	0.66	0.39	-	-	-	-	-	-

Table 5. Nominal parameters of the refrigeration vapour compression system.

Parameters	Value	
$\dot{Q}_{e,t,N}$	23.06	[kW]
$\dot{Q}_{e,sen,N}$	13.00	[kW]
$\dot{Q}_{c,t,N}$	30.32	[kW]
$\dot{W}_N$	7.53	[kW]
$\dot{V}_N$	4600	[m^3 h^{-1}]

2.3.4 Heating coil with heat pump model

The heating coils of both systems studied, Fig. 1 and Fig. 2, were fed by a constant water flow, which was heated by an air-water heat pump. The thermal power exchanged by the heating coil was obtained by Eq. (6).

$$\dot{Q}_{HC} = \dot{V}_{a,i} \cdot \rho_{a,i} \cdot \left(h_{a,o} - h_{a,i}\right) \quad (6)$$

The selected air-water heat pump covered all the required sensible heat. This heat pump is fitted with a scroll inverter compressor. The technical characteristics of the heat pump were: a nominal heating capacity of 28.1 kW, a nominal electric power consumption 9.6 kW and a nominal COP of 2.93 [33].

In order to obtain the electric power consumption of the heat pump, the simplified experimental model obtained by the manufacturer was used [33]. The output variable of the model was the heating electrical input ratio, EIR, which is the inverse of COP. The estimate EIR value was calculated from Eq. (7), where EIR_N is its nominal value, EIR_T is a second order polynomial equation based on the outdoor air temperature and outlet water temperature, as shown in Eq. (3), and EIR_{PLF} is a third order polynomial based on the partial load factor, expressed by Eq. (4). The estimated parameters of the estimate EIR value are shown in Table 6.

$$EIR = EIR_N \cdot EIR_T \cdot EIR_{PLF} \quad (7)$$

Table 6. Estimated parameters of the air-water heat pump model.

b_x	X_i	EIR_T x10^3	b_x	X_i	EIR_{PLF} x10^3
b_0	-	805.57	b_0	-	30.39
b_1	$T_{w,o}$	-4.20	b_1	PLF	1518.51
b_2	$T_{w,o}^2$	0.11	b_2	PLF^2	-1323.27
b_3	T_{OA}	-5.68	b_3	PLF^3	774.38
b_4	T_{OA}^2	0.11	-	-	-
b_5	$T_{w,o} \cdot T_{OA}$	-0.15	-	-	-

2.3.5 Filter

Filters were characterized by a constant pressure drop in the air circuit. Several filters with F8 or G4 protection were considered, as shown in Fig. 1 and Fig. 2. The pressure drop of these filters are shown in Table 7. However, the increase of their pressure drop due to dust accumulation was not considered.

2.3.6 Fan model

The fans were sized to maintain the design air flow rate given the estimated system pressure drop. The air pressure drop of each component is shown in Table 7. The fans were modelled using manufacturer data from Sodeca QuickFan software [38]. Three centrifugal fans were selected for the DX system and another three for the DW-IEC system, as shown in Fig. 1 and Fig. 2. The return and exhaust fans of the DX systems were the same. These fans were also the same for the DW-IEC systems, but different from those of the DX system. The estimated parameters of the fan models are shown in Table 8, where the output variables were static pressure, P, and electric power consumption of the fans, $\dot{W}$. The relationship between the output and input variables was expressed by second order polynomials, according to Eq. (3).

Table 7. Pressure drop of each component for the systems analysed.

Component	Pressure drop [Pa]
Desiccant wheel (process side)	350
Desiccant wheel (regeneration side)	380
Indirect evaporative cooler	146
Evaporator	40
Condenser	27
Heating coil	35
Air box with dampers	40
Filter (G4 protection)	60
Filter (F8 protection)	100
Air duct	40

Table 8. Estimated parameters of the fan models.

		DX system				DW-IEC system			
		Fan1		Fan2 and Fan3		Fan1		Fan2 and Fan3	
b_x	X_i	P x10^3 [mmca]	$\dot{W}$ x10^3 [kW]	P x10^3 [mmca]	$\dot{W}$ x10^3 [kW]	P x10^3 [mmca]	$\dot{W}$ x10^3 [kW]	P x10^3 [mmca]	$\dot{W}$ x10^3 [kW]
b_0	-	35478.6	339.9	8824.7	162.2	191371	463.03	76510.9	194.7
b_1	$\dot{V}$	11.653	0.057	14.669	0.039	77.617	0.522	- 4.768	0.192
b_2	$\dot{V}^2$	0.004	-	- 0.004	-	-0.077	-	- 0.005	-

2.4 Climate zones

The performance of the DX and DW-IEC systems under several climatic conditions was evaluated according to ASHRAE climate classification [39]. This classification consists of 8 climate zones, depending on the cooling degrees-day, CDD, and heating degrees-day, HDD. In this study, both systems were simulated for the climate zones 1 to 6, from very hot to cold. Climate zones 7 and 8, very cold and subarctic, respectively, were not used in this study because they are very dry, and therefore, do not require

a dehumidification system. The simulations were performed using the Meteonorm weather data library [40]. One city from each of the 6 selected climate zones was chosen, see Table 9. A world representation of the different climate zones with the selected cities is shown in Fig. 4.

Table 9. Selected cities from each of the climate zone defined by ASHRAE.

Climate zone[a]	City	Thermal criteria[b] [ºC]
1	Singapore	5000 < CDD
2	Taipei	3500 < CDD ≤ 5000
3	Tunis	CDD ≤ 2500 and HDD ≤ 2000
4	Barcelona	CDD ≤ 2500 and HDD ≤ 3000
5	Budapest	3000 < HDD≤ 4000
6	Ottawa	4000 < HDD ≤ 5000

[a] 1- Very hot, 2- hot, 3- warm, 4- mixed, 5- cool, 6- cold

[b] T_{base}= 10ºC for CDD; T_{base}= 18ºC for HDD

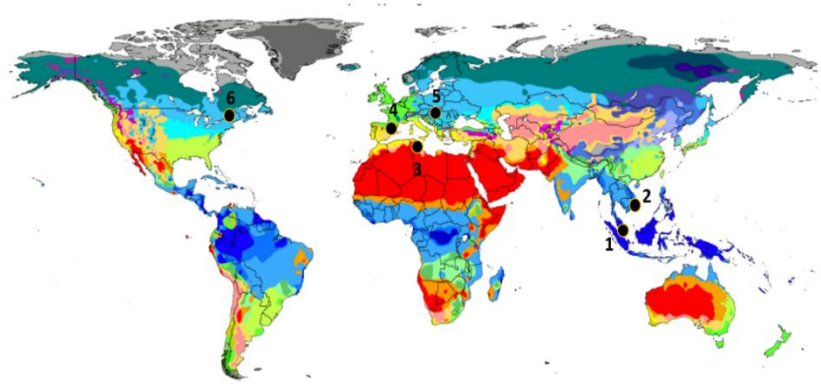

Fig. 4. World representation of the different climate zones with the selected cities.

2.5 Energy simulation

Several detailed energy simulations were carried out with the assumption that both HVAC systems served a spa with high latent loads. All the energy simulations were carried out with the TRNSYS 17 software [34], using a time step of 15 minutes. The simulations were performed for the selected six climate zones throughout the whole year.

The HVAC systems were evaluated according to the following parameters: electric power consumption, $\dot{W}$, sensible and latent energy delivered, $\dot{Q}_{sen}$ and $\dot{Q}_{lat}$, respectively, the seasonal mean coefficient of performance, SCOP, expressed by Eq. (8), and the energy consumption per unit of dehumidified water, E_{cons}, expressed by Eq. (9). The latter was calculated from the $\dot{W}$ and MRC parameters of the HVAC system, only when it was in dehumidification mode, i.e. when air dehumidification was demanded by the system.

$$SCOP = \frac{\int (\dot{Q}_{sen} + \dot{Q}_{lat})\, dt}{\int \dot{W}\, dt} \quad (8)$$

$$E_{cons} = \frac{\int \dot{W}\, dt}{\int MRC\, dt} \quad (9)$$

3 Results and analysis

The energy analysis of the simulations is presented in daily, monthly and annual analysis to correctly understand the behaviour of both HVAC systems.

3.1 Daily behaviour analysis

The daily analysis was performed for the climatic conditions of Barcelona. A typical winter day, January 10th, and a typical summer day, July 10th, were selected.

3.1.1 Daily behaviour of the DX system

The thermal behaviour and energy consumption of the DX system for a typical winter day and a typical summer day are represented in Fig. 5. Regarding the winter day, in the first process of the DX system, the

outdoor air stream was mixed with return air stream, increasing its temperature and humidity, see Fig. 5a. Nevertheless, this humidity was lower than the set point air humidity, therefore the dehumidification mode was not activated and the air stream was not handled by the EV. The mixing air stream was heated by the HC until the set point temperature value was achieved, and finally supplied to the building. The energy consumption values of the compressor and Fan 3 were equal to zero, as air dehumidification was not required, see Fig. 5b. The energy consumption of the HC was reduced when the outdoor temperature increased and the partial load factor of the heat pump decreased. Regarding the summer day, the mixing process also raised the humidity, therefore it was necessary to activate the dehumidification mode it order to reduce it, see Fig. 5c. The mixing air stream was dehumidified and cooled by the EV until the set point humidity was achieved. Then, the dry air flow was heated by the HC and supplied to the building. In this case study, the compressor consumed a significant amount of energy, as the latent energy required by the EV was high, Fig. 5d. The fans maintained low and constant energy consumption values throughout the day, and small oscillations were found for the HC.

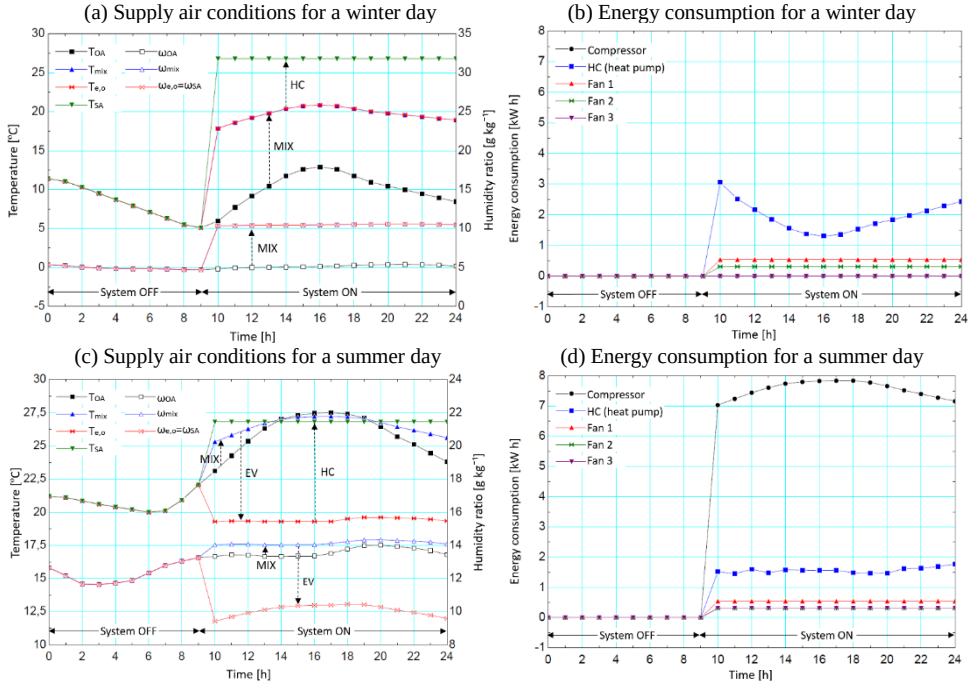

Fig. 5. Daily operational characteristics of the DX system for the climatic conditions of Barcelona.

3.1.2 Daily behaviour of the DW-IEC system

The results of the daily simulations for the DW-IEC system on a typical winter day and a typical summer day in Barcelona are represented in Fig. 6. Regarding the winter day, the outdoor air humidity was lower than the set point air humidity, see Fig. 6a, so air dehumidification was not necessary and the mode of operation Mode 1-H was activated, deactivating the DW, HC1 and Fan3, see Fig. 3. In this case, the outdoor humidity was the supply humidity. Then, the air process stream was handled by the IEC unit, which was used as a SHE, recovering sensible heat from the return air stream. However, the outlet air temperature of the SHE was lower than the set point temperature, so a post-heating by HC2 was required to increase the air temperature, according to Mode 3-T. As a result of this, the energy consumption of the DW, HC1 and Fan3 were zero, the energy consumption of HC2 varied according to the outdoor air temperature and the PLF values of the heat pump, and the energy consumption of Fan 1 and Fan 3 were constant throughout the day, see Fig. 6b. The highest energy consumption values

were those of Fan 1, due to the process side pressure losses.

On the summer day analysed, the outdoor air humidity was higher than the set point humidity, see Fig. 6c, so the Mode 2-H control activates the DW and HC1. All simulations were carried out under assumption that the DW is regenerated with air heated to relatively low temperature values (40–60 ºC). The outlet process air temperature of the DW was higher than the set point air temperature. Therefore, Mode 1-T was activated and the process air stream was cooled by the IEC, thus achieving the set point air conditions and supplying the air stream to the building. HC1 showed the highest energy consumption values for the summer day, due to the regeneration energy required by the DW. The energy consumption of post-heating by HC2 was not required, so this was zero.

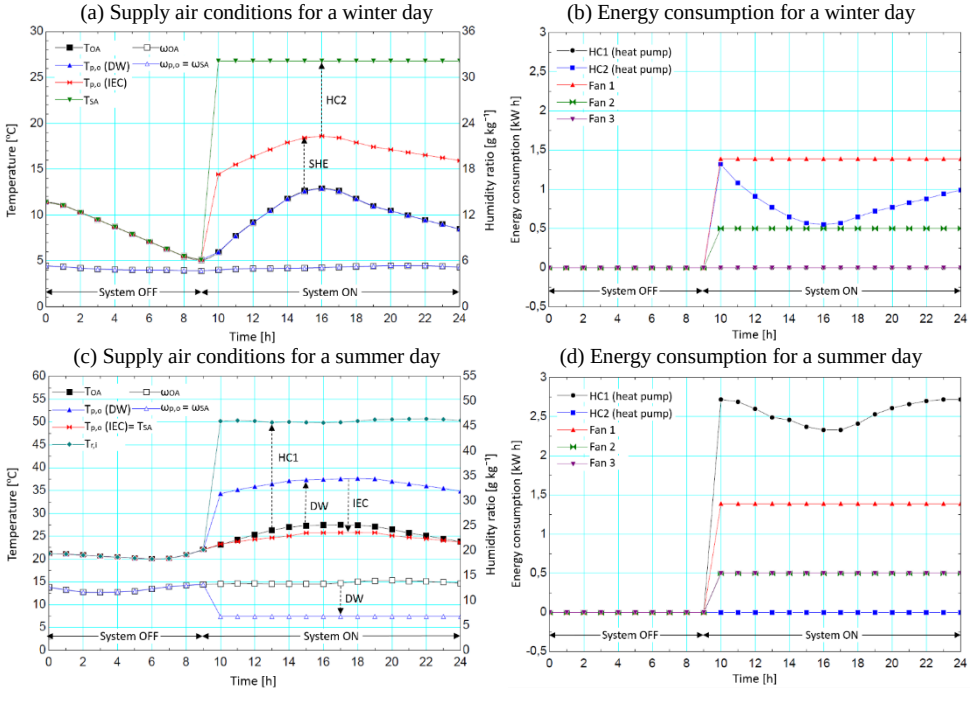

Fig. 6. Daily operational characteristics of the DW-IEC system for the climatic conditions of Barcelona.

It can be observed that the supply air humidity of the DW-IEC system was lower than the supply air humidity of the DX system, because the process air flow rate of the DW-IEC system was lower than that of the DX system. Thus, the latent energy delivered to the building with both systems was similar.

These case studies show that the modes of operation set for both systems provided the required indoor air conditions in the building in every season.

3.2 Monthly energy analysis

A monthly energy analysis for both HVAC systems for the climatic conditions of Barcelona was performed. Monthly sensible and latent energy delivered and monthly energy consumption by the DX and DW-IEC systems were obtained.

3.2.1 Monthly energy analysis of the DX system

The sensible and latent energy delivered of the DX system for the climatic conditions of Barcelona, climate zone 4, are represented in Fig. 7. This figure shows energy delivered of each element and the total monthly energy. The negative energy values indicate that the elements reduced the air temperature and humidity ratio, and the positive energy values indicate that the elements increased the air temperature and humidity ratio. It can be observed that the process of mixing air slightly increased the sensible energy delivered, see Fig. 7a, thus increasing the outlet air

temperature of the mixing box. This process caused the sensible energy required by the HC to decrease, especially in January and December, where the sensible energy delivered in the process of mixing air is greater than in the remaining months, 7.2 kWh m^{-2} and 7.5 kWh m^{-2}, respectively. However, the mixing air also increased the latent energy delivered, see Fig. 7b, thus increasing the outlet air humidity of the mixing box. For example, the latent energy values delivered in January and December were 15.2 kWh m^{-2} and 16.2 kWh m^{-2}, respectively. Therefore, the mixing air did not improve the dehumidification system performance for the climate conditions of Barcelona.

The EV delivered sensible and latent energy during the months with dehumidification demand, i.e. when the mixed air humidity ratio was higher than the set point air humidity ratio, from April to November. The maximum sensible and latent energy values delivered by the EV were obtained in July and August. The building did not require dehumidification from December to March, therefore, the sensible and latent energy delivered by the EV was zero.

The sensible energy delivered by the HC was maintained throughout the year, due to the heating demand, i.e. when the inlet air temperature to the HC was lower than the set point air temperature. This temperature was lower the set point air temperature from November to April, due mainly to the outdoor air, and from May to October, due to the low outlet air temperature of the EV.

Finally, it can be observed that the annual sensible and latent energy values delivered by the DX system were 365.7 kWh m^{-2} $year^{-1}$ and -260.2 kWh m^{-2} $year^{-1}$, respectively.

(a)

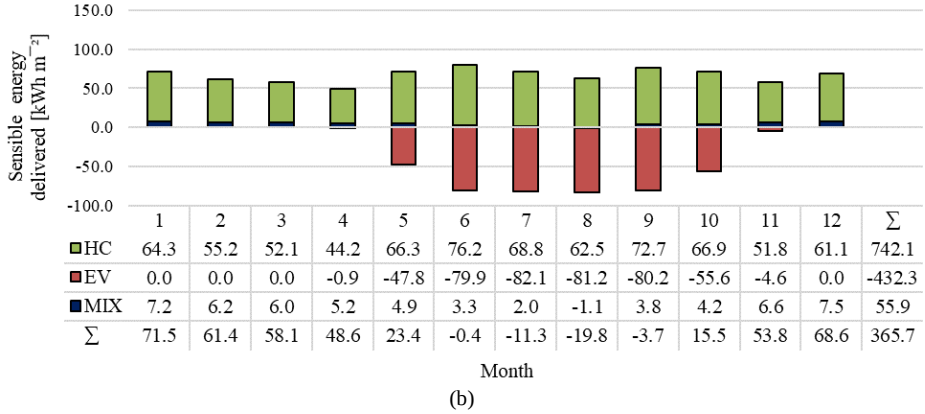

	1	2	3	4	5	6	7	8	9	10	11	12	∑
HC	64.3	55.2	52.1	44.2	66.3	76.2	68.8	62.5	72.7	66.9	51.8	61.1	742.1
EV	0.0	0.0	0.0	-0.9	-47.8	-79.9	-82.1	-81.2	-80.2	-55.6	-4.6	0.0	-432.3
MIX	7.2	6.2	6.0	5.2	4.9	3.3	2.0	-1.1	3.8	4.2	6.6	7.5	55.9
∑	71.5	61.4	58.1	48.6	23.4	-0.4	-11.3	-19.8	-3.7	15.5	53.8	68.6	365.7

(b)

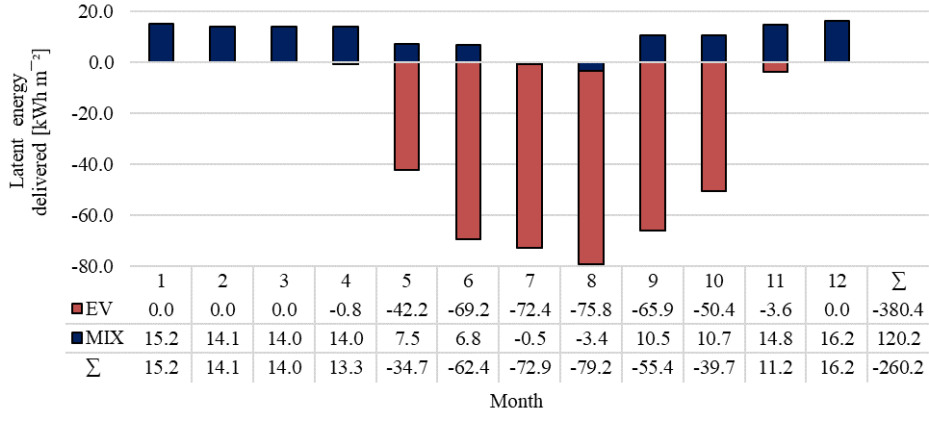

	1	2	3	4	5	6	7	8	9	10	11	12	∑
EV	0.0	0.0	0.0	-0.8	-42.2	-69.2	-72.4	-75.8	-65.9	-50.4	-3.6	0.0	-380.4
MIX	15.2	14.1	14.0	14.0	7.5	6.8	-0.5	-3.4	10.5	10.7	14.8	16.2	120.2
∑	15.2	14.1	14.0	13.3	-34.7	-62.4	-72.9	-79.2	-55.4	-39.7	11.2	16.2	-260.2

Fig. 7. Energy delivered by each element for the DX system for the climatic conditions of Barcelona, (a) sensible energy delivered and (b) latent energy delivered.

The monthly energy consumption of the DX system is represented in Fig. 8. This figure shows the monthly energy consumption of each element and the total monthly consumption. It can be observed that the highest energy consumption values were those for the compressor, which was activated during the months with dehumidification demand. The operation Fan3 was linked to that of the compressor, see Fig. 1, therefore, the energy consumption of Fan3 was zero during the months that the compressor was not in operation, from December to March. The energy consumption of the HC was maintained throughout the year, due to its sensible energy demand, as shown in Fig. 7a. The energy consumption of the HC was that of the heat pump. Regarding the monthly energy consumption, the maximum values were found from May to October, due mainly to the high dehumidification demand. The energy consumption was less during cold months with high heating demand, from November to February, and warm months, such as March and April. It can also be observed that the annual energy consumption for the climatic conditions of Barcelona with the DX system was 493.1 kWh m^{-2} $year^{-1}$, see Fig. 8.

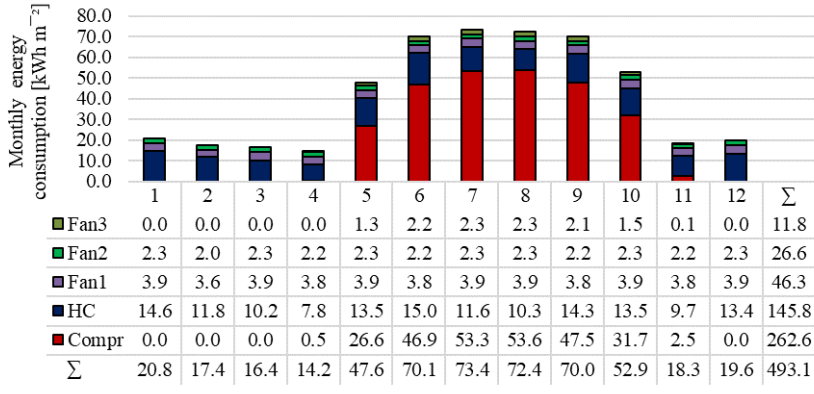

	1	2	3	4	5	6	7	8	9	10	11	12	∑
Fan3	0.0	0.0	0.0	0.0	1.3	2.2	2.3	2.3	2.1	1.5	0.1	0.0	11.8
Fan2	2.3	2.0	2.3	2.2	2.3	2.2	2.3	2.3	2.2	2.3	2.2	2.3	26.6
Fan1	3.9	3.6	3.9	3.8	3.9	3.8	3.9	3.9	3.8	3.9	3.8	3.9	46.3
HC	14.6	11.8	10.2	7.8	13.5	15.0	11.6	10.3	14.3	13.5	9.7	13.4	145.8
Compr	0.0	0.0	0.0	0.5	26.6	46.9	53.3	53.6	47.5	31.7	2.5	0.0	262.6
∑	20.8	17.4	16.4	14.2	47.6	70.1	73.4	72.4	70.0	52.9	18.3	19.6	493.1

Fig. 8. Monthly energy consumption of each element for the DX system for the climatic conditions of Barcelona.

3.2.2 Monthly energy analysis of the DW-IEC system

The sensible and latent energy delivered of the DW-IEC system for the climatic conditions of Barcelona is shown in Fig. 9, broken down by the elements. It can be observed that the DW delivered high latent energy values from April to November, as shown in Fig. 9b, due to the dehumidification demand. The peak values, corresponding to July and August, are due to the high outdoor air humidity. The operation of HC1 was linked to that of the DW, in order to regenerate it, see Fig. 2 and Fig. 3. The sensible energy of HC1 was not delivered to the building, but outside. The activation of the IEC was caused by the sensible energy delivered during the dehumidification process of the DW. As a consequence, sensible energy delivered by the IEC is obtained from April to November, in order to reduce the process air temperature, see Fig. 9a. The SHE recovered a large amount of energy during the months with heating demand and the DW was not in operation, thus reducing the energy required by HC2. The highest sensible energy values delivered by HC2 was found during the months with high heating demand, from November to March, months with low outdoor temperatures. Nevertheless, the sensible energy delivered by HC2 was zero from June to September, as shown in Fig. 9a.

(a)

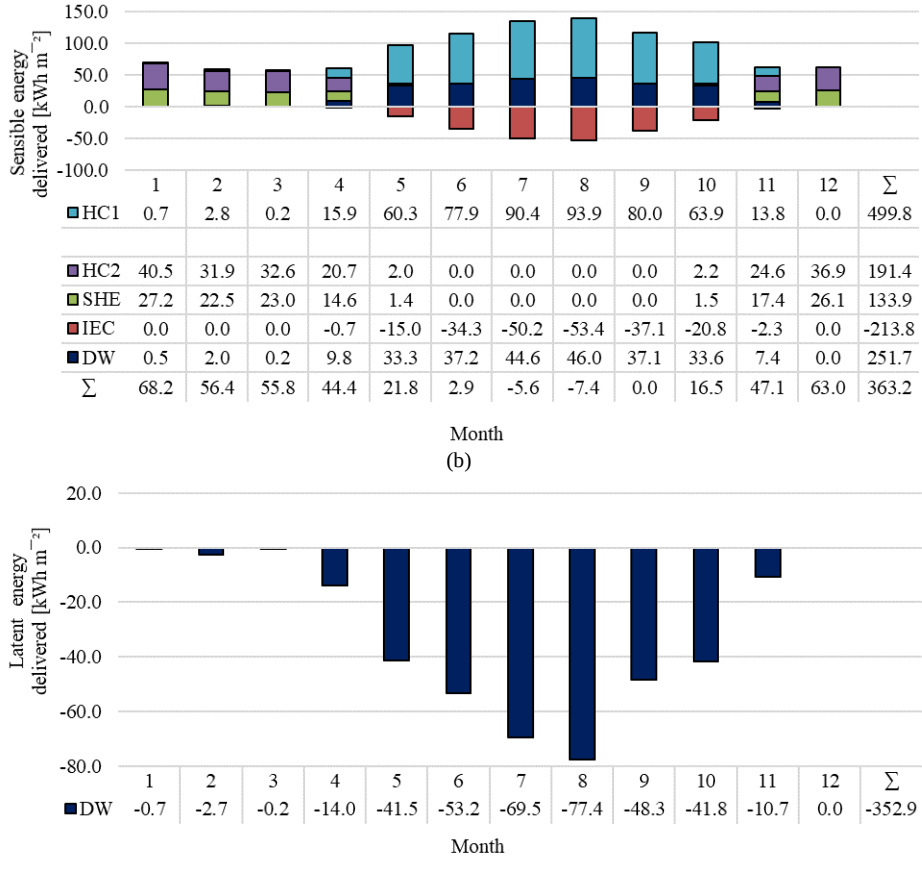

	1	2	3	4	5	6	7	8	9	10	11	12	Σ
HC1	0.7	2.8	0.2	15.9	60.3	77.9	90.4	93.9	80.0	63.9	13.8	0.0	499.8
HC2	40.5	31.9	32.6	20.7	2.0	0.0	0.0	0.0	0.0	2.2	24.6	36.9	191.4
SHE	27.2	22.5	23.0	14.6	1.4	0.0	0.0	0.0	0.0	1.5	17.4	26.1	133.9
IEC	0.0	0.0	0.0	-0.7	-15.0	-34.3	-50.2	-53.4	-37.1	-20.8	-2.3	0.0	-213.8
DW	0.5	2.0	0.2	9.8	33.3	37.2	44.6	46.0	37.1	33.6	7.4	0.0	251.7
Σ	68.2	56.4	55.8	44.4	21.8	2.9	-5.6	-7.4	0.0	16.5	47.1	63.0	363.2

	1	2	3	4	5	6	7	8	9	10	11	12	Σ
DW	-0.7	-2.7	-0.2	-14.0	-41.5	-53.2	-69.5	-77.4	-48.3	-41.8	-10.7	0.0	-352.9

Fig. 9. Energy delivered by each element for the DW-IEC system for the climatic conditions of Barcelona, (a) sensible energy delivered and (b) latent energy delivered.

Finally, comparing these results with those obtained with the DX system, it can be observed that the monthly sensible and latent energy delivered to the building by each system was similar, see Fig. 7 and Fig. 9. The slight variations in the energy values delivered between both systems were mainly due to the different control systems used.

The monthly energy consumption by each element of the DW-IEC system are shown in Fig. 10. It can be observed that the element with the highest energy consumption values throughout the year was Fan1, 119.1 kWh m-2, due to the high pressure drop of the proposed system. High energy consumption values by HC1 were found during the months with high dehumidification demand, from April to November. However, very low dehumidification demand was obtained from December to March, so the monthly energy consumption values by HC1 were very low or zero, see Fig. 10. The energy consumption of HC1 and HC2 were those of the heat pump. It can also be observed that the trend of energy consumption by HC2 was contrary to that of HC1. The highest energy consumption values by HC2 were found November to April, due to the heating demand, and the lowest values from May to October, because the outlet process air temperature of the DW was usually higher than the set point air temperature. The energy consumption of Fan3 was very low during the months that the DW was not in operation, since the operation of Fan2 was linked to that of the DW, see Fig. 2 and Fig. 3. The maximum monthly energy consumption values were found from May to October, due mainly to the high dehumidification demand, and then, as with the DX

system. Finally, the annual energy consumption for the climatic conditions of Barcelona with the proposed DW-IEC system was 314.7 kWh m^{-2} $year^{-1}$, as shown in Fig. 10. Therefore, the annual energy consumption of the DW-IEC system was 36.2 % lower than that of the DX system for the climatic conditions of Barcelona, see Fig. 8 and Fig. 10.

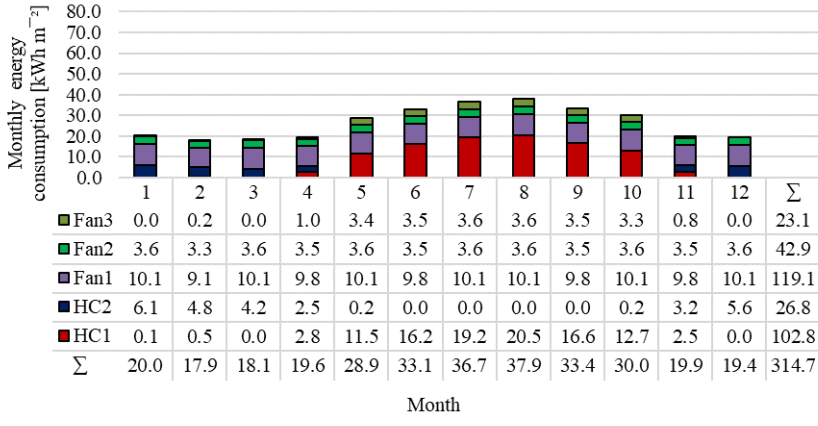

	1	2	3	4	5	6	7	8	9	10	11	12	∑
Fan3	0.0	0.2	0.0	1.0	3.4	3.5	3.6	3.6	3.5	3.3	0.8	0.0	23.1
Fan2	3.6	3.3	3.6	3.5	3.6	3.5	3.6	3.6	3.5	3.6	3.5	3.6	42.9
Fan1	10.1	9.1	10.1	9.8	10.1	9.8	10.1	10.1	9.8	10.1	9.8	10.1	119.1
HC2	6.1	4.8	4.2	2.5	0.2	0.0	0.0	0.0	0.0	0.2	3.2	5.6	26.8
HC1	0.1	0.5	0.0	2.8	11.5	16.2	19.2	20.5	16.6	12.7	2.5	0.0	102.8
∑	20.0	17.9	18.1	19.6	28.9	33.1	36.7	37.9	33.4	30.0	19.9	19.4	314.7

Fig. 10. Monthly energy consumption for the DW-IEC system for the climatic conditions of Barcelona.

3.3 Annual energy analysis

In this section, the annual energy consumption of the proposed DW-IEC system was compared with those of the DX system. The comparative analysis was carried out for the 6 climate zones, as shown in Table 9.

3.3.1 Annual energy consumption

The operating annual energy consumption of both systems for the 6 climate zones is shown in Fig. 11. It can be observed that the maximum annual consumption values for both systems were obtained for the climate zone 1, a very hot climate zone, due to the high dehumidification demand. The energy consumption values were significantly reduced for cool climatic conditions, such as in climate zone 5. The consumption decreased by 51 % and 37 % between the climate zone 1 and 5 for the DX system and the DW-IEC system, respectively. However, the annual energy consumption values increased for climate zone 6, a cold climate zone, compared to those of zones 3, 4 and 5. This increase was caused mainly by the high heating demand. This trend of annual energy consumption was also obtained for the monthly energy consumption analysed in section 3.2, where the highest monthly consumption values were found for the months with high dehumidification demand, then, the months with high heating demand and finally, the remaining months.

It can be observed that the annual energy consumption of the DW-IEC system was always lower than that of the DX system, obtaining significant energy savings, always over 27.8 %, see Fig. 11. The highest energy savings were found for the climate zones with the highest annual energy consumption and the highest dehumidification demand, zones 1 and 2, with 43.5 % and 46.8 %, respectively.

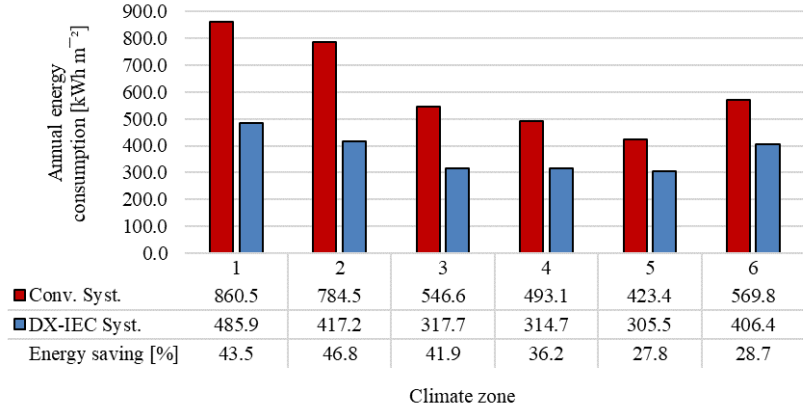

Fig. 11. Comparative analysis of annual energy consumption of the DW-IEC system and the DX system in each climate zone.

3.3.2 Seasonal mean coefficient of performance

The seasonal mean coefficient of performance, SCOP, of both systems, was calculated using Eq. (8). The SCOP values for the 6 climate zones are represented in Fig. 12. It can be observed that the maximum SCOP value for the DX system was 1.9, obtained from a cool climate zone, zone 5. Nevertheless, the maximum SCOP value for the DW-IEC system was 2.8, obtained from a very hot climate zone, zone 1.

The SCOP values of the DW-IEC system were always higher than that of the DX system, always over 27 %, as shown in Fig. 12. The greatest differences in SCOP between both systems, ΔSCOP, were found for climate zones 1 and 2, and the lowest for climate zones 5 and 6. The trend of ΔSCOP was similar to the trend of annual energy saving, as shown in Fig. 11, since the sensible and latent energy delivered to the building by each system were the same, so ΔSCOP depended exclusively on energy consumption.

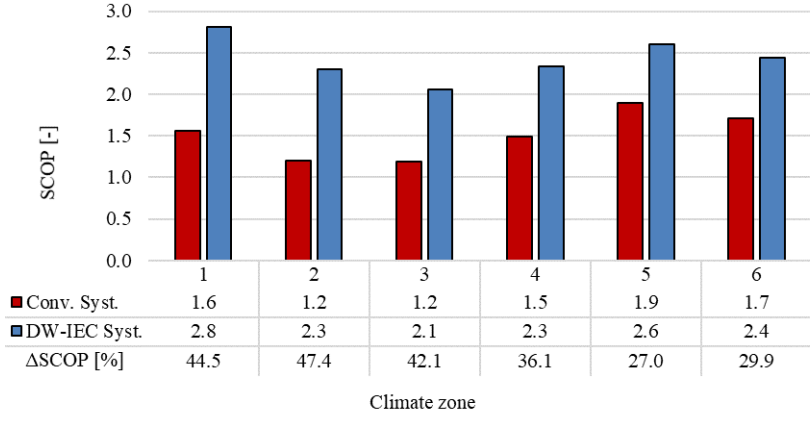

Fig. 12. SCOP values of the DW-IEC system and the DX system in each climate zone.

3.3.3 Energy consumption per unit of dehumidified water

The energy consumption per unit of dehumidified water, E_{cons}, was obtained for both system, in order to know the energy used only when the dehumidification demand was required. The E_{cons} results for each system and climate zone, are shown in Fig. 13. It can be observed that the lowest E_{cons} values were obtained for very hot climatic conditions, such as in climate zone 1

and the highest E_{cons} values for cool conditions, such as in climate zone 5. The trend of E_{cons} is contrary to that obtained for annual energy consumption, see Fig. 11. Comparing both systems studied, it can be observed that the E_{cons} values from the DX system were always higher than those from the DW-IEC system. The highest energy saving, ΔE_{cons}, was obtained for zone 1, 34.6 %. However, small energy savings were found for zones 5 and 6, 4.4 % and 1.7 %, respectively, climate zones with low dehumidification demand.

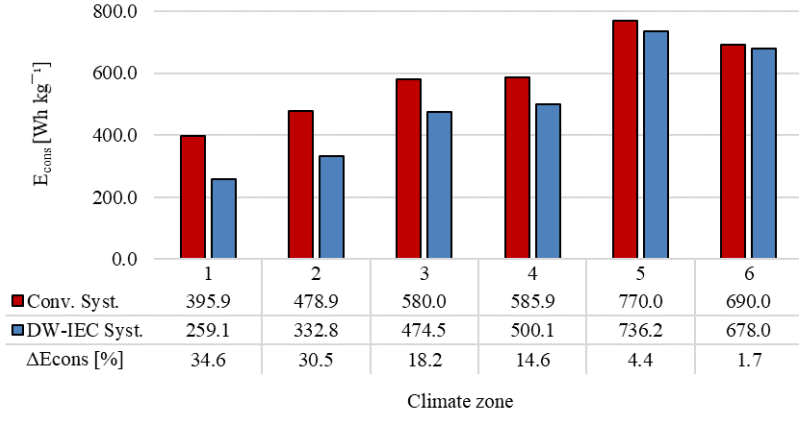

	1	2	3	4	5	6
Conv. Syst.	395.9	478.9	580.0	585.9	770.0	690.0
DW-IEC Syst.	259.1	332.8	474.5	500.1	736.2	678.0
ΔEcons [%]	34.6	30.5	18.2	14.6	4.4	1.7

Fig. 13. E_{cons} values of the DW-IEC system and the DX system in each climate zone.

4 Conclusions

In the present work, the energy potential and desiccant capacity of two air handling systems were analysed. The first system was composed mainly of a DW and an IEC, DW-IEC system, and the second system of a direct expansion conventional unit, DX system. Several detailed energy simulations were carried out with the assumption that both systems served a spa room. 6 different climatic conditions, from very hot zones to cold zones, were used to performed the simulations.

The results showed that the systems satisfactorily achieved the set point air conditions. Both systems delivered similar sensible and latent energy values to the building. The IEC system reduced the high air temperatures generated by the adsorption process of the DW.

The annual energy consumption of the DW-IEC system was lower than that of the DX system for the 6 climate zones, achieving significant energy savings, especially for hot climate zones with high dehumidification demand, where a 46.8 % annual energy saving was obtained. The lowest energy saving was achieved for a cool climate zone, 27.8 %. These energy savings resulted in better SCOP values for the DW-IEC system. The highest SCOP value was 2.8, obtained for a very hot climatic zone. The difference in SCOP between both systems was always greater than 25% for all climate zones.

Finally, the energy consumption per unit of dehumidified water, E_{cons}, of both systems was analysed for the 6 climate zones. Significant energy savings were obtained with the proposed DW-IEC system for very hot climate zone, due to the high dehumidification demand, achieving up to 34.6% savings. However, the energy savings of the DW-IEC system were lower for cool and cold climate zones, 4.4 % and 1.7 %, respectively, climate zones with low dehumidification demand and high heating demand.

The results suggest that the proposed system with a DW and an IEC could be a serious alternative to the DX systems composed of direct expansion units, to handle air in small buildings with high latent loads and low supply air flow rates, such as spas.

Acknowledgments

This work is related to a research stay at the Energy Department of Politecnico di Milano, Italy, and funded by the University of Cordoba, Spain.

References

[1] W.-S. Lee, C.-K. Kung, Optimization of heat pump system in indoor swimming pool using particle swarm algorithm, Appl. Therm. Eng. 28 (2008) 1647–1653. doi:10.1016/j.applthermaleng.2007.11.003.

[2] M.M. Shah, Prediction of evaporation from occupied indoor swimming pools, Energy Build. 35 (2003) 707–713. doi:10.1016/S0378-7788(02)00211-6.

[3] P. Torrero, DTIE 10.04. Covered swimming pools air-conditioned only with outdoor air, ATECYR, 2008.

[4] P. Sun, J.Y. Wu, R.Z. Wang, Y.X. Xu, Analysis of indoor environmental conditions and heat pump energy supply systems in indoor swimming pools, Energy Build. 43 (2011) 1071–1080. doi:10.1016/j.enbuild.2010.08.004.

[5] R. Tubío, N. Molero, M. Zamora, DTIE 10.06. Covered swimming pools. Systems of air conditioning, dehumidification and energy saving using heat pumps, ATECYR, 2013.

[6] L. Johansson, L. Westerlund, Energy savings in indoor swimming-pools: comparison between different heat-recovery systems, Appl. Energy. 70 (2001) 281–303. doi:10.1016/S0306-2619(01)00043-5.

[7] J.L. Míguez Tabarés, M. Gándara Alvarez, L.M. López González, P. Fernández Viar, Feasibility study for the installation of HVAC for a spa by means of energy recovery from thermal water - Part I: Energy analysis, Renew. Energy. 23 (2001) 135–149. doi:10.1016/S0960-1481(00)00162-2.

[8] J.L. Míguez Tabarés, M. Gándara Alvarez, L.M. López González, P. Fernández Viar, Feasibility study for the installation of HVAC for a spa by means of energy recovery from thermal water - Part II: Energy analysis, Renew. Energy. 23 (2001) 135–149. doi:10.1016/S0960-1481(00)00162-2.

[9] B. Delcroix, M.A. Leduc, M. Kummert, Modeling of a portable electric spa: Model development, experimental validation and application to winter demand response, Appl. Therm. Eng. 111 (2017) 183–192. doi:10.1016/j.applthermaleng.2016.09.078.

[10] L.G. Harriman III, The dehumidification handbook, second ed., Munters Corp. Amesbury, MA. (2003).

[11] K.S. Rambhad, P. V. Walke, D.J. Tidke, Solid desiccant dehumidification and regeneration methods - A review, Renew. Sustain. Energy Rev. 59 (2016) 73–83. doi:10.1016/j.rser.2015.12.264.

[12] D.B. Jani, M. Mishra, P.K. Sahoo, Solid desiccant air conditioning - A state of the art review, Renew. Sustain. Energy Rev. 60 (2016) 1451–1469. doi:10.1016/j.rser.2016.03.031.

[13] G. Angrisani, F. Minichiello, C. Roselli, M. Sasso, Experimental analysis on the dehumidification and thermal performance of a desiccant wheel, Appl. Energy. 92 (2012) 563–572. doi:10.1016/j.apenergy.2011.11.071.

[14] F. Comino, M. Ruiz de Adana, F. Peci, Experimental study of the moisture removal capacity of a desiccant wheel activated at low and high temperature, in: CLIMA 2016 - proceedings of the 12th REHVA World Congress. Aalborg University, Department of Civil Engineering., 2016.

[15] L. Yadav, A. Yadav, Mathematical investigation of purge sector angle for clockwise and anticlockwise rotation of desiccant wheel, Appl. Therm. Eng. 93 (2016) 839–848. doi:10.1016/j.applthermaleng.2015.10.062.

[16] C.R. Ruivo, A. Carrillo-Andres, J.J. Costa, F. Dominguez-Munoz, Exponential correlations to predict the dependence of effectiveness parameters of a desiccant wheel on the airflow rates and on the rotation speed, Appl. Therm. Eng. 51 (2013) 442–450. doi:10.1016/j.applthermaleng.2012.08.037.

[17] F. Comino, M. Ruiz de Adana, Experimental and numerical analysis of desiccant wheels activated at low temperatures, Energy Build. 133 (2016) 529–540. doi:10.1016/j.enbuild.2016.10.021.

[18] C. Aprea, A. Greco, A. Maiorino, The application of a desiccant wheel to increase the energetic performances of a transcritical cycle, Energy Convers. Manag. 89 (2015) 222–230. doi:10.1016/j.enconman.2014.09.066.

[19] D.B. Jani, M. Mishra, P.K. Sahoo, Performance prediction of rotary solid desiccant dehumidifierin hybrid air-conditioning system using artificial neural network, Appl. Therm. Eng. 98 (2016) 1091–1103. doi:10.1016/j.applthermaleng.2015.12.112.

[20] J. Zhu, W. Chen, A novel multivariate linear prediction model for the marine rotary desiccant air-conditioning by adding a dynamic correction factor, Appl. Therm. Eng. 78 (2015) 101–109. doi:10.1016/j.applthermaleng.2014.12.049.

[21] Z. Duan, C. Zhan, X. Zhang, M. Mustafa, X. Zhao, B. Alimohammadisagvand, et al., Indirect evaporative cooling: Past, present and future potentials, Renew. Sustain. Energy Rev. 16 (2012) 6823–6850. doi:10.1016/j.rser.2012.07.007.

[22] B. Porumb, P. Ungureşan, L.F. Tutunaru, A. Şerban, M. BĂlan, A Review of Indirect Evaporative Cooling Technology, Energy Procedia. 85 (2016) 461–471. doi:10.1016/j.egypro.2015.12.228.

[23] A. Sohani, H. Sayyaadi, S. Hoseinpoori, Modeling and multi-objective optimization of an M-cycle cross-flow indirect evaporative cooler using the GMDH type neural network, Int. J. Refrig. 69 (2016) 186–204. doi:10.1016/j.ijrefrig.2016.05.011.

[24] M. Tu, C.Q. Ren, L.A. Zhang, J.W. Shao, Simulation and analysis of a novel liquid desiccant air-conditioning system, Appl. Therm. Eng. 29 (2009) 2417–2425. doi:10.1016/j.applthermaleng.2008.12.006.

[25] W.Z. Gao, Y.P. Cheng, A.G. Jiang, T. Liu, K. Anderson, Experimental investigation on integrated liquid desiccant e Indirect evaporative air cooling system utilizing the Maisotesenko e Cycle, Appl. Therm. Eng. 88 (2015) 288–296. doi:10.1016/j.applthermaleng.2014.08.066.

[26] H.J. Kim, S.J. Lee, S.H. Cho, J.W. Jeong, Energy benefit of a dedicated outdoor air system over a desiccant-enhanced evaporative air conditioner, Appl. Therm. Eng. 108 (2016) 804–815. doi:10.1016/j.applthermaleng.2016.07.185.

[27] P. Finocchiaro, M. Beccali, B. Nocke, Advanced solar assisted desiccant and evaporative cooling system equipped with wet heat exchangers, Sol. Energy. 86 (2012) 608–618. doi:10.1016/j.solener.2011.11.003.

[28] D. Pandelidis, S. Anisimov, W.M. Worek, P. Drag, Comparison of desiccant air conditioning systems with different indirect evaporative air coolers, Energy Convers. Manag. 117 (2016) 375–392. doi:10.1016/j.enconman.2016.02.085.

[29] M. Goldsworthy, S. White, Optimisation of a desiccant cooling system design with indirect evaporative cooler, Int. J. Refrig. 34 (2011) 148–158. doi:10.1016/j.ijrefrig.2010.07.005.

[30] E. Elgendy, A. Mostafa, M. Fatouh, Performance enhancement of a desiccant evaporative cooling system using direct/indirect evaporative cooler, Int. J. Refrig. 51 (2015) 77–87. doi:10.1016/j.ijrefrig.2014.12.009.

[31] J.D. Chung, D.Y. Lee, Contributions of system components and operating conditions to the performance of desiccant cooling systems, Int. J. Refrig. 34 (2011) 922–927. doi:10.1016/j.ijrefrig.2011.03.003.

[32] S.D. White, P. Kohlenbach, C. Bongs, Indoor temperature variations resulting from solar desiccant cooling in a building without thermal backup, Int. J. Refrig. 32 (2009) 695–704. doi:10.1016/j.ijrefrig.2009.01.019.

[33] CIAT, http://www.grupociat.es/, (accessed 05.07.17).

[34] Klein, S.A. 2006. TRNSYS 17: A Transient System Simulation Program, SEL, University of Wisconsin, Madison USA.

[35] RITE 2007. Reglamento de instalaciones térmicas en los edificios, Real Decreto. (2007) 35931–35984.

[36] F. Comino, S. Milani, S. De Antonellis, C.M. Joppolo, M. Ruiz de Adana, Indirect evaporative coolers: development of a simplified correlation and comparison with a phenomenological model and experimental data, Energy Build, submitted to the journal.

[37] F. Comino, A. Cerezuela, M. Ruiz de Adana, M. Zamora, F. Peci, Numerical study of hybrid HVAC systems with desiccant wheel, in: V Ibero-American Congress of sciences and techniques of the cold., Tarragona, Spain, 2014: pp. 433–443.

[38] SODECA, http://www.sodeca.es/, (accessed 05.07.17).

[39] ASHRAE STANDARD 90.1 Energy Standard for Buildings Except Low-Rise Residential Buildings, Society. 8400 (2007) 404–636. doi:http://dx.doi.org/10.1108/17506200710779521.

[40] Meteotest (2003). Meteonorm handbook, Parts I, II and III. Meteotest, Bern, Switzerland. http://www.meteotest.ch, (accessed 05.07.17).

Appendix E

Numerical study of hybrid HVAC systems with desiccant wheel

The paper presented in this appendix is published in the *V Ibero-American Congress of Sciences and Techniques of the Cold*, Tarragona, Spain, 2014: pp. 433–443.

AVANCES EN CIENCIAS Y TECNOLOGÍAS DEL FRÍO VII

Estudio numérico de sistemas de climatización híbridos con rueda desecante

F. Comino Montilla[1], **A. Cerezuela Parish**[2], **M. Ruiz de Adana Santiago**[1], **M. Zamora García**[2*] **and F. Peci López**[1]

[1] Área de Máquinas y Motores Térmicos – Edificio Leonardo Da Vinci - Campus de Rabanales - Universidad de Córdoba, Ctra. Madrid-Cádiz km 396 a – 14071 Córdoba

[2] CIAT. Departamento de I+D+i. Pol. Llanos de Jarata s/n. 14550 Montilla, Córdoba, España

[*]Corresponding author: manuel.ruiz@uco.es

Palabras clave: deshumidificación, rueda desecante, sistemas híbridos.

Resumen

El uso de ruedas desecantes, DW, en sistemas de climatización puede reducir el coste de la energía empleada por un equipo para deshumidificar el aire. Los sistemas híbridos de climatización combinan ruedas desecantes, DW, con baterías de expansión directa, DX. En el presente trabajo se ha estudiado el comportamiento de dos sistemas híbridos para la climatización, DX-DW y DX-DX-DW. Se han empleado modelos empíricos para los sistemas convencionales de expansión directa y un modelo numérico simplificado para la rueda desecante. En ambos sistemas se han analizado las prestaciones del sistema en función del factor de calor sensible, SHF, del coeficiente de eficiencia energética, EER, así como de la capacidad desecante del equipo, MRC.

En primer lugar, se ha modelado el sistema híbrido DX-DW y se ha analizado su comportamiento. El modelo ha sido validado con resultados obtenidos por otros autores. A continuación, se han analizado y comparado los sistemas DX-DW y DX-DX-DW para diferentes condiciones de aire exterior.

Los resultados de este trabajo muestran que se produce una mayor penalización del EER con el sistema DX-DX-DW, hasta un 4,6% respecto al sistema DX-DW. Sin embargo, el sistema DX-DX-DW permite aumentar el MRC hasta un 7,6 %. Con ambos sistemas se obtuvieron valores de SHR próximos a cero, por lo que ambos sistemas resultan adecuados para climatizar locales con altas cargas latentes.

Introducción

El control del contenido humedad en el aire es necesario para mantener las condiciones ambientales requeridas para el confort térmico o para determinados procesos industriales. En el ámbito de la climatización de edificios, las aportaciones latentes procedentes del aire exterior o del propio local producen un incremento en el contenido de humedad, por lo que es necesario emplear sistemas para controlar la humedad absoluta del aire.

Nomenclatura:

EER	Coeficiente de eficiencia energética
DX	Batería de expansión directa
DW	Rueda desecante
HR	Humedad relativa [%]
MRC	Capacidad desecante [kg/h]
PA	Potencia absorbida [kW]
PF	Potencia frigorífica [kW]
PFS	Potencia frigorífica sensible [kW]
PFL	Potencia frigorífica latente [kW]
SHR	Factor de calor sensible
T	Temperatura [°C]
$\dot{V}$	Caudal volumétrico de aire [m^3/h]

Símbolos Griegos:

ω	Humedad absoluta [g/kg]
ρ	Densidad de aire [kg/m^3]
Subíndices:	
DX,b	Batería de baja potencia de expansión directa
DX,p	Batería principal de expansión directa
imp	Impulsión
reg	Regeneración de la rueda desecante
T	Total
vent	Ventilador

Los equipos de climatización empleados en los procesos de deshumidificación en edificios contienen baterías de refrigeración, que enfrían el aire por debajo de su punto de rocío. En estos equipos, la cantidad de agua deshumidificada es función de la temperatura de rocío existente a la salida de la batería de refrigeración, de forma que cuanto más se enfríe el aire, más se deshumidifica. El control de humedad interior con estos equipos no resulta adecuado y se producen fluctuaciones en la temperatura del aire, debido a la dependencia entre la temperatura y la humedad de salida de la batería. El control de humedad requiere un posterior calentamiento del aire para obtener las condiciones de impulsión deseadas. La solución a este problema conlleva un mayor consumo energético y en algunos casos un sobredimensionamiento del equipo, con el consiguiente sobre coste económico [1].

En los últimos años, se ha empleado la rueda desecante con sistemas desecantes activos. El uso se estos sistemas se ha extendido en los sistemas de climatización en los edificios comerciales que requieren un control de la humedad, como en el caso de supermercados, centros comerciales o almacenes frigoríficos [2].

En aplicaciones de climatización donde el caudal de aire exterior represente más del 15% del aire impulsado al local, los sistemas tradicionales pueden presentar problemas para tratar de forma combinada la carga sensible y latente [3], por lo que las combinaciones de sistemas convencionales con ruedas desecantes pueden resultar ventajosas. Los equipos de climatización que emplean rueda desecante tienen una gran capacidad de deshumidificación, ya que pueden adsorber una gran cantidad de humedad del aire de proceso. Estos sistemas permiten un control independiente de la temperatura y humedad de impulsión al local, por lo que, es posible mantener estables las condiciones de impulsión de forma prolongada, como se requiere en edificios donde la temperatura y humedad de productos o máquinas deba ser constante.

La principal desventaja de emplear sistemas desecantes, como la rueda desecante, es que el calor generado en el proceso de adsorción es entregado al aire de impulsión a su paso por la sección de proceso de la rueda desecante. En aquellos sistemas híbridos que empleen rueda desecante y deban impulsar aire a una temperatura baja, es necesario enfriar el aire de proceso antes o después de su paso por la rueda desecante. Para ello es necesario emplear equipos regenerativos como ruedas entálpicas y/o baterías de refrigeración.

Los sistemas híbridos que combinan ruedas desecantes y baterías de refrigeración permiten reducir el factor de calor sensible, SHR, del proceso de tratamiento de aire. Sin embargo, los sistemas híbridos presentan un menor coeficiente de eficiencia energética, EER. Estos sistemas requieren un ventilador adicional para vencer las pérdidas de carga de la rueda desecante por lo que el EER es menor que en sistemas tradicionales.

En este trabajo se ha realizado un estudio numérico de dos configuraciones de sistemas híbridos DX-DW y DX-DX-DW. El objetivo del trabajo consiste en analizar las relaciones entre el SHR y el EER de sistemas híbridos y explorar las posibilidades que presentan los sistemas híbridos para reducir el SHR, penalizando lo menos posible el EER.

Metodología

Los dos sistemas híbridos estudiados están compuestos de ciclos de compresión de vapor y una rueda desecante. La disposición de los elementos que componen los sistemas híbridos se realiza para obtener unas condiciones de aire de impulsión óptimas. Con los sistemas híbridos se pretende obtener aire de impulsión con baja temperatura, T_{imp}, y baja humedad absoluta, ω_{imp}. A continuación se define la configuración de ambos sistemas.

- Sistema DX-DW. El equipo emplea un circuito convencional de compresión de vapor, con el que se enfría y deshumidifica el aire de entrada al sistema, aire de proceso, mediante una batería de expansión directa, DX. El aire de salida del evaporador es tratado por la rueda desecante, impulsándose finalmente hacia el local, ver figura 1a. La rueda desecante es activada térmicamente con el aire de retorno del local, tras calentarse con el condensador del circuito de compresión de vapor.

- Sistema DX-DX-DW. El diseño del sistema DX-DX-DW es similar al anterior, pero se le añade otro circuito de compresión de vapor de baja potencia, con el objetivo de reducir la temperatura del aire de impulsión, ver figura 1b. En este sistema, el aire exterior es previamente tratado por las dos baterías evaporadoras, primero la evaporadora del circuito de compresión de vapor de baja potencia, y posteriormente por la evaporadora del circuito principal. A continuación, el aire pasa por el lado de proceso de la rueda desecante y se impulsa al local. La rueda desecante se activa térmicamente con el calor de condensación correspondiente al circuito principal de compresión de vapor. Algunos fabricantes, como Munters [4], emplean un sistema similar en sus equipos.

En las figuras 1a y 1b se observa la evolución del aire, mediante diagramas psicrométricos, tras ser tratado por los diferentes elementos que componen los sistemas híbridos DX-DW y DX-DX-DW, respectivamente.

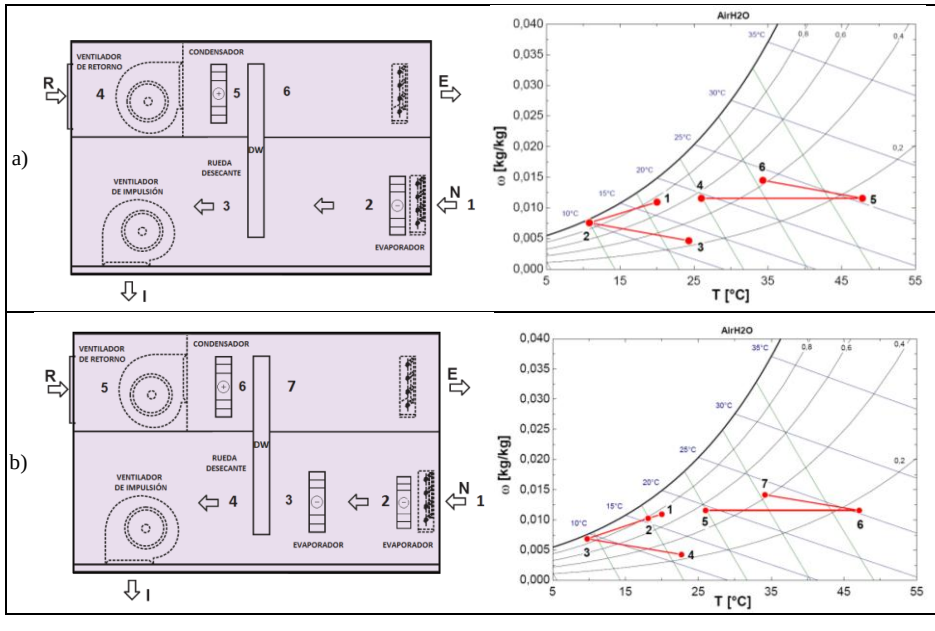

Figura 1. Configuración de los sistemas híbridos y diagramas psicrométricos a) DX-DW b) DX-DX-DW.

En este trabajo se ha desarrollado un modelo numérico para el estudio de sistemas híbridos. El modelo numérico integra el modelado de sistemas de compresión de vapor así como el modelado de ruedas desecantes.

El modelado de los sistemas de compresión de vapor, se ha realizado a partir del modelo desarrollado por la empresa CIAT [5]. El sistema de compresión de vapor principal está diseñado para un caudal nominal de 4000 m3/h y una potencia frigorífica nominal de 23 kW, así como una potencia frigorífica nominal de 6,2 kW para el sistema de compresión de vapor de baja potencia.

El estudio del comportamiento de la rueda desecante ha sido estudiado por diversos autores [6-8]. Beccali [6] desarrolló un modelo con ecuaciones empíricas ajustadas a partir de correlaciones de datos experimentales, el cual permite obtener las variables de temperatura y humedad absoluta del aire a la salida del lado de proceso de una rueda desecante. Ruivo [8] investigó la viabilidad de un método de simulación simplificado para ruedas desecantes basado en el concepto de la eficiencia. En el presente trabajo se ha empleado un modelo de rueda desecante no lineal de funciones potenciales características desarrollado por Panaras [7]. Este modelo permite predecir la temperatura y humedad del aire de salida de proceso de la rueda desecante en un amplio rango de condiciones operativas.

El modelado de los sistemas híbridos DX-DW y DX-DX-DW ha sido implementados en el software EES [9].

Para la evaluación de los sistemas híbridos se ha realizado con los siguientes parámetros:

- Coeficiente de eficiencia energética, EER, en modo refrigeración.

$$EER = \frac{PF_T}{PA_T} \quad [1]$$

Siendo,

$$PF_T = PFS_T + PFL_T \quad [2]$$

$$PFS_T = PFS_{DX} + PFS_{DW} \quad [3]$$

$$PFL_T = PFL_{DX} + PFL_{DW} \quad [4]$$

$$PA_T = PA_{DX} + PA_{vent,imp} + PA_{vent,exp} \quad [5]$$

- Factor de calor sensible, SHR, definido como la relación del calor sensible con respecto al calor total, siendo este último la suma de los calores sensible y latente.

$$SHR = \frac{|PFS_T|}{|PFS_T| + |PFL_T|} \quad [6]$$

Este parámetro representa el factor de calor sensible del equipo, es decir, la evolución que sigue el aire desde que entra en el equipo hasta que es impulsado hacia el local. Valores de SHR cercanos a cero corresponden a un equipo que debe emplearse para un local con una elevada carga latente, es decir grandes necesidades de deshumectación. Valores de SHR cercanos a uno, corresponden a un equipo el cual debe emplearse para un local con una elevada carga sensible.

- La capacidad desecante, MRC, o flujo másico de agua condensada producida por los elementos que componen al sistema híbrido, batería de frío, DX y rueda desecante, DW.

$$MRC = \rho_{imp} \cdot \dot{V} \cdot \Delta\omega \quad [7]$$

Siendo,

$$MRC = MRC_{DX} + MRC_{DW} \quad [8]$$

E n primer lugar, se ha sido estudiado el comportamiento del sistema híbrido DX-DW en diferentes condiciones a partir del modelo desarrollado. Se ha estudiado la configuración del sistema DX-DW con regeneración por calor residual y del sistema DX-DW con regeneración del circuito de compresión de vapor.

Kosar [10] realizó un estudio de configuración para el modelo DX-DW con una regeneración activa de la rueda desecante aportada por el calor residual de un condensador, para una temperatura constante de 46 ºC. En el estudio de Kosar, se analizó la tendencia de SHR frente a EER al aumentar el caudal de aire de entrada al equipo.

Los resultados numéricos del modelo DX-DW con regeneración por calor residual han sido comparados con los obtenidos por Kosar [10], lo que ha permitido validar el modelo desarrollado. También se ha estudiado el sistema DX-DW para el caso en el que el calor de condensación del circuito de compresión de vapor es empleado para regenerar la rueda desecante. En ambos casos, se han empleado las condiciones de aire empleadas de Kosar [10], condiciones ARI [11], y los caudales de aire de 2500, 4000 y 5500 m^3/h.

En segundo lugar, se ha realizado un estudio de comportamiento de los sistemas híbridos DX-DW y DX-DX-DW, para diferentes condiciones del aire exterior, analizándose en cada caso SHR, EER y MRC, así como las potencias frigoríficas y potencias absorbidas. Las condiciones del aire exteriores del estudio se muestran en la tabla 1, para un caudal de aire de 4000 m^3/h.

Tabla 1. Condiciones del aire para el estudio de los sistemas híbridos.

Condiciones del aire	**Aire exterior**		**Aire interior**	
	T [ºC]	**HR [%]**	**T [ºC]**	**HR [%]**
A	20	75	26	55
B	25	70		
C	30	65		
D	35	60		

Resultados y discusión

- Validación del sistema DX-DW.

En la tabla 2 se muestran los resultados de las potencias frigoríficas sensibles, latentes y totales de la batería evaporadora y rueda desecante, para el modelo de Kosar y los dos casos estudio del modelo DX-DW. El primer caso del modelo DX-DW se realiza para una regeneración de la rueda a temperatura constante, y el segundo con temperaturas de regeneración variables, obtenidas con el calor del ciclo de compresión de vapor, DX. A partir de estas potencias, se han obtenido los parámetros SHR y EER del sistema híbrido.

Tabla 2. Cargas del sistema Kosar y DX-DW para temperatura de regeneración constante y variable.

Modelos	$\dot{V}$	**PFS [kW]**			**PFL [kW]**			**PF_T [kW]**			**EER**	**SHR**
	[m^3/h]	**DX**	**DW**	**Total**	**DX**	**DW**	**Total**	**DX**	**DW**	**Total**		
Kosar	2500	18,14	-6,29	11,85	12,12	3,94	16,06	30,26	-2,35	27,91	2,71	0,42
	4000	21,74	-10,54	11,20	10,24	7,39	17,63	31,99	-3,15	28,84	2,61	0,39
	5500	25,56	-15,16	10,40	8,16	11,05	19,21	33,72	-4,11	29,61	2,50	0,35
DX-DW (T_{reg} constante)	2500	14,92	-5,84	8,82	8,63	4,00	12,73	23,55	-1,84	21,55	3,05	0,41
	4000	18,39	-9,93	8,25	7,00	7,58	14,7	25,39	-2,35	22,95	2,80	0,36
	5500	21,12	-13,71	7,42	5,22	10,84	16,06	26,34	-2,87	23,47	2,51	0,32
DX-DW (T_{reg} variable)	2500	14,92	-9,72	5,20	8,63	7,75	16,38	23,55	-1,97	21,58	3,03	0,26
	4000	18,39	-12,62	5,77	7,00	10,77	17,77	25,39	-1,88	23,51	2,84	0,27
	5500	21,12	-14,40	6,68	5,22	12,62	17,84	26,34	-1,82	24,52	2,62	0,29

La relación entre el SHR y el EER del sistema DX-DW al aumentar el caudal de aire se representan gráficamente en la figura 2 para temperatura de regeneración constante y variable. En el caso de temperatura de regeneración constante, se observa que el aumento del caudal de aire de entrada en el sistema híbrido DX-DW, reduce el SHR, a pesar de que la deshumidificación del sistema completo es menor. Esto es debido al incremento de la capacidad desecante de la rueda, al aumentar el caudal de aire y permanecer constante la temperatura de regeneración.

La reducción del SHR va acompañada de una disminución del EER, debido al incremento del consumo de energía de los sistemas de deshumectación y ventiladores instalados. Kosar [10] tras realizar su estudio, obtuvo una tendencia del SHR frente al EER similar a la obtenida en el presente trabajo, por lo que, el sistema DX-DW queda validado con resultados obtenidos por similares estudios.

Si la rueda desecante del sistema DX-DW es activada térmicamente mediante el calor de condensación correspondiente al ciclo de compresión de vapor, DX, la temperatura de regeneración varía. En este caso el parámetro SHR sigue una tendencia inversa a la obtenida con temperatura de regeneración constante. Esto es debido a que una temperatura de regeneración más baja reduce la deshumectación del aire en la rueda desecante. Los resultados se muestran en la figura 2.

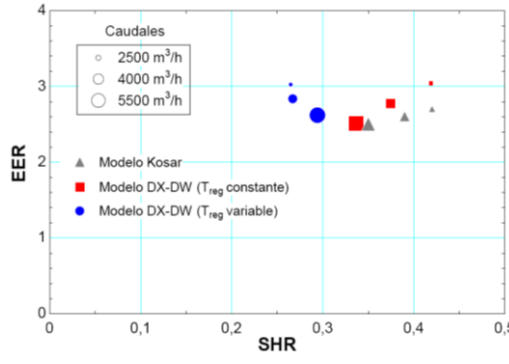

Figura 2. Comparativa SHR-EER del modelo de Kosar [10] para temperatura de regeneración constante; modelo DX-DW para temperatura de regeneración constante; y modelo DX-DW para temperatura de regeneración variable.

- Estudio de los sistemas híbridos DX-DW y DX-DX-DW.

Se ha obtenido el comportamiento de los sistemas híbridos DX-DW y DX-DX-DW para las condiciones del aire mostradas en la tabla 1. Los resultados se muestran en la tabla 3.

Tabla 3. Resultados de los sistemas híbridos DX-DW y DX-DX-DW.

Sistema híbrido	Condición del aire	T_{imp} [°C]	ω_{imp} [g/kg]	PF_T [kW]	PFS_T [kW]	PA_T [kW]	MRC [kg/h]	EER	SHR
DX-DW	**A**	24,31	4,64	15,02	6,38	8,10	29,76	1,85	0,23
	B	29,67	6,07	19,35	6,92	8,27	36,28	2,34	0,21
	C	35,06	7,92	23,83	7,51	8,43	42,98	2,83	0,19
	D	40,39	10,24	28,42	8,01	8,58	49,65	3,31	0,18
DX-DX-DW	**A**	22,68	4,27	18,53	4,17	10,03	31,69	1,85	0,15
	B	27,94	5,56	23,41	4,59	10,27	38,85	2,28	0,14
	C	33,26	7,25	28,47	5,10	10,49	46,30	2,71	0,13
	D	38,55	9,39	33,67	5,58	10,70	53,78	3,15	0,12

En la tabla 3, se observa que el aire con menor humedad absoluta se obtiene en las condiciones A, dado que las condiciones exteriores son menos húmedas. Sin embargo, la mayor eliminación de humedad se produce para las condiciones D, reduciéndose hasta 11,21 g/kg la humedad exterior con el sistema DX-DW y 12,10 g/kg con el sistema DX-DX-DW. Esto se debe a que la rueda desecante aprovecha su capacidad deshumectadora en condiciones exteriores húmedas. En las figuras 3a y 3b se puede observar la evolución del aire mediante diagramas psicrométricos, para los sistemas híbridos DX-DW y DX-DX-DW, respectivamente, para todos los casos a estudio.

La deshumectación del aire exterior con los dos sistemas híbridos fue muy elevada. Sin embargo, se obtuvieron temperaturas del aire de impulsión elevadas, ver figuras 3a y 3b. Estas temperaturas del aire de impulsión no resultan adecuadas para locales con necesidades de refrigeración. El mayor incremento de temperatura se produjo en las condiciones D, con diferencias entre el aire exterior y el aire de impulsión de hasta 5,4 y 3,5 ºC, en los sistemas DX-DW y DX-DX-DW, respectivamente.

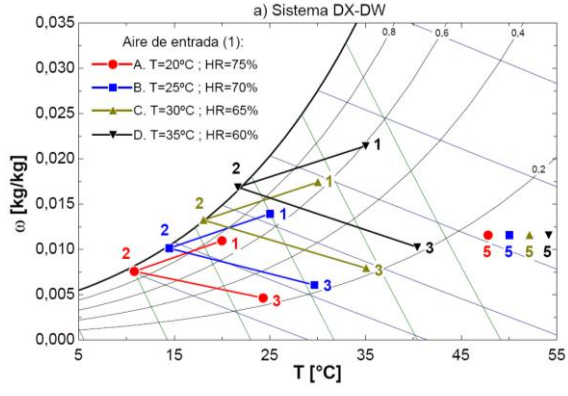

Figura 1. Gráficos psicrométricos de los sistemas híbridos a) DX-DW b) DX-DX-DW, para las diferentes condiciones estudiadas.

Analizando los resultados obtenidos de las potencias frigoríficas totales, PF_T, ver tabla 3, se observa que al aumentar la temperatura y humedad absoluta del aire exterior se incrementa PF_T. Debido a que, en dichas condiciones las diferencias de temperaturas y humedades absolutas entre el aire exterior y el aire de impulsión son mayores, produciéndose unas diferencias máximas del 45 y 47 % para el sistema DX-DW y DX-DX-DW, respectivamente, entre las condiciones del aire A y D.

Las potencias absorbidas totales, PA_T, de los sistemas híbridos se mantienen aproximadamente constantes para las diferentes condiciones de aire exterior, con diferencias menores del 6%. El aumento de la potencia absorbida en el sistema DX-DX-DW frente al sistema DX-DW, es producido por las pérdidas de carga del sistema de compresión de vapor de baja potencia añadido.

Para el cálculo de la capacidad desecante, MRC, se ha considerado como referencia las condiciones del aire exterior. En la tabla 3, se observa que el mayor MRC se produjo para las condiciones D, condiciones de aire exterior con alta temperatura y alta humedad. Se observa que el valor de MRC es mayor cuando aumenta la diferencia de temperatura y humedad entre el aire de entrada y de salida. Se obtiene un incremento máximo de 7,6 % en el valor de MRC del sistema DX-DX-DW respecto al sistema DX-DW, para las condiciones estudiadas.

Analizando los resultados de SHR, se observa que los valores obtenidos son cercanos a cero, por lo que, estos sistemas son adecuados para climatizar locales con grandes necesidades de deshumectación. Se ha obtenido un valor mínimo de SHR de 0,12, con el sistema DX-DX-DW.

El sistema DX-DX-DW presenta un EER menor que el sistema DX-DW, dado que se suman las pérdidas de carga producidas por el circuito de compresión de vapor de baja potencia. No obstante, el incremento de MRC con el sistema DX-DX-DW es mayor que la reducción del EER. La disminución del EER con el sistema DX-DX-DW frente al sistema DX-DW es de 4,8%, en las condiciones D, mientras que el aumento de MRC es de 7,6% para el mismo caso a estudio.

Conclusiones

En este trabajo se ha analizado y comparado dos modelos híbridos en distintas condiciones operativas. Se han analizado las relaciones entre el SHR y el EER de sistemas híbridos y se han explorado las posibilidades que presentan los sistemas híbridos para reducir el SHR, analizando el impacto sobre el EER. Los resultados obtenidos permiten alcanzar las siguientes conclusiones:

- Se ha integrado un modelo simplificado de rueda desecante en dos modelos de sistemas híbridos para la climatización de un local, que incluyen sistemas de compresión de vapor. Al integrar la rueda desecante se reduce el contenido de humedad absoluta del aire de impulsión en todos los casos a estudio. Sin embargo, las temperaturas del aire de impulsión son elevadas, debido al calentamiento del aire tratado por la rueda desecante. El modelo DX-DX-DW integra un segundo sistema de compresión de vapor de baja potencia, que permite reducir la temperatura del aire de impulsión.
- Con los modelos híbridos estudiados se obtiene valores bajos del factor de calor sensible, SHR. La mayor reducción del SHR se produce con el modelo DX-DX-DW, con valores cercanos a cero, por lo que, estos sistemas son adecuados para climatizar locales con altas cargas latentes, es decir, locales con grandes necesidades de deshumectación.
- La mayor penalización del EER se produce en el sistema DX-DX-DW. Este sistema reduce su EER hasta un 4% más frente al sistema DX-DW. Sin embargo, es posible aumentar la capacidad desecante, MRC, del sistema DX-DX-DW, hasta un 7% por encima del sistema DX-DW.

En consecuencia, los sistemas híbridos constituyen una alternativa para realizar el tratamiento de aire en locales con altas cargas latentes. La reducción del SHR y su impacto sobre el EER debe valorarse en cada caso y su análisis detallado será objeto de futuros trabajos.

Referencias

1. Sand, J.R. and J.C. Fischer, Active desiccant integration with packaged rooftop HVAC equipment. Applied Thermal Engineering, 2005. 25(17-18): p. 3138-3148.
2. Harriman III, L.G., The dehumidification handbook, 2nd ed. . Munters Corporation, Amesbury, MA., 2003.
3. Center, A.G.C.C.A.G.C., Applications Engineering Manual for Desiccant Systems, in Arlington. 1996.
4. Munters. http://www.munters.es/es/es/. Consulta: 14 Enero 2014.
5. CIAT. http://www.grupociat.es/. Consulta: 14 Febrero 2014.
6. Beccali, M., Butera, F., Guanella, R. and Adhikari, R. S. Simplified models for the performance evaluation of desiccant wheel dehumidification. International Journal of Energy Research, 2003. 27(1): p. 17-29.
7. Panaras, G., Mathioulakis, E., Belessiotis, V. and Kyriakis, N., Experimental validation of a simplified approach for a desiccant wheel model. Energy and Buildings, 2010. 42(10): p. 1719-1725.
8. Ruivo, C.R., Carrillo-Andres, A., Costa, J. J. and Dominguez-Munoz, F., Exponential correlations to predict the dependence of effectiveness parameters of a desiccant wheel on the airflow rates and on the rotation speed. Applied Thermal Engineering, 2013. 51(1-2): p. 442-450.
9. EES, Enginering Equation Solver. 2013, Klein S.A.
10. Kosar, D., Dehumidification system enhancements. Ashrae Journal, 2006. 48(2): p. 48-+.
11. Air-Conditioning & Refrigeration Institute, Unitary Air-Conditioning and Air-Source Heat Pump Equipment, in Standard 210/240. 2005.

Appendix F

Application of the DOE technique to the modelling of desiccant wheels for hybrid HVAC systems

The paper presented in this appendix is published in the *Scientific Congress of Researchers in Training*, Cordoba, Spain, 2014.

UNIVERSIDAD D CORDOBA

APLICACIÓN DEL DOE AL MODELADO DE RUEDAS DESECANTES PARA SISTEMAS HÍBRIDOS DE CLIMATIZACIÓN

IV Congreso Científico de Investigadores en Formación

Departamento de Química Física y Termodinámica Aplicada, EPS, Leonardo Da Vinci, Campus de Rabanales, 14014 Córdoba

Comino Montilla F., Ruiz de Adana Santiago M.

1. Objetivos: Desarrollar un modelo matemático para una rueda desecante

- Análisis de los distintos modelos matemáticos empleados por distintos autores en los últimos años
- Desarrollar un nuevo modelo matemático que represente adecuadamente el comportamiento de ruedas desecantes
- Análisis comparativo de todos los modelo matemáticos estudiados, seleccionando el modelo con mejor precisión.

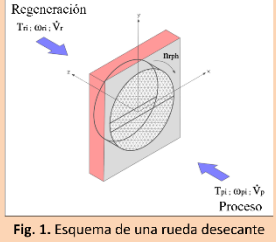

Fig. 1. Esquema de una rueda desecante

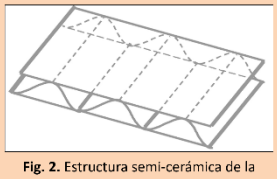

Fig. 2. Estructura semi-cerámica de la rueda desecante

2. Material y métodos

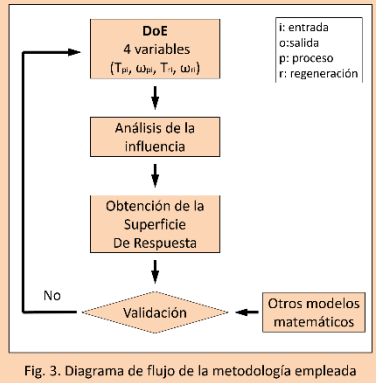

Fig. 3. Diagrama de flujo de la metodología empleada

Diseño de experimentos:
- Diseño de Box-Behnken (27 ensayos)
- Entradas: Tpi, ωpi, Tri y ωri
- Salidas: Tpo y ωpo

Herramientas empleadas:
- Ecodry
- Statgraphics
- EES

Parámetros de validación:
- ΔT y Δω (modelo vs Ecodry)
- RMSET y RMSEω

3. Principales aportaciones

- Los modelos basados en la eficiencia presentan ventajas, sin embargo es necesario un gran número de ensayos.
- Con el DoE se ha obtenido un modelo matemático con una precisión muy buena y número de ensayos reducido.
- Con el modelo del DoE se obtiene errores más pequeños frente al resto de modelos, con RMSET y RMSEω inferiores al 90 %.

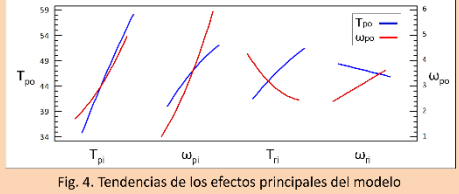

Fig. 4. Tendencias de los efectos principales del modelo

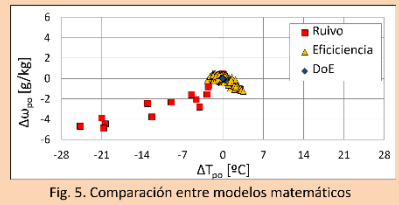

Fig. 5. Comparación entre modelos matemáticos

4. Principales referencias

- Panaras, G., Mathioulakis, E., Belessiotis, V., y Kyriakis, N., Theoretical and experimental investigation of the performance of a desiccant air-conditioning system. Renewable Energy, 2010. 35(7): p. 1368-1375.
- Ruivo, C.R., Carrillo-Andres, A., Costa, J.J., y Dominguez-Munoz, F., A new approach to the effectiveness method for the simulation of desiccant wheels with variable inlet states and airflows rates. Applied Thermal Engineering, 2013. 58(1-2): p. 670-678.

Appendix G

Design and building of a test facility for experimentation of desiccant wheels

The paper presented in this appendix is published in the *IX National Congress Engineering Thermodynamics*, Cartagena, Spain, 2015: pp. 295–302.

DISEÑO Y CONSTRUCCIÓN DE UNA PLANTA EXPERIMENTAL PARA LA EXPERIMENTACIÓN DE RUEDAS DESECANTES

COMINO MONTILLA, Francisco [(1)]; RUIZ DE ADANA SANTIAGO, Manuel [(1)]

CEREZUELA PARISH, Adoración [(2)]; ZAMORA GARCÍA, Miguel [(2)]; PECI LÓPEZ, Fernando [(1)]

p72comof@uco.es

[(1)]Universidad de Córdoba, Escuela Politécnica Superior, Departamento de Química Física y Termodinámica Aplicada

[(2)]CIAT, Departamento de I+D+i. Pol. Llanos de Jarata s/n. 14550 Montilla, Córdoba, España.

RESUMEN

La información comercial disponible de ruedas desecantes es limitada en muchos casos. Sin embargo, el diseño de algunos sistemas de tratamiento de aire requiere un conocimiento detallado del comportamiento de las ruedas desecantes bajo distintas condiciones operativas.

En este trabajo, se presenta el diseño y construcción de una planta experimental para el ensayo de ruedas desecantes. La planta experimental se compone de unidades de tratamiento de aire así como equipos humidificadores. Un sistema de monitorización permite hacer un seguimiento de los parámetros relevantes de funcionamiento, como caudal de aire, temperatura y humedad.

El trabajo recoge resultados de las pruebas de servicio realizadas para la puesta en funcionamiento de todos los equipos que componen la planta experimental. Estas pruebas analizan los consumos eléctricos, los caudales de aire para diferentes situaciones de trabajo, la capacidad térmica de los equipos o el sistema de control de temperatura y humedad del aire.

La planta experimental permite ensayar ruedas desecantes en distintas condiciones de funcionamiento. Los resultados experimentales permiten obtener información relevante a partir de la cual se realiza la caracterización de ruedas desecantes.

Palabras clave: deshumidificación, rueda desecante, planta experimental.

1. Introducción

El objetivo principal de un sistema climatización es proporcionar unas condiciones ambientales adecuadas para obtener el confort térmico. En regiones cálidas y húmedas del sur de Europa, como ciudades próximas al mar Mediterráneo, el consumo eléctrico en verano es muy elevado, debido a las condiciones climáticas exteriores y a la enorme población turística, siendo muy importante los costos de operación de los sistemas de aire acondicionado, por lo que, es necesario realizar una buena elección del sistema de climatización. En el ámbito de la climatización de edificios, las aportaciones latentes procedentes del aire exterior o del propio local producen un incremento en el contenido de vapor de agua del aire, por lo que es necesario emplear sistemas para reducir y controlar la humedad absoluta del aire.

Nomenclatura

HR	Humedad relativa [%]
P	Presión [mbar]
RMSE	Raíz cuadrada del error cuadrático medio
T	Tiempo [s]
T	Temperatura [ºC]
T_r	Temperatura de rocío [ºC]
V	Tensión eléctrica [V]
W	Potencia eléctrica [kW]
ZN	Zona neutra

Símbolos griegos

Δ	Diferencial
ω	Humedad absoluta [g/kg]

Los sistemas de deshumidificación basados en sistemas desecantes, atraen la humedad del aire creando un área de baja presión de vapor de agua en la superficie del desecante. Debido a la diferencia entre la presión parcial de vapor de agua en el aire y la existente en la superficie del desecante, las moléculas de agua se mueven desde el aire al desecante, de forma que el aire se deshumidifica. La corriente de aire que se desea deshumidificar se denomina aire de proceso. Los sistemas desecantes requieren emplear una energía para regenerar el desecante, eliminando la humedad del desecante. Esta energía de reactivación o regeneración permite extraer la humedad del desecante para poder iniciar un nuevo ciclo desecante.

La rueda desecante es un equipo de deshumidificación de aire, el cual consta de una rueda giratoria que contiene una estructura semi-cerámica, similar a cartón corrugado, que se integra en la forma de la rueda, figura 1. La rueda gira lentamente, típicamente entre 10 y 40 rph, intercambiando humedad entre las corrientes de aire de proceso y aire de regeneración.

Diversos trabajos de investigación experimentales y numéricos han sido realizados para la caracterización de los parámetros de funcionamiento que influyen en el comportamiento global de las ruedas desecantes [1][2][3]. Sin embargo, los enfoques adoptados en la mayoría de los trabajos no son muy prácticos.

En otros trabajos de investigación se han desarrollado modelos matemáticos empíricos [4][5][6], los cuales estiman el comportamiento de las ruedas desecantes. Sin embargo, los modelos matemáticos hay que interpretarlos como una aproximación a los resultados reales de funcionamiento de la rueda desecante, siendo válidos para los rangos de las variables que fueron validados.

Dada la falta de datos experimentales para el estudio de comportamiento de la rueda desecante, resulta adecuada la construcción de una planta experimental, con la cual estudiar empíricamente los procesos de transferencia de calor y masa entre la superficie de la rueda desecante y las corrientes de aire que pasan por la rueda.

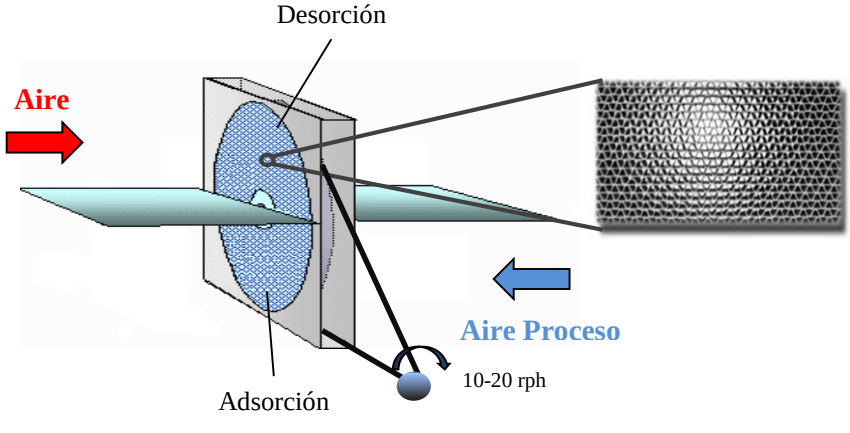

Figura 1: Esquema de una rueda desecante.

2. Objetivo

El objetivo general de este trabajo es el montaje, instalación, puesta a punto y control de la planta experimental, la cual permita una caracterización de la rueda desecante, determinando su comportamiento.

3. Configuración general experimental

En la figura 2 se muestra un esquema del diagrama de la planta experimental. Se aplicó un diseño de contraflujo entre dos corrientes de aire a través de una rueda desecante. Dos circuitos de aire fueron construidos con chapa galvanizada, aislados térmicamente con una manta termo acústica de fibra de vidrio y revestido de un velo negro, para simular las condiciones de aire de proceso y aire de regeneración.

Para simular las ganancias sensibles y latentes del aire de proceso y aire de regeneración, en la planta experimental se ha instalado componentes que realizan el tratamiento del aire para adecuarlo a las condiciones requeridas, en temperatura, humedad y caudal del aire. Los elementos que forman ambos sistemas de aire proceso y aire de regeneración son una unidad de tratamiento de aire, UTA, y un humidificador isotérmico. La UTA, consta de

ventilador de impulsión y retorno, baterías de agua fría y/o caliente, además, se compone de una resistencia eléctrica de postcalentamiento. Los humidificadores instalados en la planta experimental son equipos que producen vapor no presurizado por medio de elementos resistivos inmersos en agua contenida en un calderín, hasta alcanzarse la temperatura de ebullición. El vapor producido es distribuido en el aire que circula por los conductos de la instalación mediante una lanza de distribución de vapor.

La rueda desecante se ubica en una carcasa con juntas de goma entre ambos lados de proceso y regeneración, accionada por un motor de velocidad constante a través de un engranaje. Los canales de la rueda desecante, en forma de panal de abeja, están compuestos de fibra de vidrio recubiertos con silica gel. La rueda desecante se caracteriza con una relación de áreas 50% de flujo de aire de proceso y 50 % de flujo de aire de regeneración. Algunos de los detalles de diseño pertenecientes a la rueda se muestran en la tabla 1.

Cuatro ventiladores centrífugos de velocidad variable fueron instalados, dos aguas abajo y dos aguas arriba, con los cuales se regula la velocidad de flujo de aire. Para variar la velocidad del aire en la instalación, los ventiladores disponen de un potenciómetro, el cual permite variar la tensión eléctrica del ventilador. Además, para lograr mayor estabilidad del flujo de aire, se ha instalado en los conductos cuatro acondicionadores de flujo, un acondicionador antes de cada punto de medida de caudal y otro acondicionador después. Estos elementos reducen las distorsiones de flujo de aire que se produce tras pasar por los diferentes equipos que compone la planta.

La instalación experimental está compuesta de dos cajas de mezcla, las cuales permiten la recirculación de ambas corrientes de aire, o bien, la expulsión del aire tratado y/o la entrada del aire nuevo. Asimismo, las cajas permiten la mezcla del aire exterior con el aire tratado por la planta experimental, en el porcentaje de aire requerido. Las cajas de mezclan están instaladas después de los elementos de tratamiento de aire, tanto en proceso como en regeneración.

Tabla 1: Especificaciones de la rueda desecante.

Parámetros	**Valores**
Diámetro del rotor	550 mm
Anchura	200 mm
Material desecante	Silica-gel
Forma del canal	Panal de abeja
Capacidad desecante nominal	15 kg/h
Caudal nominal	2300 m^3/h
Velocidad del rotor	42 rph
Peso	57 kg
Potencia	1x230 V – 50/60 Hz

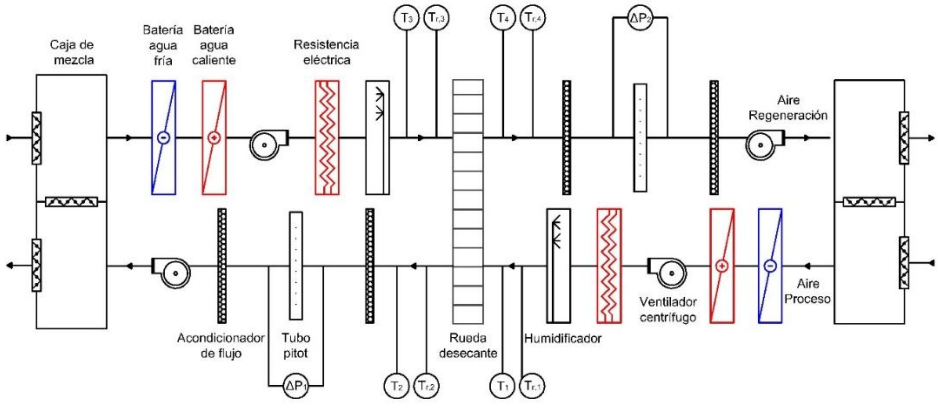

Figura 2: Esquema de la planta experimental y su instrumentación.

4. Sistema de control

El sistema de control empleado en la planta experimental controla las variables temperatura y humedad del aire a la salida en los sistemas de aire proceso y regeneración, estados 1 y 3, respectivamente, ver figura 2. En la figura 3, se muestra mediante un diagrama de bloques la estrategia del sistema de control para obtener las condiciones deseadas del aire de salida, siendo la posición de las electroválvulas instaladas en las baterías de calefacción y refrigeración, la potencia eléctrica de las resistencias eléctricas y la potencia eléctrica de los humidificadores, las variables de control.

El controlador empleado permite la gestión de las unidades de tratamiento de aire, mediante la conexión de sondas de temperatura y humedad.

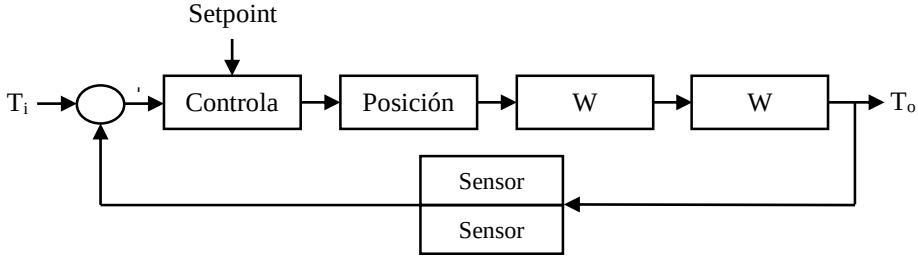

Figura 3: Diagrama de la estrategia del sistema de control.

5. Instrumentación y monitorización de datos

La planta experimental dispone de un sistema de monitorización, el cual permite hacer un seguimiento de los valores recopilados por todos los sensores y realizar un posterior análisis. En la tabla 3 se recoge la instrumentación de medida que se emplea en la instalación experimental, indicándose el tipo de sonda y su incertidumbre de medida. La instrumentación empleada son sondas de temperatura PT100, sondas de temperatura de rocío de espejo frío y capacitivo, y un transmisor de presión diferencial, con el cual se mide el caudal que circula en el sistema experimental a su paso por los tubos de Pitot.

Tabla 2: Especificaciones de los sensores.

Sondas	**Tipo**	**Incertidumbre de medida**
T	PT 100	± 0,12 ºC
T_r1	Espejo frío	± 0,15 ºC
T_r2	Capacitivas	± 0,4 ºC
HR	0-100%	± 3 %
ΔP	Trans. presión diferencia	± 0,3 % (0 a 1 mbar)

Para el sistema de monitorización se dispone de una interfaz para visualizar los datos capturados en la pantalla del ordenador. Este nos permite obtener estadísticas, gráficas o realizar consultas de un historial de datos.

Debido a las dimensiones de la planta experimental, los tramos de conductos de aire que conectan elementos de tratamiento de aire corresponden a tramos de conductos de longitud reducida. Estos tramos de conductos de poca longitud, pueden condicionar la homogeneización de las condiciones del aire después de su paso por los elementos de tratamiento de temperatura, baterías, y tratamiento de humedad, humidificadores. Por este motivo, se han instalado soportes metálicos en las estaciones de medida, que permiten desplazar las sondas en sentido horizontal. Este sistema permite realizar la medición de las condiciones del aire a diferentes distancias del eje horizontal.

Para garantizar y verificar el buen funcionamiento de los equipos de medida es necesario su calibración. El procedimiento de calibración permite determinar el estado operacional de los sensores durante el periodo de funcionamiento. En el presente trabajo solo se han calibrado las sondas de temperatura de aire seco, dado que, para el resto de instrumentación el fabricante ha facilitado un certificado de calibración de sondas.

6. Metodología

Con el propósito de obtener las capacidades operativas y asegurar la obtención de resultados experimentales fiables, se ha seguido la metodología mostrada en la tabla 4 para la puesta en marcha de la planta piloto.

En primer lugar se han calibrado las sondas empleadas, y se han instalado y probado. Todas las sondas de medida están conectadas externamente a un equipo de registro de datos, que permite registrar la información de todas las sondas en un equipo informático para su posterior corrección, análisis y postprocesado. A continuación, se ha realizado las pruebas correspondientes al análisis de capacidad y control de los equipos que componen la planta experimental. Para ello, los equipos se prueban en diferentes condiciones de funcionamiento, variando la temperatura, humedad y caudal del aire. Con estas pruebas, la planta experimental está en condiciones de realizar la caracterización de la rueda desecante.

Tabla 3: Metodología para la puesta en marcha de la planta experimental.

Pasos		**Ensayos**
Calibración e instalación de las sondas		
Sondas	1	Temperatura (PT100)
	2	Humedad (Punto de rocío)
	3	Humedad (Espejo frío)
	4	Caudal (Transmisor de Presión Diferencial)
Capacidad y control de los equipos		
Equipos	5	Baterías agua fría UTA
	6	Baterías agua caliente UTA
	7	Resistencias UTA
	8	Humidificadores
Estudio completo		
Climatización	9	Rueda desecante

7. Pruebas de servicio

7.1. Consumo eléctrico

El consumo eléctrico de los elementos que componen la planta experimental se registra mediante un analizador de redes. Este instrumento permite una medida programable y un registro de los parámetros eléctricos en una red monofásica y trifásica. La aplicación principal del analizador de redes en esta planta experimental es un estudio de las potencias eléctricas consumidas en los equipos que la componen, mediante la medición de la intensidad y tensión de corriente.

7.2. Caudal de aire

La instalación está compuesta de 4 ventiladores centrífugos de caudal variable. El ajuste de la velocidad de cada ventilador permite disponer en la planta experimental de un determinado caudal de aire. Se han determinado los caudales de aire que circulan por la planta experimental en dos condiciones de funcionamiento. En primer lugar, cuando la instalación trabaja con todo aire exterior, expulsando e impulsando todo el aire atmosférico. Para este caso el acoplamiento se produce con 2 ventiladores en el lado de proceso y 2 ventiladores en el lado de regeneración. El segundo caso, cuando la instalación trabaja con aire en recirculación, circulando todo el tiempo el mismo aire en la planta. De esta manera se acoplan los 4 ventiladores. En la tabla 5 se muestra los caudales de aire obtenidos para ambas pruebas, así como sus respectivos RMSE.

Tabla 4: Rangos de los caudales de aire en la planta experimental.

	Tensión [V]	**Aire de proceso**		**Aire de regeneración**	
		Caudal [m^3/h]	RMSE [m^3/h]	Caudal [m^3/h]	RMSE [m^3/h]
Todo aire exterior	Máxima	2088,21	± 31,23	1670,88	± 34,81
	Mínima	1216,49	± 15,38	1040,99	± 20,01
Aire en recirculación	Máxima	2142.11	± 35,63	2142.11	± 38,59
	Mínima	1096.28	± 9,71	1096.28	± 16,79

7.3. Capacidad de los equipos de climatización

En la tabla 5 se muestra los rangos de temperatura y humedad absoluta del aire que pueden mantenerse de forma continua y estable en la planta experimental, para la corriente de aire de proceso y aire de regeneración. Estos rangos han sido obtenidos para el caudal máximo de aire que circula en la planta experimental, expuesto en la tabla 4. Los valores máximos alcanzados para aire de proceso son 35ºC y 31 g/kg, y los valores mínimos 15ºC y 8,5 g/kg. En el caso del aire de regeneración, los valores máximos alcanzados son 45 ºC y 31 g/kg, y los valores mínimos 29 ºC y 9 g/kg, ver figura 4.

Tabla 5: Rangos de trabajo de temperatura y humedad absoluta del aire en la planta experimental.

Capacidad	**Aire de proceso**		**Aire de regeneración**	
	T [ºC]	ω [g/kg]	T [ºC]	ω [g/kg]
Máxima	35	31	45	31
Mínima	15	8,5	26	9

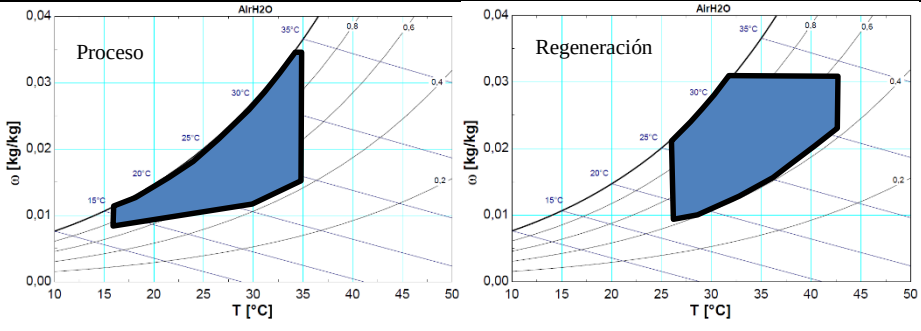

Figura 4: Rangos de trabajo para a) sistema de proceso; b) sistema de regeneración.

7.4. Control de temperatura y humedad del aire

Debido a la dependencia de la humedad relativa del aire con la temperatura, en primer lugar, se realiza la regulación de la temperatura del aire, y a continuación, el control de la humedad del aire.

El equipo de control permite la programación de diferentes tipos de regulación. Para el control de la temperatura y humedad, se ha empleado un control PID. En la tabla 6 se muestra la configuración de la regulación para ambos parámetros con el objetivo de conseguir la máxima estabilidad en temperatura y humedad relativa. El procedimiento seguido para obtener dicha configuración fue la realización de múltiples ensayos variando los parámetros de control, como el diferencial de calor y frío, la zona neutra de calor y frío o el tiempo integral y derivativo.

Configuración de control de temperatura y humedad absoluta del aire.

Variable	ZN calor	ZN frío	Δ calor	Δ frío	$t_{integral}$ [s]	$t_{derivativo}$ [s]
T [ºC]	0	0	6	5	1000	30
HR [%]	0	0	10	10	1000	40

Al analizar las tres acciones de la regulación, proporcional, integral y derivativo, se observa que el tiempo de la acción integral seleccionado es muy alto, dado que el tiempo de actuación de los elementos de regulación es muy elevado (hasta 80 s las electroválvulas de las baterías).

La acción integral genera una corrección proporcional a la integral del error y asegura que aplicando un esfuerzo de control suficiente el error de seguimiento se reduce al mínimo. Sin embargo, el tiempo necesario para la estabilidad es muy alto, habitualmente se requieren 40 minutos para alcanzar la estabilidad de la temperatura del aire. Las oscilaciones máximas generadas para la temperatura del aire son de ±0,35ºC, para el rango de temperatura de impulsión 15-45ºC.

Para la configuración de control de humedad seleccionada, las oscilaciones máximas de la humedad absoluta cuando se realiza la deshumectación del aire son muy pequeñas, ±0,75 g/kg. Sin embargo, las oscilaciones se incrementan cuando se realiza la humidificación del aire, dado que el tiempo de actuación de los humidificadores es muy alto. Las oscilaciones máximas de la humedad absoluta cuando se realiza la humidificación del aire son de ±2 g/kg. Para alcanzar dicha estabilidad del aire es necesario emplear 60 minutos.

8. Conclusiones

Del presente trabajo se extraen las siguientes conclusiones:

- Se ha diseñado y construido una planta experimental con la que se pueden realizar los ensayos necesarios para caracterizar el comportamiento de una rueda desecante.
- Con las pruebas de servicio realizadas se han establecido las condiciones de ensayo en la planta experimental. La planta experimental permite ensayar en rangos de temperatura de entre 15ºC a 45ºC, rangos de humedad absoluta de entre 8,5 a 31 g/kg y rangos de caudal del aire de entre 1100 a 2300 m^3/h, respectivamente.
- Con el sistema de control instalado en la planta, se obtiene una estabilidad de temperatura del aire de ±0,35 ºC, así como, una estabilidad de la humedad absoluta del aire de ± 2 g/kg. El tiempo medio necesario para alcanzar la estabilidad del aire es de 60 minutos.

Por tanto, la planta experimental permite realizar ensayos experimentales de ruedas desecantes en distintas condiciones de funcionamiento dentro de los rangos establecidos y en unas condiciones operativas de temperatura y humedad relativa muy estables. Los resultados experimentales permiten obtener información relevante a partir de la cual se realiza la caracterización de ruedas desecantes.

9. Agradecimientos

El presente trabajo es parte del proyecto DESSECA *Investigación en deshumectación y secado de aire*, promovido por la empresa CIAT y cofinanciado por la Agencia de Innovación y Desarrollo de Andalucía Expte. IDEA 360097 y por la Corporación Tecnológica de Andalucía Expte CTA 12/612. (2012-2014)

10. Referencias

[1] G. PANARAS, E. MATHIOULAKIS, y V. BELESSIOTIS, «Solid desiccant air-conditioning systems - Design parameters», ENERGY, vol. 36, n.o 5, pp. 2399-2406, may 2011.
[2] G. ANGRISANI, F. MINICHIELLO, C. ROSELLI, y M. SASSO, «Experimental analysis on the dehumidification and thermal performance of a desiccant wheel», Applied Energy, vol. 92, pp. 563-572, 2012.
[3] S. YAMAGUCHI y K. SAITO, «Numerical and experimental performance analysis of rotary desiccant wheels», International Journal of Heat and Mass Transfer, vol. 60, pp. 51-60, 2013.
[4] J. Y. SAN y S. C. HSIAU, «Effect of axial solid heta-conduction and mass diffusion in a rotary heat and mass regenerator», International Journal of Heat and Mass Transfer, vol. 36, n.o 8, pp. 2051-2059, 1993.
[5] C. R. RUIVO, J. J. COSTA, y A. R. FIGUEIREDO, «On the behaviour of hygroscopic wheels: Part I - channel modelling», International Journal of Heat and Mass Transfer, vol. 50, n.o 23-24, pp. 4812-4822, 2007.
[6] F. E. NIA, D. VAN PAASSEN, y M. H. SAIDI, «Modeling and simulation of desiccant wheel for air conditioning», Energy and Buildings, vol. 38, n.o 10, pp. 1230-1239, 2006.

Appendix H

Experimental study of the moisture removal capacity of a desiccant wheel activated at low and high temperature

The paper presented in this appendix is published in the *CLIMA 2016 - 12th REHVA World Congress*, Aalbor, Denmark, 2016.

EXPERIMENTAL STUDY OF THE MOISTURE REMOVAL CAPACITY OF A DESICCANT WHEEL ACTIVATED AT LOW AND HIGH TEMPERATURE

Francisco Comino[#1], Manuel Ruiz de Adana[#2], Fernando Peci[#3]

[#]Departamento de Química-Física y Termodinámica Aplicada, Escuela Politécnica Superior, Universidad de Córdoba, Campus de Rabanales, Antigua Carretera Nacional IV, km 396, 14072

[1]p72comof@uco.es

[2]manuel.ruiz@uco.es

[3]fernando.peci@uco.es

Abstract

Desiccant dehumidifiers can be combined with refrigeration vapour compression systems to reduce and control the humidity ratio in buildings and certain industrial processes. These combined systems are referred to as hybrid systems.

Many studies about hybrid systems with desiccant wheels, DW, have been carried out. In these hybrid systems, a significant energy consumption is required for thermally activate the DW.

The objectives of this piece of work are to determine empirically the main variables which influence the moisture removal capacity, MRC, of a DW activated at low and high temperature, and analyse the variability of these on MRC. In order to compare the results obtained for a DW activated at low and high temperature, a secondary objective is to obtain the theoretical cooling energy needed to achieve the supply air set conditions. In this paper, values below 60°C were considered as low regeneration temperatures for a DW and values above 60ºC were considered as high regeneration temperatures. The methodology used was based on the statistical technique of design of experiments, DOE, which allows to study the behaviour of DW with a reduced number of experimental tests.

The results showed a significant influence of the inlet humidity ratio of the air process and the air regeneration on MRC. Using high regeneration temperatures, the MRC values were found 61% higher than using low regeneration temperatures. However, high regeneration temperatures led to higher process air temperatures and thus more cooling energy was required to achieve the supply air set conditions.

Keywords - desiccant wheel; low temperature activated systems; dehumidification

1. Introduction

Controlling the humidity ratio content in the air is necessary to maintain the required indoor air conditions in buildings and certain industrial processes. Desiccant dehumidifiers can be combined with refrigeration vapour compression systems to reduce and control the humidity ratio in buildings. These combined systems are referred to as hybrid systems.

Many studies about hybrid systems with desiccant wheels, DW, have been carried out [1,2]. Desiccant wheels are usually activated thermally at temperatures above 60ºC. In a DW the desiccant material is heated by the regeneration air stream. The higher the temperature of the desiccant material, the easier moisture is removed, so the regeneration air temperature has a strong effect on performance [3]. Therefore, a significant energy consumption is required to regenerate the DW, and energy savings are usually obtained when the DW is regenerated using waste heat from other processes [4]. However, in some cases waste heat energy is not available or the corresponding temperature level is not adequate. Other studies have analysed the use of solar energy to regenerate a DW [5], but the solar thermal system involves a significant increase in the overall cost of the system.

Several studies integrated DW into hybrid systems operated at low regeneration temperatures reaching acceptable desiccant capacities [6,7]. A DW activated at low temperature could be integrated in refrigeration vapour compression systems in a building or industrial environment. In this paper, values below 60°C were considered as low regeneration temperatures and values above 60ºC were considered as high regeneration temperatures.

ASHRAE defines Moisture Removal Capacity (MRC) as a primary figure of merit for desiccant wheel performance, as reported in [8]. In previous studies the desiccant capacity was analysed through the MRC [9–11].

The objectives of this work are to determine empirically the main variables which influence the moisture removal capacity, MRC, of a DW activated at low and high temperature, and analyse the variability of these on MRC. In order to compare the results obtained for a DW activated at low and high temperature, a secondary objective is to obtain the theoretical cooling energy needed to achieve the supply air set conditions. To achieve these objectives an experimental hybrid system was built and several tests were carried out using the statistical technique of design of experiments, DOE.

2. Methodology

2.1. Experimental Setup

An experimental test rig was built to analyse the performance of DW under different working conditions. A schematic representation of the experimental setup is shown in Fig. 1. Process and regeneration air streams were configured in a countercurrent flow. The inlet temperature and humidity ratio of both process and regeneration streams were set using cooling and heating coils (CC, HC), an electric heater (EH) and a steam humidifier (SH) [12]. The process and regeneration airflow rates were set using variable speed fans (F). Two Pitot tubes (PT) were used to measure the airflow rate.

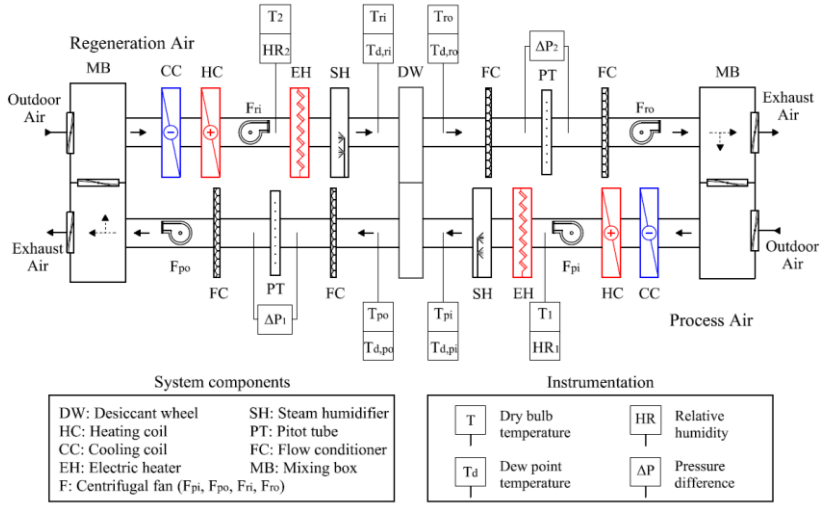

Fig. 1 Layout of test facility.

The DW is divided into two equal partitions and rotates at a constant speed of 42 rph. The matrix of the DW consists of alternate layers of flat and corrugated sheets of silica gel and metal silicates, chemically bonded into a tissue of inorganic fibres. Physical and operational characteristics of the DW are shown in Table 1.

Table 1. Characteristics of the desiccant wheel.

Parameters	Value	Unit
Rotor diameter	550	[mm]
Rotor length	200	[mm]
Desiccant material	Silica gel	
Channel shape	Honeycomb	
Nominal capacity	15	[kg h^{-1}]
Nominal air flow	2300	[m^3 h^{-1}]
Rotation speed	42	[rph]
Weight	57	[kg]
Power supply	230	[Vac]

The sensors locations are shown in Fig. 1. Temperature was measured using PT100 sensors, dew point temperature using chilled mirror hygrometer sensors, relative humidity using capacitive sensors, and pressure difference using pressure transmitter sensors [12]. All the experimental tests were carried out at steady-state conditions. The sampling time step was 3 s and the values were averaged every 20 min.

2.2. Design of Experiment

The statistical technique DOE was used to identify and analyze the influential variables on MRC of a DW [13,14]. The number of required experimental tests can be reduced if they are optimally designed. In this work, two case studies were carried out with four input variables: inlet air process temperature, Tpi, inlet air process humidity ratio, ωpi, inlet air regeneration temperature, Tri and inlet air regeneration humidity ratio, ωri. In case 1 low regeneration temperatures were considered, and in case 2 high regeneration temperatures were considered.

Two regression models were obtained from both case studies. Regression models illustrate the relationship between MRC and the set of process parameters.

In both case studies, the effect of the four input variables was studied applying a factorial design [13]. These designs were carried out defining two grids to cover the range of validity of the process and regeneration air streams, as shown in Fig. 2. Four inlet limit states for the process airflow were selected, P1 to P4, and an additional fifth inlet state P5 located inside the four-sided polygon previously defined. The regeneration inlet conditions were defined introducing another set of five points R1 to R5.

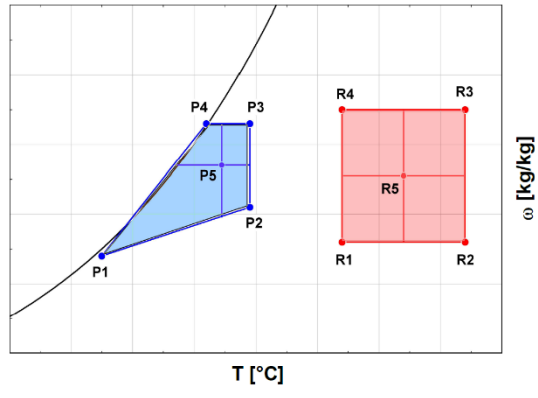

Fig. 2 Grid considered for the inlet states of the process and regeneration airflow for case studies 1 and 2.

The inlet process air flow temperature range was from 17.5 ºC to 29.5 °C, and the humidity range from 12 g·kg-1 to 21.5 g·kg-1 for both case studies. For the regeneration air stream, the inlet air humidity ratio range was also considered the same in both cases: from 13 g·kg-1 to 22.5 g·kg-1. However, the regeneration inlet air temperature ranges were different in each case. The case study 1 was carried out for low regeneration temperatures, from 34 to 42.5°C. The case study 2 was carried out for high regeneration temperatures, from 70 to 80°C, an increase of 60%. The air flow rate was set to 2100 m3/h in both process and regeneration air streams for all cases.

2.3. Process Air Cooling Energy

In order to obtain the theoretical energy needed to achieve the supply air set conditions in a building, two case studies for MRC maximum values were carried out. The first case was evaluated for usual summer air supply conditions, Tsupply=18 ºC and HRsupply=80 %. The second case was studied for usual winter air supply conditions, Tsupply=27 ºC and HRsupply=20 %.

3. Results and Analysis

3.1. Statistical Analysis

The results of the statistical analyses for the two case studies are summarized in Table 2. This table shows the main estimated effects, the standard error of each effect, the statistical parameter F-Ratio, and the statistical parameter P-value and the lack-of-fit test. Positive and negative effects on MRC for the different input variables were observed. All variables were found significant at 95% confidence level, as the P-values were lower than 0.05 in

all cases. The results for case studies 1 and 2 showed that the most influential variables on MRC were ωpi and ωri. Both design of experiments were also found to be suitable for the observed data at 95 % confidence level, as the P-values for lack-of-fit tests were greater than 0.05 in all cases.

Table 2. Effects of input variables on MRC.

Case study 1				
Effect	Estimate	Stnd. Error	F-Ratio	P-value
Average	4.91	0.11		
T_{pi}	-1.44	0.27	28.93	0.0329
ω_{pi}	3.66	0.22	273.74	0.0036
T_{ri}	0.85	0.12	48.30	0.0201
ω_{ri}	-3.91	0.12	1024.81	0.0010
	Lack-of-fit P-value: 0.9991			
Case study 2				
Effect	Estimate	Stnd. Error	F-Ratio	P-value
Average	16.31	0.08		
T_{pi}	-3.19	0.19	271.90	0.0037
ω_{pi}	4.79	0.15	904.05	0.0011
T_{ri}	1.93	0.08	478.45	0.0021
ω_{ri}	-2.25	0.08	654.88	0.0015
	Lack-of-fit P-value: 0.9727			

3.4. Regression Model

The results of the set of experiments were used to fit the parameters of a first order model expressed by Eq. (1):

$$\hat{Y} = a_0 + \sum_{i=1}^{k=1} \sum_{\substack{j=2 \\ j>i}}^{k} a_{ij} \cdot X_i \cdot X_j \qquad (1)$$

Where k is the number of parameters, ai…aij are the regression coefficients, showing the weight each one has in the equation, a0 is the average response in the design of experiments, Xi are the single input variables or their interactions, and Ŷ is the output variable, corresponds to MRC.

The models adjusted by regression of the data obtained from the experimental tests are shown in Table 3. These show the relationship between MRC and the set of process parameters. It can be observed that the parameters with the highest weight were a2 and a4, ωpi and ωri variables, respectively.

Table 3. Estimated parameters for case studies.

Estimated parameters	Xi	MRC ($x10^3$) of case 1 [kg h^{-1}]	MRC ($x10^3$) of case 2 [kg h^{-1}]
a_0	-	45719.00	12252.40
a_1	T_{pi}	146.52	260.75
a_2	ω_{pi}	-3017.17	698.15
a_3	T_{ri}	495.84	5.12
a_4	ω_{ri}	884.04	578.38
a_5	$T_{pi} \cdot \omega_{pi}$	45.87	13.55
a_6	$T_{pi} \cdot T_{ri}$	17.59	4.25
a_7	$T_{pi} \cdot \omega_{ri}$	20.42	5.45
a_8	$\omega_{pi} \cdot T_{ri}$	47.33	0.13
a_9	$\omega_{pi} \cdot \omega_{ri}$	28.96	6.45
a_{10}	$T_{ri} \cdot \omega_{ri}$	12.19	4.81

The results of the accuracy of the models are presented in Table 4. It can be observed that the accuracy of the designs was guaranteed. R2 values greater than 99 % and standard errors of the estimate lower than 0.3 were obtained for both cases. R2 values in very good agreement, 98% for Tpo and 99% for ωpo, were obtained in a DW experimental model proposed by Beccali, called Model 54 [15].

Table 4. Correlation coefficients and standard errors of estimation.

Case study	R^2 [%]	Stnd. Error of Est.
1	99.91	0.22
2	99.89	0.16

3.2. Response Surfaces

The trends of the main effects on MRC for case studies 1 and 2 are shown in Fig. 3. It can be observed that the trends for both cases were similar. MRC increased when Tpi and ωri were reduced and ωpi and Tri were increased. This suggested that, if removing high amount of moisture were necessary, the inlet regeneration humidity ratio, ωri, did not have to be very high. These trends were found consistent with the positive and negative estimated effects in Table 2.

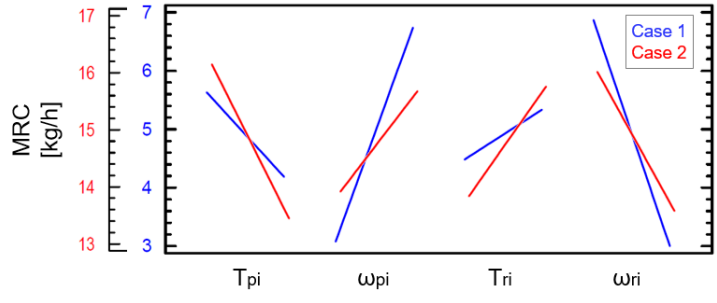

Fig. 3 Trends of the main effects on MRC for case studies.

The response surfaces for both case studies are shown in Fig. 4. In Fig. 4a, MRC is represented as a function of Tpi and ωpi. Tri and ωri were fixed at constant values: for case 1, 42.5 °C and 17.75 g kg-1, respectively, and for case 2, 80 °C and 17.75 g kg-1, respectively. The trends of MRC were similar for different values of Tri and ωri. For case 1, it can be observed that MRC increased when ωpi was increased. MRC values also increased when Tpi was reduced and ωpi low values. The MRC trends obtained in case 2 were in good agreement with case 1, see Fig. 4a. In case 2, MRC increased as ωpi was increased and Tpi was reduced.

Fig. 4b shows MRC as a function of Tri and ωri. Tpi and ωpi were fixed at constant values in both case studies, 23 °C and 17 g kg-1, respectively. The trends of MRC were similar for different values of Tpi and ωpi. In both case studies, MRC increased as Tri was increased and ωri was reduced. It can be observed that in both cases MRC presented low gradients compared to the first response surface. This suggested that the influence of the regeneration air stream conditions on MRC was lower than that of the process air stream.

The MRC maximum value achieved for case study 1 was 8.3 kg h-1, an acceptable value compared to the MRC nominal value, 15 kg h-1, see Table 1. The MRC maximum value achieved for case study 2 was 21.5 kg h-1, a difference of 61 % between both case studies. However, the sensible load generated in the adsorption process was delivered to the supply air when it passed through the process section of a DW outlet air process. For MRC maximum values, the air process outlet temperatures were 37 ºC and 54 ºC for case studies 1 and 2, respectively, a difference of 31.5 %.

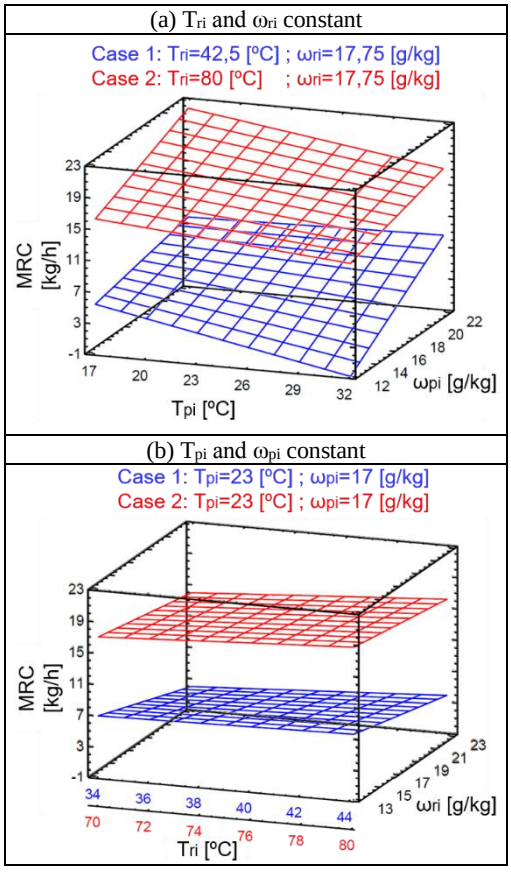

Fig. 4 Response surfaces for case studies 1 and 2 when (a) Tri and ωri remain constant; (c) and (b) Tpi and ωpi remain constant.

3.3. Cooling Energy

The theoretical cooling energy required for usual summer air supply conditions was 25.93 kW for case 1, and 28.42 kW for case 2, which was an increase of 9 %. The theoretical energy required for usual winter air supply conditions was 29.78 kW for case 1 and 32.07 kW for case 2, which was an increase of 7 %. The results showed that the DW activated at high temperature requires higher cooling energy, due to the high air process outlet temperatures derived from the higher heat rejection in the adsorption process.

4. Conclusions

In the present work, the moisture removal capacity of a DW was studied empirically for low and high regeneration temperature. Both cases were conducted varying the air process inlet temperature and humidity ratio and the air regeneration inlet temperature and humidity ratio. The methodology used is based on the statistical technique of design of experiments, DOE, which allowed to study the behaviour of DW with 19 experimental tests. The results allowed to reach the following conclusions:

- The methodology of DOE allowed the identification of the most influential psychrometric variables on MRC of a DW activated at low and high temperature. In both cases, the results showed a significant influence of the inlet humidity ratio of the air process and the air regeneration on MRC.

- MRC was analyzed from the influential variables. Using high regeneration temperatures, the MRC values were found 61% higher than using low regeneration temperatures. Nevertheless, with low temperatures MRC acceptable values were achieved compared to MRC nominal value.
- The theoretical cooling energy needed to achieve the supply air set conditions for MRC maximum values were obtained. The results showed that the DW activated at high temperature requires higher cooling energy, due to the high air process outlet temperatures derived from the higher heat rejection in the adsorption process.

In buildings where MRC extremely high is not required, a DW activated at low temperature needs lower cooling energy to achieve the supply air set conditions.

Acknowledgment

This work is related to the research project dehumidification and air drying, DESSECA, promoted by the company CIAT and co-funded by the Agency for Innovation and Development of Andalusia, expedient IDEA 360097, and by the Technological Corporation of Andalusia, expedient CTA 12/612, (2012-2014).

References

[1] A.G.C.C. American Gas Cooling Center. Applications Engineering Manual for Desiccant Systems, Arlington, 1996.
[2] Y. Sheng, Y. Zhang, N. Deng, L. Fang, J. Nie, L. Ma, Experimental analysis on performance of high temperature heat pump and desiccant wheel system, Energy Build. 66 (2013) 505–513.
[3] L.G. Harriman III, The dehumidification handbook, 2nd ed. , Munters Corp. Amesbury, MA. (2003).
[4] Y. Guan, Y. Zhang, Y. Sheng, X. Kong, S. Du, Feasibility and economic analysis of solid desiccant wheel used for dehumidification and preheating in blast furnace: A case study of steel plant, Nanjing, China, Appl. Therm. Eng. 81 (2015) 426–435.
[5] K.F. Fong, T.T. Chow, C.K. Lee, Z. Lin, L.S. Chan, Advancement of solar desiccant cooling system for building use in subtropical Hong Kong, Energy Build. 42 (2010) 2386–2399.
[6] D. Kosar, Dehumidification system enhancements, Ashrae J. 48 (2006) 48–58.
[7] J. Wrobel, P. Morgenstern, G. Schmitz, Modeling and experimental validation of the desiccant wheel in a hybrid desiccant air conditioning system, Appl. Therm. Eng. 51 (2013) 1082–1091.
[8] S.J. Slayzak, J.P. Ryan, Desiccant Dehumidification Wheel Test Guide, NREL Tech. Report, NREL/TP-550-26131. (2000).
[9] G. Angrisani, F. Minichiello, C. Roselli, M. Sasso, Experimental analysis on the dehumidification and thermal performance of a desiccant wheel, Appl. Energy. 92 (2012) 563–572.
[10] J.D. Chung, D.Y. Lee, S.M. Yoon, Optimization of desiccant wheel speed and area ratio of regeneration to dehumidification as a function of regeneration temperature, Sol. Energy. 83 (2009) 625–635.
[11] S. De Antonellis, C.M. Joppolo, L. Molinaroli, Simulation, performance analysis and optimization of desiccant wheels, Energy Build. 42 (2010) 1386–1393.
[12] F. Comino Montilla, M. Ruiz de Adana Santiago, A. Cerezuela Parish, M. Zamora García, F. Peci López, Design and building of a test facility for experimentation of desiccant wheels, Minutes B. Natl. Congr. Eng. Thermodyn. (2015) 295–302.
[13] D.C. Montgomery, Design and analysis of experiments, 6th Edition, Wiley, 2004.
[14] Statgraphics Centurion XV, (2006). available from http://www.statgraphics.com/ (accessed 05.12.15).
[15] M. Beccali, F. Butera, R. Guanella, R.S. Adhikari, Simplified models for the performance evaluation of desiccant wheel dehumidification, Int. J. Energy Res. 27 (2003) 17–29.

Appendix I

Experimental analysis of the desiccant capacity of hybrid HVAC systems based on desiccant wheels activated at low temperature by vapor compression refrigeration systems

The paper presented in this appendix is published in the *X National Congress Engineering Thermodynamics*, Lleida, Spain, 2017.

10CNIT-F179

ANÁLISIS EXPERIMENTAL DE LA CAPACIDAD DESECANTE DE SISTEMAS HÍBRIDOS BASADOS EN RUEDAS DESECANTES ACTIVADAS A BAJA TEMPERATURA MEDIANTE SISTEMAS DE REFRIGERACIÓN POR COMPRESIÓN DE VAPOR

Francisco Comino[1], Manuel Ruiz de Adana[1]

[1] Universidad de Córdoba, Escuela Politécnica Superior, Departamento de Química Física y Termodinámica Aplicada, Campus de Rabanales, Córdoba, España, e-mail: francisco.comino@uco.es

1. Introducción

El uso de ruedas desecantes, DW, en sistemas de climatización puede reducir el coste de la energía empleada por un equipo para deshumidificar el aire [1]. Los sistemas híbridos de climatización combinan ruedas desecantes, DW, con baterías de expansión directa, DX [2]. Para el estudio de sistemas de climatización con rueda desecantes, ASHRAE define la capacidad desecante, MRC, y el factor de calor sensible, SHR, como los parámetros principales para estudiar el rendimiento de estos sistemas [3] y [4].

El análisis experimental de la capacidad desecante de dos configuraciones diferentes de sistemas híbridos, mediante los parámetros MRC y SHR, es el principal objetivo de este trabajo.

2. Materiales y Métodos

Dos configuraciones diferentes de sistemas híbridos compuestos de un ciclo de compresión de vapor y una rueda desecante se han montado en el Laboratorio de Climatización de la Universidad de Córdoba para analizar el MRC y SHR bajo distintas condiciones de operación. La disposición de los elementos que componen ambos sistemas híbridos se muestra en la Figura 1.

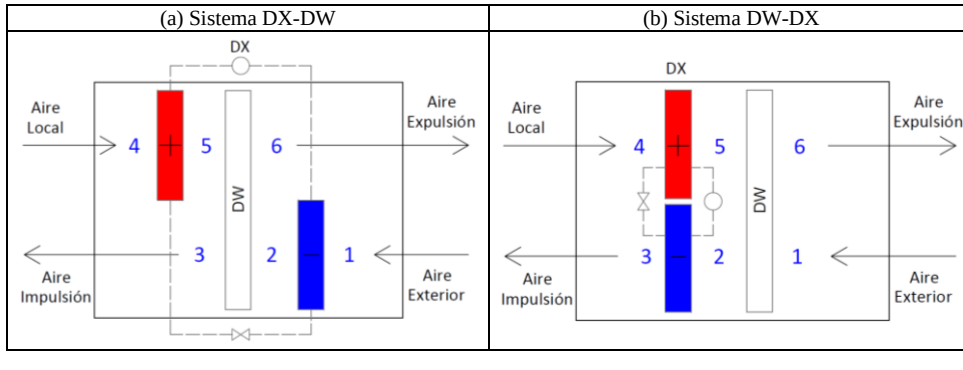

Figura 1. Configuración de los sistemas híbridos (a) DX-DW y (b) DW-DX.

La configuración y características técnicas de la planta experimental han sido publicadas en anteriores trabajos [4]. Las prestaciones de ambos sistemas híbridos, en términos de MRC y SHF se han analizado bajo diferentes condiciones del aire exterior y condiciones de aire interior, que corresponden con los cuatro casos a estudio que se muestran en la Tabla 1.

Tabla 1. Condiciones del aire para el estudio de comportamiento de los sistemas híbridos.

Caso a estudio	Aire exterior		Aire interior	
	T [ºC]	HR [%]	T [ºC]	HR [%]
1	16	88	27	65
2	32	34		
3	26	94		
4	32	66		

3. Resultados y Discusión

Los resultados del análisis experimental realizado en ambos sistemas híbridos se muestran en la Figura 2. El mayor valor de MRC en ambos sistemas corresponde al caso a estudio 3, alcanzándose valores de 18,3 kg/h y 14,7 kg/h, para el sistema DX-DW y DW-DX, respectivamente. Se observa un incremento de la capacidad desecante de la rueda desecante para condiciones exteriores húmedas y cercanas a la saturación del aire. Asimismo, los menores valores de MRC fueron obtenidos para el caso 2. La ubicación del evaporador en la corriente de aire de proceso antes de la rueda desecante en el sistema DX-DW genera unas condiciones de aire de proceso a la entrada de la rueda más favorables para potenciar la deshumidificación en la rueda desecante. En consecuencia, el sistema DX-DW, en la mayoría de los casos, presenta valores de MRC superiores al sistema DW-DX.

Analizando los valores de SHR, se observa que los menores valores, en valor absoluto, fueron alcanzados para los casos a estudio 3 y 4. Estos resultados indican que, para condiciones exteriores húmedas, estos sistemas híbridos son adecuados para climatizar locales con altas cargas latentes y bajas cargas sensibles interiores. Al comparar ambos sistemas híbridos se observa que en la mayoría de los casos con el sistema DW-DX se obtiene menores valores de SHR.

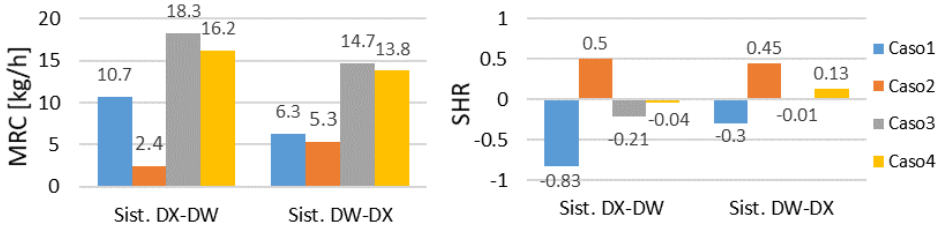

Figura 2. Resultados de los sistemas híbridos DX-DW y DW-DX (a) MRC y (b) SHR, para los cuatro casos a estudio.

4. Conclusiones

Los resultados experimentales obtenidos permiten alcanzar las siguientes conclusiones:

- El sistema híbrido DX-DW presenta en general una capacidad desecante superior a la del sistema DW-DX. La ubicación del evaporador antes de la rueda desecante en la corriente de proceso incrementa la capacidad desecante de la rueda en el sistema DX-DW.

- Con el sistema híbrido DW-DX, se obtienen valores de SHR cercanos a cero. Esta característica hace que el sistema DW-DX resulte adecuado para climatizar locales con altas cargas latentes.

En consecuencia, los sistemas híbridos basados en ruedas desecantes activadas a baja temperatura mediante sistemas de refrigeración por compresión de vapor constituyen una alternativa para realizar el tratamiento de aire en locales con altas cargas latentes.

5. Referencias

[1] L.G. Harriman III, The dehumidification handbook, 2nd ed. , Munters Corp. Amesbury, MA. (2003).

[2] D. Kosar, Dehumidification System Enhancement, ASHRAE J. 48 (2006) 48–58.

[3] ASHRAE, Method of Testing for Rating Desiccant Dehumidifiers Utilizing Heatfor the Regeneration Process, ASHRAE standard, 2007.

[4] F. Comino, M. Ruiz de Adana, Experimental and numerical analysis of desiccant wheels activated at low temperatures, Energy Build. 133 (2016) 529–540.